UNIVERSITY OF CALIFORNIA, SAN DIEGO

SAN DIEGO STATE UNIVERSITY

Degenerate Four-Wave Mixing Interfaced with Capillary Electrophoresis as a Bioanalytical Method for Small Molecules, Peptides, and Proteins

A dissertation submitted in partial satisfaction of the
requirements for the degree of Doctor of Philosophy

in

Chemistry

by

Manna Frances Iwabuchi

Committee in charge:

University of California, San Diego

Professor Thomas Hermann
Professor Michael J. Tauber

San Diego State University

Professor William G. Tong, Chair
Professor Chun-Ta Lai
Professor Diane K. Smith

2015

The dissertation of Manna Frances Iwabuchi is approved, and it is acceptable in quality and form for publication on microfilm and electronically:

_____

_____

_____

_____

_____

Chair

University of California, San Diego

San Diego State University

2015

DEDICATION

This dissertation is dedicated to my Grandmother Barbra Stuher,
Grandfather Walter Stuher,
my family,
Michael Doud, and Brutus Iwabuchi,
and all I love

EPIGRAPH

研究室で研究をしていなければ暇だというのか？

この世に無駄な研究なんかはない。

福山雅治　～ガリレオより

TABLE OF CONTENTS

LISTS OF FIGURES

LISTS OF TABLES

ACKNOWLEDGEMENTS

I do not have many chances to think about people who have supported me through my education this far and I appreciate them deeply. I would like to use this opportunity to express this appreciation. First, I would like to thank my parents. 父、岩渕育雄様。私がアメリカに住む様になっても、いざという時に頼れる安心感があったおかげでパニックにならず、ここまで来る事が出来ました。いつも、娘達のベストを考えてくれてサンキュー。To my mother, Deborah Iwabuchi. I appreciate that you came so far from California to Japan. I am so glad I have both Japanese and US in me so I was able to come to the US and accomplish my Ph.D. degree. I know editing my thesis took time and you were always happy to help me. My sister, Hikari. We came to the US at the same time to start graduate school. I had courage to come here since I knew you would be here. Now I am going to start a new stage of my life, which you have already started, and I truly appreciate your advice.

I was inspired to make the most of the projects I have here by my grandmother, Barbara Stuhr who passed away two years ago. I always loved you and wanted to make your life easier when you were struggling from Parkinson's disease. I hope I was a granddaughter you could be proud of. Grandfather, Walter Stuhr. I respect you for the fact you earned a Ph.D. degree before there were computers, and of course for your knowledge. I learned from you to be patient and supportive the way you were for Grandma. I would also like to thank my relatives in North and

South California, and all other places in the US. I did not have too many problems adapting to U.S. culture because you always accepted me as I am, and supported me through my life. I love you all.

I would like to thank people from San Diego State University. Kathy, thank you for being supportive and always willing to give me advice. I cannot count how many times I stopped by your lab to have a "therapy session." To Dr. Huxford and Harrison; I truly appreciate the scientific knowledge you shared with me to accomplish my projects. I learned to look at experimental issues from different perspectives and you helped me to become a better scientist.

Dr. Tong, if you were not my adviser, I think I would not have pursued a Ph.D. degree. I was not confident, but I could challenge myself with your words, "It's going to be ok, just try." I gained so much experience, knowledge, and met lots of people who I would not have met if I were not in the Joint Doctoral Program.

I always appreciate all the members, past and present, from the Tong Lab. To those who taught me the degenerate four-wave mixing when I joined Tong lab, especially Marc; thank you for helping me and giving me advice while you were a graduate student and even after you graduated. Ashley, Sashary, Linda, Doug, Diane, I was so fortunate to work with undergraduates who had great work ethics and interest in science. Sashary, you joined Tong's lab when you were a freshman and we are both graduating together. You always challenged yourself to make yourself and your life better and better. You inspired me a lot. To my colleagues, Tiffany, Eric, Sebastian, Alex, and Jeff. It was a pleasure to work with you. I enjoyed talking about our research, science in general, and ideas for future plans. To one of my best friends

and colleagues, Marcel. We had so much fun in and outside of lab. You taught me all about American humor. I learned about your culture, language, and points of view. Having a great friendship is the best way to like where you are. I am also very proud of what we have overcome and accomplished. Thank you for being my support all the time.

To people in Japan. I am truly grateful to all my undergraduate chemistry professors. I learned chemistry is an exciting area to learn and research, and research doesn't end since there are so many topics and issues to fix in the world. Also, I would like to thank you for the mental support that I had from you. You always cared about me, and wished for my best. Dr. Mizoguchi and Dr. Nakamura. When I first met you, I didn't have any specific goals for my life and career. You slowly guided me so that I could find them by myself. It was the most important skill I got in my life. And I know you still care about me! I cannot thank you enough.

All the Douds I have met. Thank you for your love, advice, mental support, and delicious *EverCrisp* and all sorts of apples that you sent to San Diego.

My handsome emotional support cat, Brutus, you loved hanging out with me when I was writing my thesis. Partially from the warmth of the computer, but I am sure you also love me as much as I love you.

Last, Michael Doud! I am glad we both supported each other throughout this rough time and survived. I cannot thank you enough for how much time you spent editing my dissertation. We also had fun by going to lots of places, cooking, and eating delicious food! I appreciated you for validating my feelings, cheering me up, and giving me advice every time I was down or facing some huge wall.

I truly appreciate ARCS Foundation for supporting my graduate student career. You have provided me with more than grants. I was always motivated by the the people in the foundation to contribute to society and learned how important it is to keep up my motivation, challenge myself, and be persistence in my research as ARCS scholar. I have come so far thanks to your support.

Chapter 5: The majority of the material for this chapter comes directly from a manuscript entitled "Sensitive Analysis of α-Synuclein by Nonlinear Laser Wave Mixing Coupled with Capillary Electrophoresis," by Manna F. Iwabuchi, Marcel M. Hetu, and William G. Tong, submitted in Anal. Biochmeistry., 2015. The dissertation author is the primary author of this manuscript.

Chapter 6: The majority of the material for this chapter comes directly from a manuscript entitled "Zepto- and Yocto-mole Detection of Native and Labeled Neurotransmitters by Nonlinear Wave-Mixing Spectroscopy Coupled with Capillary Electrophoresi.," by Manna F. Iwabuchi, Marcel M. Hetu, Sashary Ramos, and William G. Tong, to be submitted. The dissertation author is the primary author of this manuscript.

Chapter 7: The majority of the material for this chapter comes directly from a manuscript entitled "Ultrasensitive Detection of Alzheimer's Disease Biomarkers Aβ1-42 and Aβ1-40," by Manna F. Iwabuchi, Marcel M. Hetu, and William G. Tong, to be submitted. The dissertation author is the primary author of this manuscript.

VITA

2007	B.A., Natural Science, International Christian University
2015	Ph.D., Chemistry, University of California, San Diego, San Diego State University

PUBLICATIONS

Iwabuchi, M. I., Hetu, M. M., Tong, W. G. "Sensitive Analysis of α-Synuclein by Nonlinear Laser Wave Mixing Coupled with Capillary Electrophoresis." Submitted to *Anal. Biochem,* **2015**.

Iwabuchi, M., Hetu, M., Maxwell, E., Pradel, S., Ramos, S., Tong, W. G. "Nonlinear Multi-Photon Laser Wave-Mixing Optical Detection in Microarrays and Microchips for Ultrasensitive Detection and Separation of Biomarkers for Cancer and Neurodegenerative Diseases." Submitted to *SPIE,* **2015**.

Hetu, M., **Iwabuchi, M.**, Maxwell, E., Wu, H., Ramos, S., Tong, W.G. "Zepto-Mole Detection in Microfluidics by Novel Nonlinear Multi-Photon Laser Wave-Mixing Spectroscopy for Biomedical and Environmental Applications." *Proc. SPIE*, **2014**, *9193*, 7.

Gregerson, M., Hetu, M., **Iwabuchi, M.**, Jimenez, J., Warren, A., Tong, W. G. "Ultrasensitive Standoff Chemical Sensing Based on Nonlinear Multi-Photon Laser Wave-Mixing Spectroscopy." *Proc. SPIE*, **2012**, *8497*, 31.

Iwabuchi, M. F., Hetu, M. M., Ramos, S., Tong, W. G. "Zepto- and Yocto-mole Detection of Native and Labeled Neurotransmitters by Nonlinear Wave-Mixing Spectroscopy Coupled with Capillary Electrophoresi." Manuscript to be submitted.

Iwabuchi, M. I., Hetu, M. M., Tong, W. G. "Ultrasensitive Detection of Alzheimer's Disease Biomarkers Aβ1-42 and Aβ1-40." Manuscript to be submitted.
Hetu, M. M., **Iwabuchi, M. F.**, Maxwell, E. J., Tong, W. G. "Zeptomole Detection of Nitroaromatic Explosives and Ammonium Nitrate in Liquid Capillary Flow Cells and on Surfaces Using Laser Wave-Mixing Spectroscopy." Manuscript to be submitted to *Anal. Methods.*

Hetu, M. M., **Iwabuchi, M. F.**, Tong, W. G. "Ultrasensitive Detection of HIV-1 P24 Capsid by Degenerate Four-Wave Mixing." Manuscript to be submitted.

FIELDS OF STUDY

Major Field: Analytical Chemistry

Studies in Laser Wave-Mixing Spectroscopy

Professor William G. Tong, Chair

ABSTRACT OF THE DISSERTATION

Degenerate Four-Wave Mixing Interfaced with Capillary Electrophoresis as a Bioanalytical Method for Small Molecules, Peptides, and Proteins

by

Manna Frances Iwabuchi

Doctor of Philosophy in Chemistry

University of California, San Diego, 2015

San Diego State University, 2015

Professor William G. Tong, Chair

Degenerate four-wave mixing (DFWM) is demonstrated as an ultrasensitive detection method for the study of neurodegenerative disease-related biomolecules in a capillary electrophoresis system. Nonlinear absorption-based wave mixing offers important advantages including high spatial resolution, small probe volumes down to

picoliter, small sample requirements, effective signal collections, and low background noise levels. The laser wave mixing is easily interfaced with microcapillaries for a continuous-flow mode detection and a capillary electrophoresis-mode detection.

The optimal conditions for laser wave mixing and capillary electrophoresis is investigated to perform ultrasensitive detection and molecular weight-based separation for proteins. A cost-effective fluorophore is employed to target analytes, bovine serum albumin (BSA), antibody of HIV-1 capsid protein p24, and monoclonal antibody of breast cancer marker CA15-3. Concentration (and mass) detection limits of 1.4×10^{-10} M (1.0×10^{-20} mol), 6.6×10^{-10} M (5.1×10^{-20} mol), and 6.7×10^{-12} M (5.2×10^{-22} mol) are determined for BSA, p24 antibody, and CA15-3 antibody.

For the first time, α-synuclein is analyzed using fluorescein isothiocyanate (FITC), QSY35 acetic acid succinimidyl ester, and Chromeo^{TM} P503 by wave mixing-based capillary zone electrophoresis and capillary sieving electrophoresis. Detection limits of 1.4×10^{-13} M (1.1×10^{-23} mol), 1.4×10^{-10} M (1.1×10^{-20} mol), and 3.8×10^{-13} M (3.0×10^{-23} mol) are determined for FITC, QSY35, and Chromeo^{TM} P503-conjugated α-synuclein. Tetramer α-synuclein is observed to be the most abundant species in the buffer system in which separation is executed.

Native label-free adenosine and dopamine, and chromophore-conjugated glutamate and γ-aminobutyric acid are detected at ultrasensitive concentration levels using wave mixing-based micellar electrokinetic chromatography. Detection limits of 1.0×10^{-13} M (5.6×10^{-24} mol corresponds to 4 molecules), 1.2×10^{-9} M (6.6×10^{-20} mol), 3.7×10^{-10} M (2.9×10^{-20} mol), and 4.1×10^{-11} M (3.2×10^{-21} mol) are determined for native label-free adenosine and dopamine, dabsylated glutamate and γ-aminobutyric

acid.

β-Amyloid 1-42 and 1-40 peptides are investigated using wave mixing based capillary zone electrophoresis. Detection limits of 8.2×10^{-13} M (6.5×10^{-23} mol) and 1.2×10^{-12} M (9.5×10^{-23} mol) are determined for Aβ1-42 and Aβ1-40.

CHAPTER 1
INTRODUCTION TO LASER SPECTROSCOPY

1.1 Sensitive Detection of Biomolecules by Laser Spectroscopy

1.1.1 MOTIVATIONS

Spectroscopy involves both the investigation and measurement of spectra produced when matter interacts with radiated energy. Researchers use several types of spectroscopic methods including ultraviolet (UV) and infrared (IR) absorption, Raman scattering, laser-induced fluorescence, and nonlinear laser methods such as degenerate four-wave mixing (DFWM) laser spectroscopy. Nonlinear DFWM laser spectroscopy is an optical absorption-based technique that is suitable for detecting varieties of molecules at picomolar concentration levels and zeptomole and yoctomole mass detection limits. This ultrasensitive detection method is suitable for exploring early stage diagnostics and novel studies for brain chemistry. The motivation for the research in this dissertation is to demonstrate that DFWM coupled with capillary electrophoresis (CE) is suitable for ultrasensitive detection, quantification, and molecular weight sizing for biomolecules related to Parkinson's Disease (PD), Alzheimer's Disease (AD), breast cancer, and Human Immunodeficiency Virus (HIV).

Developing an accurate and field deployable instrument would help to better understand the mechanisms of neurodegenerative diseases, such as PD and AD, and could help establish biomarkers for early stage diagnostics. The only effective and FDA-approved treatment of Parkinson's disease (PD) involves brain stimulation with radio frequencies. The exact mechanism behind this type of brain treatment is still

being explored. Real time monitoring of neurotransmitters may provide critical information on how deep brain stimulation (DBS) treatments affect the symptoms of PD. Several biomarker targets have been explored for both PD and AD; however, mechanisms of neurodegenerative diseases are very complicated and no one biomarker has been established as a reliable diagnostic marker for these diseases. Categorizing and identifying different forms of biomarker, peptides and proteins may help in developing early-stage diagnostic methods for these diseases. Nonlinear absorption-based laser spectroscopy is an ultrasensitive technique that provides excellent sensitivity and high specificity levels, and when coupled with an appropriate separation method, it is useful for early diagnostic studies and monitoring of diseases, and investigating brain chemistry.

1.2 Advantages of lasers for use in spectroscopy

1.2.1 LASER AS A TOOL FOR SPECTROSCOPY

Throughout this work, lasers are used as the light source for nonlinear degenerate wave-mixing detection systems. Laser systems are used in many sophisticated spectroscopic instruments. They provide a magnitude of improvements in sensitivity and selectivity when compared to other spectroscopic techniques where a laser is not used as the excitation source. Laser-induced fluorescence, Raman spectroscopy, laser-induced breakdown spectroscopy, laser absorption spectroscopy and DFWM require the use of an appropriate laser source. Lasers offer special features such as monochromaticity, low divergence, extreme brightness, and spatial and temporal coherences, making them attractive for laser-based spectroscopic

methods.

1.2.2 HIGHLY MONOCHROMATIC LIGHT SOURCE

Unlike ordinary incoherent white light sources, a laser emits a single wavelength of light with a narrow linewidth. The laser light typically comes from one atomic transition with a single precise wavelength, giving laser light a single spectral color and an almost pure monochromatic wavelength. The laser light, however, is not a fully monochromatic, single-frequency light. True monochromatic light requires a wave train of infinite duration. Due to the Doppler effect resulting from moving atoms or molecules, the spectral line from which laser radiation originates does have a finite linewidth in the order of a few MHz or KHz depending on the laser, but orders of magnitude narrower than those of conventional light sources.[1] Highly monochromatic light source like lasers improve selectivity levels in chemical analysis.

1.2.3 SMALL DIVERGENCE

Divergence is a measure of how much the diameter of a light beam spreads out as the laser beam travels. One of the special features of a laser is that its beam has a small divergence and the beam can travel great distances and remain relatively collimated as compared to incoherent light sources. Photons inside a laser cavity bounces back and forth between two mirrors before exiting from the laser cavity.[2] These internal reflections make the effective length of the laser cavity longer than the distance between the two mirrors. These mirrors allow the buildup of the photons aligned only in certain propagation directions back and forth inside the cavity.

Figure 1.1 shows a typical helium-neon laser with a laser cavity defined by the two reflecting mirrors. To narrow or focus the beam in the middle of the cavity, these mirrors are curved slightly. The output mirror is designed to allow a fraction of the light to be transmitted in order to create the laser output beam. The beam radius ω is defined as the distance from the center of the beam to where the intensity has fallen to 37% (100% x 1/e; e=2.78). At the beam waist, the Gaussian profile is depicted as ω_0. The divergence of the beam is characterized by the angle Φ/2 and described as:

$$\phi = \frac{1.27\,\lambda}{2\,\omega_0} \tag{1.1}$$

Small divergence of lasers play an important role in DFWM since two laser beams must be tightly focused at the sample to create a probe volume that is in the nano- to picoliter range.

1.2.4 LASER BRIGHTNESS

High radiance of the laser beam is the result of compact, collimated, and highly monochromatic laser beam. As described in equation 1.2, radiant intensity depends on the power of the laser (P), unit solid angle (Ω), and area of the source (A).

$$\text{Radiance} = \frac{P}{A\Omega} \tag{1.2}$$

Lasers have a high spectral brightness that can be quantified and expressed as brightness per unit of frequency. Spectral distribution or frequency widths give a number of frequencies output by the light source. Power per frequency is smaller if the power of a source comes from a wide range of frequencies. Figure 1.2 illustrates three types of frequency distributions denoted as g(υ). It describes the distribution of

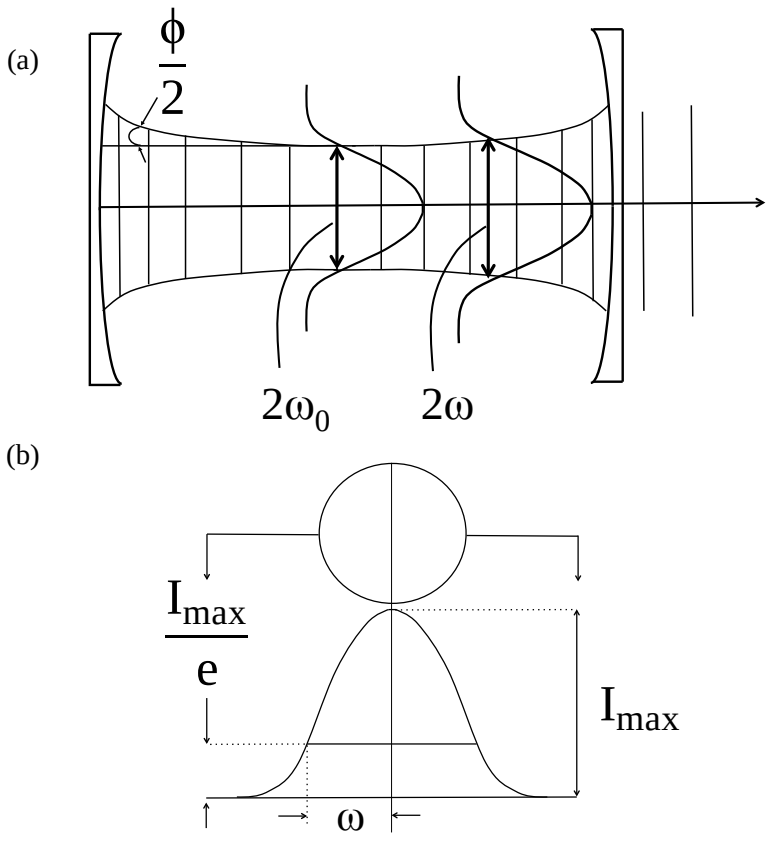

Figure 1.1 a) Typical helium-neon laser cavity: two mirrors facing each other. Gaussian cross-sectional profile is presented, where the beam intensity maximizes at the beam center and decreases according to a Gaussian distribution as distance from the center. b) Cross-sectional profile of a laser beam and the Gaussian profile. The laser beam intensity is plotted. The profile of the beam varies depending on lasers. All lasers used for this work have the TEM_{00} profile depicted in this figure.

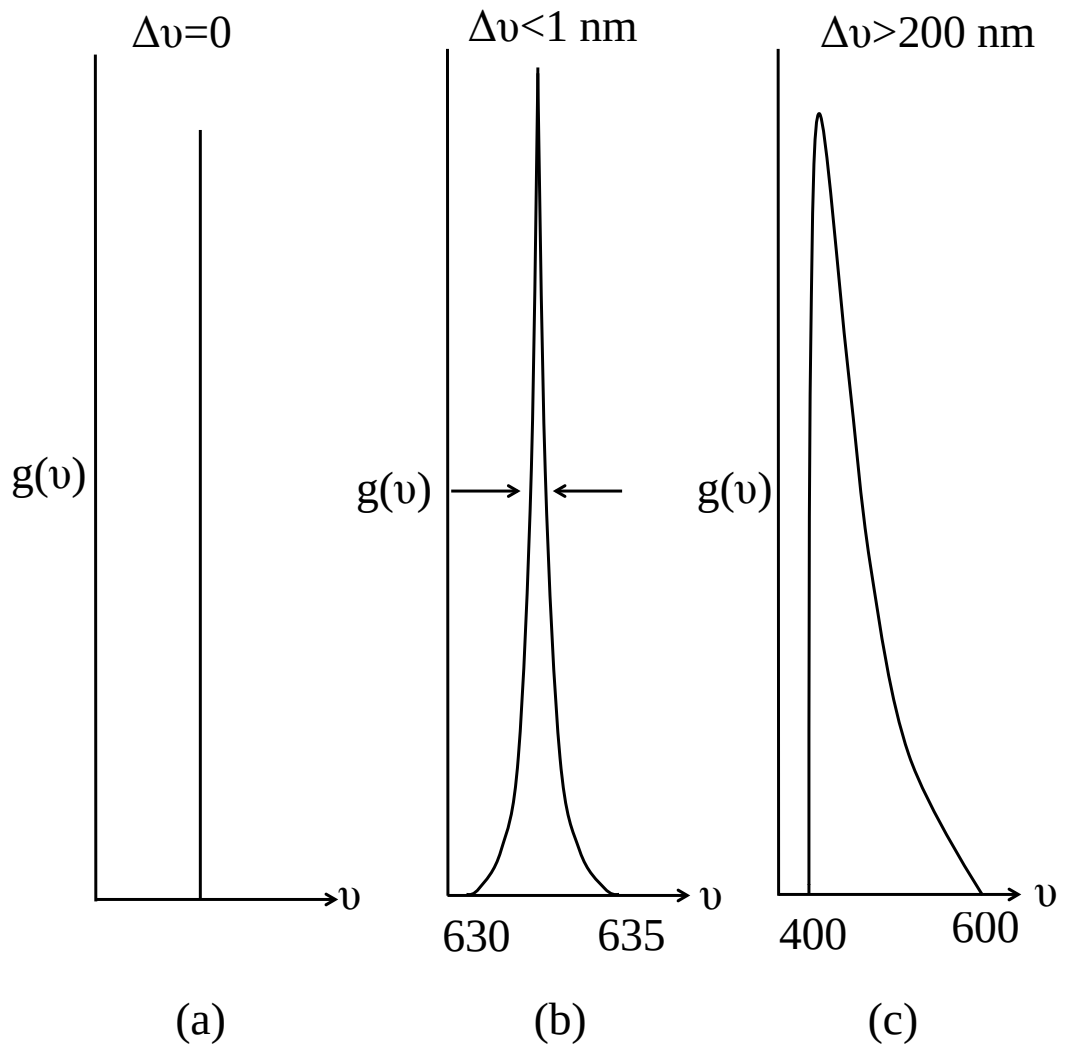

Figure 1.2 Three examples of frequency distributions. (a) Intensity of the source output at single frequency. (b) Frequency distribution of a typical laser. (c) Spectral width of a typical black body.

the energy radiated at different wavelengths. The spectral width of the laser always enhances its output compared to conventional incoherent light source.

1.2.5 SPATIAL AND TEMPORAL COHERENCES

Coherence is the most unique aspect of lasers that distinguishes them from other light sources. There are two types of coherences; spatial and temporal. A coherent light typically exhibits the same wavelength radiating in the same direction with a uniform phase or polarization. Spatial coherence describes the correlation between electromagnetic waves at different points. When all points of the wave are coherent, then the wave is spatially coherent. If two waves oscillate in the same manner from one point in time to the next, they are temporally coherent. The coherence time (t_c), a quantitative measure of temporal coherence, is given by equation 1.3 where l_c is the coherence length and c is the speed of light.

$$t_c = \frac{l_c}{c} \tag{1.3}$$

Both spatial coherence and temporal coherence relate to the monochromaticity of the laser. The degree of monochromaticity depends on the range of the frequency ν that the laser outputs. The center frequency can be denoted as ν_0. Frequency distribution is denoted as g(ν) in Figure 1.2 and bandwidth as Δν.

$$l_c = \frac{c}{\Delta\upsilon} \tag{1.4}$$

$$t_c = \frac{1}{\Delta\upsilon} \tag{1.5}$$

Equations 1.4 and 1.5 explain physical concepts of coherence; if the light source

emits a single frequency, it stays spatially and temporally coherent. Due to high monochromaticity, the laser is the only light source that can generate light that is coherent over relatively long distances and times.

1.3 Basis of lasers

1.3.1 HISTORY OF LASER

The paper containing both the concept and theory of stimulated emission was first published by Albert Einstein in 1917.[3] Charles H. Townes came up with an idea to build stimulated emission at microwave frequencies in 1951. He and his graduate student, James Gordon, built a device called MASER (Microwave Amplification by the Stimulated Emission of Radiation) in 1954.[4] He was awarded Nobel Prize in Physics (1964), though, the first person to build a laser was Theodore Maiman in 1960.[5] The new device, LASER, was a pulsed laser produced from crystal of synthetic ruby with a high intensity flash lamp. Now lasers have become a popular source for studying spectroscopy including laser-induced fluorescence, Raman spectroscopy, and DFWM.[6-8]

1.3.2 BASIC LASER PROCESSES

Laser is an acronym for Light Amplification by Stimulated Emission of Radiation. The concept of stimulated emission is at the foundation of the laser. Figure 1.3 is an energy diagram and it illustrates three basic processes: absorption, spontaneous emission, and stimulated emission. Spontaneous emission happens randomly when molecules in an excited electronic state (E_2) lose energy and return to the lower energy level (E_1). Incoherent light is emitted during this process.

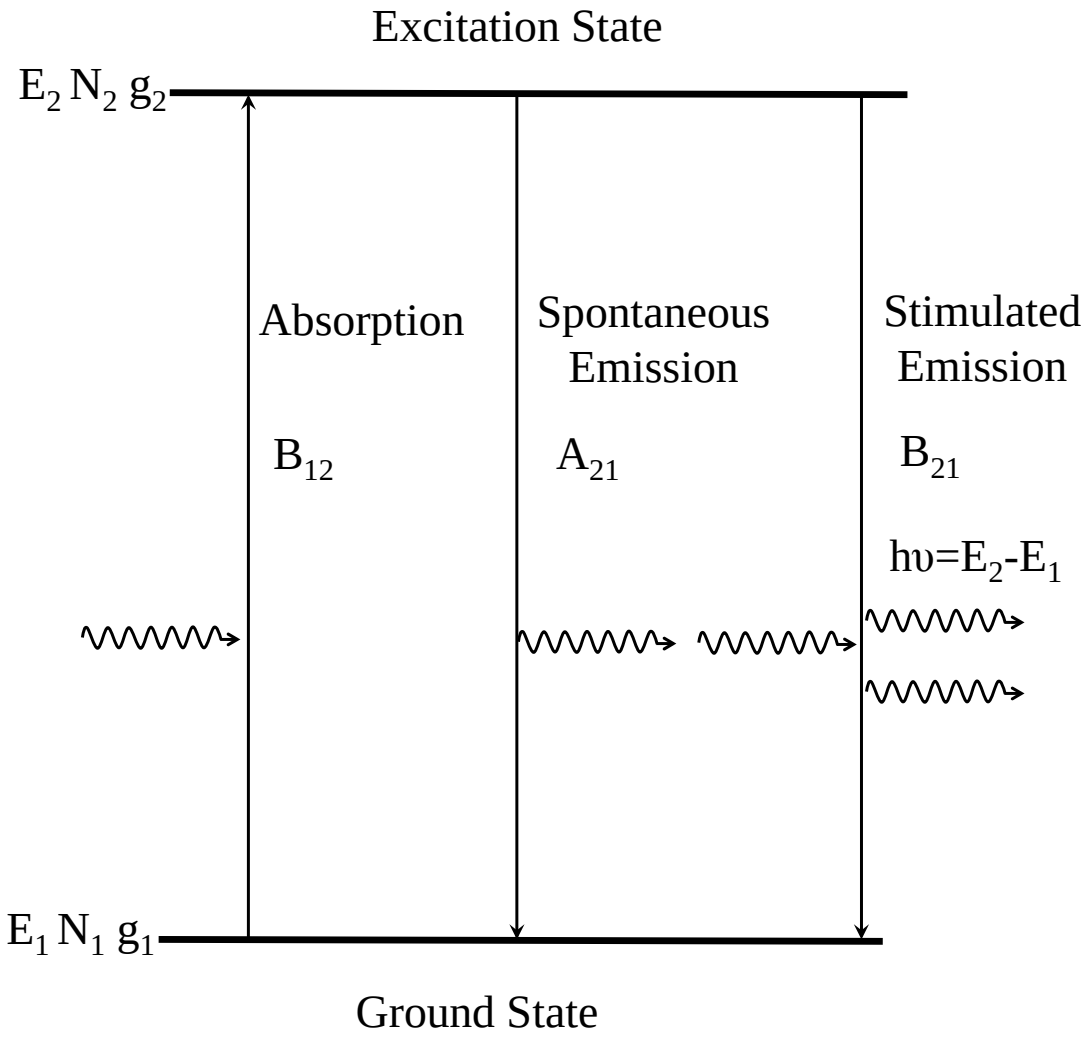

Figure 1.3 Energy diagram for stimulated absorption, spontaneous emission, and stimulated emission. B_{12}, A_{21}, and B_{21} are Einstein coefficients for each process. Population is indicated by N and quantum mechanical factors are characterized by g_1 and g_2.

Absorption from E_1 to E_2 occurs when a molecule absorbs light. Stimulation of a population in an excited state induces emission with energy that equals the product of Planck constant (*h*) and frequency associated with the electromagnetic wave (ν). In stimulated emission, emitted photons and excitation photons are in phase traveling in the same direction and combined to yield the total stimulated emission beam. Amplification of these coherent in-phase directional photons yields the output laser beam.

The rates of absorption and emission can be described by Einstein coefficients, B_{12}, B_{21}, and A_{21} as shown in Figure 1.3. B_{12} is a second-order rate constant describing absorption of a photon by the energy state E_1. B_{21} is a second-order rate constant describing the stimulated emission of a photon from the energy state E_2. The processes of both B_{12} and B_{21} depend on the radiation density $\rho(\nu_{12})$ of the light energy needed to drive a transition from the ground state to the excited state. Both Einstein coefficients are in units of $m^3J^{-1}s^{-2}$. A_{21} is a first-order rate constant describing the spontaneous emission of a photon from the energy state E_2 in units of s^{-1}. Three possible processes that can change the state of the system from E_1 to E_2 or E_2 to E_1 are described below. The rate for absorption is described as[9]:

$$\frac{dN_1}{dt} = B_{12}\,\rho(\nu_{12})\,N_1 \qquad (1.6)$$

The rate for stimulated emission depends on Einstein coefficient B_{21}.

$$\frac{dN_1}{dt} = -B_{21}\,\rho(\nu_{12})\,N_2 \qquad (1.7)$$

The rate for spontaneous emission depends on Einstein coefficient A_{21}.

$$\frac{dN_1}{dt} = -A_{21}N_2 \qquad (1.8)$$

The reciprocals of Einstein coefficients refer to lifetimes for each process. Time for spontaneous emission (τ_{A12}) from E_2 to E_1 occurs in $1/A_{21}$ seconds, and for stimulated emission (τ_{B12}) from E_2 to E_1 occurs in $1/\rho B_{21}$ seconds.

1.3.3 POPULATION INVERSION

Population inversion must be achieved first in order to amplify light in a laser, i.e., the number of photons produced by stimulated emission must exceed the number of lost photons by absorption. This condition is achieved when the population in the higher energy level exceeds that of the lower energy level. The energy gap between E_1 and E_2 is so large that the thermal energy only usually cannot overcome the energy barrier. Population in ground state (N_1) is much higher than excited-state population, and hence, absorption happens more likely than emissions. Population distribution in a gas medium obeys the Boltzman distribution as described below.[9]

$$\frac{N_2}{N_1} = \frac{g_1}{g_2}\, e^{-\frac{\Delta E}{RT}} \qquad (1.9)$$

Quantum mechanical factors are characterized by g_1 and g_2, and ΔE is the energy gap between E_2 and E_1. R is the gas law constant (8.31J/Kmol), and T is the absolute temperature in the system.

Figure 1.4 shows schematic diagram of three- and four-level laser systems and the best known examples for three- and four-level systems are ruby laser and Nd:YAG laser, respectively. The majority of the population is in the ground state (E_1) at room temperature for both systems. Sufficient energies, $h\nu_{13}$ and $h\nu_{14}$, for

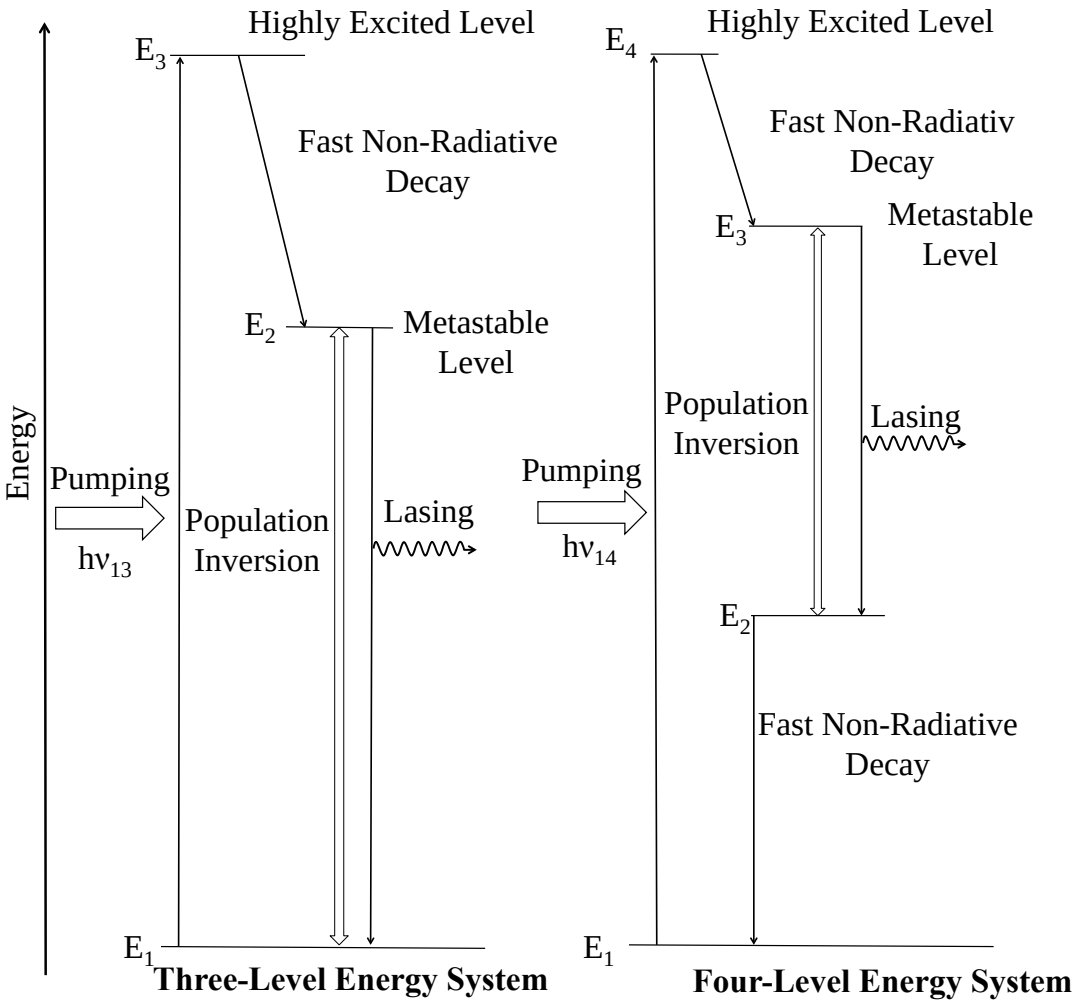

Figure 1.4 Energy diagrams of three- and four-level laser systems. The population inversion obtained by optical pumping from E_1 to E_3 or E_4 for three- or four-level system is quickly depleted to metastable states. Lasing is created when population inversion between E_3 and E_1 or E_3 and E_2 is achieved.

three- and four-level system, respectively, excite the population to highly excited states. Optical pumping or electrical pumping is used to provide external energy needed to achieve population inversion. The excited-state lifetime for most systems is short (ns); however, some metastable states of laser materials have considerably longer lifetimes (micro to millisecond) before spontaneous emission occurs. Systems with metastable states yield stimulated emission more readily.

1.4 Various types of lasers

1.4.1 CATEGORIES OF LASERS

Different types of lasers covering a wide range of wavelengths are available for spectroscopic measurements. Each region of wavelength reflects a particular type of energy level transition. Microwave and far-infrared (IR: 1 cm -50 μm) wavelengths are suitable for rotational studies, mid- and near-IR (50-1 μm) wavelengths are for vibrational studies, and near-IR, visible, UV, and VUV wavelengths (1 μm-100nm) are for electronic transitions.[10] Various types of lasers are generally classified by the light-emitting medium or material including gas, solid-state, diode, and dye lasers. This work uses mostly solid-state lasers including a 266 nm frequency quadrupled Nd:YAG laser and 405, 447, 473, and 488 nm visible solid-state lasers.

1.4.2 SOLID-STATE LASERS

Solid-state lasers contain special crystals that allow efficient population inversion. The light absorbing atoms are embedded in a solid. These embedded absorbing atoms are called the active species and the material that has the emitting atoms is called the host. The active species absorb light, get excited to a higher

energy level that, in turn, populate the metastable upper energy level. The most important active species are metals such as chromium, neodymium, erbium, ytterbium, and titanium. They are often called “ions” because they have a nominal chemical valence in the host crystal. Valance bonds with the host material and interactions with adjacent atoms affect energy levels. In the case of neodymium, 1054 nm or 1064 nm is emitted depending on the host: phosphate-base glass or yttrium aluminum garnet (YAG), respectively.

Host materials must meet optical, thermal, and mechanical requirements. Most of the pump energy that is not converted to laser energy ends up as heat, thus the thermal properties of the host are important. Heat removal is an important operating consideration since solids cannot dissipate heat efficiently like gases. Excessive heat causes thermal and mechanical stress within a laser rod. Uneven distribution of heat can leads to refractive-index differentials that degrade beam quality, reduce output power, and/or crack the rod. Crystals with good thermal properties dissipate heat efficiently and can operate at higher powers and higher repetition rates.

1.4.3 ND:YAG LASER

The Nd:YAG laser has transition metal ions embedded in a transparent ionic crystal host. The most common neodymium-based laser possesses small concentrations of Nd^{3+} ions in an yttrium aluminum garnet (YAG) crystal. Neodymium ions act as a substitute for yttrium ions that have a similar ionic size. Neodymium is present as an impurity in the YAG crystal at 1-2% by weight. High thermal conductivity between the YAG crystalline host and the medium allows

removal of the heat generated during high-power runs. The lasing medium is generally rod-shaped with a centimeter diameter and several centimeters in length, depending on the laser design and size.

The Nd:YAG laser is a classic four-level laser system shown in Figure 1.5. Neodymium is classified as a rare earth element with an incomplete 4*f* electronic subshell. A number of energy levels arise from the coupling of the spin and orbital angular momenta to yield total angular momentum states with closely spaced energies. The number of these states is defined by $2J+1$, where J is the total angular momentum quantum number. J values are represented by subscripts of each energy level. $^4F_{3/2}$ energy level has $J = 3/2$, representing that the state has 4 degenerate energy levels. Presence of the host lattice, though, separates 4 energy levels slightly. This is called crystal field splitting. The upper levels of Nd^{3+} ions are populated by pumping the ground state ions $^4I_{9/2}$ with 0.73 μm and 0.8 μm using Xe flash lamps for pulsed laser operation and tungsten arc lamps for continuous-wave (CW) operation. Population inversion between $^4F_{3/2}$ and $^4I_{11/2}$ is achieved by fast and non-radiative transitions from upper energy levels to metastable states ($^4F_{3/2}$). The transition from $^4F_{3/2}$ to $^4I_{11/2}$ produces the primary 1.06 μm laser radiation. Non-radiative decay from $^4I_{11/2}$ to $^4I_{9/2}$ subsequently occurs as the final relaxation step.[11]

Nd:YAG CW output powers range from a few milliwatts up to about 100 W. Normal pulse mode (100-1000 μs) output energy reaches 0.1-100 J, and the Q-switched mode (10-20 ns pulse) generates energy of 0.01-1 J.[12] Nonlinear frequency conversion crystals are employed for harmonic generations. The second harmonic, the third harmonic, and the fourth harmonic generation yield 532, 355 and 266 nm,

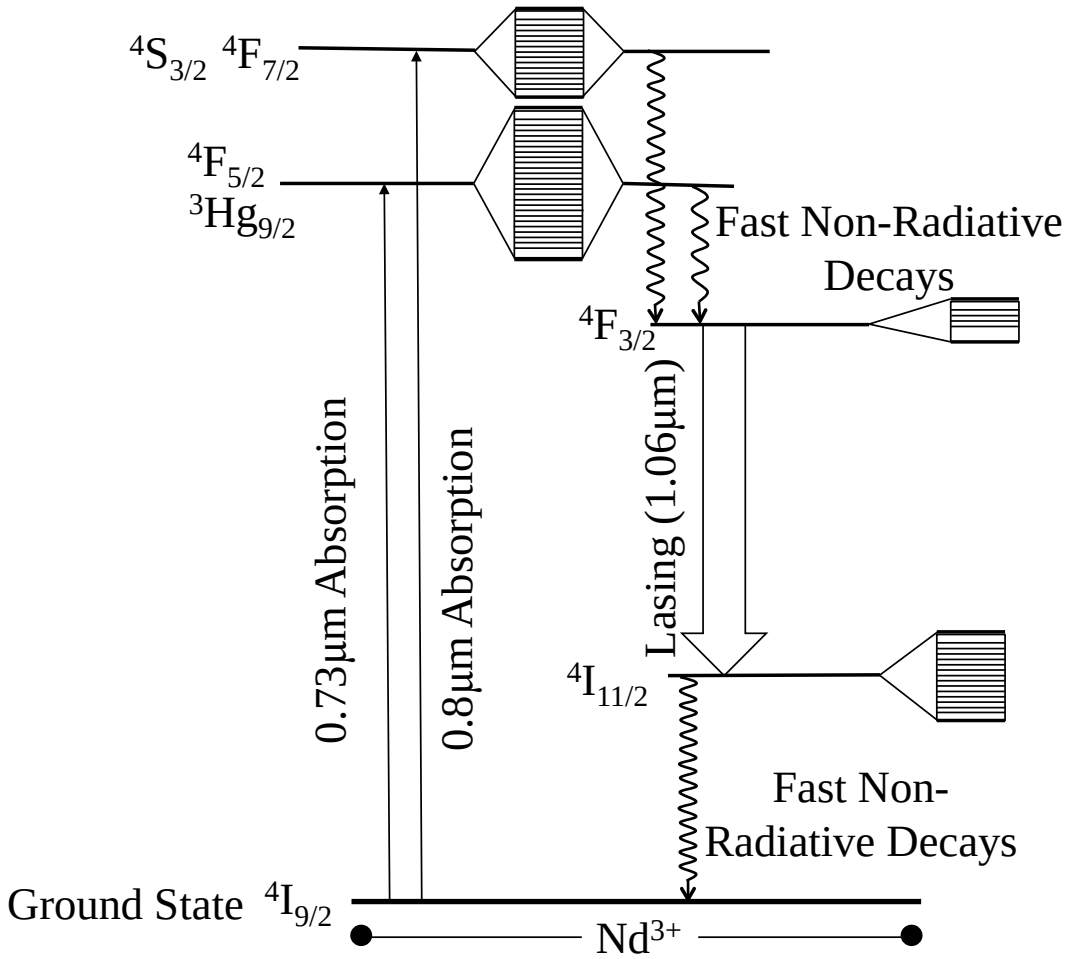

Figure 1.5 Energy diagram of four-level Nd:YAG laser system. A combination of active species Nd^{3+} and host YAG crystal generates the 1.06 μm laser radiation. Various wavelengths, 532, 355, and 266nm, are generated by using harmonic generation crystals.

respectively.

Nd:YAG lasers are widely used in various types of research including Raman spectroscopy and mass spectrometry. This work uses a Nd:YAG (266 nm) laser as an excitation source to detect numerous biological molecules including adenosine, dopamine, and various type of proteins that absorbs light in the UV wavelength range.

1.4.4 SEMICONDUCTOR LASER

The semiconductor laser is different from gas- and solid-state lasers due to the dependency of both optical and electron confinements by the multilayer structure. Figure 1.6 describes a typical semiconductor laser construction. A p-type and n-type semiconductor are constructed in parallel at a separation distance of about 1 μm to create a *p*-*n* junction. Negative and positive electrical leads are attached to *n*- and *p*-type junction, respectively, to supply certain threshold voltage to induce current. In this process, electrons are donated from the conduction band of the *n*-type material and accepted by holes in the valence band of the *p*-type semiconductor to recombine and release energy equivalent to band gap in the form of photon. The multilayer structure achieves both light amplification and population inversion differently from general light-emitting diodes. The light is confined to the active region by placing layers with lower refractive indices adjacent to the *p*-*n* junction. Both ends of a laser are polished to serve as mirrors for a cavity. The length of the laser equals to $n2/\lambda$, that is, a half-integral number of the wavelength of the light emitted.

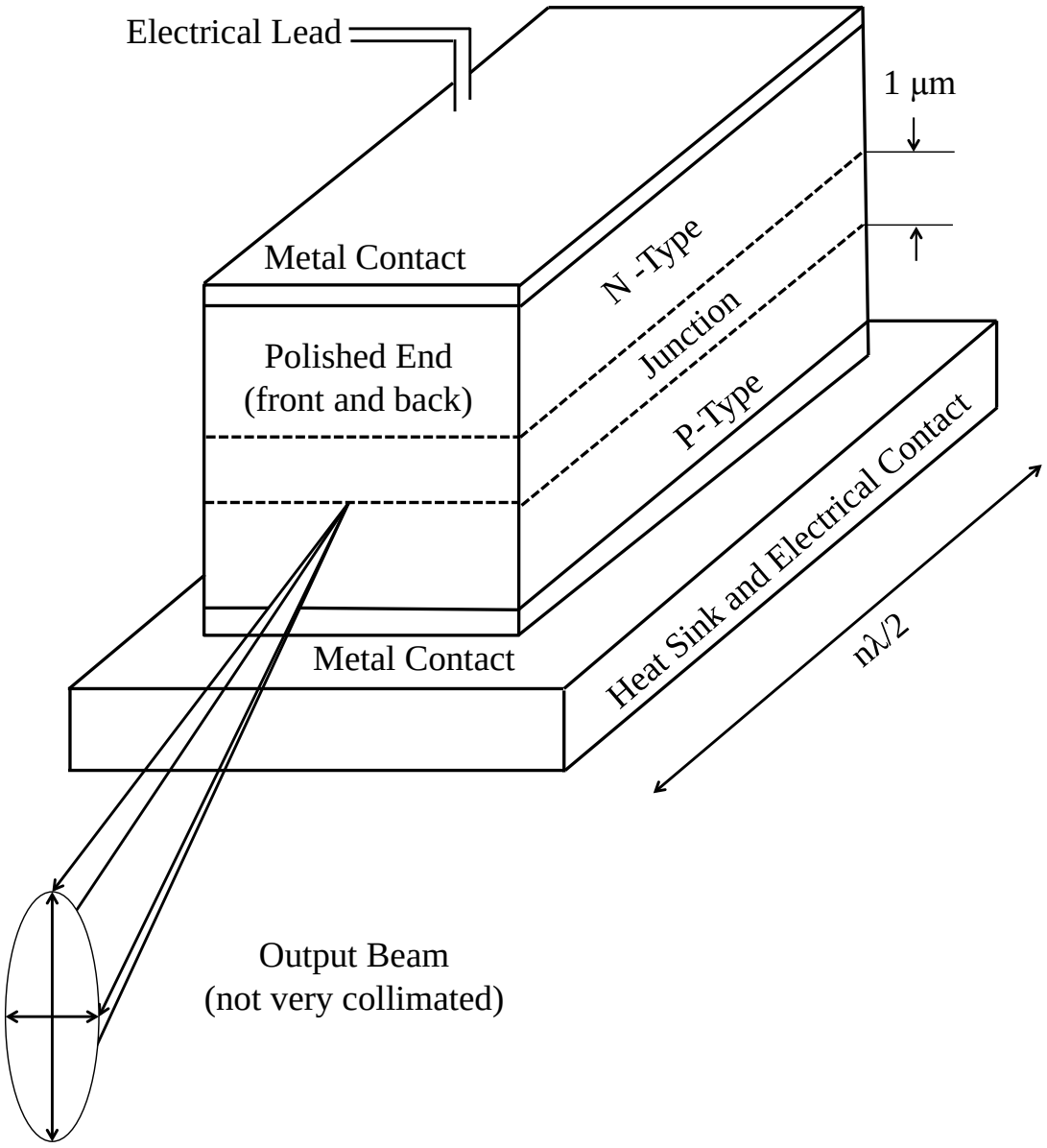

Figure 1.6 Illustrated figure of a semiconductor laser. The laser has *n*- and *p*-type materials, electrical leads, and a heat sink.

1.4.5 OPTICALLY PUMPED SEMICONDUCTOR LASER

The optically pumped semiconductor laser (OPSL) uses a diode laser to pump the gain medium such as the III-V semiconductor GaAs. The schematic diagram of an OPSL system is shown in Figure 1.7.[13] Pump absorption layers efficiently absorb pump light from the diode laser. A high-reflection (HR) mirror is used to provide optimized performance at specific wavelengths and incidence angles. Quantum wells determine the output wavelength depending on its size and stoichiometry. Emitted photons are amplified by an external mirror and HR mirror.

The OPSL has numerous advantages over gas lasers including size, efficiency, and short warm-up times. Generally, OPSLs are 150 times smaller than gas lasers and these compact laser systems are ideal for use in analytical instrumentation. Compact laser wave-mixing systems provide portability that is suitable for medical field and stand-off detection uses. The efficiency of OPSLs are 10 to 40 times higher than that of a gas laser. A gas laser often requires a special three-phase electrical power source while OPSLs can operate at normal line voltage and current. A cooling system required in a gas laser is not needed in an OPSL due to its efficiency, and OPSLs emit a laser beam instantaneously while gas lasers require some warm-up time.

1.5 Outline of dissertation

The following chapters in this dissertation demonstrate applications of DFWM-CE as a sensitive and selective laser-based spectroscopic technique to detect neurodegenerative disease related biomolecules and several other types of macromolecules. The theory behind nonlinear absorption-based laser wave mixing is

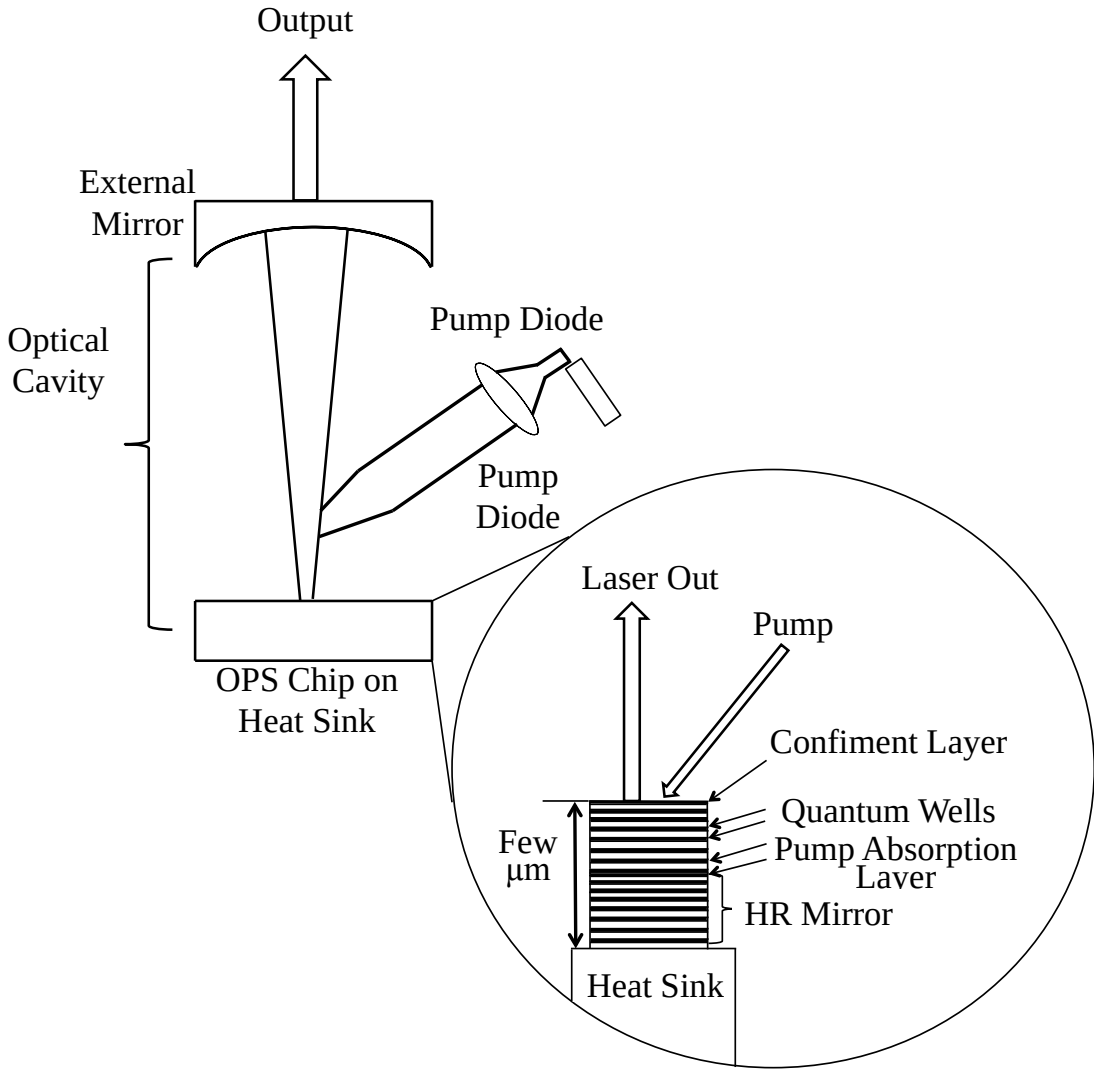

Figure 1.7 Schematic diagram of an optically pumped semiconductor laser with a close view of the chip (Reference 13).

discussed in Chapter 2, along with its properties and capabilities for ultrasensitive detection of analytes. Chapter 3 introduces the basic experimental parameters behind forward-scattering wave-mixing experiments. The basic principles of capillary electrophoresis, optimization of DFWM-CE to detect proteins at ultrasensitive levels, and the process used to separate protein analytes by molecular weight are discussed in Chapter 4. The methods and parameters discussed in this chapter are also employed to study Parkinson's disease related proteins in Chapter 5. These proteins are labeled with a chromophore and two types of fluorophores. Detection and separation of native and chromophore-labeled neurotransmitters are demonstrated in Chapter 6. Chapter 7 introduces ultrasensitive methods for peptide detection for early diagnosis of Alzheimer's disease.

1.6 References

(1) Hecht, J. *The laser guidebook*; 2nd ed.; McGraw-Hill: New York, 1992.

(2) Van Hecke, G. R.; Karukstis, K. K. *A guide to lasers in chemistry*; Jones and Bartlett: Boston, 1998.

(3) Hecht, J. *Understanding lasers : an entry-level guide*; 3rd ed.; IEEE Press ; John Wiley & Sons: Piscataway, NJ Hoboken, N.J., 2008.

(4) Gordon, J. P.; Zeiger, H. J.; Townes, C. H. *Phys Rev* **1954**, *95*, 282.

(5) Maiman, T. H. *Nature* **1960**, *187*, 493.

(6) Weiss, S. *Science* **1999**, *283*, 1676.

(7) Kneipp, K.; Wang, Y.; Kneipp, H.; Perelman, L. T.; Itzkan, I.; Dasari, R.; Feld, M. S. *Phys. Rev. Lett.* **1997**, *78*, 1667.

(8) Farrow, R. L.; Rakestraw, D. J. *Science* **1992**, *257*, 1894.

(9) Bernath, P. F. *Spectra of atoms and molecules*; Oxford University Press: New York, 1995.

(10) Andrews, D. L.; Demidov, A. A. *An introduction to laser spectroscopy*; 2nd ed.; Kluwer Academic/Plenum Publishers: New York, 2002.

(11) Andrews, D. L. *Lasers in chemistry*; 2nd ed.; Springer-Verlag: Berlin ; New York, 1990.

(12) Telle, H. H.; González Ureña, Á.; Donovan, R. J. *Laser chemistry : spectroscopy, dynamics and applications*; John Wiley & Sons: Chichester, West Sussex, England ; Hoboken, NJ, 2007.

(13) Chilla, J.; Shu, Q. Z.; Zhou, H. L.; Weiss, E.; Reed, M.; Spinelli, L. *P Soc Photo-Opt Ins* **2007**, *6451*, 45109.

CHAPTER 2
THEORY OF DEGENERATE FOUR-WAVE MIXING

2.1 Nonlinear Absorption-Based Degenerate Four-Wave Mixing

Degenerate four-wave mixing (DFWM) is an optical absorption-based technique that detects analytes at ultrasensitive concentration levels. The wave-mixing signal is created by mixing two laser beams at the same frequency in a nonlinear medium. When a target analyte absorbs the wavelength, a grating forms, and incoming photons are diffracted to yield laser-like coherent signals. Laser wave mixing provides outstanding limit-of-detection (LOD) from nanomolar to picomolar range, much better than those of conventional absorption techniques. Due to cubic dependence on laser power and quadratic dependence on concentration, the wave-mixing signal is strong enough to detect a few molecules inside the probe volume. This chapter reviews the applications of DFWM, an introduction to the wave-mixing signal generated by two types of optical geometry, and a discussion of the advantages of this detection technique.

2.2 History of Degenerate Four-Wave Mixing

Nonlinear wave mixing was originally introduced to generate a phase-conjugate mirror. Boris Zel'dovich and his colleagues first observed optical phase conjugation in 1972 by applying stimulated Brillouin scattering (SBS).[1] A pulsed ruby laser beam was aimed at a frosty glass slide to obtain a distorted beam before reaching a capillary tube of methane gas under high pressure, and an undistorted beam generated by SBS was observed when the incident beam interacted with the

methane gas (the phase-conjugation mirror). The undistorted beam traveled in the reverse direction of the incident laser beam, and the reflected beam was called a "time-reversed" replica of an incident beam with a slight frequency shift.

In 1977, Bloom and Bjorklund introduced degenerate four-wave mixing, a new type of nonlinear optical process.[2] In the same year, Ammon Yariv and David Pepper observed optical effects including amplified reflection, transmission, phase conjugation and oscillation with DFWM.[3] To prove the concept, they used four laser beams with the same frequency intersecting at a nonlinear medium (Figure 2.1). Two sets of counter propagating (I_1 and I_2, and I_3 and I_4) laser beams intersected in the nonlinear medium. Intense beams, I_1 and I_2, served as pump beams, and I_3 and I_4 served as weaker probe beams.

In 1978, Abrams and Lind demonstrated enhancement of the phase-conjugate wave by DFWM by tuning the laser frequency at a resonant electronic transition of the nonlinear medium.[4] DFWM was demonstrated as a high-resolution spectroscopic technique that has the ability to quantify analytes with minimum background noise and excellent signal-to-noise ratios.[5-9]

2.3 Ultrasensitive Detection of Chemicals by Nonlinear Wave Mixing

Nonlinear absorption-based wave-mixing technique has shown great potential for ultrasensitive detection down to zeptomole and yoctomole levels for a wide range of chemicals in gas- and liquid-phase samples.[10] The following sections discuss methods for detecting analytes using different nonlinear wave-mixing setups offering advantages including ultrasensitive detection, high selectivity, high spatial-resolution,

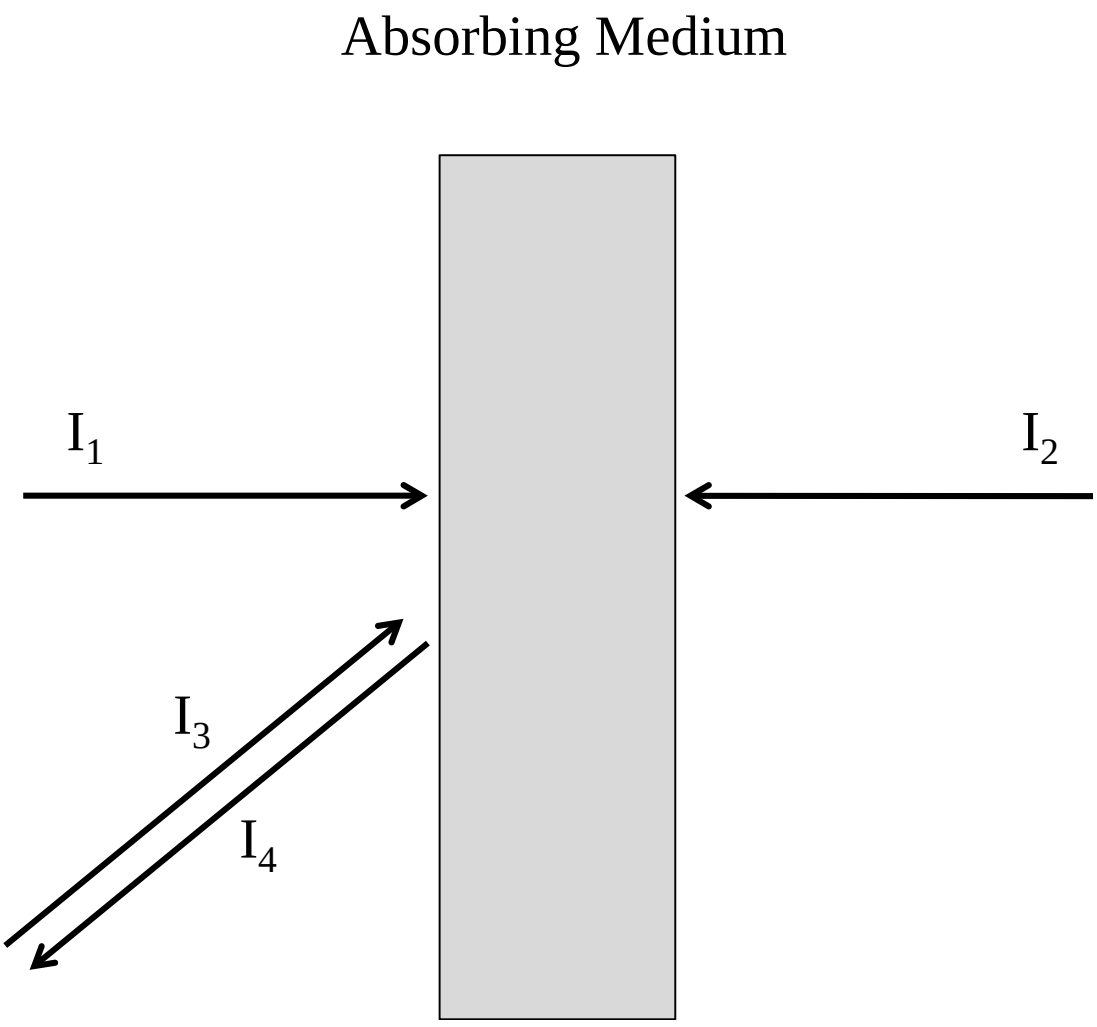

Figure 2.1 Nonlinear degenerate four-wave mixing backward-scattering optical setup with two sets of counter-propagating beams (Reference 3). and capability to interface with multiple separation methods.

and capability to interface with multiple separation methods.

2.3.1 Gas-Phase Detections by Wave Mixing

Sensitive analyses of isotopes and hyperfine structures for gas-phase samples have been obtained by laser wave mixing for Na, Ca, Ba, Li and Rb in the gas-phase.[11-15] Different types of atomizers can be used to atomize samples in a laser wave-mixing setup including graphite furnaces, flames, dc discharge plasma, and inductively coupled plasma.[16] Sub-Doppler linewidths can be obtained using a backward-scattering multi-photon wave-mixing setup, and hence, it allows high-resolution hyperfine structure analyses and isotope-ratio measurements at sub-parts-per-quadrillion concentration levels.[15]

2.3.2 Liquid-Phase Wave-Mixing Detection

Ultrasensitive detection methods for liquid-phase analytes are needed in a wide range of biomedical, environmental, and security applications. Reliable detection of trace concentration levels of biomarkers, such as amyloid-beta (Aβ) and the cancer antigen 15-3, could enable early-stage diagnoses of Alzheimer's and breast cancer. Reliable early-stage testing of HIV (human immunodeficiency virus) can be achieved by detecting trace amounts of p24 capsid proteins. Ultrasensitive detection of neurotransmitters could help us understand the mechanisms of brain chemistry and gain some new information needed to improve therapeutic treatments. Environmental contaminants that affect human health, such as malachite green and crystal violet, can be detected in trace amounts with multi-photon optical wave mixing.[17] Low-concentration detection of nitroaromatic explosives has also been accomplished using

wave mixing. DFWM can be readily interfaced to separation instruments, such as capillary electrophoresis, microchip, and high-performance liquid chromatography (HPLC), and to other analytical tools such as DNA and protein microarrays, sol-gel sensors, and enzyme-linked immunoSorbent assay (ELISA) kits.

2.4 Laser Wave-Mixing Signal

2.4.1 LASER-INDUCED DYNAMIC GRATING

The nonlinear wave-mixing signal is generated only when the following conditions are met in the absorbing medium.[18]

$$\omega_1 = \omega_2 = \omega_3 = \omega_4 \tag{2.1}$$

$$k_1 = -k_2 \tag{2.2}$$

$$k_3 = -k_4 \tag{2.3}$$

where ω_1, ω_2, ω_3 and ω_4 are frequencies of four waves and k_1, k_2, k_3 are k_4 are propagation vectors (Figure 2.2). The equations denote that both energy and momentum conservation must be satisfied to generate the wave-mixing signal.

A dynamic grating is generated when two coherent laser beams with the same wavelength intersect at a small angle to create constructive and destructive interferences. The wave-mixing signal, I, generated by the pump and probe beams, I_A and I_B, can be described by Equation 2.4.[19]

$$I = I_0\left[1+m\cdot\cos\left(\frac{2\pi x}{\Lambda}\right)\right] \tag{2.4}$$

where x is the spatial coordinate, and I_0 is the sum of I_A and I_B. The intensity of the pump beam and probe beam contribute to m, as described by Equation 2.5.

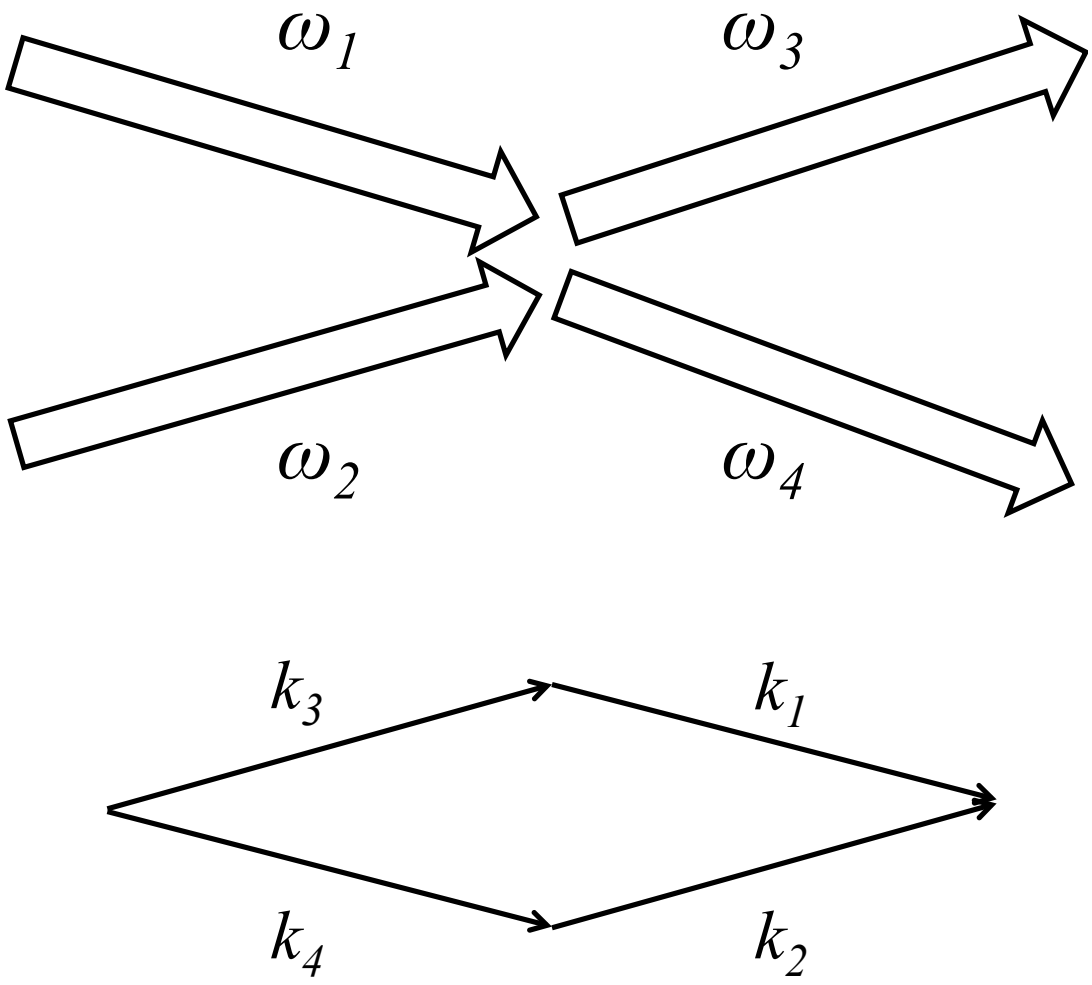

Figure 2.2 Frequencies (ω_1-ω_4) and propagation vectors (k_1-k_4) at absorbing analyte medium. Propagation vectors show phase-matching condition.

$$m=2\frac{\sqrt{I_A I_B}}{I_0} \tag{2.5}$$

The spatial grating period is denoted by Λ (Equation 2.6).

$$\Lambda = \frac{\lambda}{2\sin(\theta/2)} \tag{2.6}$$

where λ is wavelength of the laser source and θ is the angle between two incident laser beams when they intersect at the nonlinear medium (Figure 2.3). The probe volume is defined by the beam overlap volume created by the two laser beams.

2.4.2 Nonlinear Wave-Mixing Gratings

Gas- and liquid-phase analytes rely on different mechanisms in generating the nonlinear wave-mixing signal. After an interference pattern is formed by the two input beams crossing inside an absorbing medium, a population or a thermal grating is generated depending on the sample type. The population grating is responsible for signal generation when a gas-phase analyte absorbs the input beams. Thermal gratings play a significant role in liquid-phase DFWM.

2.4.3 Population Gratings for Gas-Phase Absorbing Analyte

A population grating is formed when a gas-phase analyte absorbs the input beams. Spatial separation of excited- and ground-state populations occurs when the ground state molecules or atoms absorb photons to reach the excited state.[20] A portion of the molecules promoted to excited states exist around the area of constructive interference pattern, while species around the deconstructive area remain in the ground state. The population grating diffracts incoming photons at certain angles to

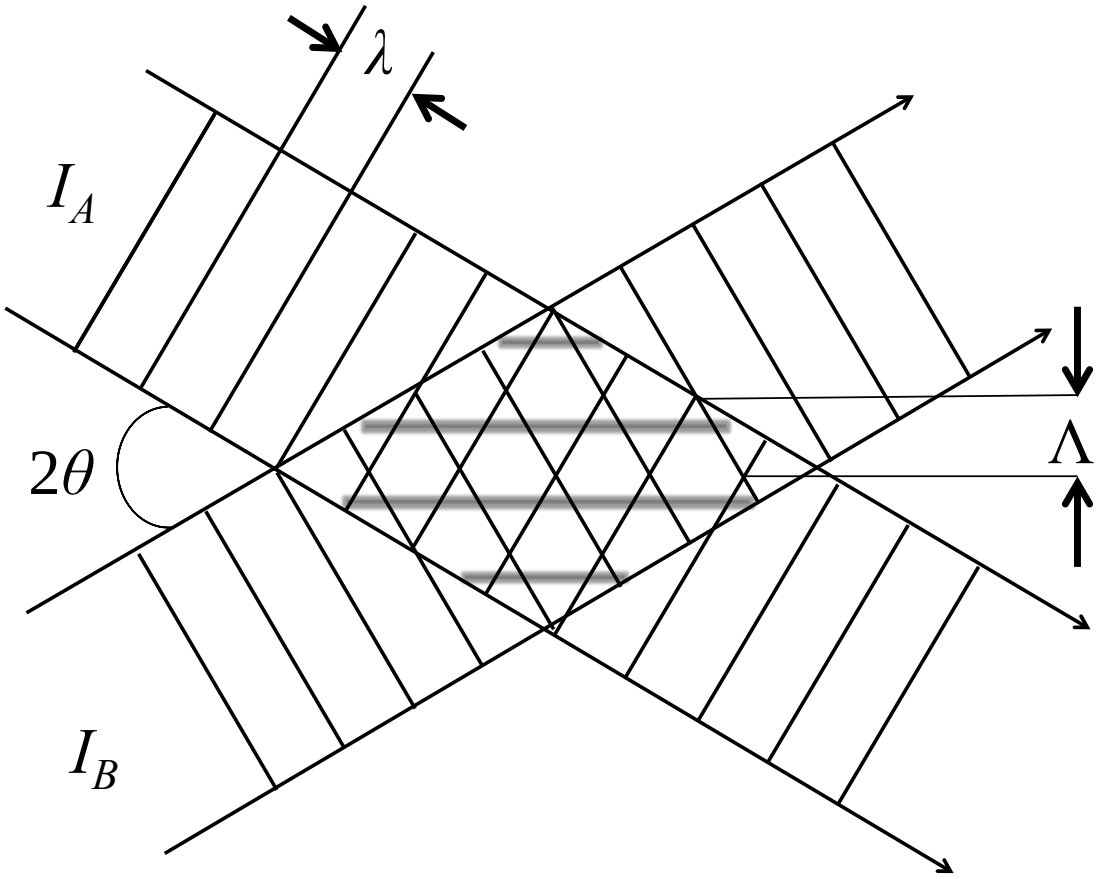

Figure 2.3 Interference grating formed by two input beams at the same wavelength (λ) crossed at a small angle θ. This pattern is produced by constructive and destructive interferences of two laser beams. Λ is the spatial grating period that depends on the wavelength and angle between the two beams.

create the wave-mixing signals.

The diffracted wave-mixing signal beam intensity, I_{signal}, depends on the intensity of the probe and pump beams, I_{probe} and I_{pump}, the line center absorption coefficient of the analyte (α_0), the length of the induced grating (L), and the intensity required to achieve an equal population of molecules or atoms in the excited and ground states, I_{sat}, as shown in Equation 2.7.[21]

$$I_{signal} \sim I_{probe}\pi\alpha^2 L^2 \left[\frac{I_{pump}}{I_{sat}}\right]^2 \tag{2.7}$$

Cubic dependence on input laser power, $I_{probe}\, I_{pump}^{\,2}$, and quadratic dependence on analyte concentration, are inherent properties of the wave-mixing signal. The relation of the absorption coefficient and analyte concentration is shown by the Beer-Lambert law (Equation 2.8)

$$A=\varepsilon lc \tag{2.8}$$

where A is absorbance of the analyte, ε is molar extinction coefficient of the molecule or atom, and l is the path length of the cell.

2.4.4 Thermal Gratings for Liquid-Phase Absorbing Analytes

In liquid-phase analytes, thermal gratings diffract incoming photons to generate the wave-mixing signal. The molecules absorb photons around the constructive interference regions created by the input laser beams and get excited to higher energy levels. Energy transferred to the surrounding medium through non-radiative relaxation yields changes in refractive index. The following equation describes the wave-mixing signal from a liquid-phase analyte.

$$I_S = C\left(\frac{b}{8\pi}\right)^2 I_1^2 I_2 \frac{\lambda}{\sin^4(\theta/2)} \left(\frac{dn}{dT}\right)^2 \frac{\alpha^2}{\kappa^2} \quad (2.9)$$

where C is a constant. The wave-mixing signal, I_s, depends on the optical path length (b), the two incident beams represented by I_1 and I_2, the wavelength of the input beams, λ, and the angle between the two incident laser beams, θ. The change in the refractive index of the medium with respect to the temperature, dn/dT, thermal conductivity of the medium, κ, and optical absorptivity of the analyte, α, also contribute to the wave-mixing signal. This equation shows that the wave-mixing signal has a cubic dependence on laser power and a quadratic dependence on concentration.

2.5 Laser Wave Mixing Optical Configurations

The wave-mixing signals can be generated by using different optical configurations. Commonly used DFWM optical configurations include three-beam backward-scattering DFWM and two-beam forward-scattering DFWM. The two waves propagate in the backwards direction for the former, and all four waves propagate in the forward direction for the latter.

2.5.1 THREE-BEAM BACKWARD-SCATTERING DFWM

The three-beam backward-scattering optical configuration consists of three input laser beams to form the gratings and the resulting signal beam. This optical geometry is commonly used for gas-phase samples[21] in order to achieve sub-Doppler spectral resolution for isotope analyses.

In a typical backward-scattering DFWM setup, two counter propagating input

beams, I_1 and I_2, at the same frequency, enter the nonlinear medium and the third input beam, I_3, with the same frequency, enters at a small angle, θ. Incoming photons at the intersection of three input beams are diffracted back exactly along the same path as the probe beam, I_3, to generate the backward DFWM signal, I_4. The signal beams are created when the phase-matching requirement is met. The following equation describes the wave-vector mismatch.[22]

$$\Delta\vec{k} = \vec{k_1} + \vec{k_2} - \vec{k_3} - \vec{k_4} \tag{2.10}$$

where $\vec{k_1}$, $\vec{k_2}$, $\vec{k_3}$, $\vec{k_4}$ are the vectors of the forward, backward, probe and the signal beams. The wave-mixing signal is maximized in an optimal condition where $\Delta\vec{k} = 0$.

2.5.2 TWO-BEAM FORWARD-SCATTERING DFWM

A forward-scattering wave-mixing configuration is commonly used for liquid-phase studies and it is much simpler than the backward DFWM optical arrangement. The work described in this dissertation uses the forward-scattering DFWM configuration. It requires only two input laser beams instead of three and these two incoming beams, I_1 and I_2, intersect in the absorbing medium at a small angle θ, and the resulting gratings diffracts photons to produce the signal beam, $I_{signal\ 1}$. To yield $I_{signal\ 1}$, I_1 and I_2 function as pump beams and I_1 also works as a probe beam. The process of generating $I_{signal\ 2}$ works similarly, but I_2 serves as both pump and probe beams.

Conservation of energy and momentum must be achieved to generate the degenerate four-wave mixing signal. Hence, following equation must be satisfied.

$$\omega_{signal\ 1} = \omega_{pump\ 1} + \omega_{probe\ 1} - \omega_{pump\ 2} \tag{2.11}$$

Frequencies of signal$_1$, pump$_1$, probe$_1$, and pump$_2$, are denoted as $\omega_{signal\ 1}$, $\omega_{pump\ 1}$, $\omega_{probe\ 1}$, and $\omega_{pump\ 2}$. Since this is "degenerate" four-wave mixing, all the incident beams have the same frequency ($\omega_{signal\ 1} = \omega_{pump\ 1} = \omega_{probe\ 1} = \omega_{pump\ 2}$). In addition, conservation of momentum is achieved when Equation 2.12 is satisfied.

$$k_{signal\ 1} = k_{pump\ 1} + k_{probe\ 1} - k_{pump\ 2} \tag{2.12}$$

Propagation vectors of signal$_1$, pump$_1$, probe$_1$, and pump$_2$, are denoted as $k_{signal\ 1}$, $k_{pump\ 1}$, $k_{probe\ 1}$, and $k_{pump\ 2}$ showing directions of the photons. The vectors shown in Figure 2.4 indicate phase-matching conditions. A minimally-tolerated mismatch denoted by Δk is observed due to imperfect parallel beams.[23]

2.6 Amplitude and Phase Gratings

In the case of liquid-phase analytes, variance in the refractive index and extinction coefficient of the analyte matrix affect the wave-mixing signal. Hence, induced wave-mixing gratings alter both the phase and the amplitude of the probe beam.

Change in amplitude, denoted by $\Delta\alpha$, of a wave is obtained when the degree of light absorbance in one part of the grating is different from that of another part. Attenuation of the amplitude of the wave in the pattern of grating is observed when the wave with uniform amplitude and phase passes through multiple modulated slits. The amplitude grating is formed by general optical saturation and media density changes.

The change in refractive index of a surrounding solvent is responsible for the formation of phase gratings. The grating changes the speed of photons depending on

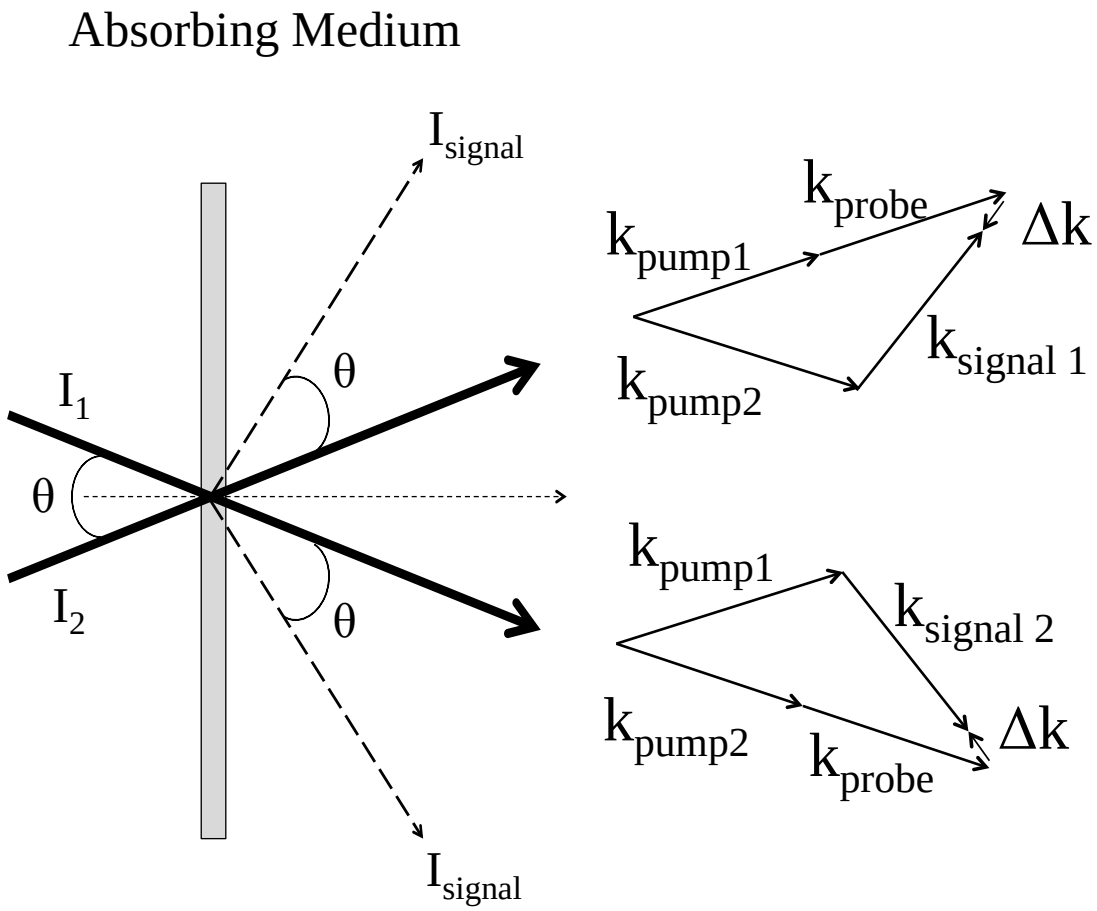

Figure 2.4 Two-beam forward-scattering DFWM optical geometry and propagation vectors. I_1 and I_2 are pump and probe beams. Two incident beams intersect at angle θ to create laser-like coherent signal beams, $I_{signal\ 1}$ and $I_{signal\ 2}$.

the refractive index. Non-radiative thermal relaxation causes the change in density within the medium that also affects the refractive index and the local concentration.

The combined effect of the amplitude and phase gratings must be considered. The probe beam involved in the DFWM signal is diffracted at an angle according to the following equation:

$$\theta_{signal} = \sin^{-1}\left(\frac{\lambda}{2\Lambda}\right) \tag{2.13}$$

where θ is the Bragg or diffraction angle, λ is the wavelength of the laser beam, and Λ is the grating period.[1] The following equation expresses the diffraction efficiency of weak absorption, weak diffraction, and thick grating at the Bragg angle.

$$\eta = \left(\frac{\pi d \Delta n}{\lambda}\right)^2 + \left(\frac{d\Delta\alpha}{4}\right)^2 \tag{2.14}$$

The diffraction efficiency has quadratic dependence on thickness of the grating, *d*, the peak-to-null difference of the refractive index, Δn, the reciprocal of the laser wavelength, $1/\lambda$, and the peak-to-null difference of the extinction coefficient, $\Delta\alpha$.

2.7 Advantages of Nonlinear Absorption-Based Wave Mixing

Nonlinear absorption-based wave mixing offers inherent advantages over other optical detection methods including ultrasensitive detection limits and compact portable detector designs. One of the most unique aspects of the DFWM signal is its quadratic dependence on analyte concentration and extinction coefficient, whereas laser induced fluorescence (LIF) and conventional absorption techniques exhibit linear dependencies. Since DFWM is an absorption-based technique, the target molecule does not have to be a fluorophore or tagged by a fluorophore label. A wide

range of biomolecules, including neurotransmitters and proteins, absorb ultraviolet wavelengths, and hence, they can be detected in their native form. The analyte absorption can be easily enhanced by a simple reaction or a conjugation of a target molecule with a dye or a reagent. Unlike fluorescence methods, wave mixing allows the use of both fluorophores and chromophores as labels.

The wave-mixing signal has a cubic dependence on laser power, and hence, one can efficiently use low laser power levels (mW). This is important because the use of high laser power levels could damage samples inside the probe volume, especially when capillaries are used as the sample cell.

The laser wave-mixing signal exhibits some unique characteristics. The signal is a coherent laser-like beam that can be separated easily from background noise. The wave-mixing signal is diffracted at a set angle depending on the angle between two input beams (Figure 2.5), and hence, one can pre-align the detector to collect the signal beam conveniently with virtually 100% optical collection efficiency.

Nonlinear absorption-based wave mixing, with all of its advantages, is capable of ultrasensitive detection for a variety of important analytes. This work further proves that DFWM is capable of ultrasensitive detection for both native and labeled molecules. Interfacing the wave-mixing optical setup to capillary electrophoresis allows one to quickly separate these analytes and detect them at trace concentration levels.

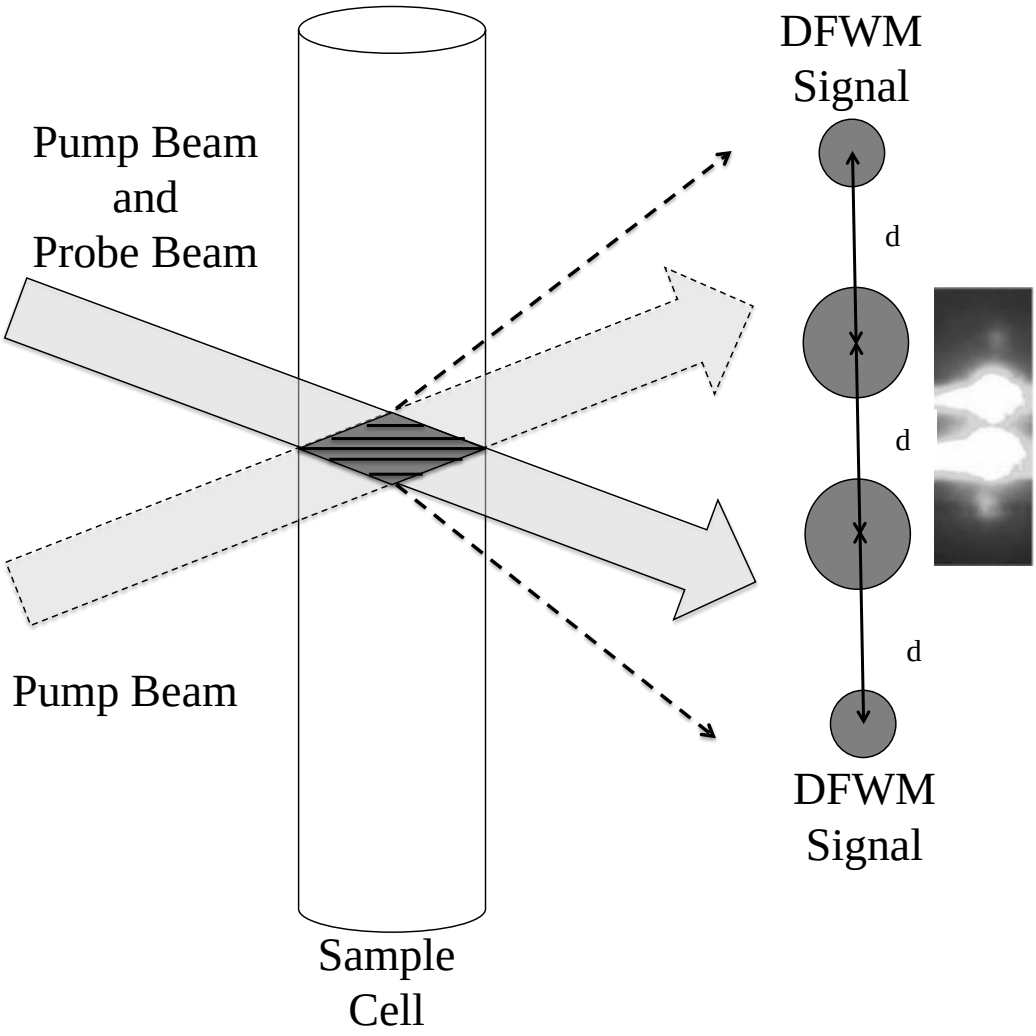

Figure 2.5 DFWM signals and real signal images. Center-to-center distances between neighboring beams are all equal.

2.8 References

(1) Atherton, A. A. Ph.D, Thesis, Univeristy of San Diego, California, **2006**.

(2) Bloom, D. M.; Bjorklund, G. C. *Appl Phys Lett* **1977**, *31*, 592.

(3) Yariv, A.; Pepper, D. M. *Opt Lett* **1977**, *1*, 16.

(4) Abrams, R. L.; Lind, R. C. *Opt Lett* **1978**, *2*, 94.

(5) Pender, J.; Hesselink, L. *Opt Lett* **1985**, *10*, 264.

(6) Ewart, P.; Oleary, S. V. *Opt Lett* **1986**, *11*, 279.

(7) Ewart, P.; Snowdon, P.; Magnusson, I. *Opt Lett* **1989**, *14*, 563.

(8) Dreier, T.; Rakestraw, D. J. *Opt Lett* **1990**, *15*, 72.

(9) Rakestraw, D. J.; Farrow, R. L.; Dreier, T. *Opt Lett* **1990**, *15*, 709.

(10) Lopez, M. M.; Atherton, A. A.; Tong, W. G. *Anal Biochem* **2010**, *399*, 147.

(11) Andrews, J. M.; Tong, W. G. *Spectrochim Acta B* **1989**, *44*, 101.

(12) Wu, Z. Q.; Tong, W. G. *Spectrochim Acta B* **1992**, *47*, 449.

(13) Andrews, J. M.; Weed, K. M.; Tong, W. G. *Appl Spectrosc* **1991**, *45*, 697.

(14) Wu, Z. Q.; Tong, W. G. *Anal Chem* **1991**, *63*, 899.

(15) Mickadeit, F. K.; Berniolles, S.; Kemp, H. R.; Tong, W. G. *Anal Chem* **2004**, *76*, 1788.

(16) Lyons, W.; Schafer, J.; Briggs, R.; Gregerson, M.; Tong, W. G. 2005; Vol. 5971, p 597109.

(17) Hetu, M.; Iwabuchi, M.; Maxwell, E.; Wu, H.; Ramos, S.; Tong, W. G. 2014; Vol. 9193, p 91930T.

(18) Lopez, M. M. Ph. D., University of California, San Diego, and San Diego State University, 2004.

(19) Simoni, F.; Cipparrone, G.; Duca, D.; Khoo, I. C. *Opt Lett* **1991**, *16*, 360.

(20) Danehy, P. M.; Paul, P. H.; Farrow, R. L. *J Opt Soc Am B* **1995**, *12*, 1564.

(21) Knittle, J. E. Ph.D, University of California, San Diego, and San Diego State University, **2004**.

(22) Lyons, W. J. Ph.D., University of California, San Diego, and San Diego State University, **2009**.

(23) Khoo, I. C.; Normandin, R.; Liu, T. H.; Michael, R. R.; Lindquist, R. G. *Phys Rev B* **1989**, *40*, 7759.

CHAPTER 3
EXPERIMENTAL

3.1 Degenerate Four-Wave Mixing Setup

A typical forward-scattering degenerate four-wave mixing (DFWM) optical setup consists of optical components and electronic instruments described in Figure 3.1. The output of a laser with the appropriate wavelength is split into two input beams of low and high intensity (R:T of 30:70). The transmitted beam serves as both the pump and the probe beam, while the reflected beam serves only as the pump beam. These two parallel input beams travel equal distances before reaching the focusing lens (L1). They are focused and mixed by the biconvex lens (focal length 100 mm) at the sample cell. Two coherent laser-like wave-mixing signals are generated when the analyte absorbs photons from the input beams. The signal beam is collected with 100% collection efficiency after pinholes and beam blockers filter out the background noise. The signal is reflected by a mirror (M4), focused by a 150 mm focal length biconvex lens (L2) on a photodetector, and digitized and monitored by a computer. An optical chopper modulates the frequency of the reflected beam at 200 Hz to maximize S/N. The chopper, photodetector, and computer are interfaced to a lock-in amplifier. The forward-scattering DFWM setup is compact since compact diode lasers and small optical components are used.

3.2 Laser Excitation Source

A variety of lasers can be used in DFWM including continuous-wave argon ion lasers, pulsed excimer-pumped dye lasers, quantum cascade lasers, and diode

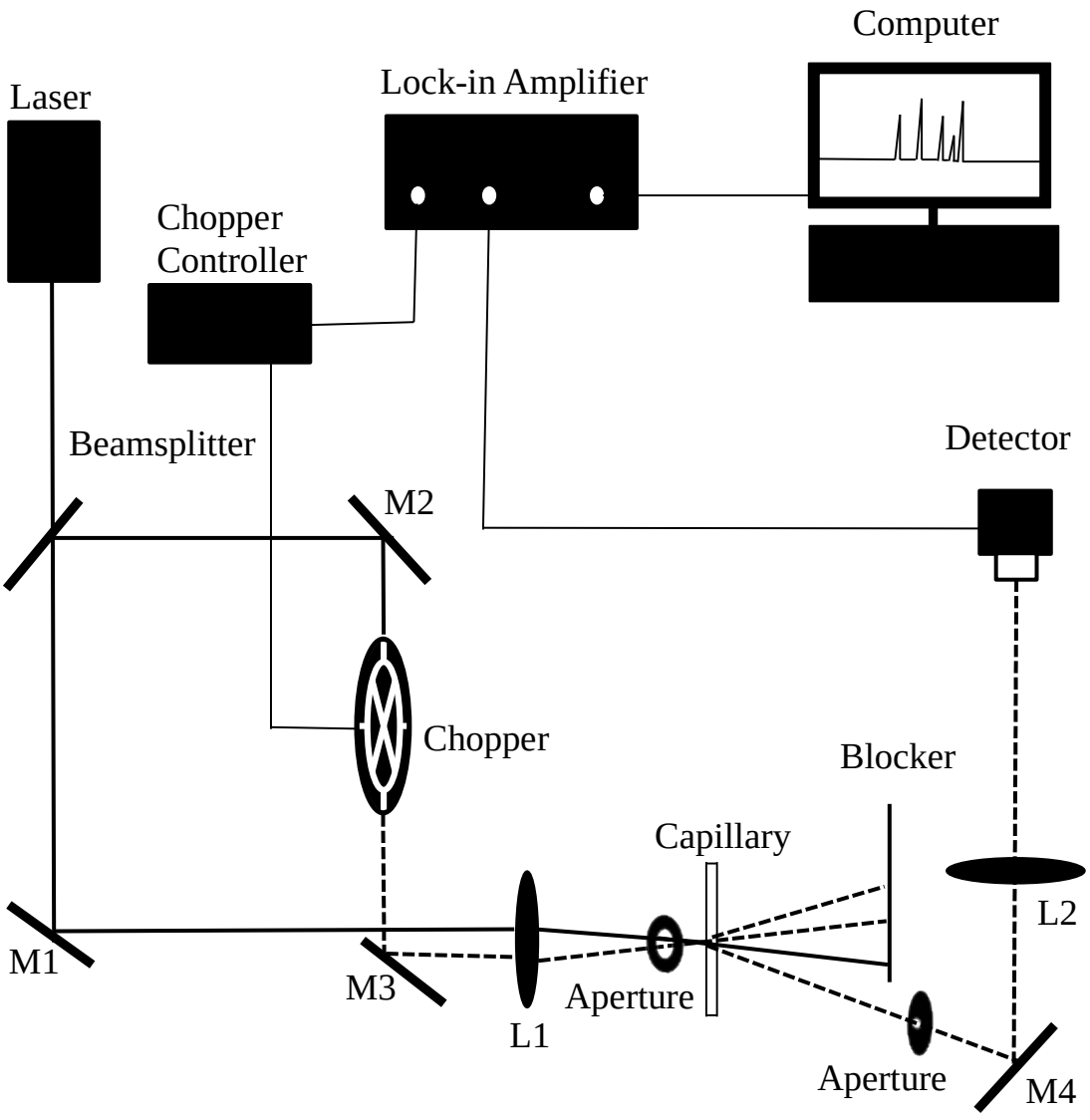

Figure 3.1 Compact forward-scattering nonlinear degenerate four-wave mixing optical setup.

lasers. Table 3.1 summarizes different lasers used in this dissertation along with their wavelengths, beam diameter, calculated beam waist, and probe volumes.

3.2.1 Ultraviolet Laser

A 266 nm Q-switched pulsed laser (CNI, Changchun, China) is used for native label-free detection of biomolecules, neurotransmitters, proteins, and peptides, which possess aromatic or conjugated systems. The laser operates at a 7 kHz repetition rate at 20 mW at 266 nm with near TEM_{00} mode structure. The Q-switched pulsed laser is compact and ready to operate relatively quickly after power stabilization.

3.2.2 Blue Diode Laser

The solid-state diode lasers at 447 nm and 473 nm (CNI, Changchun, China) emit blue continuous-wave radiation at 20 mW and 50 mW, respectively. The beams produced by these lasers feature near TEM_{00} laser modes. These lasers are used in DFWM for ultrasensitive detection of both small biomolecules and larger macromolecules since a wide range of labels, such as chromophores and fluorophores, absorb light in the blue wavelength range. Diode lasers are suitable for field applications since they are durable, cost efficient, and compact without the need for a massive cooling system. These diode lasers are used in Chapters 4, 5 and 6.

3.2.3 Optically Pumped Semiconductor Laser

Another visible excitation source is an optically pumped semiconductor laser (OPSL) emitting a 488 nm (blue) laser beam (Coherent, Santa Clara, CA, Sapphire CDRH LP). It is a reliable alternative to the argon-ion laser and much more compact

Table 3.1 Laser sources used in this dissertation for ultrasensitive detection of analytes.

Laser	Wavelength	Beam Diameter	Beam Waist	Power	Probe Volume	Chapter
266 nm Q-Switched Pulsed Laser	266 nm	1.10 mm	30.8μm	20 mW	56 pL	5, 6
447 nm Diode Laser	447 nm	4.00 mm	14.2 μm	25 mW	11.9 pL	6
473 nm Diode Laser	473 nm	1.20 mm	31.6 μm	50 mW	58 pL	4, 5
488 nm Sapphire CDRH LP	488 nm	1.70 mm	36.5 μm	Tunable	78 pL	4, 5, 6, 7

and portable. It weighs just 1.85 kg, while the argon-ion laser weighs about 150 kg. The heat sink in the OPSL is very efficient and eliminates the need for a water-cooling system. This 488 nm laser is used in the studies described in Chapters 4-7.

3.3 Sample Cells

Various types of sample cells can be readily interfaced to the DFWM setup. Fused silica capillary tubes, glass and Quartz sandwich liquid cells, microarrays and microchips can be used to hold samples.

3.3.1 Microfluidic Capillary for Continuous-Flow and Capillary Electrophoresis Detection Modes

In Chapters 4, 5, 6 and 7, fused silica capillary fibers are used as a sample cell for both continuous-flow and capillary electrophoresis (CE) detection modes. The fused silica (75 μm i.d., 360 μm o.d., Molex, Lisle, IL) is coated with polyimide to prevent it from breaking easily. A small portion of this capillary coating is removed by using a butane torch, creating a clear window for the input laser beams. The capillary is mounted on an aluminum block (Figure 3.2), and electrical tape is placed between the aluminum plates and the capillary to avoid electrical arcing during capillary electrophoresis runs. The aluminum block is mounted on a XYZ-translational stage to allow 3D adjustments in the setup. The X-axis and the Y-axis adjustments allow positioning of the capillary at the probe volume created by the two input laser beams. The Y-axis adjustment is also used to find an optimal position on the capillary to minimize scattering off the polyimide residue. Depending on the detection mode, the capillary is connected either to a syringe pump, peristaltic pump, or a CE power supply to move the analytes across the capillary.

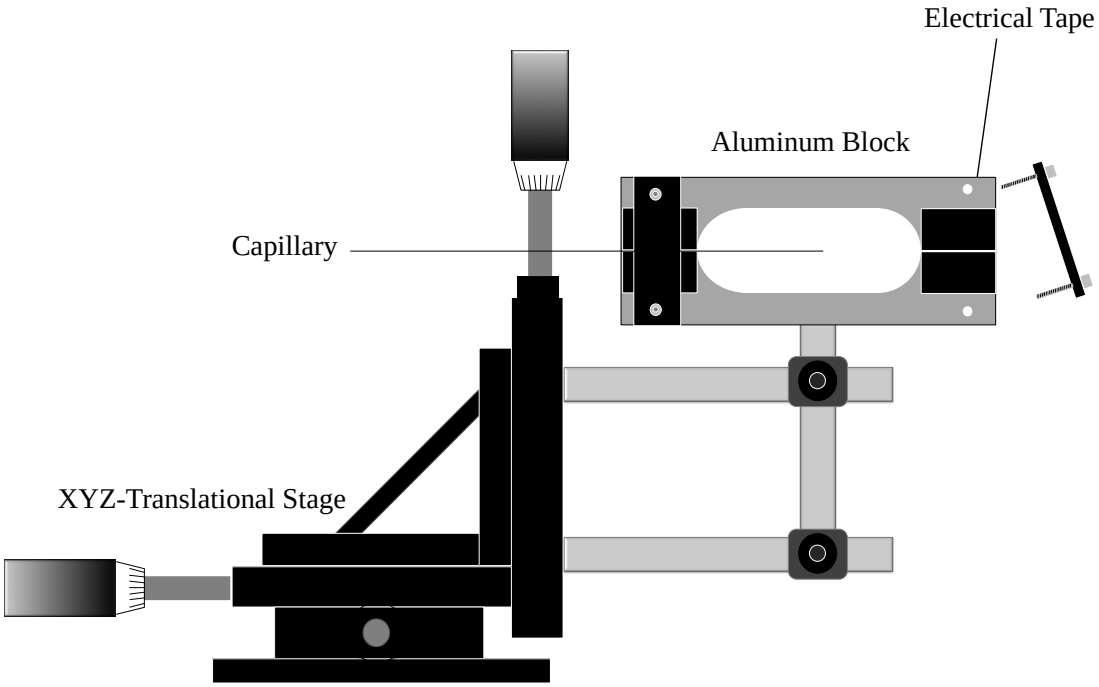

Figure 3.2 The capillary cell is mounted on an aluminum block that can be adjusted by the XYZ-translational stage.

3.3.2 SANDWICH CELL

A sandwich cell is typically used to hold liquid thin-film samples.[1] Two Quartz plates can hold a micrometer-thin sample as shown in Figure 3.3. A microliter volume of a sample can be deposited precisely with a micropipette. The thickness of the sample can be adjusted by adjusting the gap between the Quartz plates. After the sample is deposited, the sandwich cell is mounted on the XYZ-translational stage as described in Section 3.3.1.

3.4 Optical Components Used in a DFWM Setup

Laser wave mixing is a relatively simple nonlinear optical method that requires fewer optical components as compared to other multi-photon spectroscopic techniques. The optics used in this setup are mounted on either a magnetic mount or a universal post holder (Thorlabs, Newton, NJ). Some of the optical components are illustrated in Figure 3.4.

A typical visible or ultraviolet laser-based forward-scattering wave-mixing setup requires four mirrors (Thorlabs, Newton, NJ). The mirror coating is chosen for the excitation wavelength needed for the analyte. For visible lasers, SiO_2 coated aluminum mirrors are used since they offer an average reflectance of 90% from 450 nm to 2 μm. UV-enhanced aluminum mirrors offer 90% average reflectance from 250 nm to 600 nm (Newport, Irvine, CA). A beam splitter split the original laser beam into two input beams with a ratio of 30:70 (R:T). Beam blockers and pinholes are used to filter the signal and block background noise (Figure 3.4). An optical iris is placed in front of the sample cell to prevent random or reflected laser beams from

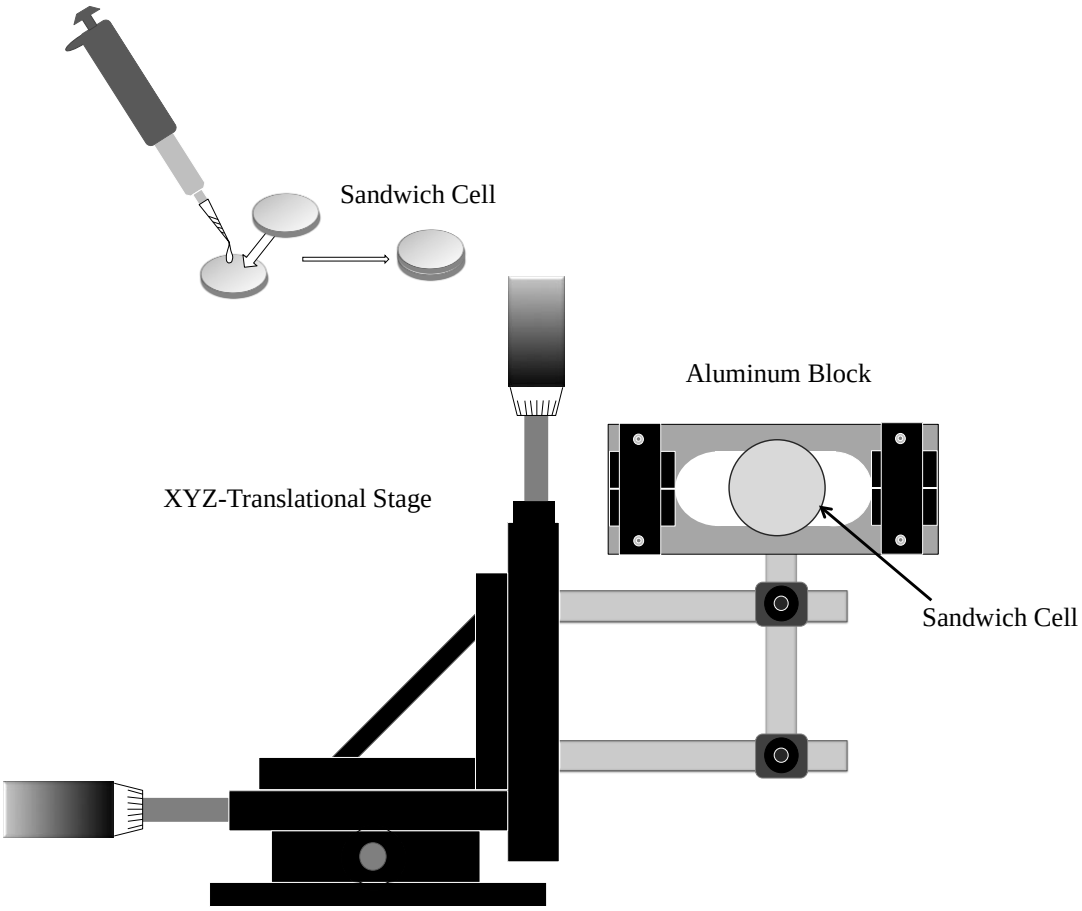

Figure 3.3 The Quartz plate sandwich cell mounted on a XYZ-translational stage. A thin-film liquid sample can be deposited using a micropipette.

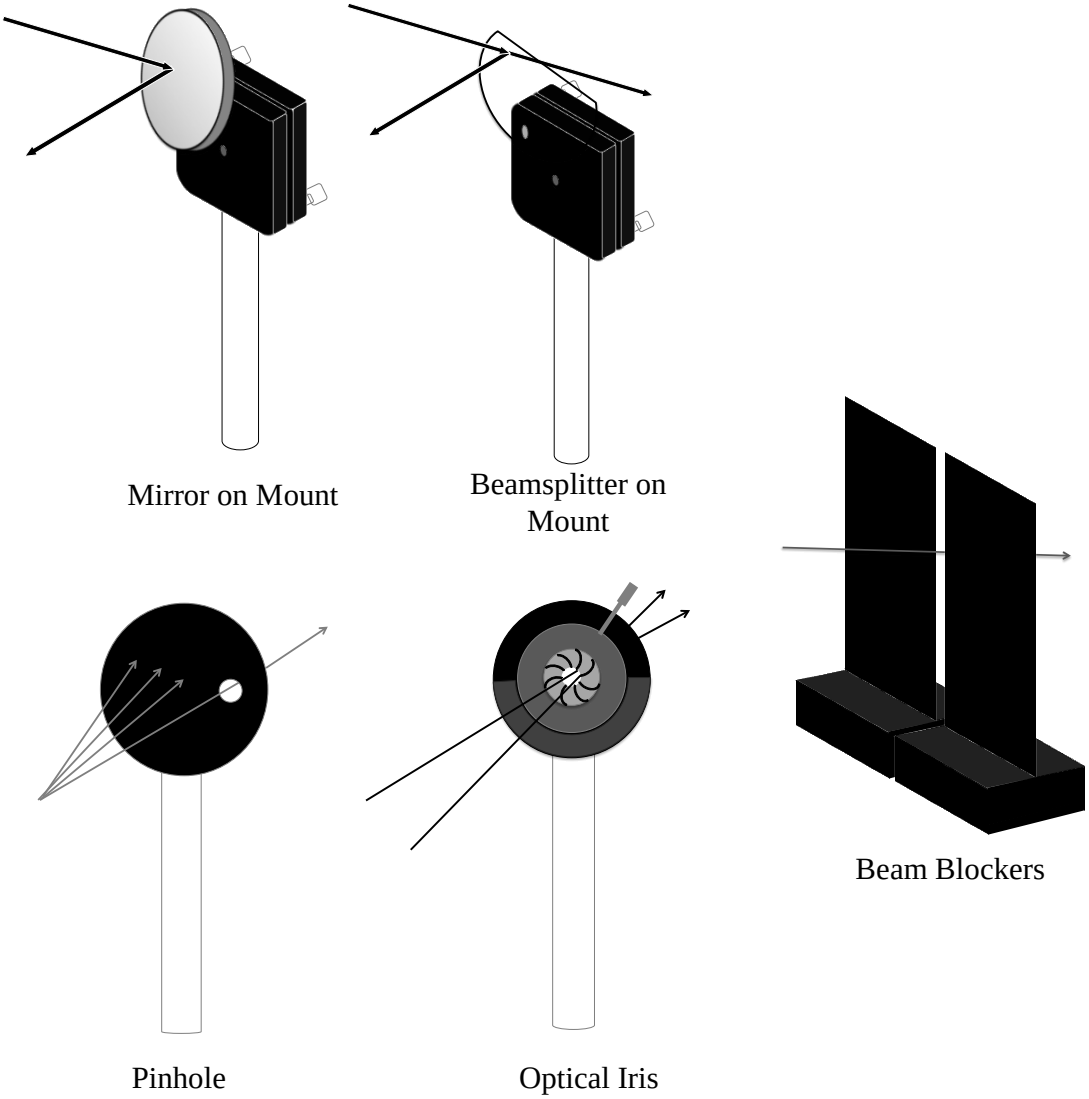

Figure 3.4 Basic optical components used in a forward-scattering DFWM setup. Mirrors and a beamsplitter are used to direct the laser beam as desired. Beam blockers, pinholes and an optical iris are used to filter the signal beam and block background noise.

entering the cell.

3.5 Electronic Instruments for Nonlinear Absorption-Based Spectroscopy

A photodetector (Thorlabs, Newton, NJ, PDA25K, 150 nm-550 nm) is interfaced to a lock-in amplifier (Stanford Research Systems, Sunnyvale, CA, SR810 DSP) and used to collect the DFWM signal. An optical chopper (Stanford Research Systems, Sunnyvale, CA, SR540,) modulates the frequency of the weaker input laser beam at 200 Hz.

3.6 Capillary Electrophoresis

Capillary electrophoresis is a powerful separation technique for small molecules, peptides and proteins that can be readily interfaced to the DFWM optical setup. Chemical matrices used for chemical separation are optimized depending on the analytes and the mode of separation.

In an electrophoresis run, the charged analytes migrate at different rates in a conductive liquid medium under the influence of an electric field. The migration time and direction depend on the charge and the size of the analyte. Further CE theories are discussed in Chapter 4.

3.7 Reference

(1) Hetu, M.; Iwabuchi, M., *et al* 2014; Vol. 9193, p 91930T.

CHAPTER 4
ULTRASENSITIVE DETECTION AND MOLECULAR WEIGHT-BASED SEPARATION OF PROTEINS USING A MULTI-PHOTON NONLINEAR ABSORPTION-BASED METHOD

4.1 Abstract

Degenerate four-wave mixing interfaced with capillary electrophoresis (DFWM-CE) offers enhanced sensitivity and selectivity levels that are suitable for biomarker studies. This multi-photon nonlinear absorption-based spectroscopic method is an effective technique for monitoring small changes in analyte concentration since the wave-mixing signal exhibits a quadratic dependence on analyte concentration. The laser wave-mixing detection limit exceeds those of conventional absorption techniques by orders of magnitude. The laser wave-mixing signal is a coherent laser-like beam that can be collected with virtually 100% collection efficiency with low optical background noise. Our wave-mixing capillary electrophoresis system offers fast analysis while conventional protein separation techniques, such as sodium dodecyl sulfate-polyacrylamide gel electrophoresis (SDS-PAGE), can take a full day to analyze. Capillary zone electrophoresis separates molecules by charge-to-mass ratio and is ideal for the ultrasensitive detection of chemical analytes. In a typical wave-mixing setup, two laser beams are focused and mixed inside a capillary where the analytes are separated and detected. The small probe volume, where the two input beams intersect, ranges from nanoliter to picoliter, and hence, it yields excellent zeptomole-level detection sensitivity.

4.2 Introduction

4.2.1 Application of DFWM-CE for Protein Analysis

Ultrasensitive detection of analytes can be achieved by a degenerate four-wave mixing (DFWM) detector interfaced to a capillary electrophoresis (CE) separation system. DFWM provides molecular specificity by tuning the wavelength of an excitation laser source to the analyte absorption peak. The specificity of analyte detection can be further enhanced by coupling wave mixing to a CE system to distinguish compounds that absorbs at similar absorption wavelengths. Capillary electrophoresis is a well-established separation technique that has been used to detect important analytes in the biomedical field.[1,2] Analytes with a wide range of molecular weights (e.g. small molecules, peptides and proteins) can be detected by DFWM-CE while requiring minimal sample preparation and small sample volumes to obtain reliable data. Depending on the purpose of analysis and the nature of various analytes, different modes of CE can be employed. Selecting the most appropriate CE mode is key to achieving optimal separation and detection of analytes.

Ultrasensitive detection of biomarkers plays a crucial role in early-stage diagnosis of various types of diseases, e.g. cancer, HIV and Alzheimer's disease (AD). Collecting a blood sample from a patient is faster, simpler and much less invasive than bone marrow aspiration sample collection. Unfortunately for cancer patients, sensitive analysis of a blood sample is still challenging since there is only one circulating tumor cell per one billion blood cells.[3] DFWM can detect at these low concentration levels due to its parts-per-trillion level sensitivity.

Laser-induced fluorescence (LIF) is often used as a sensitive detector for CE.

DFWM offers comparable or better detection sensitivity.[4,5] In addition, label-free analytes, and choromophore- or fluorophore-labeled analytes can be detected with DFWM since the laser wave-mixing method is an absorption-based technique. DFWM-CE serves as a sensitive tool for various biomedical applications as described in this chapter.

CE-based nonlinear wave mixing is cost effective and fast as compared to existing diagnostic techniques. Currently, expensive and time-consuming polymerase chain reaction (PCR) based nucleic acid testing is used for diagnostics and for viral load monitoring of HIV-1 (human immunodeficiency virus). Detection of p24 antigen, a viral protein that is detectable in earlier stages of infection, is studied as an alternative to PCR since its concentration increases with viral load. Modified enzyme-linked immunosorbent assays (ELISA)[6] and functionalized nanoparticles[7] are popular methods currently used to detect p24 antigen. These often require expensive materials and time-consuming steps while laser wave-mixing CE does not require special materials or time-consuming steps.

Laser wave mixing coupled with CE can detect key proteins related to neurodegenerative diseases, e.g., Parkinson's and Alzheimer's diseases, at ultrasensitive levels and it can also monitor oligomerization (Chapters 5 and 7). Proteins have distinguishable isoelectric points, relative molecular masses, conformations, hydrophobicities and, specific-binding capabilities - characteristics not found in small molecules. Utilizing these properties, proteins can be separated using different techniques including capillary zone electrophoresis (CZE), isotachophoresis (ITP) (electrophoretic mobility separation), micellar electrokinetic

chromatography (MEKC) (hydrophobicity separation), sieving media such as gels and polymetric matrices (size-based separation), bioaffinity electrophoresis (BAE) (separation by specific integration with other biomolecules), isoelectric focusing (IEF), and electrokinetic chromatography (EKC) with ion-exchanger pseudophase (charge-based separation).

This chapter introduces the basics of CZE, MEKC, and polymetric matrices CE, and presents ultrasensitive detection and molecular weight sizing of proteins using DFWM-CE. Important analytes including p24 antibody for HIV-1 and CA 15-3 antibody for breast cancer are detected at ultrasensitive detection levels.

4.2.2 Capillary Zone Electrophoresis

Capillary zone electrophoresis (CZE) is the simplest capillary electrophoresis (CE) method, thus CE often refers to CZE. A schematic diagram of our custom-built CE is shown in Figure 4.1. The ends of a fused silica capillary are placed in reservoirs filled with an aqueous buffer, called a running buffer. Platinum wires are connected to a high-voltage power supply and are placed inside the reservoirs to complete an electric circuit for the CE system. When a sample is injected from the anode end and power is applied, molecules in the capillary migrate with different rates and directions depending upon their electric charges and size. Cations move toward the cathode while anions move toward the anode. Charge-to-size ratios of each molecule determine the rate of migration. In addition to the injected analytes, the buffer usually travels through the capillary under the influence of the electric field. This phenomenon, termed electroosmotic flow (EOF), is directed toward the cathode in

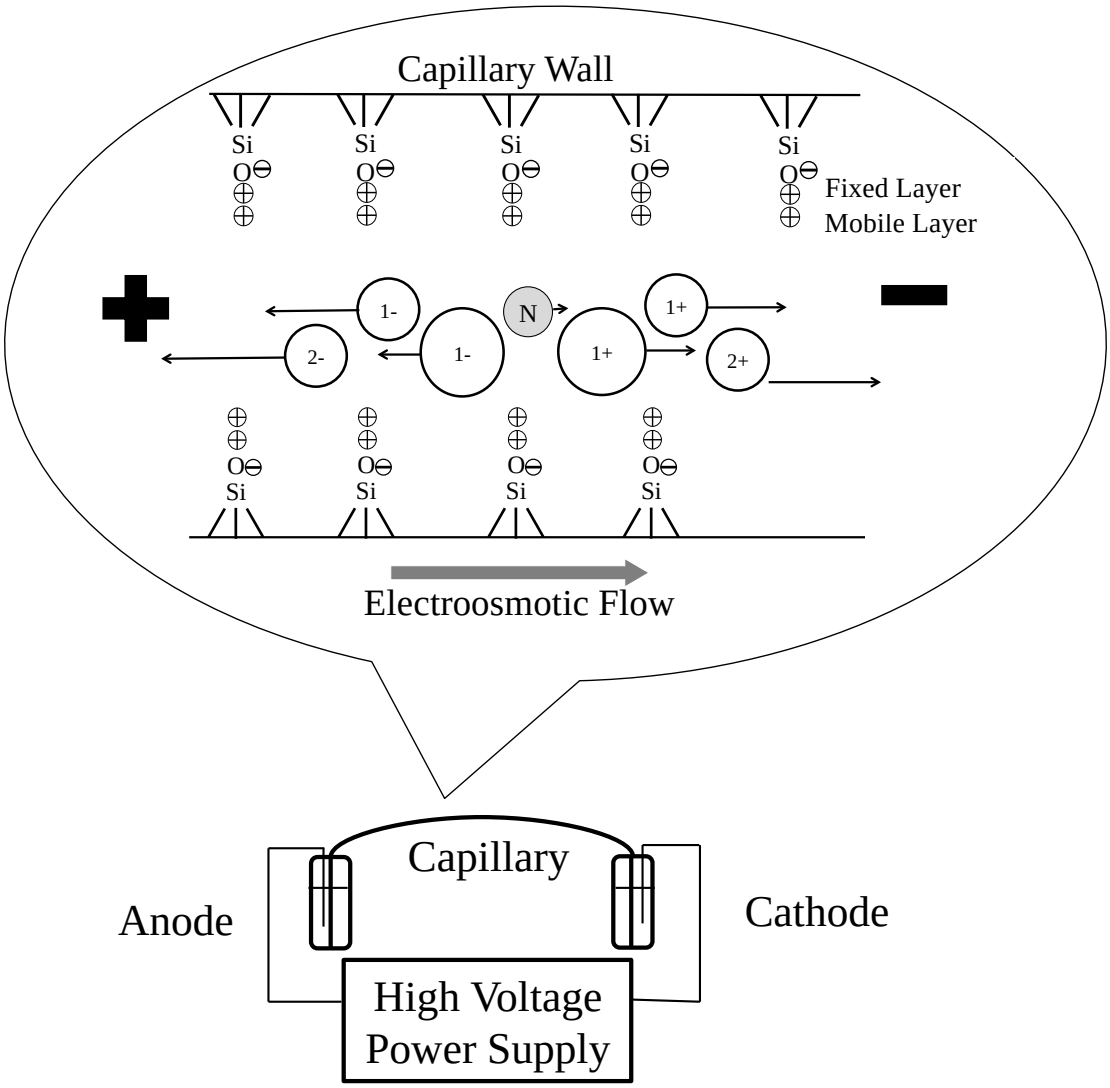

Figure 4.1 Schematic diagram of custom-built capillary electrophoresis and mechanisms of separation using capillary zone electrophoresis. EOF is generated by the negatively charged fused silica inner capillary wall, attracting the positively charged cations forming the fixed layer and the mobile layer, which is pulled toward the cathode and the bulk buffer solution travels with it.

operations, and neutral ions travel with the EOF. The velocity of EOF (v_{EOF}) and mobility (μ_{EOF}) are given by the following equations.[8]

$$v_{EOF} = \frac{\varepsilon \zeta E}{4\pi\eta} \tag{4.1}$$

$$\mu_{EOF} = \frac{\varepsilon \zeta}{4\pi\eta} \tag{4.2}$$

where ε is the dielectric constant of the buffer, ζ is the zeta potential, E is applied electric field, and η is the viscosity of the buffer.

Further enhancement of DFWM sensitivity can be achieved by optimizing CE conditions to achieve sample preconcentration. Multiple types of online preconcentration methods are available: (1) field-amplified sample stacking (FASS), (2) large-volume sample stacking (LVSS), and (3) MEKC[9] sweeping can all improve the limit of detection (LOD) without degrading the separation resolution. FASS is the simplest stacking mode; therefore, this method is mainly used for this work. Figure 4.2 illustrates the FASS theory, first introduced by Mikkers *et al.* in 1979.[10] Analytes that are introduced electrophoretically from a low-conductivity solution into a high-conductivity solution slow down dramatically at the boundary. The axial gradient in ionic conductivity is achieved by introducing analytes in lower concentration buffer than in the BGE. The sample region, called the low conductivity region, acts as a high-electrical resistance zone in series with the rest of the channel. The locally high electric field is generated within the sample region when voltage is applied.[11] Thus, sample ions migrate from high to low drift velocity regions. This leads to accumulation at the interface between high and low conductivity regions.

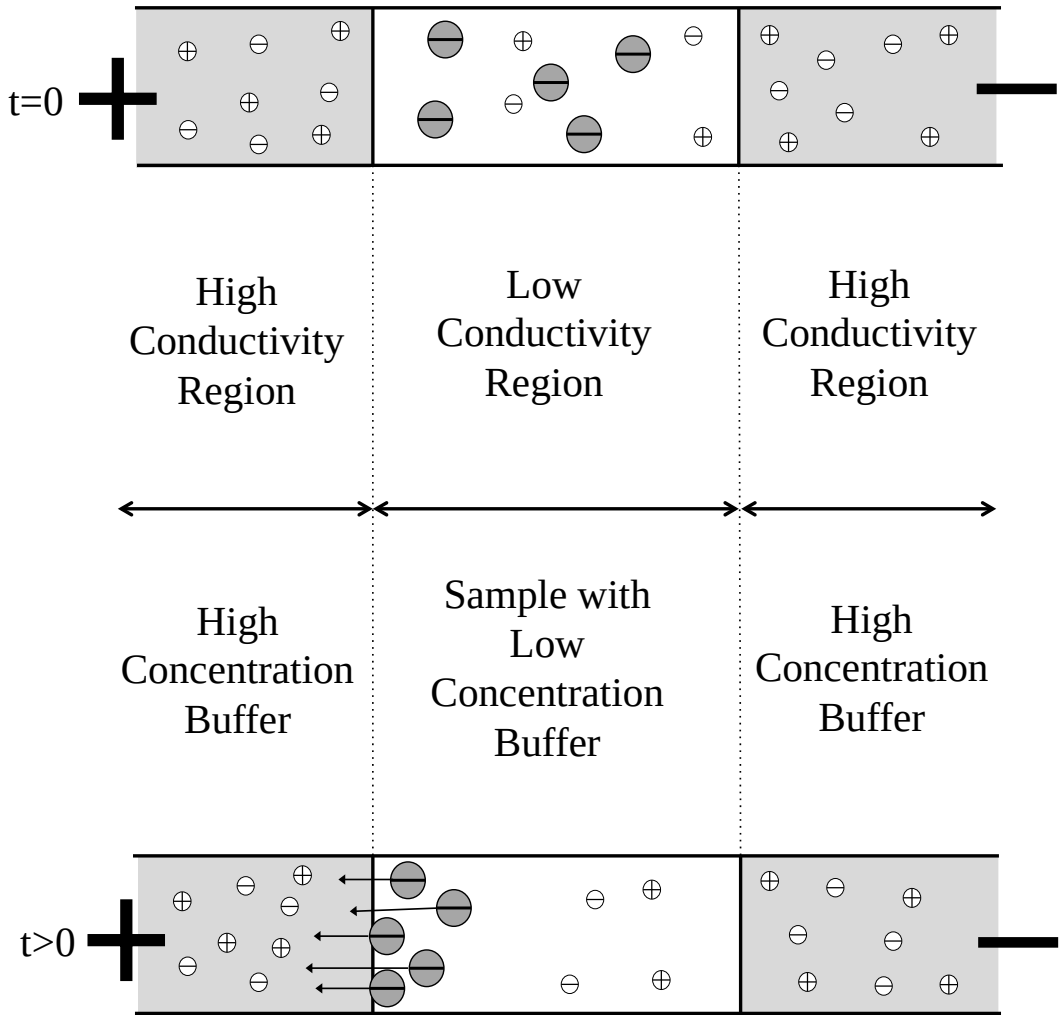

Figure 4.2 Schematic diagram of FASS principles. Introducing a running buffer with a higher concentration buffer than the electrokinetically injected sample buffer allows for online preconcentration.

4.2.3 THEORY OF MICELLAR ELECTROKINETIC CHROMATOGRAPHY

Separation of both ionic and neutral proteins can be achieved by micellar electrokinetic chromatography (MEKC), a hybrid method that combines chromatographic and electrophoretic separation principles developed in the early 1990s. Ionic micellar solution is the run buffer for MEKC, while a simple salt buffer is used for CZE. In MEKC, a surfactant containing "pseudostationary" micelles is introduced in a capillary to interact with the analytes. The EOF acts like a chromatographic "mobile phase." However, the EOF provides a relatively flat profile compared to pumped or laminar flows, as in high-performance liquid chromatography (HPLC). Thus, narrow peaks (high separation efficiency) are achieved by CE since all the solute molecules experience the same velocity component caused by EOF regardless of their cross-sectional position in the capillary.[8]

In this chapter, sodium dodecyl sulfate (SDS), commonly used as a negatively charged surfactant, is employed. When high voltage is applied, a negatively-charged micelle travels towards the anode. In reality, micelles travel toward the cathode since the EOF that counter travels is usually stronger than the electrophoretic migration of the micelles (Figure 4.3)[12] unless the capillary is treated with a special coating. The separation depends on the individual interaction between analytes and micelles, i.e., molecules that have greater interaction with micelles migrate more slowly than analytes distributed in the bulk solution.[13] Anions are first separated and detected since they remain in bulk solution due to electrostatic repulsions from the micelles. Neutral analytes are separated next due exclusively to their hydrophobicity. Cations are separated and detected last due to their strong electrostatic attraction to micelles.

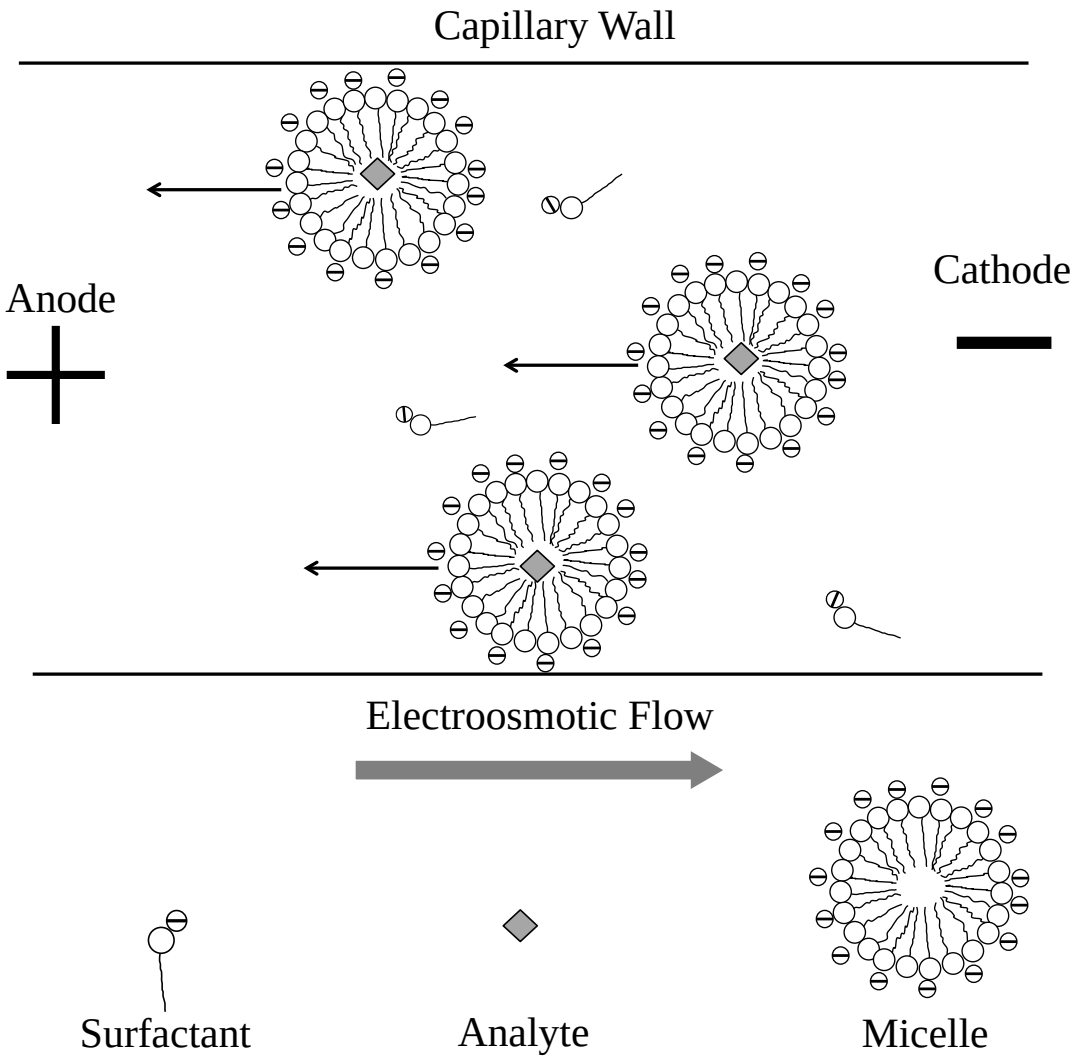

Figure 4.3 Schematic diagram for the MEKC separation process.

4.2.4 CAPILLARY SIEVING ELECTROPHORESIS

Fast, high-resolution on-column separation, and detection can be obtained by sodium dodecyl sulfate-capillary gel electrophoresis (SDS-CGE), in which a high-intensity electric field is applied to the CE system. Generally, separation and molecular mass determination of proteins and polypeptides are performed by SDS-PAGE, which is time-consuming and not suitable for accurate quantification.[14] Three types of polymers, pullulan, polyacrylamide, and poly (ethylene glycol) (PEG), can be employed by SDS-CGE to minimize analyte-wall interactions, change EOF for faster separation, improve reproducibility, and enhance resolution[15] as described in this chapter.

Pullulan, a water-soluble non-crosslinked polymer comprising α-1, 6-linked maltotriose residues, is employed as an alternative to crosslinked gels to achieve protein separation by molecular weight. The non-crosslinked polymer network is formed by a slightly branched or linear hydrophilic polymer chain entangled in solution.[16] Pullulan is generally used as a CE-format SDS protein electrophoresis assay,[14,17] since low UV absorbance, and separation resolution comparable to SDS-PAGE are offered by the polymer. However, some additives are required for pullulan due to its fragile capillary coating.

Cross-linked polyacrylamide[18,19] and linear polyacrylamide[20-22] are introduced in capillaries for slab-gel electrophoresis. Although the neutral and hydrophilic polymer layer is widely used, problems occasionally occur: polyacrylamide shrinkage and segmentation, generation of bubbles in the column, and background absorbance by leftover monomers. In addition, the method lacks reproducibility since, after the

first successful run, proteins can accumulate at the injection end of the capillary and prohibit proteins from being injected.[23]

Poly (ethylene glycol) (PEG), a replaceable and water-soluble linear polymer, is used for sieving capillary electrophoresis to improve run-to-run reproducibility and the lifetime of a capillary. Cooke *et al.* demonstrated impressive reproducibility over 400 runs for a molecular mass marker ladder of 9-116 kDa using PEG.[24] In addition, nonspecific protein absorption and EOF are avoided by using a hydrophilic PEG-coated capillary, an important feature in protein-sieving separation.[25] Thus, PEG is the matrix used in capillary sieving electrophoresis for this work.

4.2.5 Degenerate Four-Wave Mixing Signal

The wave-mixing signal exhibits excellent properties including quadratic dependence on analyte extinction coefficient, i.e. concentration, and cubic dependence on intensity of the excitation laser source. The wave-mixing signal can be described with the following equation.[26]

$$I_3 = \left(\frac{b}{8\pi}\right)^2 I_1^2 I_2 \frac{\lambda}{\sin^4(\theta/2)} \left(\frac{dn}{dT}\right)^2 \frac{\alpha^2}{\kappa^2} \qquad (4.3)$$

The intensity of the DFWM signal (I_3) produced by the probe and pump beams depends on the cross section of the path length of a laser beam (b), intensities of excitation laser source (I_1 and I_2), the wavelength of the laser source (λ), the angle between the probe and pump beams (θ), a derivative of the refractive index with respect to solvent temperature change (dn/dT), the extinction coefficient (α), and thermal conductivity (κ). This equation indicates that the wave-mixing detection

technique allows more effective measurement of small changes in analyte concentration as compared to conventional absorption and fluorescence methods. Both sensitivity and selectivity levels are enhanced when DFWM is coupled with CE. Excellent separation resolutions, zeptomole-level sensitivity, high speed analysis, and the small sample required to perform separation[27,28] are some of the advantages of DFWM-CE.

4.3 Experimental

4.3.1 NONLINEAR WAVE-MIXING EXPERIMENTAL SETUP FOR PROTEIN ANALYSIS

A schematic diagram of a nonlinear four-wave mixing setup interfaced to capillary electrophoresis (CE) is shown in Figure 4.4. The visible lasers used in these experiments are a 40 mW continuous-wave 488 nm blue laser with adjustable power (Coherent, Santa Clara, CA), and a 50 mW 473 nm diode laser (CNI, Changchun, China). Two input beams are created by splitting the original laser source with a 30:70 (R:T) beam splitter. The stronger beam serves as both pump and probe beams while the reflected weaker beam serves only as a pump beam. The two input laser beams travel equal distances to a focusing lens (L1), which focuses the two input beams. The diameters of 488 nm and 473 nm beams are 1.70 and 1.20 mm, respectively, and their mixing angles are 0.95° and 1.5°, respectively. The calculated probe volumes, where two input beams intersect, are 79 pL and 58 pL for 488 nm and 473 nm lasers, respectively. A 75 μm i.d. and 360 μm o.d fused-silica capillary, the sample holder for this setup, is purchased from Molex (Lisle, IL). A small portion (under 1 cm) of the capillary coating is removed using a butane flame so that the

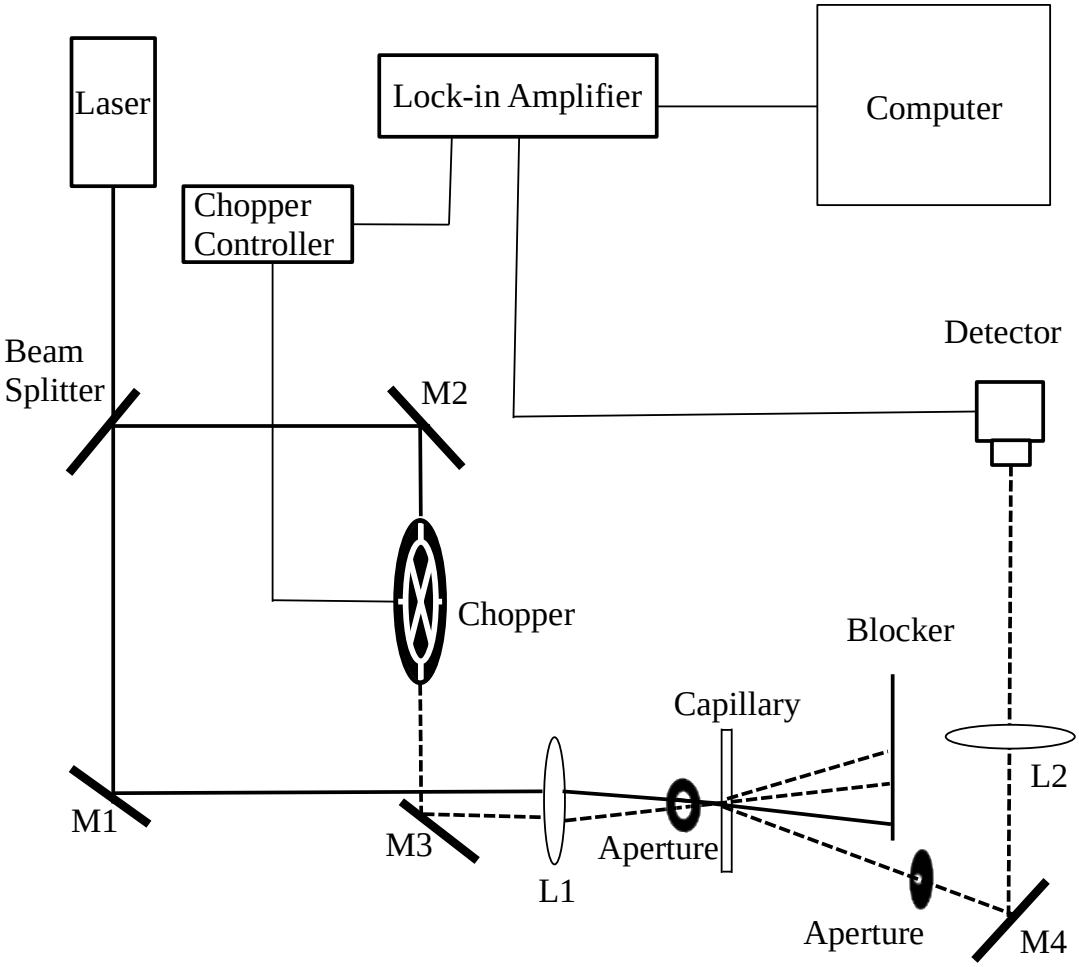

Figure 4.4 DFWM setup for protein detection. Two coherent excitation laser sources are mixed at the capillary to generate the wave-mixing signals from an absorbing analyte.

input laser beam can propagate across the capillary. Two coherent laser-like signals are generated when absorbing analytes are present in the capillary. The wave-mixing signal that is adjacent to the unchopped input beam is the stronger signal beam. The wave-mixing signal is chopped at 200 Hz by an optical chopper (Stanford Research Systems, Sunnyvale, CA, SR541), focused by a 150 mm focal-length biconvex lens (L2), and collected by a simple photodetector (Thorlabs, Newton, NJ, PDA25K). The optical chopper, photodetector and computer are interfaced to a DSP lock-in amplifier (Stanford Research Systems, Sunnyvale, CA, SR810) where the signal is amplified and the S/N enhanced.

4.3.2 CHEMICALS

Buffers and solutions are prepared using distilled water from a compact water distillation system (Waterwise, Leesburg, FL, 4000). Borax, Tris base, sodium dodecyl sulfate (SDS), acrylamide, β-lactoglobulin, FITC-conjugated bovine serum albumin (BSA), linear polyacrylamide, and poly (ethylene glycol) (PEG, 10,000) are purchased from Sigma-Aldrich (St. Louis, MO). Succinimidyl 6-(N-(7-nitrobenz-2-oxa-1,3-diazol-4-yl)amino) hexanoate (NBD-X, SE) is obtained from Marker Gene Technologies (Eugene, OR). 5-(and 6)-Carboxytetramethylrhodamine, succinimidyl ester (NHS-rhodamine), fluorescein isothiocyanate (FITC), sodium carbonate, sodium bicarbonate, CHES, hydrochloric acid, sodium hydroxide, unstained protein ladder, p24 antibody, N,N-*Dimethylformamide* (DMF), and dialysis tubing (MW_{CO} 12-14 kDa) are purchased from Thermo Fisher Scientific (Waltham, MA). A capillary is coated with Ultratrol LN (Target Discovery, Palo Alto, CA), and some of the sieving

matrix for CE is prepared with pullulan (TCI America, Portland, OR). Breast cancer biomarker CA 15-3 antibody is obtained from MP Biomedicals (Santa Ana, CA).

4.3.3 PROTEIN LABELING

Sodium borate buffer (50 mM) is prepared by dissolving Borax (1.907 g) in water (100 mL). Optimal pH (8.6) is obtained by using 1.0 M hydrochloric acid. Proteins are dissolved in conjugation buffer (50 mM sodium borate, pH 8.6) at 2 mg/mL in a 1.5 mL centrifuge tube. Labels are dissolved in DMF (10-20 mg/mL) to react with proteins at 1:20 ratio. The mixture is allowed to react for 1 hour in the dark at room temperature. The mixture is dialyzed into Tris-CHES (25 mM) with SDS (0.1%) solution to remove the excess label.

The unstained protein ladder contains seven proteins, lysozyme (14.4 kDa), β-lactoglobulin (18.4 kDa), REase Bsp98I (25.0 kDa), lactate dehydrogenase (35.0 kDa), ovalbumin (45.0 kDa), bovine serum albumin (66.2 kDa) and β-galactosidase (116 kDa), at various concentration levels (0.1 – 0.2 mg/mL). An aliquot of 150 µL is taken from the stock solution and dialyzed into conjugation buffer to react with FITC using the protocol stated earlier.

4.3.4 CAPILLARY ELECTROPHORESIS

Tris-CHES, carbonate, borate buffers (50mM, pH 9.0) are prepared to test optimal conditions for the CE system. Tris-CHES buffer: Tris (1.04 g) and CHES (0.607 g) are dissolved in distilled water (100 mL), pH is adjusted to 9.0. Carbonate buffer: Sodium carbonate (2.65 g) and sodium bicarbonate (2.10 g) are dissolved in

distilled water to obtain 0.1 M solution, and a pH 9.0 buffer is obtained by combining 3 mL and 27 mL solution, respectively. The mixture is diluted by distilled water to obtain 50 mM. borate buffer: Borax (1.907 g) is dissolved in 100 mL distilled water, sodium hydroxide is added in drops until the desired pH is reached. The current of each buffer is tested and recorded by changing voltage multiple times with a high voltage supply controller to obtain Ohm's Law plot.

Sieving matrices are prepared by dissolving pullulan or PEG at different concentration levels into Tris-CHES buffer (100 mM) with 0.1% high purity electrophoresis-grade sodium dodecyl sulfate (SDS).

All CE runs are performed by a custom-built CE system. The setup consists of a fused silica capillary (75 μm i.d., 360 μm o.d., 30 cm length, 15 cm effective length) and a high voltage power supply (Glassman High Voltage, High Bridge, NJ) that is connected to platinum wires. Voltage is controlled by a custom-built controller and the voltage and current levels are monitored by voltmeters. Plastic vials containing running buffer or samples are placed at each end of the capillary. The capillary is rinsed with 0.1 M NaOH, distilled water and CE running buffer for 2 minutes before each run.

4.3.5 UV-Visible Absorption Spectrum

A bench-top UV-visible diode-array spectrometer (Agilent, Santa Clara, CA 8453) is used for conventional absorption measurements. A Quartz cuvette (1.0 cm path length) is used as a sample cell. The instrument is blanked with buffers used to dissolve each sample before each measurement.

4.4 Results and Discussion

4.4.1 Excitation source wavelength selection

The first step to build DFWM is selecting the wavelength of the laser, since a molecule that selectively absorbs the wavelength of an excitation laser source produces a strong wave-mixing signal. Biomolecules have strong absorption around the range that can be detected with a UV laser (266 nm). Small molecules and neurotransmitters such as adenosine and dopamine can be detected label free with excellent detection sensitivity using a 266 nm laser (Chapter 6). Aromatic amino acids such as tryptophan, tyrosine and phenylalanine allow proteins to absorb UV wavelengths; however, a visible laser with lower power is ideal for protein detection since macromolecules consisting of long chain amino acids tend to degrade with high laser power. Figure 4.5 shows conventional UV-visible absorption spectra of β-lactoglobulin and label-conjugated proteins. Fluorescein isothiocynate (FITC) is a fluorescein derivative with λ_{max} at 495 nm designated for blue lasers (488 nm or 473 nm). Succinimidyl 6-(*N*-(7-nitrobenz-2-oxa-1,3-diazol-4-yl)amino)hexanoate (NBD-X) is another commonly used protein and peptide label (λ_{max}=467 nm). *N*-Hydroxysuccinimide (NHS)-rhodamine forms a stable covalent amide bond with primary amines with a maximum absorption at 544 nm, which can be probed by a green 532 nm laser. For convenience, FITC is used in this chapter because of the availability of blue lasers and its stronger absorptivity as compared to that of NBD-X. Since DFWM is an absorption-based technique, both chromophores and fluorophores can be used as labels (Chapter 6).

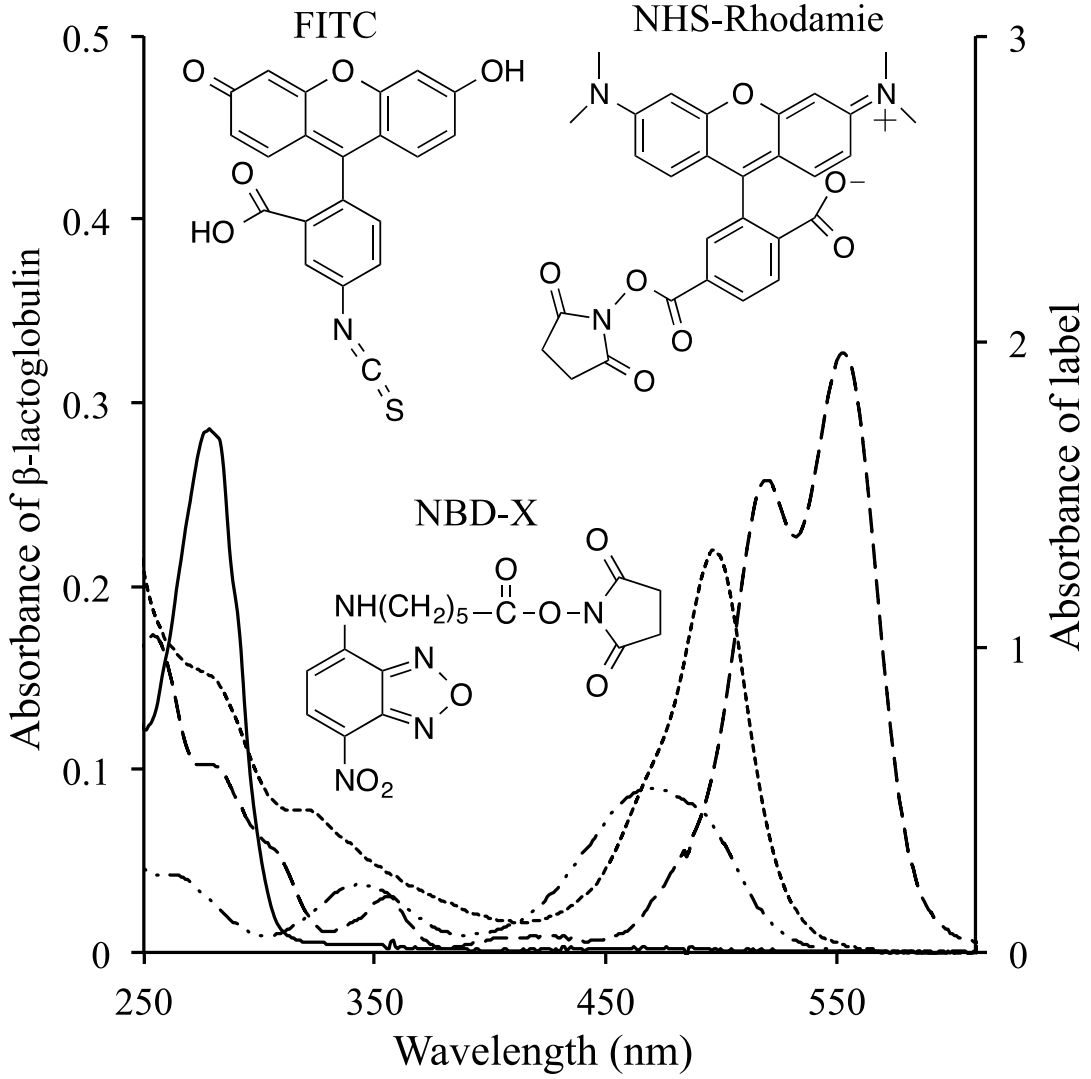

Figure 4.5 Chemical structures and conventional UV-visible absorption spectra of common labels used for protein labeling. —— = β-lactoglobulin (1.1 x 10^{-5} M), — •• — = NBD-X labeled β-lactoglobulin, ------ = FITC labeled β-lactoglobulin (1.1 x 10^{-5} M), and — — — = NHS-Rhodamine (1.1 x 10^{-5} M). Protein-labeled samples are dissolved in a pH 8.6 borate buffer (100 mM).

4.4.2 SELECTION OF ELECTROLYTES

Running buffers play a critical role in obtaining good detection and separation levels in capillary electrophoresis runs. A background electrolyte (BGE) is selected based on desirable characteristics including lack of interference with analytes of interest, minimum optical absorption at the excitation laser wavelength, good solubility for analytes, and buffering capacity through analysis.

Generally, a relatively high ionic strength buffer is preferred to suppress ion-exchange effects between the charged analyte and the ionized silanol groups on the capillary wall in order to obtain high resolution CE separation. Various concentrations of running buffers (50-100 mM) are studied to observe the effect on peak height for pre-conjugated protein (Figure 4.6). Figure 4.7 (A) and (B) show peak heights/currents versus BGE concentration plots. The current of the buffer system has a linear dependence on concentration. The highest running buffer concentration yields the highest peak due to enhanced FASS and higher current levels. However, buffer concentration is restricted by several parameters including capillary length, inner diameter of capillary, the applied electrical field strength, efficiency of the capillary thermostating/cooling system, and induction of excessive current (Joule heating).[29] A longer capillary may yield less Joule heating with a tolerable current, but this may compromise some separation parameters. Alternatively, buffers with relatively low current levels can be selected for CE separation.

An Ohm's law plot, described by Nelson *et al.* allows comparison of different types of running buffers and the maximum voltage that can be applied to particular buffer systems.[29] Figure 4.8 shows current versus applied voltage for Tris-CHES,

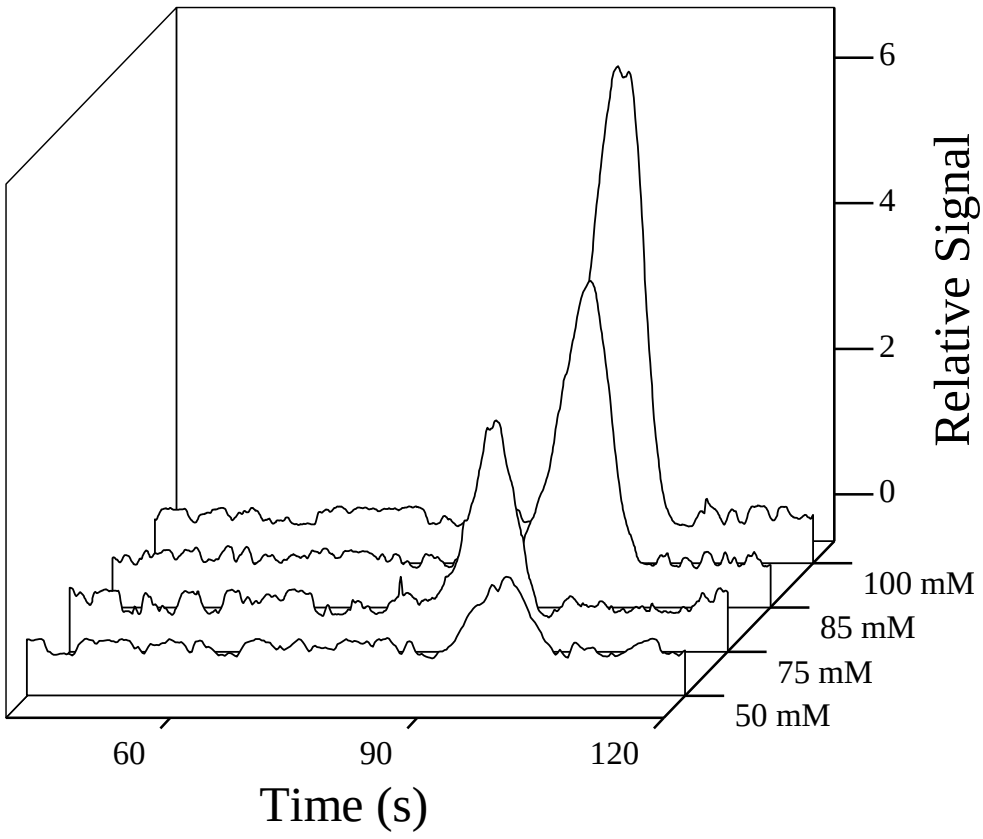

Figure 4.6 Electropherograms of capillary zone electrophoresis with different concentrations of Tris-CHES as BGE (50, 75, 85 and 100 mM) at pH 8.9. The capillary is rinsed with NaOH (0.1 M) and water, coated with UltraTrol, and filled with running buffer. Capillary: 75 μm i.d., 30 cm (15 cm effective length), -18.3 kV. FITC-conjugated BSA (3.0 x 10^{-6} M) in Tris-CHES (25 mM) is injected electrokinetically for 6 s. Detection at 488 nm.

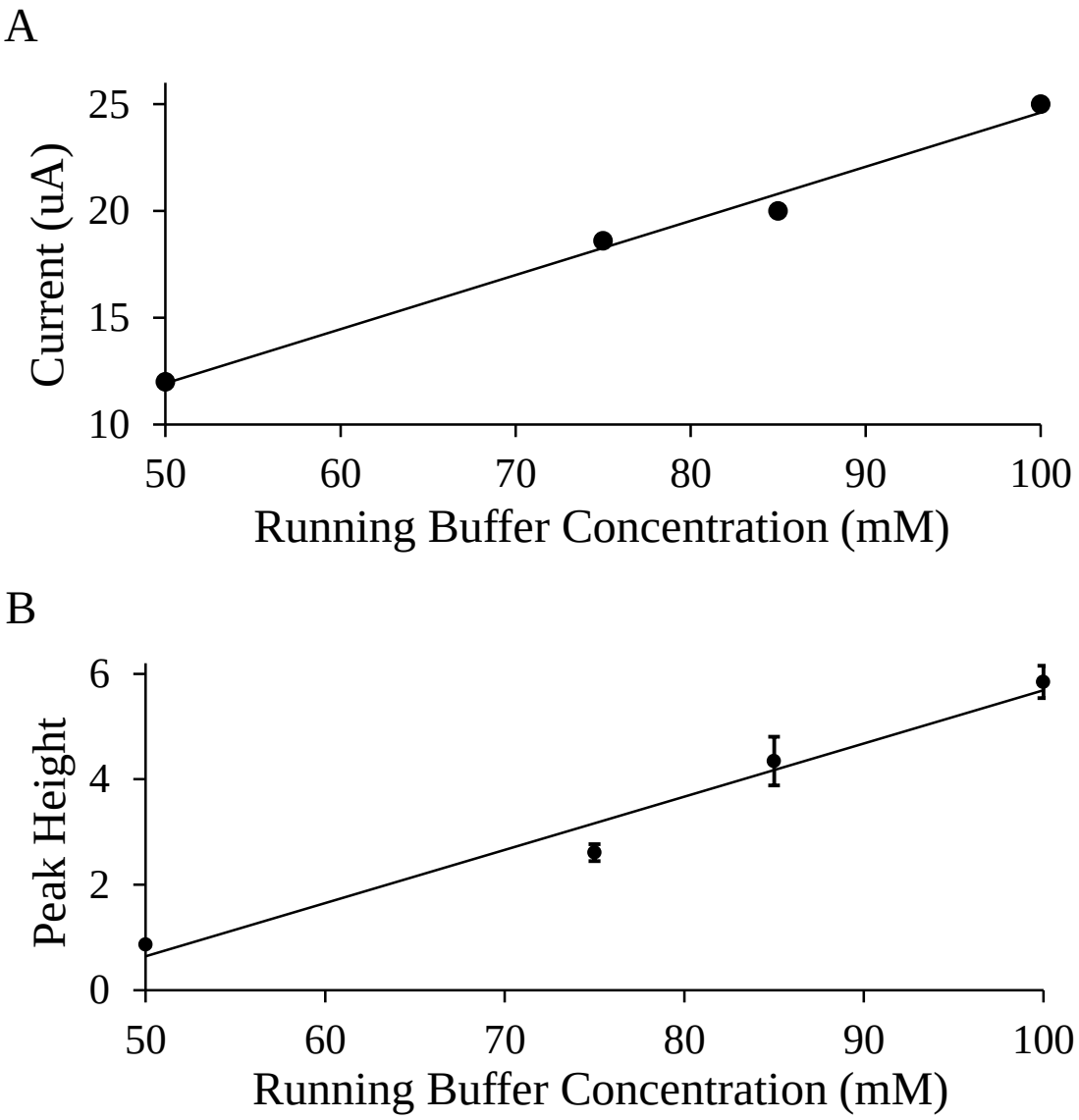

Figure 4.7 Relationships between current, BGE concentration and peak height. A: Current versus running buffer concentration plot. A capillary is filled with 50, 75, 85 and 100 mM Tris-CHES (pH 8.9) to measure currents. Capillary: 75 μm i.d., 30 cm (15 cm effective length), -18.3 kV. B: Peak heights obtained by capillary zone electrophoresis under the same conditions.

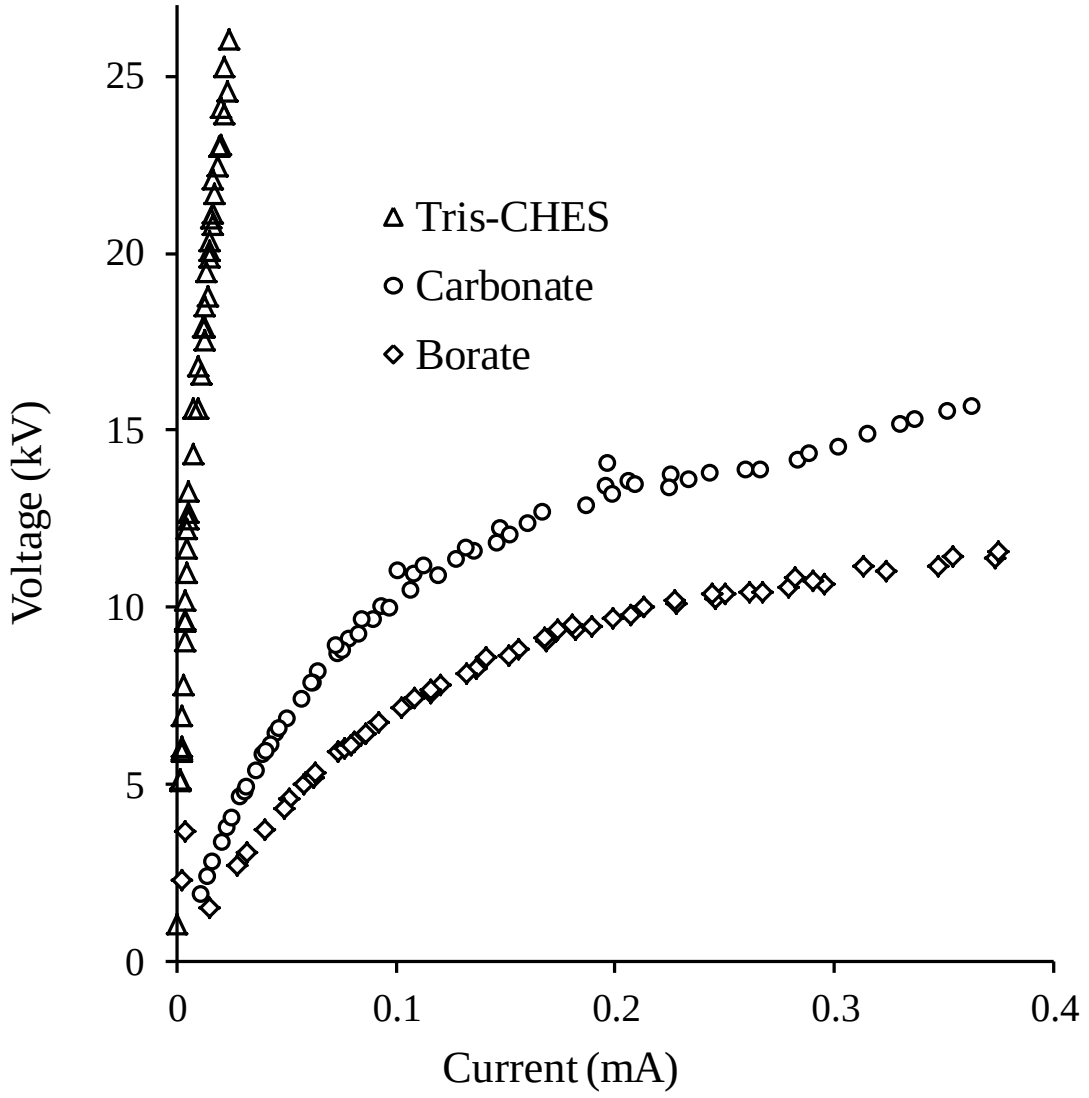

Figure 4.8 Ohm's plot of Tris-CHES, sodium carbonate and borate buffer. Currents are measured in a custom-built CE system. Capillary: 75 μm i.d., 30 cm total length (15 cm effective length), BGE, 50 mM Tris-CHES (pH 9.0), sodium carbonate buffer (pH 8.9), and borate buffer (pH 9.3).

carbonate, and borate buffer systems. The plot is obtained by filling a capillary with the desired buffer system and applying a voltage for about one minute to record the current. The capillary temperature is adequately maintained when a current versus voltage plot shows linearity, and thermostating capacity is exceeded at the point where linearity is lost. Tris-CHES is mainly used for this study since linearity is preserved beyond 25 kV and a low current that maintains the high voltage level for the CE systems is observed.

4.4.3 DETECTION LIMIT STUDY WITH CAPILLARY ZONE ELECTROPHORESIS

Determination of optimal SDS concentration for capillary electrophoresis is obtained by plotting current versus sodium dodecyl sulfate (SDS) concentration (Figure 4.9). SDS concentration of 0.1% or 3.3 mM (less than the critical micelle concentration of 8.2 mM) is selected to maintain a low current for CZE runs. For smaller molecules, higher SDS concentration is used to form micelles to separate analytes with similar charges and Tris-CHES is selected based on a previous study.

Figure 4.10 presents the detection limit study of FITC-conjugated BSA, with concentration of 3.0×10^{-8} M (bottom) and 3.0×10^{-10} M (top). Relatively cost effective pre-labeled BSA is used to test optimal conditions before detecting our p24 antibody and CA 15-3 antibody samples. A concentration detection limit of 1.4×10^{-10} M (S/N 2) is determined for FITC-conjugated BSA. Based on the probe volume used, a mass detection limit of 1.0×10^{-20} mol is determined. The analyte is dissolved in 25 mM Tris-CHES buffer, and Tris-CHES 100 mM BGE is used to perform FASS for online preconcentration. BSA migration times for the 3.0×10^{-8} M and 3.0×10^{-10} M

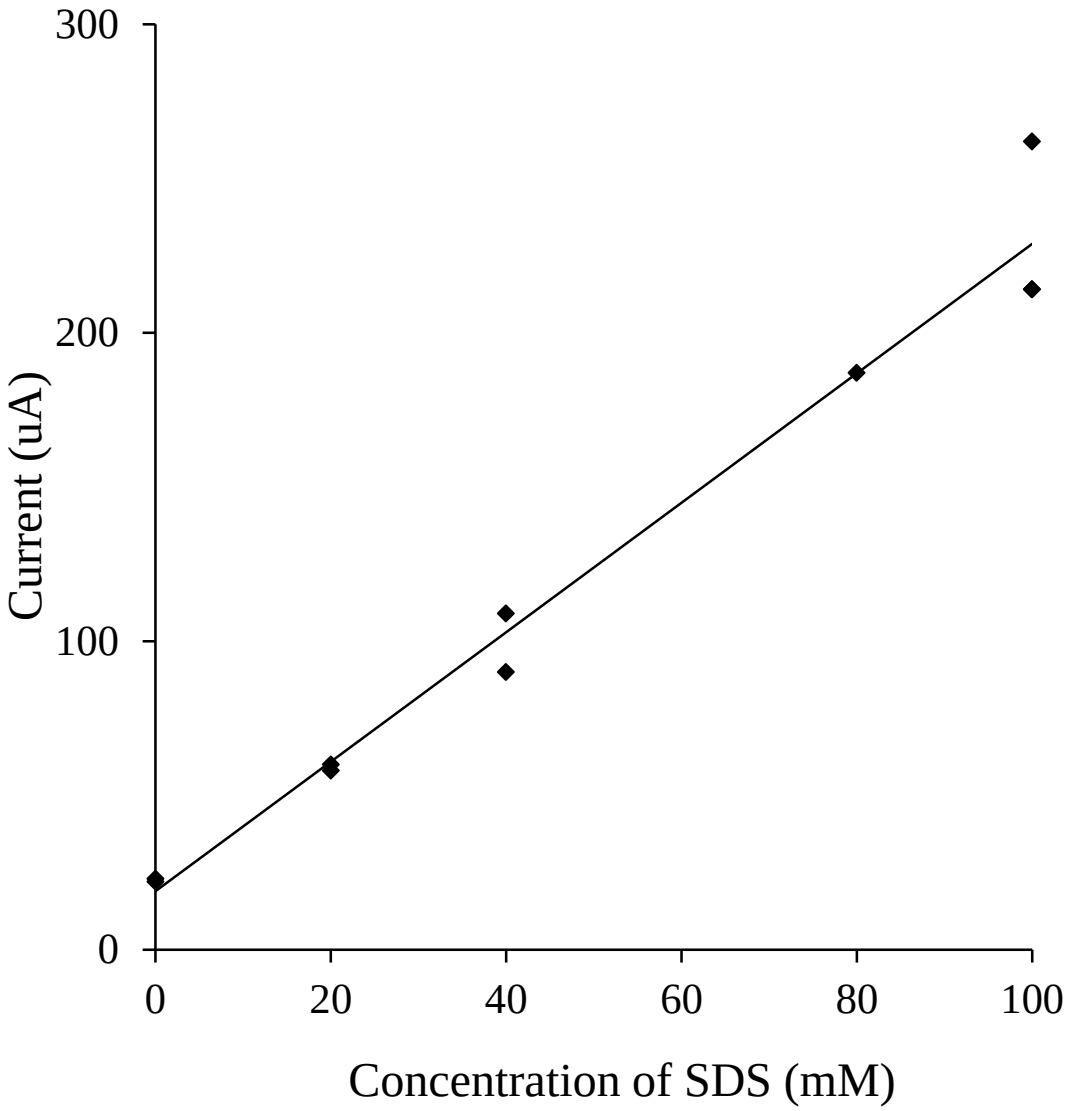

Figure 4.9 Plot of current versus running buffer with various SDS concentrations. A capillary is filled with 0, 20, 40, 60, 80 and 100 mM SDS dissolved in Tris-CHES (100 mM, pH 8.9) to measure currents. Capillary: 75 μm i.d., 30 cm (15 cm effective length). 18.3 kV.

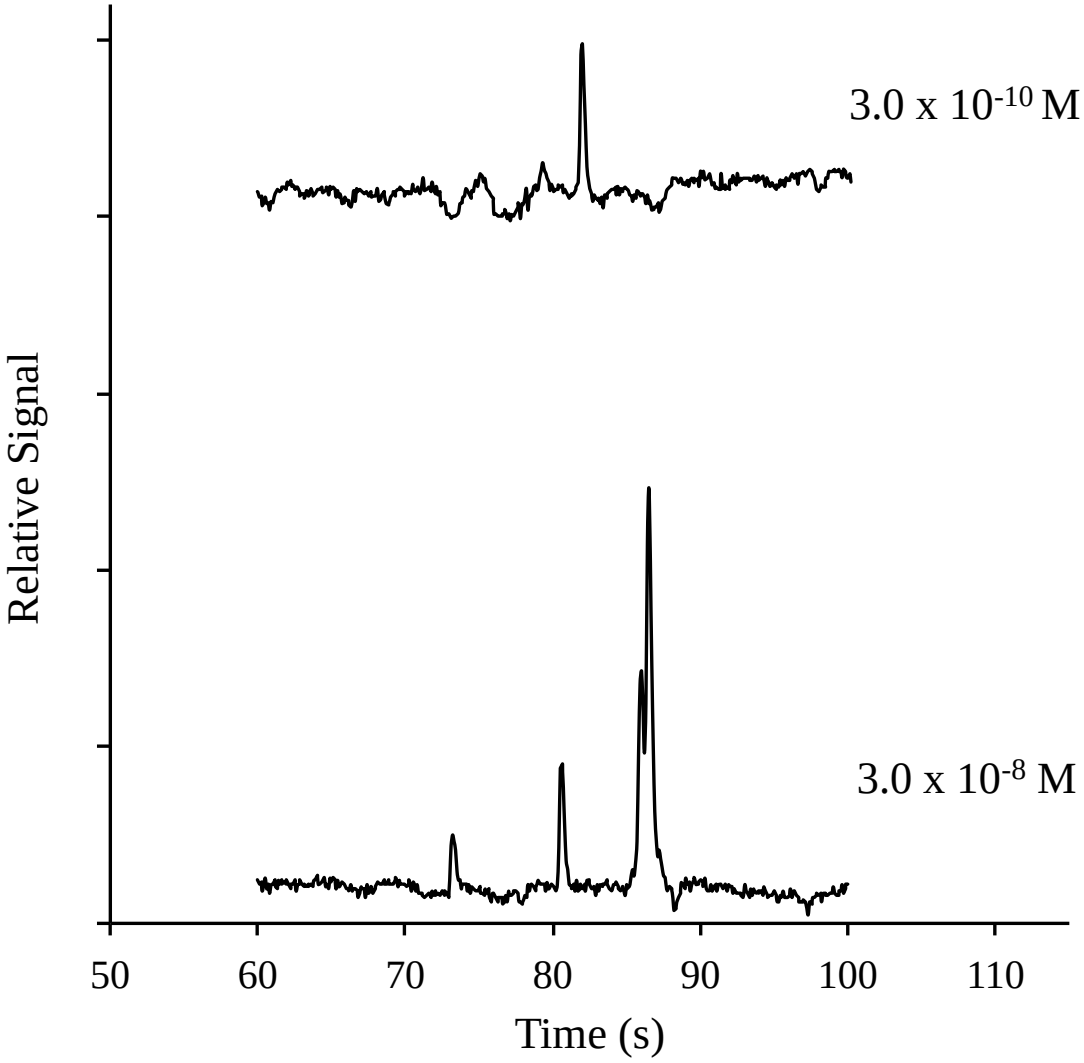

Figure 4.10 Electropherograms of capillary zone electrophoresis of FITC-conjugated BSA 3.0 x 10^{-8} M (bottom) and 3.0 x 10^{-10} M (top). Capillary is rinsed with NaOH (0.1 M), water, UltraTrol, and running buffer (pH 8.9, 100 mM Tris-CHES with 0.1% SDS) for 3 minutes. Capillary: 75 μm i.d., 30 cm (15 cm effective length). -17.9 kV (32 μA and 35 μA for each system). The samples are injected electrokinetically for 20 and 25 s. Detection is performed using a 488 nm laser.

analytes are slightly out of alignment due to subtle mismatch of averaged currents (32 μA and 35 μA) resulting from the manual operation of the custom-built CE switch and the lack of a temperature control system. The wave-mixing setup is realigned and the sensitivity scale on the lock-in amplifier is adjusted between runs in addition to optimization of injection time to obtain the best detection limit. Thus, a drastic change in peak height is not observed even though the analyte concentrations are two orders of magnitude apart; however the S/N values reflect the concentration levels.

The detection of the HIV-1 biomarker, p24 antibody, takes less than 2 minutes by DFWM-CZE while enzyme-linked immunosorbent assay (ELISA) and Western blot methods take a day. Figure 4.11 shows reproducible electropherograms for FITC-conjugated p24 antibody using the same concentration (6.6×10^{-10} M). Sensitive DFWM techniques can result in less signal intensity due to subtle misalignment of optics and capillary position, although small adjustments of the Y-axis and optical alignment can bring back optimal sensitivity levels. A mass detection limit of 5.1×10^{-20} mol is determine for p24 antibody.

Figure 4.12 presents ultrasensitive detection of a fluorophore-conjugated CA15-3 antibody. The concentration detection limit of 6.7×10^{-12} M and a mass detection limit of 5.2×10^{-22} mol are determined. Two peaks in the electropherogram are caused by multiple labeling sites with various reactivity of the protein.[25] The smaller peak disappears when the sample is diluted to nano- or picomolar levels. Different injection times (sample size) result in some deviation from the quadratic dependence of peak height on concentration.

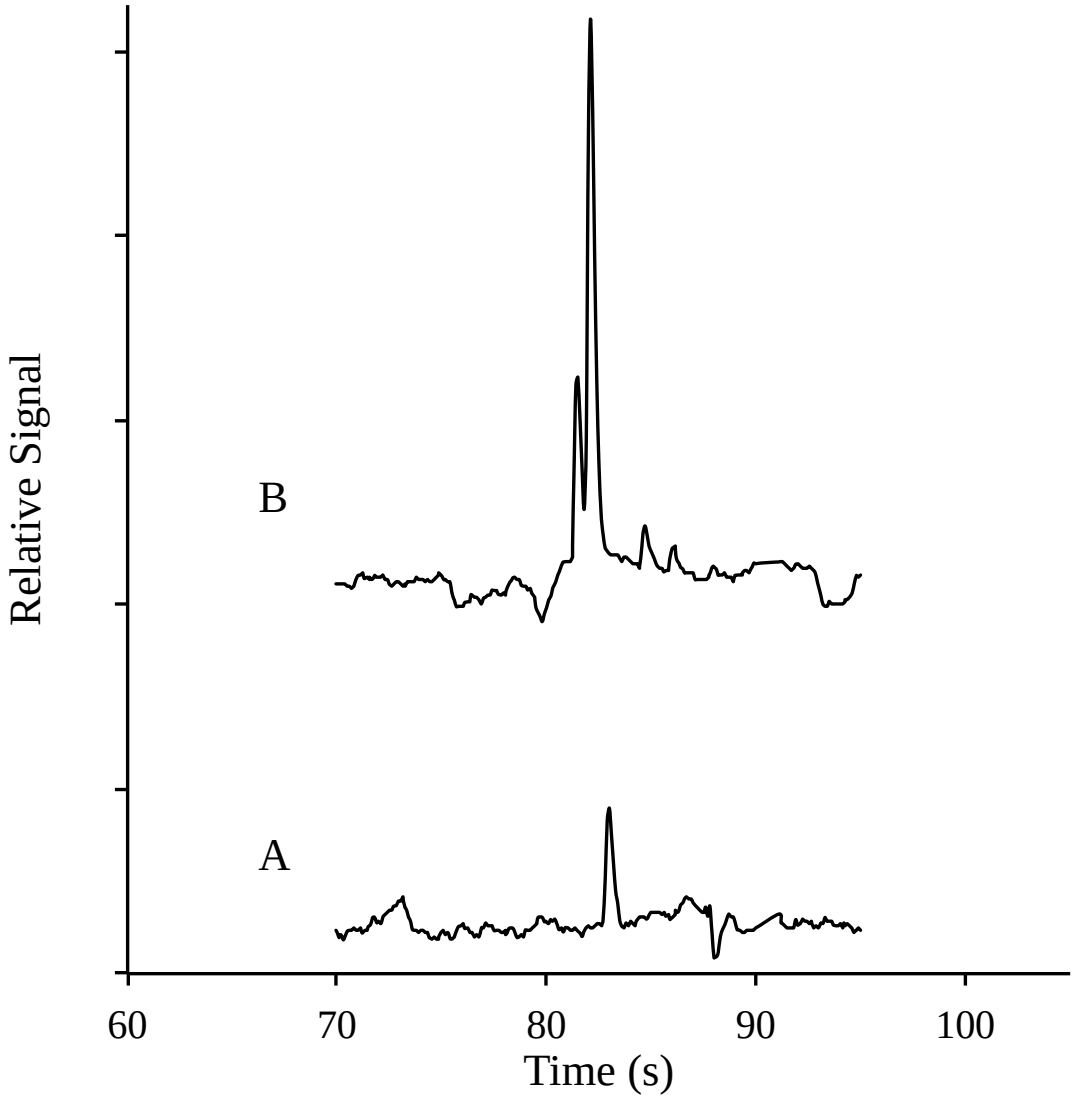

Figure 4.11 Reproducible electropherogram of FITC-conjugated p24 antibody (6.6 x 10^{-10} M) in 25 mM Tris-CHES buffer (pH 8.9). (A) sample is injected without aligning DFWM setup after the previous run. (B) signal enhanced by minor realignment. Capillary is rinsed with NaOH (0.1 M), water, UltraTrol and BGE for 3 minutes between runs. BGE: 100 mM Tris-CHES (pH 8.9) with 0.1% SDS. Capillary: 75 μm i.d., 30 cm length (15 cm effective length), -17.6 kV, 33 μA. The samples are injected electrokinetically for 25 s. Detection by DFWM using a 488 nm excitation laser source.

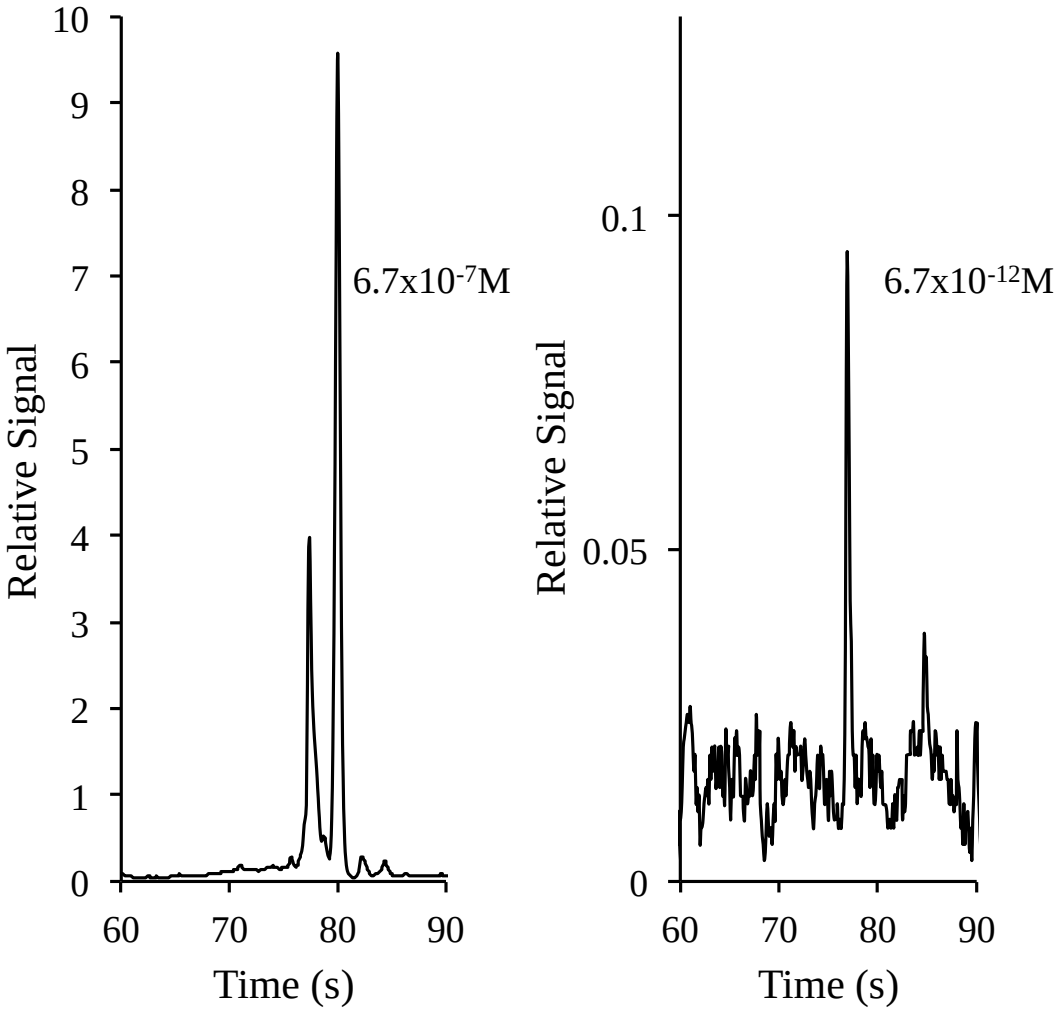

Figure 4.12 DFWM electropherograms of CA15-3 antibody in 25 mM Tris-CHES (pH 8.9) buffer at different concentration levels of 6.7 x 10^{-7} M and 6.7 x 10^{-12} M. Capillary are each rinsed with NaOH (0.1 M), water, UltraTrol and running buffer for 3 minutes. BGE: 100 mM Tris-CHES (pH 8.9) with 0.1% SDS. Capillary: 75 μm i.d., 30 cm length (15 cm effective length), -18.4 kV, 20 s and 25 s electrokinetic injections, DFWM detection using a 488 nm laser.

4.4.4 SODIUM DODECYL SULFATE-CAPILLARY GEL ELECTROPHORESIS

Sodium dodecyl sulfate-capillary gel electrophoresis (SDS-CGE) has been widely used as an on-column, high resolution, and high-speed mass determination method as an alternative to SDS-PAGE. Preferably, a low UV-visible absorbance matrix is used for this technique to obtain low background noise. Figure 4.13 shows a conventional optical UV-visible absorption spectra of sieving matrices dissolved in Tris-CHES (100 mM) that are commonly used for SDS-CGE. Although linear polyacrylamide separates proteins by molecular mass, it is used rarely due to its background absorption in UV and visible wavelength ranges.[14] Relatively UV transparent matrices such as poly (ethylene glycol) (PEG) and pullulan are favorable for a wave-mixing system. Figure 4.14 shows photos of excitation laser profiles after passing through the capillary filled with a sieving matrix. Tris-CHES, the base buffer, shows mostly a circular profile after the beam travels through the capillary with the running buffer. PEG exhibits a similar profile as Tris-CHES buffer that generates the best wave-mixing signal, while linear polyacrylamide and pullulan shrink and distort laser beams.

Performance of SDS-CGE depends on some sample preparation steps including protein denaturing to avoid fluctuation in migration time. The SDS reagent may denature protein in three different ways: the denaturing process can be done first before labeling the protein, the denaturing and labeling processes can be performed simultaneously, or the labeling process can be done prior to denaturing the protein.[5] The first method prohibits a label from accessing protein sites since SDS binds to protein chains with its hydrocarbon tail.[30] The last method provides the best labeling

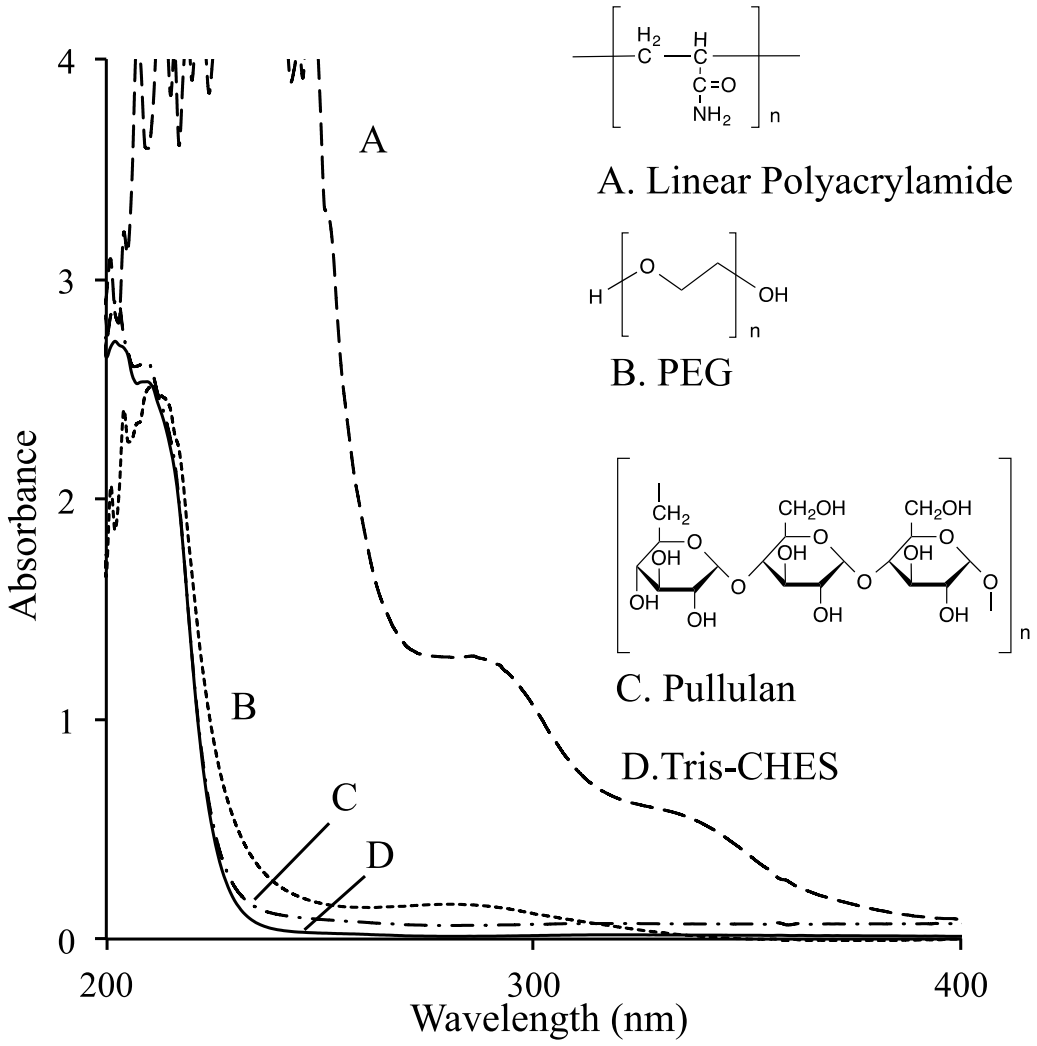

Figure 4.13 Conventional UV-visible absorption spectra of (A) linear polyacrylamide 4%, (B) PEG (3%), (C) pullulan (6%), and (D) Tris-CHES buffer (100 mM). SDS-CGE matrices are dissolved in 100 mM Tris-CHES buffer.

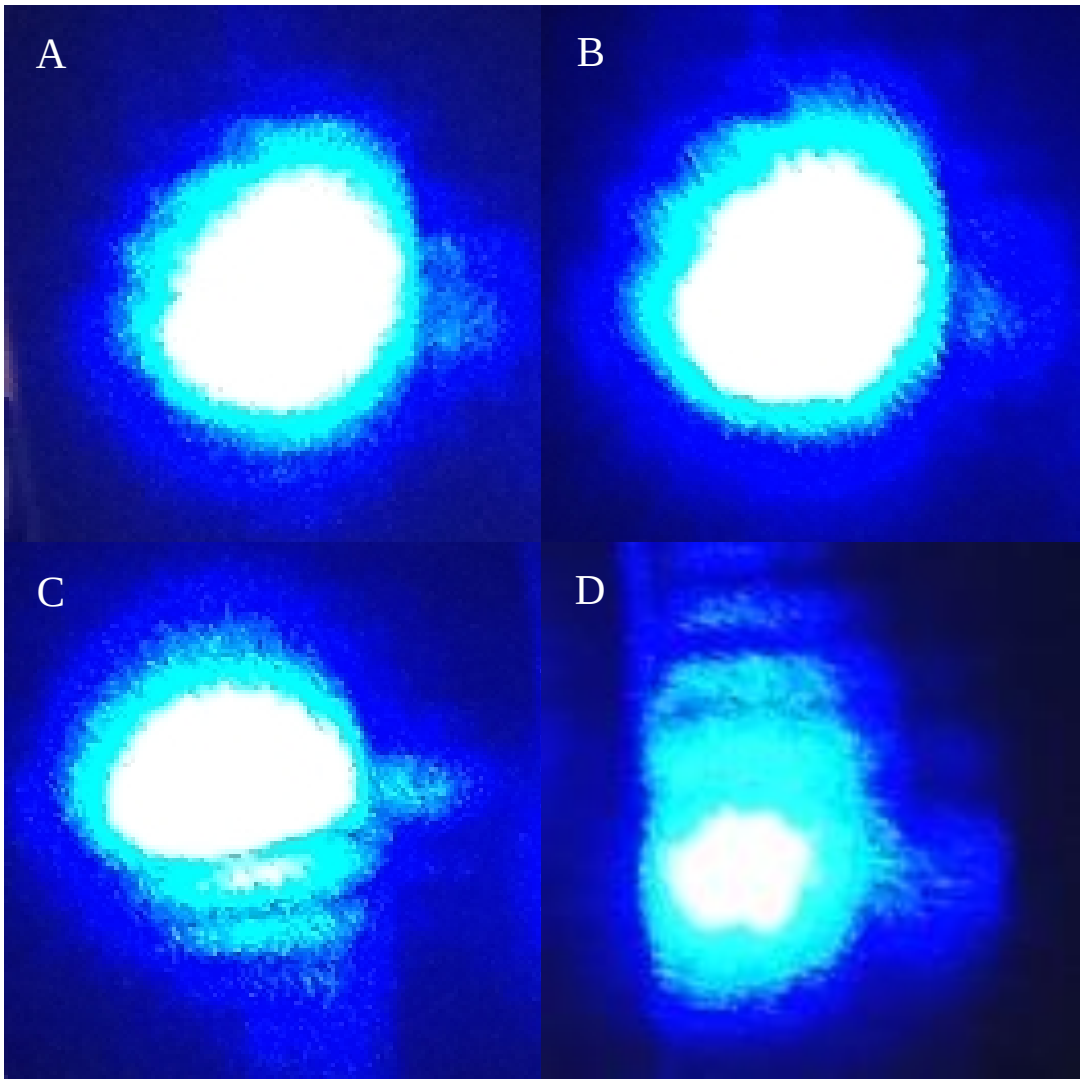

Figure 4.14 Photos of excitation laser beam profiles after passing through the capillary filled with (A) 100 mM Tris-CHES buffer, (B) PEG (3%), (C) linear polyacrylamide (4%), and (D) pullulan (6%). All the sieving matrices are dissolved in 100 mM Tris-CHES buffer.

efficiency, as confirmed UV-visible absorption data.

The use of a proper dynamic coating and a gel matrix in SDS-CGE is critical in successful separation of proteins. Figure 4.15 shows electropherogram for FITC-conjugated β-lactoglobulin and bovine serum albumin (BSA) in an UltraTrol-LN-coated capillary filled with a sieving matrix, without recoating, with refreshed dynamic coating, and with gel matrix after consecutive runs. In run 1, the first two peaks are from FITC-conjugated β-lactoglobulin. If FITC conjugates to a protein before it is fully labeled, the excess free label can be hindered from accessing the protein due to the protein structure or protein-conjugated labels that may result in inconsistent charges, yielding multiple peaks. Runs 2 and 3 demonstrate the necessity of recoating and refilling the dynamic coating of PEG for reproducible runs. The untreated capillary leads to gradual extrusion of the matrix out of the capillary due to the electroosmotic pressure when water-soluble and low viscosity polymer matrix is employed.[14] Thus, UltraTrol™ is introduced into the capillary as a dynamic pre-coating to overcome this problem. UltraTrol™ LN is used to pre-coat the silica capillary to suppress EOF for the CE run; however, the coating is easily removed by rinsing with a strong base. Due to the nature of PEG and the dynamic coating, it is necessary to recoat the capillary and refresh the matrix after each run, which only takes 4 to 8 minutes.

Figure 4.16 shows DFWM SDS-CGE electropherograms for seven standard proteins using different percentages of PEG (1.0, 3.0 and 5.0 %). Although 5.0% PEG provides better resolution than 3.0% and 1.0 % PEG, the higher PEG system requires a longer analysis time, which could lead to poor reproducibility due to current

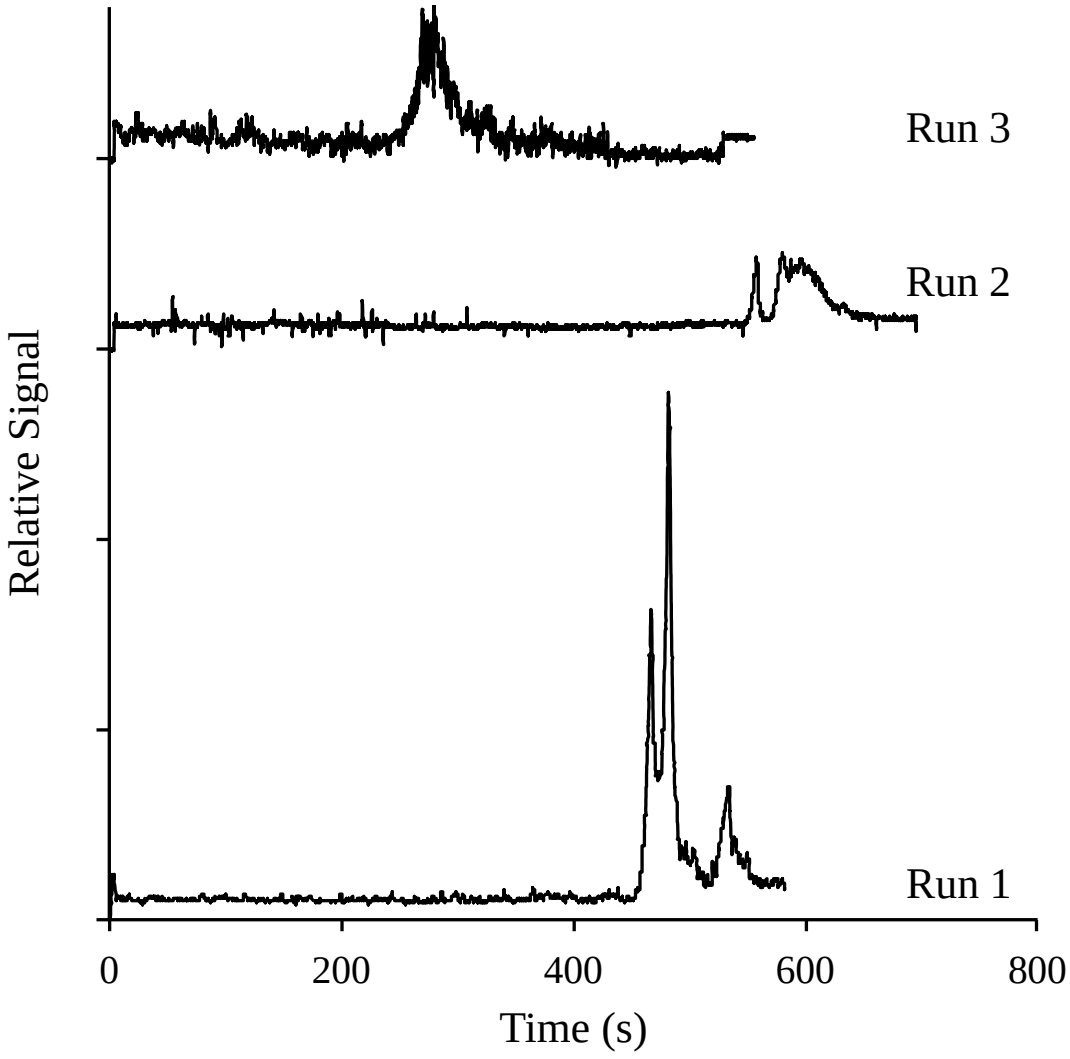

Figure 4.15 Electropherograms of consecutive CE separation runs for FITC-conjugated β-lactoglobulin and BSA (1 mg/mL) where the coating and sieving matrices are not refreshed after each run. UltraTrol LN-coated capillary, 75 µm i.d., 50 cm (30 cm effective length), -15 kV, 12 µA, electrokinetic injection for 5 s, 100 mM Tris-CHES (pH 8.9) BGE and 3% PEG. Detection by DFWM using a 473 nm laser.

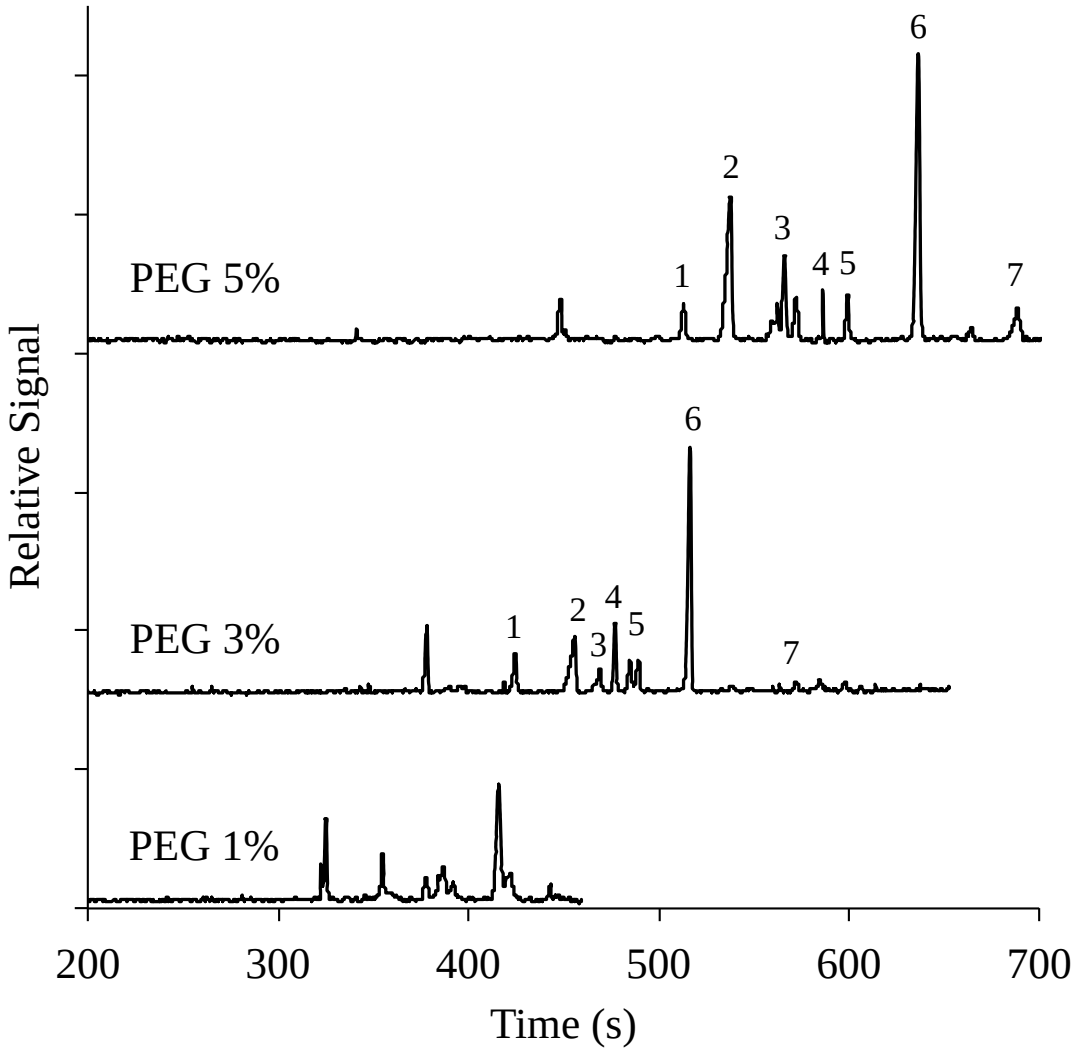

Figure 4.16 Electropherograms of FITC-conjugated standard proteins in different concentrations of PEG. Peak 1, lysozome (14.4 kDa); 2, β-lactoglobulin (18.4 kDa); 3, REase Bsp98I (25.0 kDa); 4, lactate dehydrogenase (35.0 kDa); 5, ovalbumin (45.0 kDa); 6, bovine serum albumin (66.2 kDa); and 7, β-galactosidase (116 kDa). Protein standards are denatured prior to labeling. Capillary: 75 µm i.d., 50 cm (30 cm effective length), -15 kV, 12 µA, 2 s injections. Sieving buffer: 100 mM Tris-CHES, 0.1% SDS and PEG (1, 3, or 5%). Protein concentration (0.1-0.2 mg/mL).

fluctuations. PEG at 3% yields reproducible protein separation that is sufficient to determine molecular weight with shorter analysis time as compared to that of 5% PEG. In addition, the lower percentage provides less viscosity to the solution, which is desirable for refreshing gel matrix between runs.

Figure 4.17 shows electropherograms of seven standard proteins including lysozome, β-lactoglobulin, REase Bsp98I, lactate dehydrogenase, ovalbumin, BSA and β-galactosidase obtained under different applied voltage levels. The optimal range of voltage for a CE system depends on its BGE, sieving matrix and capillary length. The resolution does not change drastically between 19 kV and 16 kV. Each peak becomes lower and wider as the voltage decreases, as expected, and it is kept above 16 kV for this system to obtain sufficient separation. The migration times for proteins decrease as separation voltage is increased. Current levels fluctuate when applied voltage is set over 19 kV, leading to poor reproducibility.

Figure 4.18 presents reproducible separation of FITC-conjugated standard proteins by CGE-DFWM using a 488 nm laser. The CE separation parameters, as discussed earlier: running buffer 100 mM Tris-CHES, 0.1% SDS and 3% PEG, 17.9 kV, and 5 s injection time. A linear relationship (R^2=0.99) is observed by plotting the logarithm of the molecular mass of standard proteins (14,400-116,000 Da) and average migration time of the protein standards (Figure 4.19). The calibration curve is mostly introduced to determine the molecular mass of a protein. The statistical data are summarized in Table 4.1. Relative standard deviations for migration time (RSD_T) range from 0.79-1.4%. The slight drift of migration time may have been due to some drift in the capillary temperature.[5]

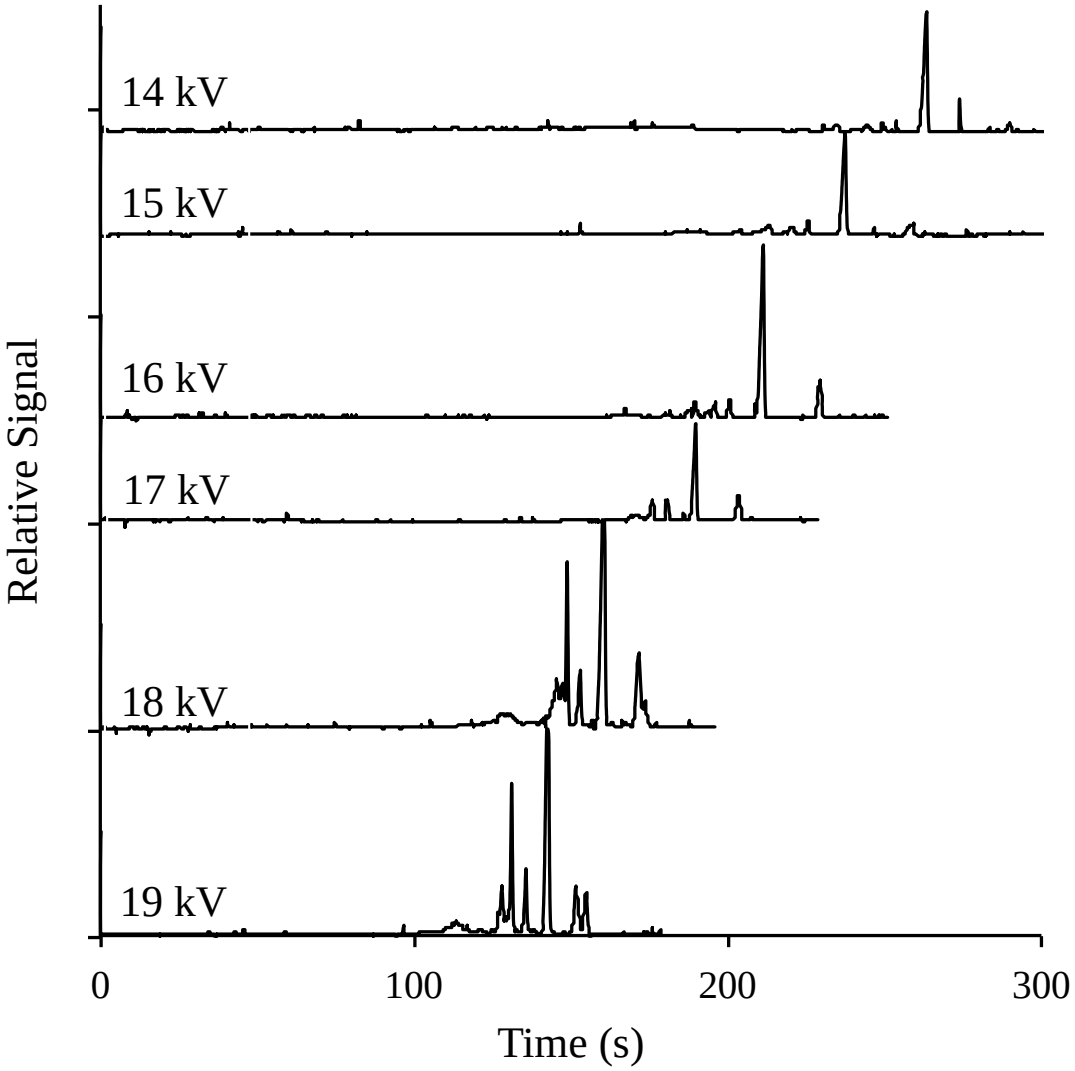

Figure 4.17 Electropherograms of standard proteins under different applied CE voltage levels. Capillary: 75 µm i.d., 30 cm (15 cm effective length), -19 kV to -14 kV, 2-s injection. Sieving buffer: 100 mM Tris-CHES, 0.1% SDS and 3% PEG. Protein concentration: 0.1-0.2 mg/mL.

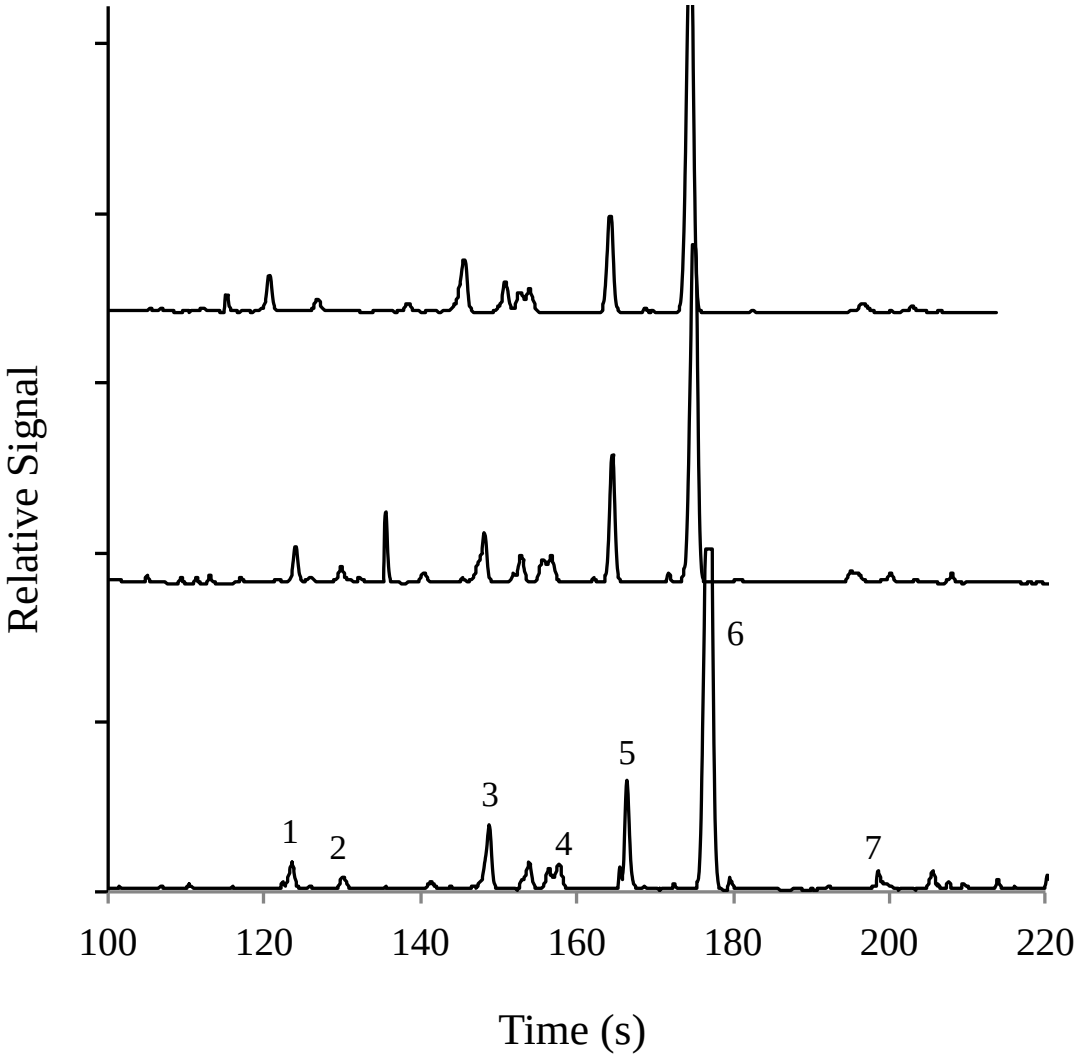

Figure 4.18 Reproducible electropherograms of seven standard proteins. Peak 1, lysozome (14.4 kDa), 2, β-lactoglobulin (18.4 kDa), 3, REase Bsp98I (25.0 kDa), 4, lactate dehydrogenase (35.0 kDa), 5, ovalbumin (45.0 kDa), 6, bovine serum albumin (66.2 kDa), and 7, β-galactosidase (116 kDa). The concentrations of the proteins range from 10 to 20 μg/mL. Capillary: 75 μm i.d., 30 cm (15 cm effective length), -17.9 kV, 5 s injection, sieving buffer 100 mM Tris-CHES, 0.1% SDS and 3% PEG.

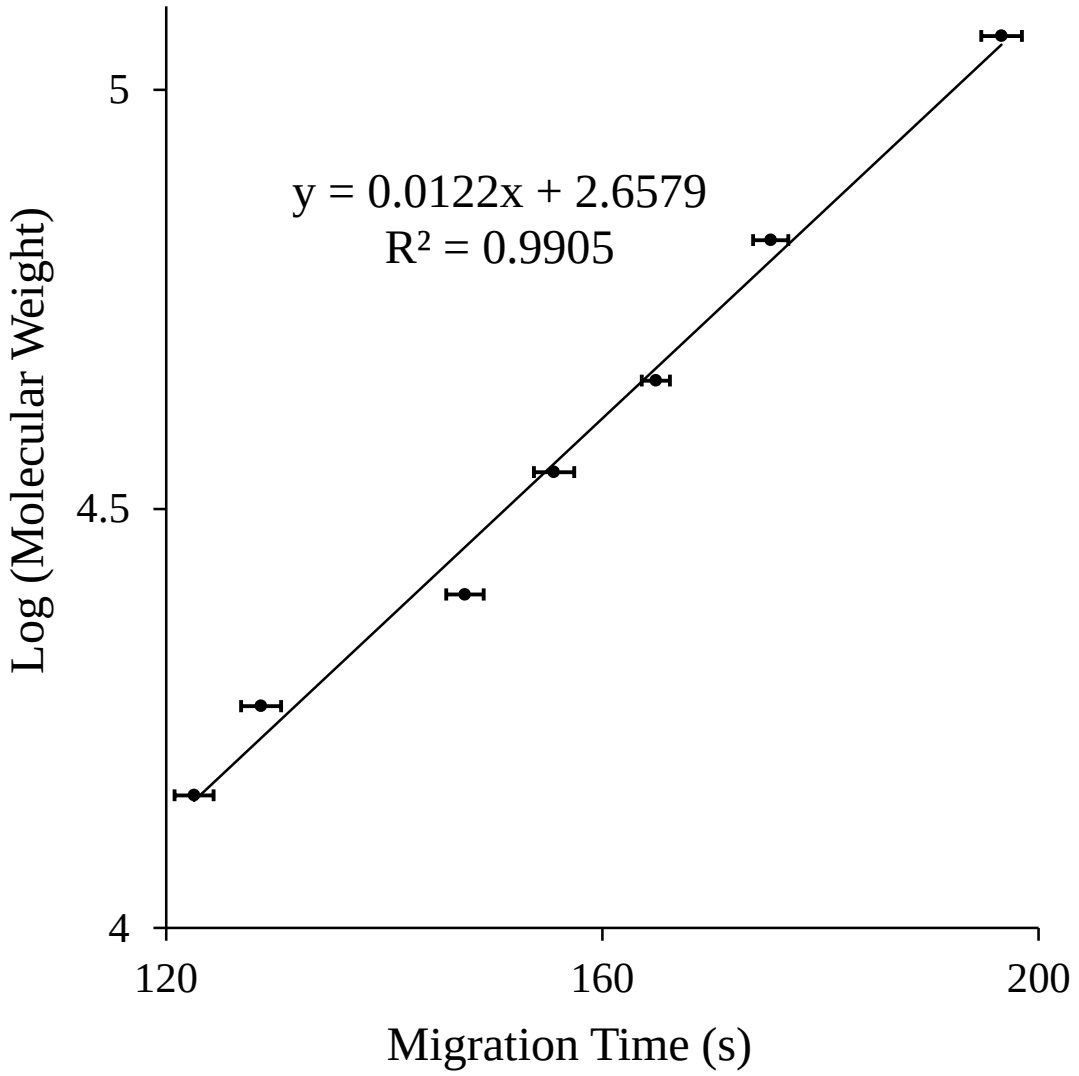

Figure 4.19 Molecular weight standard curves obtained by plotting the logarithm of molecular weights versus migration times for FITC-conjugated protein standards using DFWM-CGE.

Table 4.1 Statistical data of standard protein ladder with CGE and DFWM

Peak Number	Protein	Molecular weight (g/mol)	Average migration time (s)	RSD_T (%)
1	lysosome	14,400	124.6	1.4
2	β-lactoglobulin	18,400	128.7	1.4
3	REase Bsp98I	25,000	147.4	1.2
4	lactate dehydrogenase	35,000	155.6	1.2
5	Ovalbumin	45,000	164.9	0.79
6	bovine serum albumin	66,200	175.4	0.93
7	β-galactosidase	116,000	196.6	1.1

4.5 Conclusion

DFWM-CE provides ultrasensitive absorption-based optical detection and reliable molecular weight-based separation of various FITC-conjugated proteins. The DFWM signal has a quadratic dependence on analyte concentration, and protein detection limits of picomolar and zeptomole are determined. Capillary electrophoresis allows separation based on various modes: (1) size-to-charge ratio, (2) hydrophobicity and (3) molecular weight. DFWM offers unique and significant advantages, including small probe volume, coherent laser-like signals, virtually 100% optical signal collection efficiency, zeptomole detection sensitivity, compact and portable detection setup, low laser power requirements, and the ability to detect both fluorescing and non-fluorescing molecules.

4.6 Reference

(1) Pedersen, J. T.; Heegaard, N. H. H. *Anal Chem* **2013**, *85*, 4215.

(2) Pryor, N. E.; Moss, M. A., *et al Electrophoresis* **2014**, *35*, 1814.

(3) Ghazani, A. A.; Castro, C. M., *et al Neoplasia* **2012**, *14*, 388.

(4) Chen, Z.; Wu, J., *et al J. Chromatogr. A* **2001**, *914*, 293.

(5) Hu, S.; Jiang, J., *et al Electrophoresis* **2002**, *23*, 3136.

(6) Sutthent, R.; Gaudart, N., *et al Journal of clinical microbiology* **2003**, *41*, 1016.

(7) Tang, S.; Hewlett, I. *The Journal of infectious diseases* **2010**, *201 Suppl 1*, S59.

(8) Baker, D. R. *Capillary electrophoresis*.

(9) Osbourn, D. M.; Weiss, D. J., *et al Electrophoresis* **2000**, *21*, 2768.

(10) Mikkers, F. E. P.; Everaerts, F. M., *et al J Chromatogr* **1979**, *169*, 11.

(11) Bharadwaj, R.; Santiago, J. G. *J Fluid Mech* **2005**, *543*, 57.

(12) Hancu, G.; Simon, B., *et al Advanced pharmaceutical bulletin* **2013**, *3*, 1.

(13) Altria, K. D.; McLean, R. *J Pharmaceut Biomed* **1998**, *18*, 807.

(14) Nakatani, M.; Shibukawa, A., *et al J Chromatogr A* **1994**, *672*, 213.

(15) Horvath, J.; Dolnik, V. *Electrophoresis* **2001**, *22*, 644.

(16) Guttman, A. *Electrophoresis* **1996**, *17*, 1333.

(17) Hu, S.; Zhang, L., *et al Electrophoresis* **2001**, *22*, 3677.

(18) Cohen, A. S.; Karger, B. L. *Journal of Chromatography* **1987**, *397*, 409.

(19) Tsuji, K. *Journal of Chromatography* **1991**, *550*, 823.

(20) Widhalm, A.; Schwer, C., *et al Journal of Chromatography* **1991**, *549*, 446.

(21) Zhu, M. D.; Hansen, D. L., *et al Journal of Chromatography* **1989**, *480*, 311.

(22) Werner, W. E.; Demorest, D. M., *et al Anal Biochem* **1993**, *212*, 253.

(23) Zhang, K.; Yang, L., *et al Analyst* **2014**, *139*, 2379.

(24) Yao, S.; Anex, D. S., *et al Proceedings of the National Academy of Sciences of the United States of America* **1999**, *96*, 5372.

(25) Zhu, Z. F.; Lu, J. J., *et al Analytica Chimica Acta* **2012**, *709*, 21.

(26) Nunes, J. A.; Tong, W. G. *Anal Chem* **1993**, *65*, 2990.

(27) Prata, C.; Bonnafous, P., *et al Electrophoresis* **2001**, *22*, 4129.

(28) García-Cañas, V.; Cifuentes, A. *Electrophoresis* **2008**, *29*, 294.

(29) Lander, J. P. *Handbook of Capillary and Microchip Electrophoresis and Associated Microtechniques*; Third ed.; CRC Press: Boca Raton, Florida, US, 2007.

(30) Bhuyan, A. K. *Biopolymers* **2010**, *93*, 186.

CHAPTER 5
ANALYSIS OF α-SYNUCLEIN BY DEGENERATE FOUR-WAVE MIXING COUPLED WITH CAPILLARY ELECTROPHORESIS

5.1 Abstract

Multi-photon nonlinear laser wave-mixing spectroscopy is a novel absorption-based technique that offers excellent detection sensitivity for biomedical applications including early diagnosis and investigation of neurodegenerative diseases. α-Synuclein is linked to Parkinson's disease (PD), and characterization of its oligomers and quantification of the protein may contribute to understanding PD. The laser wave-mixing signal intensity has a quadratic dependence on analyte concentration, and hence, the technique is effective in monitoring small changes in concentration within biofluids. A wide variety of labels can be employed for laser wave-mixing detection due to its ability to detect both chromophores and fluorophores. In this chapter, three types of labels are described for the detection of α-synuclein: two types of fluorophores and a chromophore. Wave mixing detection limits of PD-related protein conjugated with fluorescein isothiocyanate; QSY 35 acetic acid, succinimidyl ester, and Chromeo P503 are 1.4 x 10^{-13} M, 1.4 x10^{-10} M and 1.9 x 10^{-13} M, corresponding to mass detection limits of 1.1 x 10^{-23} mol, 1.1 x 10^{-20} mol, and 1.5 x 10^{-23} mol, respectively. This chapter also presents molecular-based separation and quantification of α-synuclein by degenerate four-wave mixing coupled with capillary electrophoresis.

5.2 Introduction

5.2.1 PARKINSON'S DISEASE

Parkinson's disease (PD) is the second most predominant neurodegenerative disease in the U.S., afflicting 1-2 % of the population aged 65 and over.[1] The disease is clinically characterized by the progressive dysfunction of several motor and non-motor neurological functions.[2] Degeneration of dopamine producing neurons of the substantia nigra pars compacta region of the basal ganglia that helps control voluntary movement has been confirmed for PD patients.[3] Patients generally show the following symptoms: slowness of movement, tremors, rigidity, poor balance, cognitive and psychiatric disturbance.[3] One of the challenges for Parkinson's is early diagnosis at preclinical stages. A series of studies shows that intercellular accumulation of Lewy bodies (LB), the hallmark of PD, appears 6 years or more before the symptoms emerge.[4] Thus, accurate quantifications and detection of LB-related proteins such as α-synuclein[5] at a sensitive level is key to pave the way to understanding PD. This chapter demonstrates sensitive detection at picomolar levels and quantification of α-synuclein and separation of monomer from oligomers by the nonlinear absorption detection method interfaced with capillary gel electrophoresis (CE).

5.2.2 α-SYNUCLEIN AS CANDIDATE BIOMARKER FOR PARKINSON'S DISEASE

α-Synuclein is a 14 kDa, 140-residue neural protein highly expressed in central neurons and localized in presynaptic terminals.[6] The protein is a major component of LBs (aggregated proteins), the hallmark pathology of PD and those

with dementia.[7,8] The mechanisms and inclusion of α-synuclein in LBs do not explain the pathogenesis of the neurodegenerative disease, and it remains unclear whether LBs are a cause or a symptom.[9]

Parkinson's disease was believed to be genetically inherited, since several families with PD history were found to possess a mutation of α-synuclein. Based on this finding, numerous studies developed a hypothesis that both point mutations and multiplications in the α-synuclein gene cause PD.[3] Lee and Trojanowski suggested that β-sheet structure of α-synuclein, readily oligomerized and aggregated, is induced by both pathogenic mutations and elevated levels of α-synuclein.[10] The aggregation of the protein (5-25 μm)[11] is accelerated by various types of post-translational modification, such as Ser-129 phosphorylation, calpain-mediated cleavage, O-glycosylation, tyrosine nitration, methionine oxidation, and C-terminal truncation.[12]

Currently, the toxicity of the oligomerized and protofibril intermediate α-synuclein is widely accepted.[13,14] In addition to the LB hallmark, destruction of dopaminergic neurons are observed in early stages of PD.[15-17] Conway *et al.* executed a study indicating that the formation of oligomerized α-synuclein can be accelerated by dopamine, although the mechanism remains unclear.[18] Südhof *et al.* recently suggested that the formation of soluble N-ethylmaleimide sensitive factor attachment protein receptor (SNARE) complex, critical to the vesicle fusion leading to dopamine release, is promoted by α-synuclein binding to a vesicular SNARE protein, synaptobrevin-2.[19] On the other hand, in 2013, Choi *et al.* performed a study indicating that large α-synuclein oligomers inhibit neuronal SNARE-meditated vesicle lipid mixing (Figure 5.1).[8]

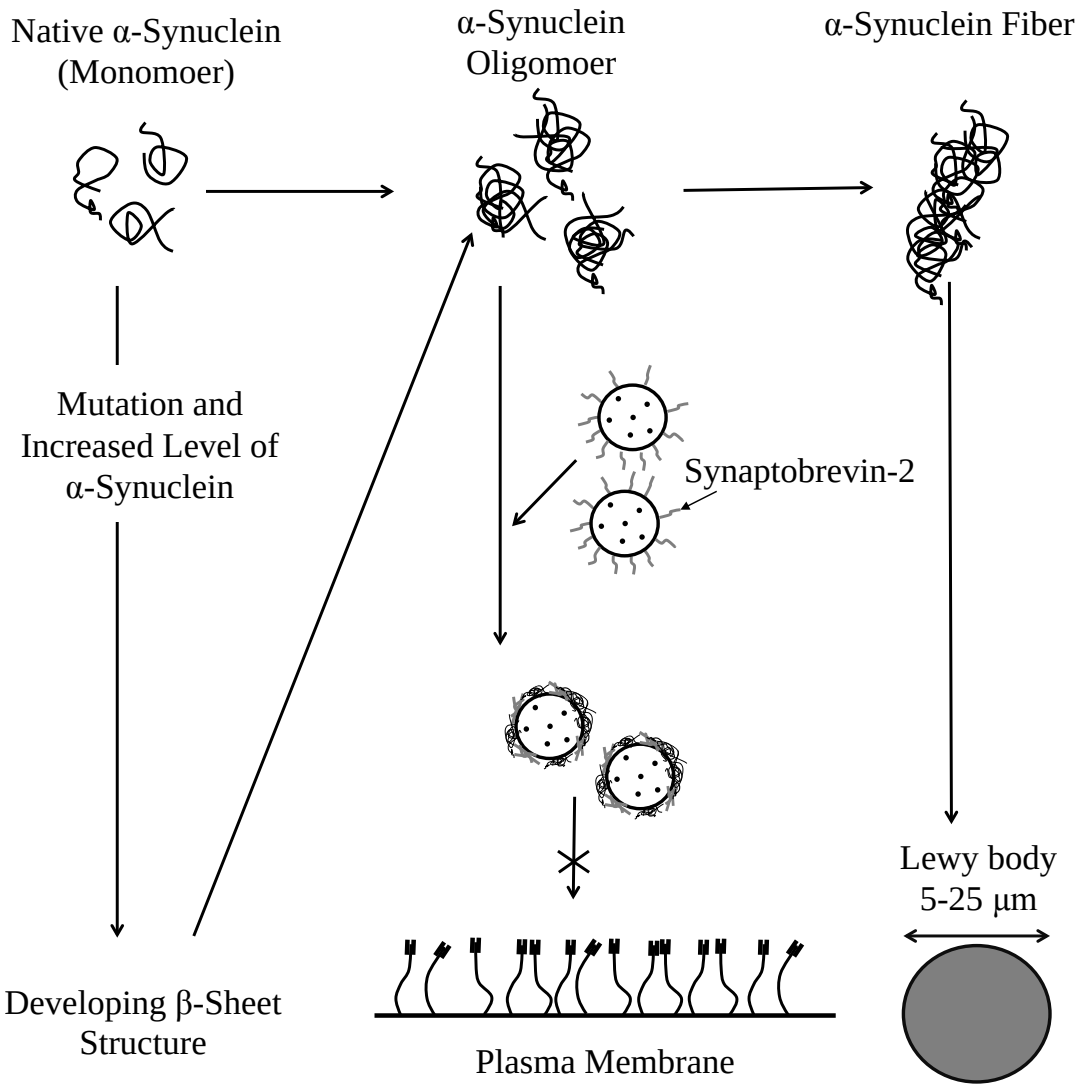

Figure 5.1 Possible toxicity pathways of the monomer, oligomerized, and fibril α-synuclein (Ref 8 and 10).

In addition to cerebrospinal fluid (CSF) analysis, levels of α-synuclein in blood samples have been investigated to develop less invasive diagnostic methods for PD. Kasuga *et al.* reviewed studies of blood samples of a control group and PD patients to compare α-synuclein levels. They concluded that, due to the lack of a simple and prominent ultrasensitive detection and quantification method that can differentiate α-synuclein species, such as truncated, phosphorylated, monomeric, and oligomeric forms[20], the levels of PD-related proteins are inconsistent in the literature studies. In the next section of this chapter, the capabilities of DFWM and how they can resolve these issues are discussed.

5.2.3 CLINICALLY USED DETECTION AND QUANTIFICATION METHOD FOR α-SYNUCLEIN

A sensitive detection method is needed in order to develop an early diagnostic tool for Parkinson's disease. Currently, enzyme-linked immunosorbent assay (ELISA) is commonly used for detecting monomeric and oligomeric forms of α-synuclein in CSF and serum; however, ELISA is usually designed specifically for analyzing a single analyte and cannot be coupled to a separation device. As shown in Figure 5.2, sandwich ELISA is a time-consuming assay that requires multiple steps to detect and quantify a target protein. The ELISA well is coated with a target protein-specific antibody that binds to the protein when a sample is introduced. The enzyme-linked antibody may react with an unbound site of the protein. Free antibodies that do not react with the protein are removed by washing. Additionally, ELISA yields inconsistent results (Table 5.1)[21-26] for control groups due to background absorption and cross-reactivity interference.[27] The assay may yield false-positive results, i.e., a

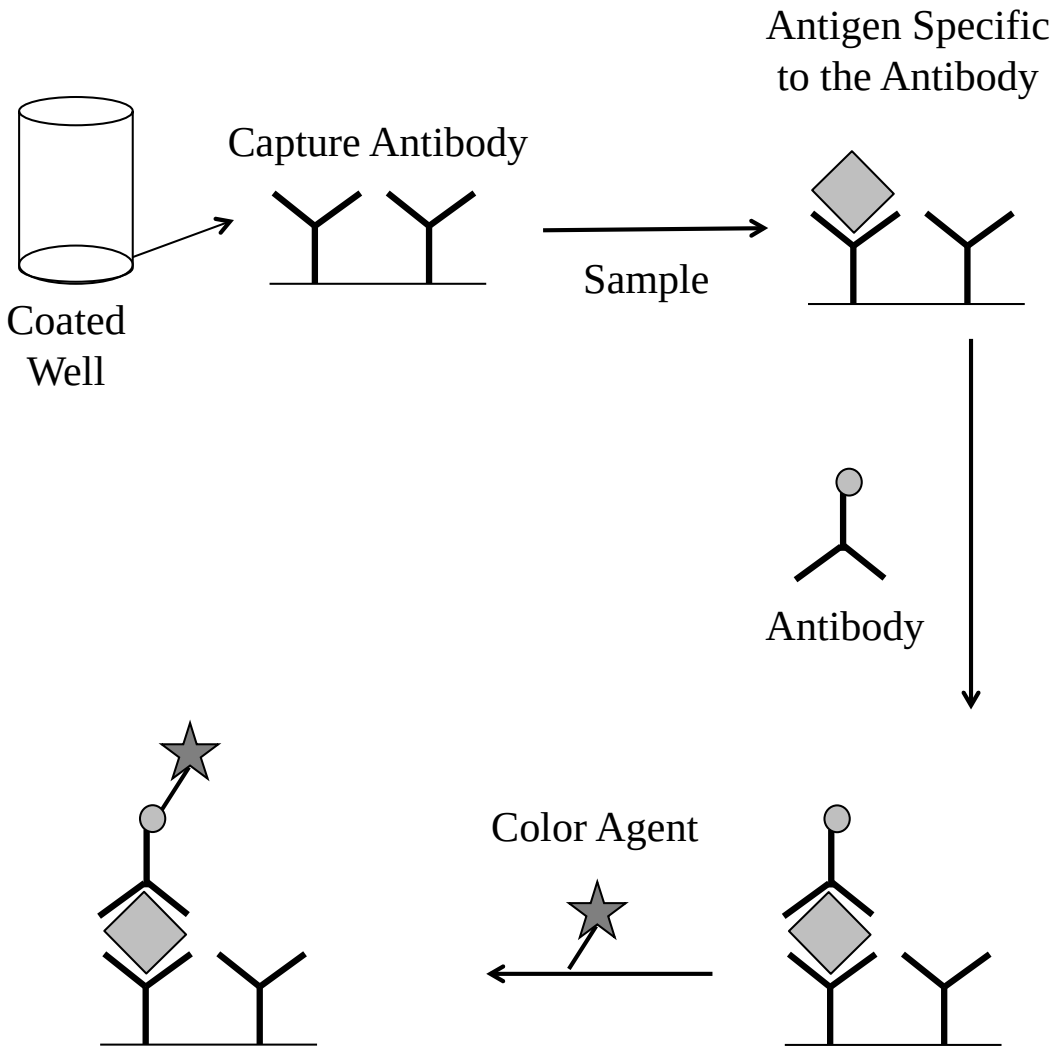

Figure 5.2 Mechanisms of sandwich ELISA. Quantification is allowed by an enzyme that can generate color. Multiple steps are required for the quantification.

Table 5.1 ELISA provides inconsistent quantification results for the control group.

Level of α-synuclein	Detection method	Concentration of α-synuclein for control group	Concentration of α-synuclein for PD patients	References
CSF ↓	ELISA	2.3×10^{-10} M	1.9×10^{-10} M	21
CSF ↓	ELISA	4.1×10^{-10} M	2.0×10^{-10} M	22
CSF ↓	ELISA	4.8×10^{-9} M	3.0×10^{-9} M	23
Plasma ↑	ELISA	5.2×10^{-12} M	5.5×10^{-12} M	24
Plasma ↑	ELISA	8.2×10^{-10} M	8.2×10^{-10} M	25
Plasma →	Flow cytometric assay	2.7×10^{-9}M	2.7×10^{-9} M	26

signal may not be generated by α-synuclein antigen-antibody reaction or specify monomeric and oligomeric forms.

The wave-mixing detection limit is orders of magnitude better than those of conventional absorption techniques, and comparable or better than those of ELISA. Laser wave mixing also provides better specificity without the use of expensive antibody and shorter analysis times. Sodium dodecyl sulfate-capillary gel electrophoresis (CGE) or capillary zone electrophoresis (CZE) can distinguish monomeric and oligomeric forms. Unlike laser-induced fluorescence (LIF), DFWM is capable of detecting both fluorophores and chromophores. Moreover, the DFWM signal is a coherent laser-like signal and it can be detected conveniently with high collection efficiency and high S/N.

5.2.4 DFWM AS AN ALTERNATIVE TO CURRENT α-SYNUCLEIN DETECTION METHODS

The wave-mixing signal has a quadratic dependence on extinction coefficient, and hence, it can measure smaller changes in analyte properties more efficiently. DFWM yields excellent sensitivity and high spatial resolution and it can effectively probe analytes in a thin capillary (Figure 5.3). Two input laser beams are focused and mixed by a biconvex lens on the capillary. The diameter of the laser beam is calculated by the following equation (Equation 7.1)

$$2\omega_0 = \left(\frac{4\lambda}{\pi}\right)\frac{F}{D} \qquad (1)$$

where, $2\omega_0$ represents the beam diameter at the focal point and it depends on the wavelength of the excitation laser source (λ), the diameter of the input beam before it

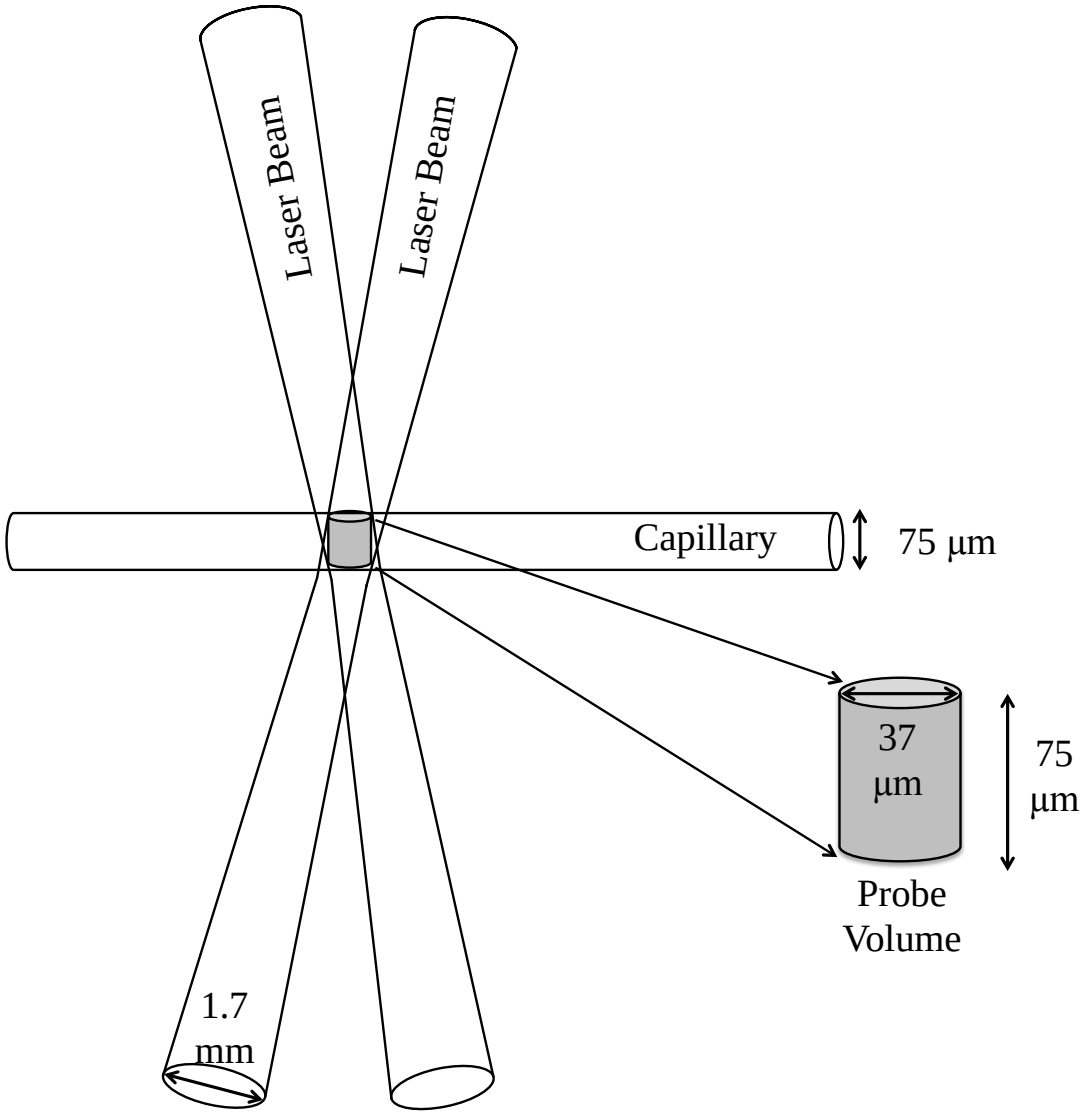

Figure 5.3 DFWM yields excellent mass detection limits since the analyte probe volume is very small (nanoliter to picoliter range).

is focused (*D*), and the focal length of the lens (*F*). The laser probe volume in DFWM

is in the picoliter range, and hence, the required sample size is small.

5.3 Experimental

5.3.1 Forward-Scattering DFWM Experimental Setup

Figure 5.4 shows a schematic diagram of forward-scattering DFWM optical setup interfaced to a CE system. A continuous-wave 488 nm blue laser with adjustable power tuned to 40 mW (Coherent, Santa Clara, CA) and a 50 mW 473 nm diode laser (CNI, Changchun, China) are used for visible-wavelength DFWM. A 266 nm UV pulsed laser (CNI, Changchun, Jilin, China, 20 mW, 7kHz) is used in UV DFWM detection of α-synuclein. The laser output is first split by a beamsplitter (R:T 30:70) to create 2 input beams. The weaker (reflected) input beam is modulated by an optical chopper (Stanford Research Systems, Sunnyvale, CA, SR541) at 200 Hz. The two input laser beams travel the same distances and then cross at an angle of 0.95° (488 nm laser), 1.5° (473 nm laser), and 1.5° (266 nm laser). The excitation lasers yield beam diameters of 1.70 mm (488 nm), 1.20 mm (473 nm) and 1.10 mm (266 nm), and probe volumes of 78 pL (488 nm), 58 pL (473 nm), and 55 pL (266 nm). A 75 μm i.d. fused-silica capillary (Molex, Lisle, IL) is used as the analyte cell, and a small portion of the capillary coating is removed by a butane flame so that the input laser beams can propagate across the capillary. The wave-mixing signal is collected by a photodetector (Thorlabs, Newton, NJ, PDA25K). The optical chopper, the photodetector and the computer are interfaced to a lock-in amplifier (Stanford Research Systems, Sunnyvale, CA, SR810 DSP).

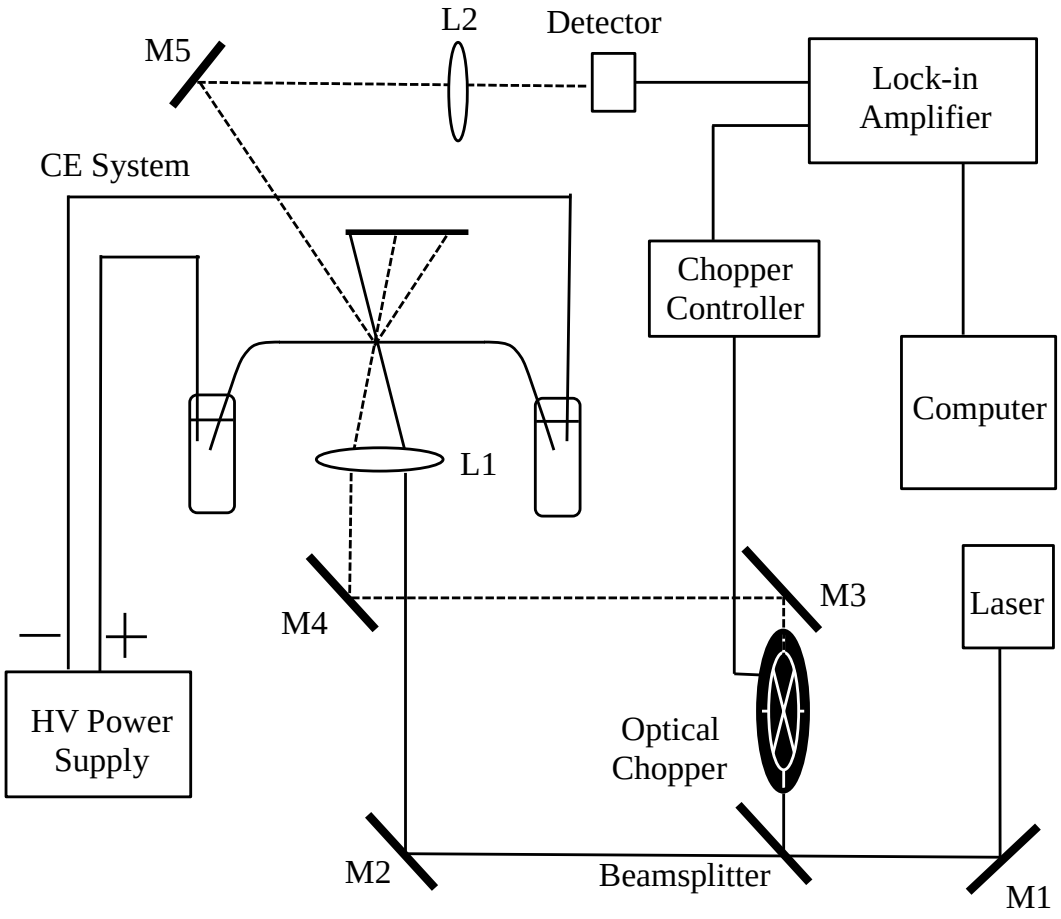

Figure 5.4 Forward-scattering DFWM experimental setup coupled with CE system for α-synuclein detection.

5.3.2 CHEMICALS

Solutions used for this study are prepared with distilled water from a compact water distillation system (Waterwise, Leesburg, FL, 4000). Borax, Tris base, sodium dodecyl sulfate (SDS), sodium bicarbonate, and poly (ethylene glycol) (PEG, 10,000)

are purchased from Sigma-Aldrich (St. Louis, MO). Fluorescein isothiocyanate (FITC), CHES, hydrochloric acid, sodium hydroxide, unstained protein ladder, N,N-*Dimethylformamide* (DMF), and dialysis tubing (MW_{CO} 12-14 kDa) are purchased from Thermo Fisher Scientific (Waltham, MA). The chromophore label, QSY 35 acetic acid, succinimidyl ester is obtained from Life Technologies (Carlsbad, CA). The capillary is coated with Ultratrol LN (Target Discovery, Palo Alto, CA) by flowing through the solution for 2 to 5 minutes, and a sieving matrix is prepared by flowing PEG in the sample cell. Recombinant α-synuclein, a DNA sequence encoding the human α-synuclein sequence, is expressed in *E. coli* (rPeptide, Bogart, GA). Fluorophore protein label, Chromeo^{TM} P503, is purchased from Active Motif (Carlsbad, CA).

5.3.3 FLUORESCEIN ISOTHIOCYANATE-CONJUGATED PROTEIN

Sodium borate reaction buffer (50 mM, pH 8.6) is prepared by dissolving borax in distilled water, and pH is adjusted by using 1.0 M HCl. Proteins are dissolved in the buffer at 2.0-2.2 mg/mL. FITC, a fluorophore label, is dissolved in DMF (10-20 mg/mL) to react with proteins. The mixture of FITC and protein(s) is allowed to proceed for 1 hour in the dark. Dialysis is performed to remove free FITC using regenerated cellulose dialysis tubing (MW_{CO} 12,000 kDa – 14,000 kDa) and buffer exchange is performed simultaneously to prepare FITC-conjugated protein in Tris-CHES buffer (25 mM) with SDS (0.1%).

Molecular weight and migration time calibration curves are generated by running FITC-conjugated protein ladder that includes seven proteins: lysozyme (14.4 kDa), β-lactoglobulin (18.4 kDa), REase Bsp98I (25.0 kDa), lactate dehydrogenase (35.0 kDa), ovalbumin (45.0 kDa), bovine serum albumin (66.2 kDa), and β-galactosidase (116 kDa). The unstained proteins are present in the solution at various concentration levels (0.10 – 0.20 mg/mL). The stock solution (150 µL) is aliquoted and dialyzed into conjugation buffer for the protein ladder to react with FITC using the previously stated protocol.

5.3.4 QSY 35 ACETIC ACID, SUCCINIMIDYL ESTER-CONJUGATED α-SYNUCLEIN

Lyophilized α-synuclein is resuspended in 450 µL water to obtain 2.2 mg/mL protein in Tris-HCl and NaCl buffer (pH 7.4). The buffer is replaced with sodium carbonate-sodium bicarbonate reaction buffer (100 mM, pH 8.3) using regenerated cellulose dialysis tubing. α-Synuclein is reacted with QSY 35 in DMF (20 mg/mL) for 1 hour in the dark (1:20). Excess dye is removed by dialysis while carbonate buffer is changed to Tris-CHES (100 mM) with 0.1% SDS.

5.3.5 CHROMEO P503-CONJUGATED PROTEIN

Using an aliquot of 2.2 mg/mL α-Synuclein (100 µL) prepared in section 5.3.4, Chromeo P503 is dissolved in DMF (5.0 mg/mL) and added to the aliquot dropwise to obtain a 1:4 ratio or greater. The solution is gently mixed for 30 minutes until the original color of the dye (blue) changes to red.

5.3.6 Capillary electrophoresis

Background electrolyte (BGE) Tris-CHES is prepared by dissolving Tris (1.04 g) and CHES (0.607 g) in distilled water (100 mL), and adjusting pH to 9.0. Sieving matrix is prepared by dissolving PEG (3%) into Tris-CHES buffer (100 mM) with 0.1% high purity electrophoresis-grade sodium dodecyl sulfate (SDS).

All the capillary electrophoresis (CE) runs are performed by a custom-built CE system described in previous chapters. The CE system has a fused-silica capillary (Molex, Lisle, IL) and a high voltage power supply (Glassman High Voltage, High Bridge, NJ) that is connected to platinum wires. Voltage is controlled by a custom-built voltage controller. Plastic reservoirs containing running buffer/samples are placed at each end of the capillary.

5.3.7 UV-Visible Absorption Spectra

UV-visible absorption spectra are obtained by a UV-visible spectrophotometer (Agilent, Santa Clara, CA, 8453) using 1 cm Quartz cuvettes. Absorption spectra are blanked using an appropriate solvent before measuring each analyte.

5.4 Results and Discussion

5.4.1 UV-visible analysis of α-synuclein and amine-reactive labels

Since DFWM is an absorption-based technique, labels are not required when the analyte absorbs the excitation source. Measuring absorption spectra of analytes allows one to choose an appropriate laser to use in a DFWM-CE setup. Figure 5.5 shows UV-visible absorption spectra of α-synuclein and labels used in this study. α-Synuclein absorbs UV wavelengths due to aromatic amino acid residues, such as

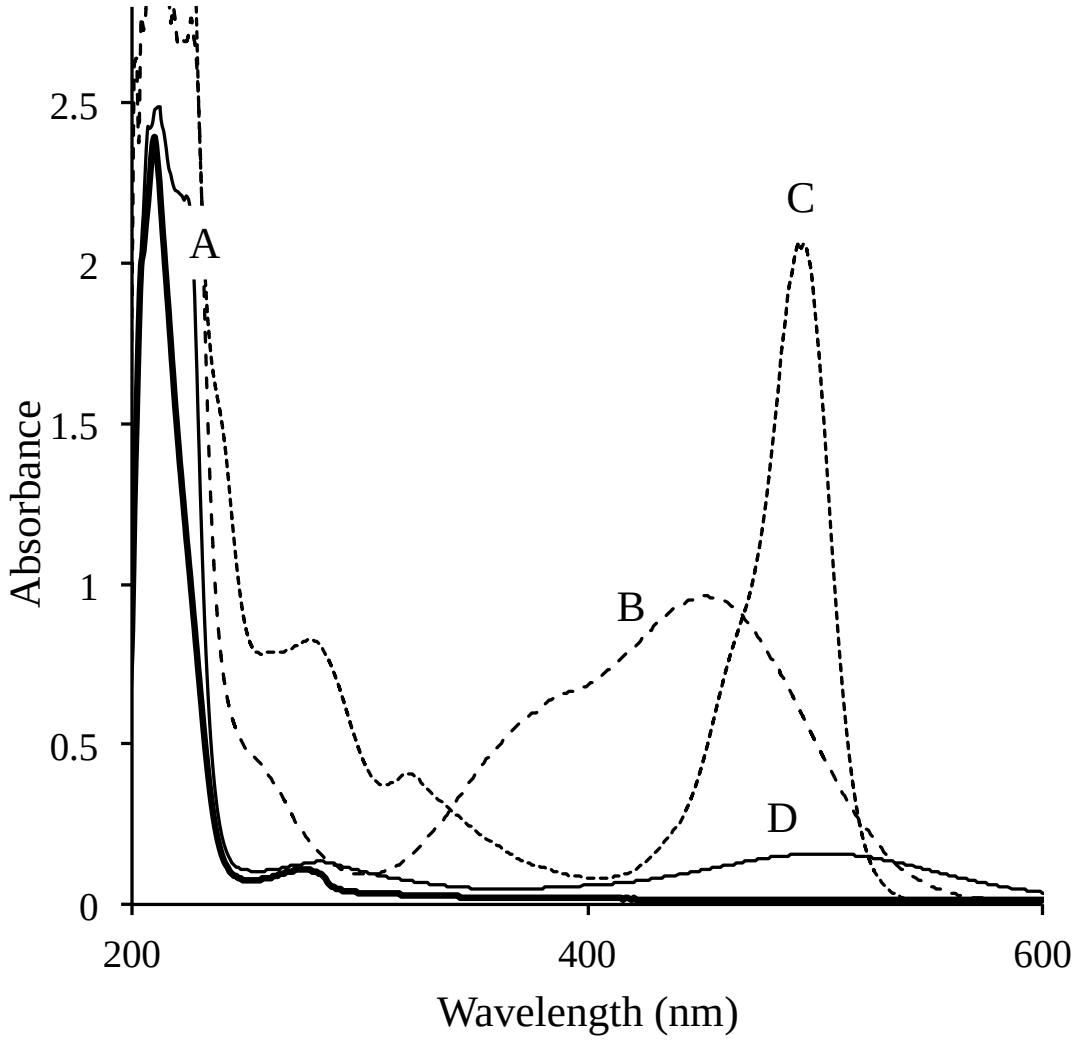

Figure 5.5 UV-visible absorption spectra of (A) α-synuclein (1.5 x 10^{-5} M), (B) QSY 35-conjugated protein (4.9 x 10^{-5} M), (C) FITC-conjugated protein (2.5 x 10^{-5} M), and (D) Chromeo P503-conjugated protein (6.4 x 10^{-6} M). A, B and D are in carbonate buffer (100 mM, pH 8.3), and C is in borate buffer (50 mM, pH 8.6).

tyrosine (Y) and phenylalanine (F); however, the protein scarcely absorbs at the 266 nm laser excitation wavelength. Nevertheless, DFWM yields good detection sensitivity and allows label-free detection of the native protein. Detection sensitivity can be significantly enhanced, by conjugating the protein with a label to increase the absorption coefficient. Since every protein possesses N-terminus, and lysine (K) is relatively abundant, amine-reactive dyes are widely used for protein labeling. According to the amino acid sequence of α-synuclein (Figure 5.6 B), 16 labeling sites are available for conjugation; however, due to steric hindrances and the protein conformation, not all the sites are accessible.

Figure 5.6 (A) shows molecular structures of amine-reactive dyes used in this study. FITC is a widely used amine-reactive fluorophore with excitation λ_{max} at 495 nm, an excitation coefficient of 70,000 $M^{-1}cm^{-1}$, and emission λ_{max} at 525 nm. In this study, 20-mole excess FITC is reacted with the protein for 1 hour before dialysis. QSY 35 is a chromophore label that is used as an acceptor of fluorescence resonance energy transfer (FRET) applications.[28] Its maximum absorbance is at 475 nm with an extinction coefficient of 23,000 $M^{-1}cm^{-1}$ that is suitable for DFWM with an excitation laser source of 488 nm or 473 nm. Chromeo^{TM} 503 displays maximum absorbance at 503 nm, and its labeling reaction time is only 30 minutes. The molecular structure of the fluorophore is unclear but Py-1 introduced by Wolfbeis appears to be an identical compound.[29]

The unique features of Chromeo P503 as a fluorophore label is shown in Figure 5.7. Its absorbance shifts in wavelength from 603 nm to 503 nm after conjugation with protein, resulting in the solution changing from red to blue.

A: α-Synuclein Labels

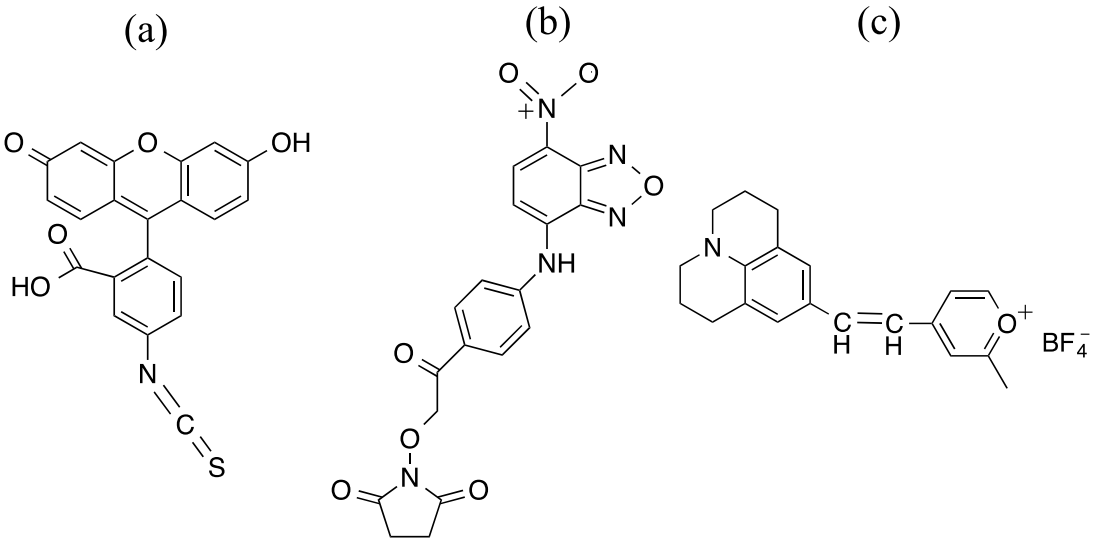

B: α-Synuclein Amino Acid Sequence: 16 Labeling Sites

10 20 30

MDVFM**K**GLS**K** A**K**EGVVAAAE **K**T**K**QGVAEAA

40 50 60

G**K**T**K**EGVLYV GS**K**T**K**EGVVH GVATVAE**K**T**K**

70 80 90

EQVTNVGGAV VTGVTAVAQ**K** TVEGAGSIAA

100 110 120

ATGFV**KK**DQL G**K**NEEGAPQE GILEDMPVDP

130 140

DNEAYEMPSE EGYQDYEPEA

Figure 5.6 (A) Amino acid sequence of α-synuclein. Lysine (K) and N-terminus are amine reactive sites. (B) Molecular structures of three amine reactive labels (a) FITC, (b) QSY 35 acetic acid, succinimidyl ester, and (c) Py-1.

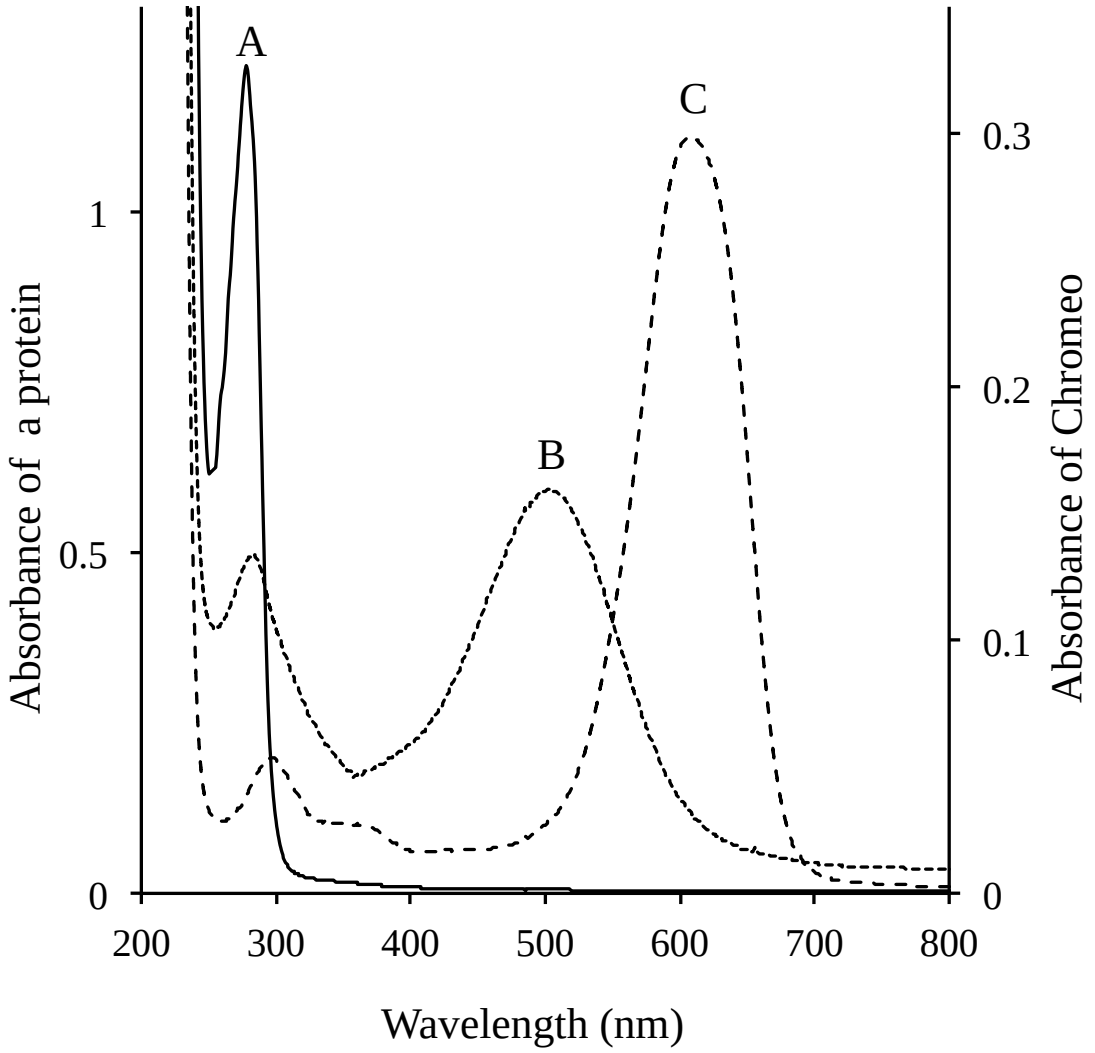

Figure 5.7 Wavelength shift observed for Chromeo P503. Conjugation with protein shifts approximately 100 nm. (A) BSA (3.0×10^{-5} M), (B) Chromeo P503-conjugated BSA (6.4×10^{-6} M), and (C) Chromeo P503 (6.4×10^{-6} M). All solutions are prepared in 100 mM sodium carbonate-sodium bicarbonate buffer (pH 8.3).

Chromeo P503-conjugated protein analysis is faster since the reaction time is shorter and it does not require dialysis when 488 nm laser is used as the excitation source. Extinction coefficient alters from 60,000 $M^{-1}cm^{-1}$ to 24,000 $M^{-1}cm^{-1}$ through the reaction when 4 molar excess label is introduced (manufacturer recommended ratio). There are more un-conjugated labeling sites on the protein as compared to the other two labels with 1:20 (protein : label) reaction ratio. Increasing Chromeo P503 concentration for the reaction can easily enhance the extinction coefficient of the analyte. In addition, Chromeo forms a relatively stable molecule, and its stock solution does not deteriorate, so it can be used for several months.[30] Moreover, the dye can be conjugated with a protein without changing the charge of the protein during the process in order to preserve its native form.[31]

5.4.2 MOLECULAR WEIGHT DETERMINATION OF α-SYNUCLEIN BY SIEVING CAPILLARY ELECTROPHORESIS

Nonlinear wave mixing, interfaced to capillary gel electrophoresis (CGE), can identify monomer, oligomerized, and fibril α-synuclein in its native conformation. Detergents have the potential to breakdown physiological assemblies, thus they are not used while performing molecular weight-based separation. Optimal conditions for sieving CE are described in Chapter 4, and here we employed PEG (3%) for CE separation. Figure 5.8 shows an electropherogram of molecular weight-based separation of α-synuclein to identify its oligomeric form. Molecular weights of the analytes are obtained by running a standard FITC-conjugated protein ladder (Figure 5.9). The main peaks around 55.3 kDa indicate that the most stable form of α-synuclein is a tetramer with some dimeric (27-39 kDa) and higher oligomeric forms

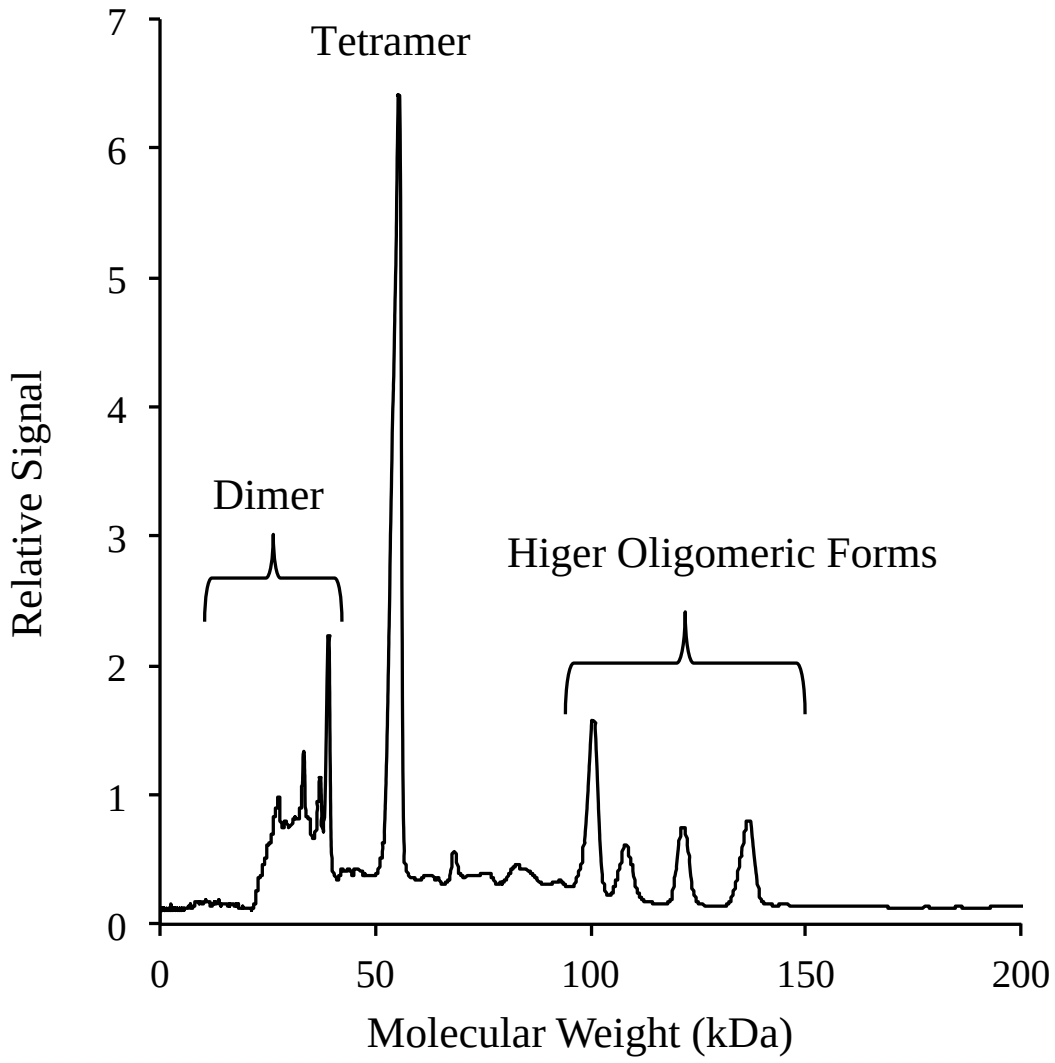

Figure 5.8 Electropherograms of size-based separation of FITC-conjugated α-synuclein (1.4 x 10^{-5} M). The capillary (75 μm i.d., 50 cm) is rinsed with NaOH (0.1 M), water and UltraTrol for 3 minutes followed by running buffer (3% PEG, 100 mM Tris-CHES, and 0.1% SDS). 15.0 kV is applied for each CE run (reverse polarity). The sample is injected electrokinetically for 5 seconds. Wave mixing detection by using a 50 mW, 473 nm laser.

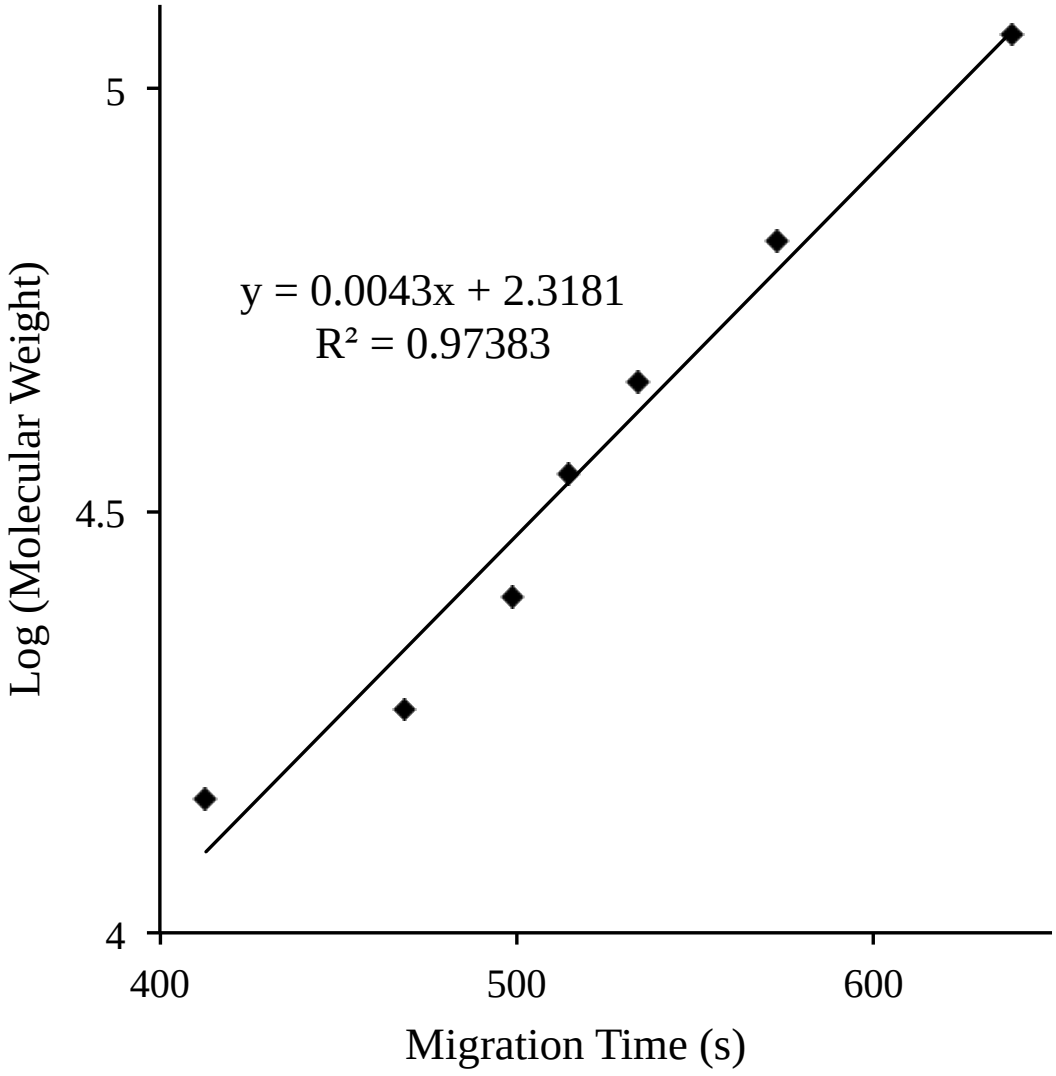

Figure 5.9 Calibration curve created by standard protein ladder for sizing FITC-conjugated α-synuclein. Log of molecular weight versus migration has a linear dependence.

(approximately 100 kDa). The results obtained by this study closely match a study by Bartels *et al,* wherein the molecular weight of the protein is determined using scanning transmission electron microscopy (STEM) under non-denaturing conditions.[32] They validated their STEM results by sedimentation equilibrium analytical ultracentrifugation (SE-AUC), which is commonly used to establish the oligomeric state of native proteins independent of their conformation. Thus, DFWM-CE is capable of providing accurate analysis of the native protein conformation and has the potential to help understand the function of α-synuclein and mechanisms of PD.

5.4.3 LABEL-FREE α-SYNUCLEIN DETECTION

Label-free native detection is desirable since it is faster and simpler without any time-consuming sample preparation steps. A 266 nm UV laser can be used for label-free native α-synuclein detection. Figure 5.10 shows electropherogram of the native protein. Optical absorption at 266 nm is very weak and DFWM only yields a detection limit of 4.1 x 10^{-4} M (S/N 2) for the native macromolecule. Thus, a label is applied to enhance the detection limit for the protein.

5.4.4 PICO- AND FEMTO-MOLAR DETECTION OF α-SYNUCLEIN

Laser wave mixing, interfaced to CE, yields excellent detection limits when using label-conjugated α-synuclein. The three types of labels discussed earlier are used in this study. Figures 5.11 - 5.13 shows electropherograms of α-synuclein conjugated with FITC, QSY 35, and Cheomeo P503. Each figure is obtained by running DFWM-CE (488 nm laser) with different concentration levels of labeled

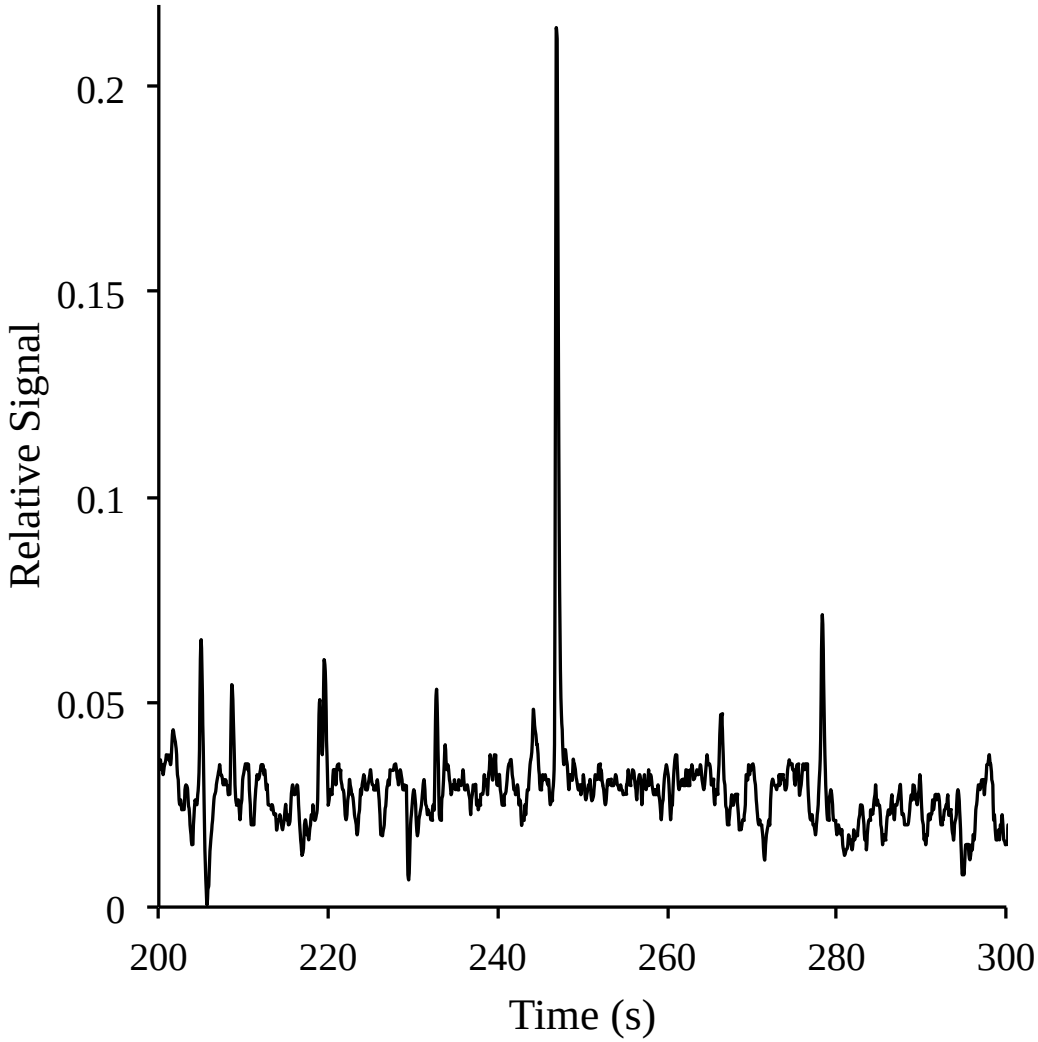

Figure 5.10 Electropherograms of label-free α-synuclein (1.5×10^{-4} M). Capillary is rinsed with NaOH (0.1 M), water and UltraTrol for 3 minutes followed by filling with running buffer (3% PEG, 100 mM Tris-CHES, and 0.1% SDS). Capillary: 75 μm i.d., 30 cm (15 cm effective length), 15.0 kV is applied (reverse polarity). The sample is injected electrokinetically for 5 seconds. Detected by a 20 mW 266 nm laser.

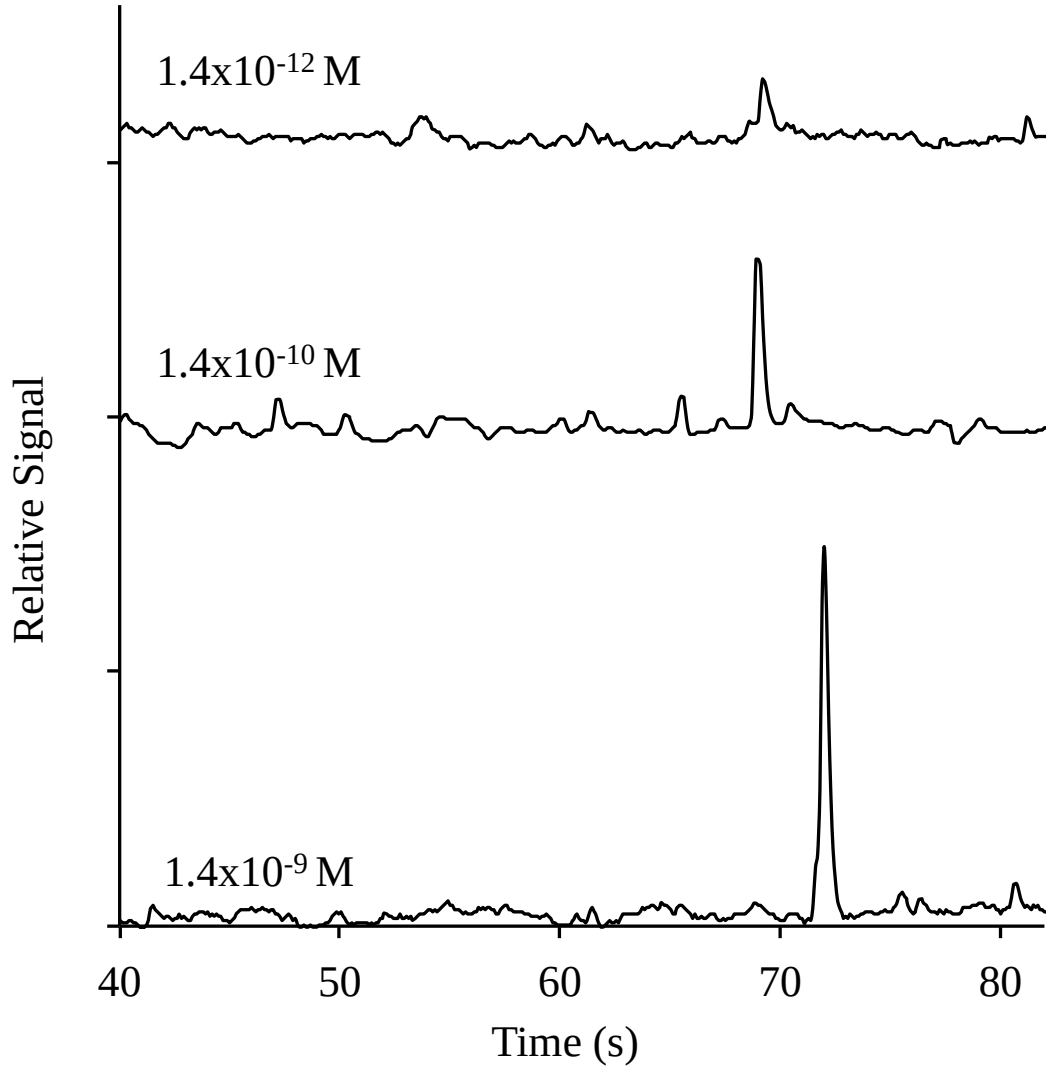

Figure 5.11 Detection limit study of FITC-conjugated α-synuclein. Different concentrations, 1.4 x 10^{-9} M, 1.4 x 10^{-10} M and 1.4 x 10^{-12} M, of the protein are detected by DFWM-CE using a 488 nm laser. Capillary is rinsed with NaOH (0.1 M), water, UltraTrol, and background electrolyte for 3 minutes. Capillary: 75 μm i.d., 30 cm (15 cm effective length). 18.5 kV is applied for each run (reverse polarity). The sample is injected electrokinetically for 20 seconds.

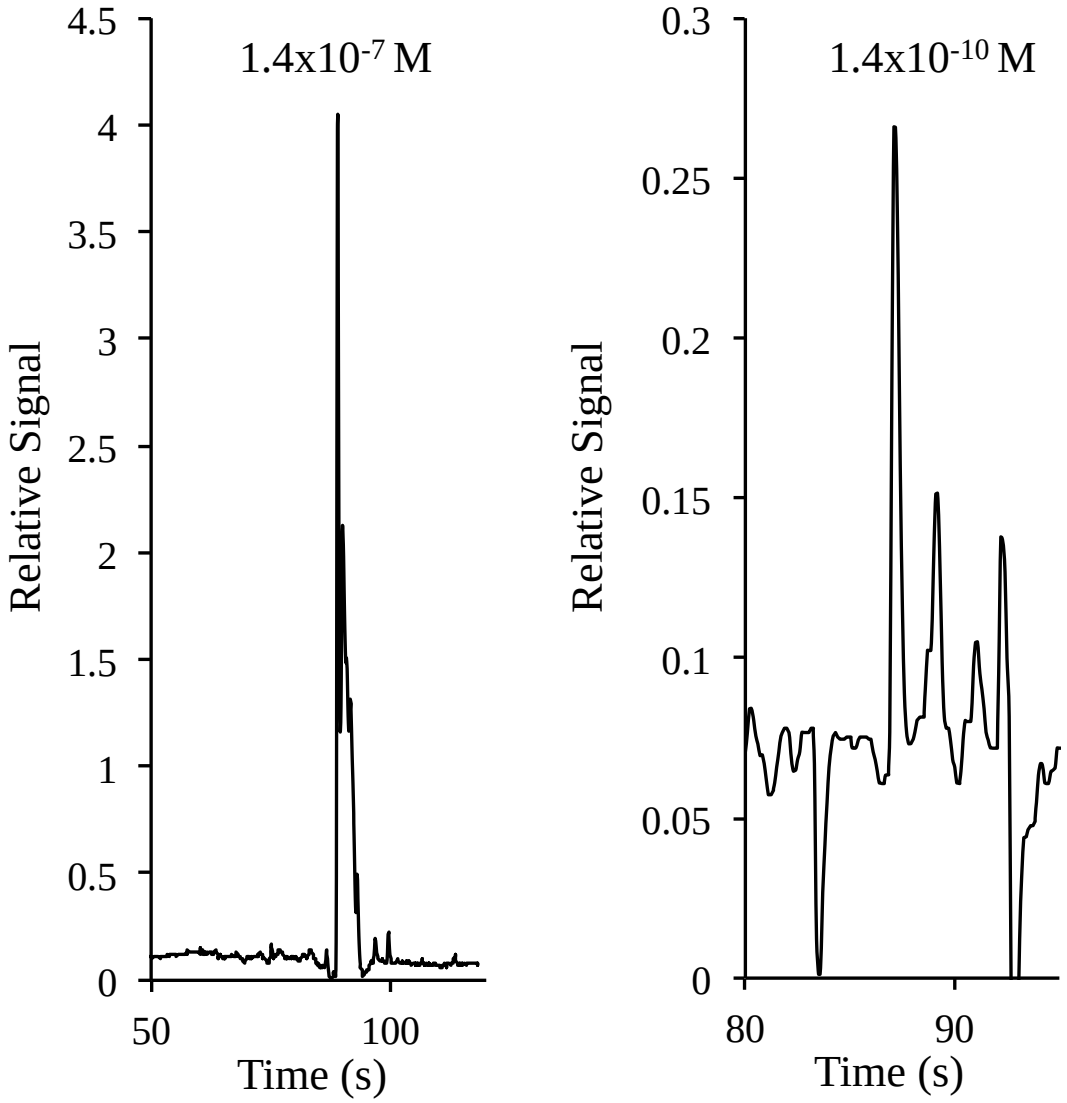

Figure 5.12 Electropherograms of QSY 35-conjugated α-synuclein (1.4 x 10^{-7}, and 1.4 x 10^{-10} M). Capillary is rinsed with NaOH (0.1 M), water, and UltraTrol for 3 minutes followed by running buffer (100 mM, pH 8.6 Tris-CHES). Capillary: 75 μm i.d., 30 cm (15 cm effective length). 18.0 kV is applied for each run (reverse polarity). The sample is injected electrokinetically for 25 seconds.

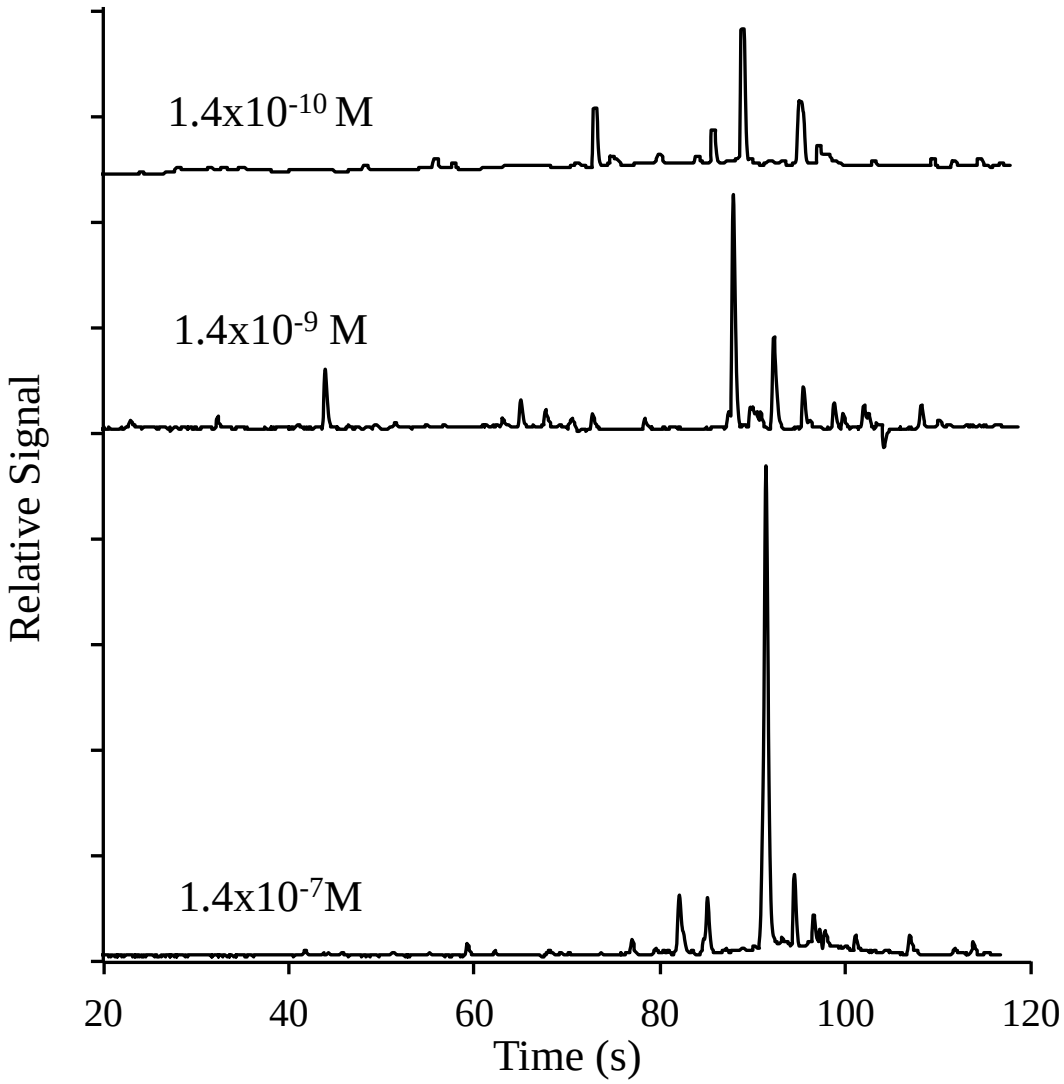

Figure 5.13 DFWM-CE detection limit study for Chromeo P503-conjugated α-synuclein. Proteins are detected at 1.4 x 10^{-7} M, 1.4 x 10^{-9} M, and 1.4 x 10^{-10} M in 25 mM Tris-CHES buffer (pH 8.6). Capillary is rinsed with NaOH (0.1 M), water and UltraTrol for 3 minutes followed by background electrolyte (100 mM, pH 8.6 Tris-CHES). Capillary: 75 μm i.d., 30 cm (15 cm effective length). 18.0 kV is applied for each run (reverse polarity). The sample is injected electrokinetically for 20, 25 and 25 seconds.

proteins. The protein is reacted with FITC and QSY 35 at a ratio of 1 to 20, and Chromeo P503 at 1 to 4, as recommended by the manufacturer for individual labels. Concentration detection limits of 1.4 x 10^{-13} M (FITC), 1.4 x10^{-10} M (QSY 35), and 1.4 x10^{-10} M (Chromeo P503) are determined for conjugated α-synuclein (Table 5.2). Based on the small probe volume used, mass detection limits of 1.1 x 10^{-23} mol (FITC), 1.1 x 10^{-20} mol (QSY 35), and 1.1 x 10^{-20} mol (Chromeo P503) are determined for conjugated proteins. This is equivalent to detecting 7 - 6,000 molecules inside the probe volume. FITC-conjugated protein has the highest extinction coefficient at 488 nm, and it reaches the best detection limit by three orders of magnitude as compared to QSY 35 and Chromeo P503-conjugated α-synuclein. Migration time for the FITC-conjugated protein is shorter than those of QSY 35 and Chromeo P503 conjugated-protein since higher voltage is applied to the system.

A protein is a large biomolecule, resulting in a wider peak width as compared to that of a small molecule and multiple peaks are observed in a capillary electrophoresis run. A negatively charged fused-silica capillary wall reacts with multiple charges on protein and causes a high tendency to absorb the protein.[33] To reduce protein-wall interaction in this study, a dynamic coating is applied. The degree of tailing of a peak differs depending on the effectiveness of the wall coating. In addition, there are multiple labeling sites and individual sites have different reactivity that results in variable labeling and multiple peaks or peak broadening.

By increasing the ratio of Chromeo P503 for conjugation reaction, the detection limit is improved by three orders of magnitude. Figure 5.14 shows correlation of reaction ratio and peak height. There are 16 available labeling sites for

Table 5.2 Extinction coefficient and detection limit of labels and label-conjugated protein.

Label	Extinction Coefficient ($M^{-1}cm^{-1}$)	Extinction Coefficient at 488 nm with Protein ($M^{-1}cm^{-1}$)	Detection Limit (M)	Mass Detection Limit (mol)	Number of Molecule
FITC	70,000	76,000	1.4×10^{-13}	1.1×10^{-23}	7
QSY 35	23,000	13,000	1.4×10^{-10}	1.1×10^{-20}	6624
Chromeo P503 1:4	24,000	23,000	1.4×10^{-10}	1.1×10^{-20}	6624
Chromeo P503 1:10	24,000	133,000	1.9×10^{-13}	1.5×10^{-23}	9

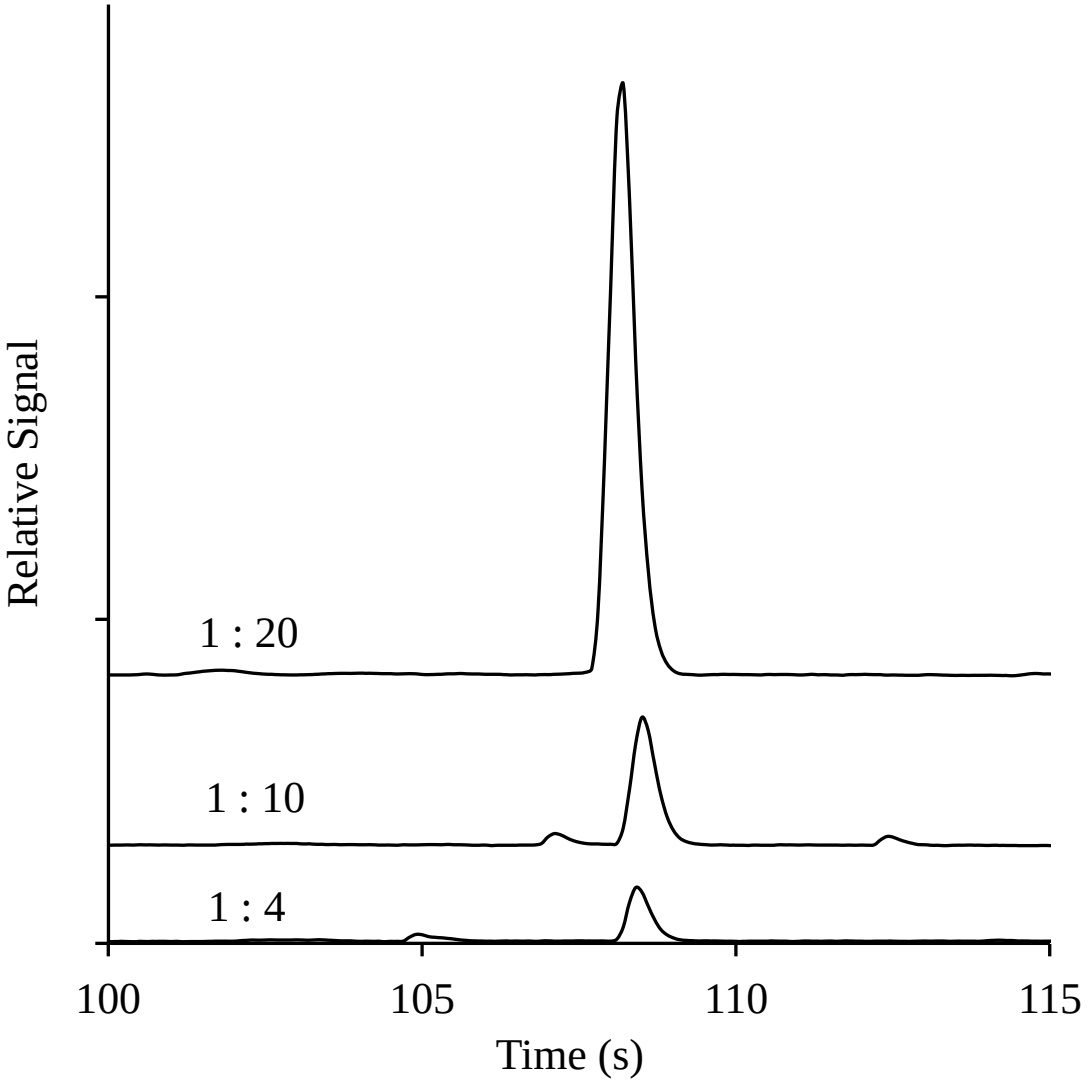

Figure 5.14 Electropherograms of Chromeo P503-conjugated α-synuclein. Analytes are prepared by using different protein-to-label ratios (1:4, 1:10 and 1:20). Capillary is rinsed with NaOH (0.1 M), water and UltraTrol for 3 minutes followed by running buffer (100 mM, pH 8.6 Tris-CHES). Capillary: 75 μm i.d., 30 cm (15 cm effective length). 18.1 kV applied to each run (reverse polarity). The sample is injected electrokinetically for 15 seconds.

α-synuclein, thus free labels are observed in UV-visible absorption spectra when 20 equivalents of Chromeo P503 are reacted. However, the free label is not observed by DFWM-CE using a 488 nm laser since free Chromeo P503 scarcely absorbs at that wavelength, shortening sample preparation time by 5.5 hours as compared to other labels that require dialysis. Minimizing preparation steps results in cleaner optical background and fewer peaks in the electropherogram.

When α-synuclein and Chromeo P503 are reacted at 1:20 ratio, a concentration detection limit of 1.9×10^{-13} M and a mass detection limit of 1.4×10^{-23} mol are determined. The mass detection limit corresponds to 9 molecules inside the probe volume. Figure 5.15 shows reproducible runs for different concentrations of α-synuclein. With optimal protein-label reaction ratio, the detection limit is further enhanced.

Our wave-mixing setup is not a commercial closed system, thus subtle capillary movement, inconsistent temperature, and other outside elements including dust and noise can affect the DFWM-CE signal. Noise levels can vary depending on the position of the capillary. To minimize this noise, capillary is moved horizontally to find the optimal position, which can lead to a migration time shift for CE runs. After multiple runs, two input beams may shift, resulting in a decrease in signal intensity. Since a cooling system is not used, inconsistent temperature levels can also affect migration times. The capillary is mounted on a XYZ-translational stage that can shift down over time, resulting in lower peak heights. To obtain a better detection limit, the position of the capillary is adjusted as needed.

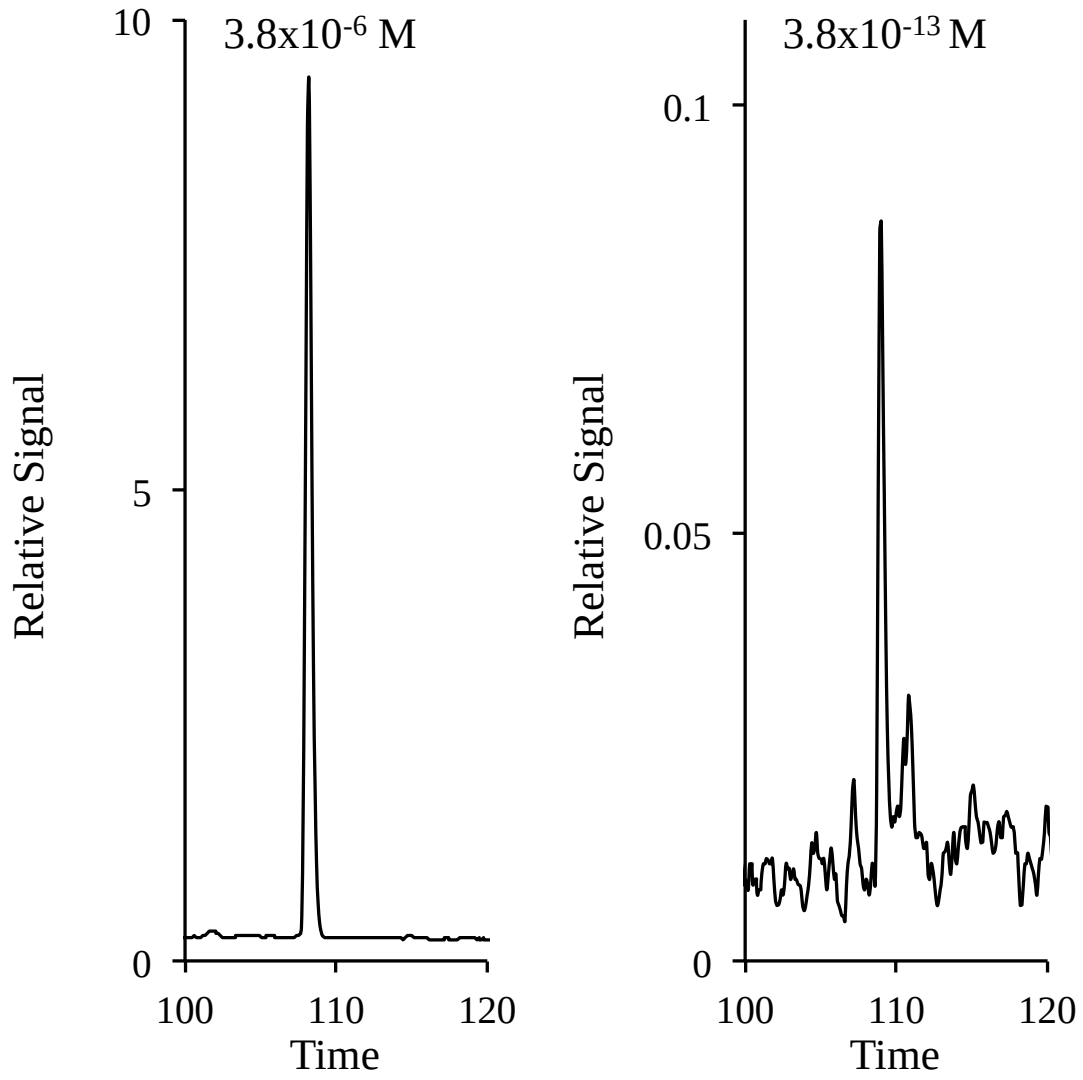

Figure 5.15 Electropherograms of un-dialyzed Chromeo P503-conjugated α-synuclein (1:20 reaction). Concentrations of the protein are 3.8 x 10^{-6} M and 3.8 x 10^{-13} M in 25 mM Tris-CHES buffer (pH 8.6). The capillary is rinsed with NaOH (0.1 M), water and UltraTrol for 3 minutes followed by running buffer (100 mM, pH 8.6 Tris-CHES). Capillary: 75 μm i.d., 30 cm (15 cm effective length). 18.0 kV is applied for each run (reverse polarity). The sample is injected electrokinetically for 15 and 25 seconds.

5.4.5 QUANTITATIVE MEASUREMENT OF A-SYNUCLEIN BY DFWM-CE

Quantitative measurement of α-synuclein is challenging due to the reasons mentioned in the previous section, although DFWM yields strong signals and high S/N. Figure 5.16 shows electropherograms of FITC-conjugated α-synuclein detected by laser wave mixing interfaced with CGE. The capillary is filled with 3% of PEG and 15 kV is applied (reverse polarity) to the system to obtain molecular weight-based separation. Taking advantage of the quadratic dependence on analyte concentration, DFWM allows more reliable monitoring of small changes in analyte concentration. The protein has been detected at the following concentration levels: 28, 56, 84, 112 and 140 μM. Peak heights and areas are measured using Origin 8.5. Figure 5.17 shows correlations between peak heights and concentrations and a quadratic dependence. Peak area vs. concentration plot also shows a nearly quadratic dependence. The slope is not exactly 2.0 (theoretical value) for peak heights and peak areas due to background noise and exterior influences.

Laser wave mixing, interfaced to CE, offers high S/N and yields reproducible CE runs, while ELISA struggles with background control absorption and cross-reactivity interferences that result in false results. Moreover, DFWM-CE is much faster than ELISA and SDS-PAGE. Thus, a nonlinear absorption-based technique is suitable for fast and reliable analyses of clinical samples.

5.4.6 FUTURE WORK: IMMUNOAFFINITY CAPILLARY ELECTROPHORESIS

Capillary electrophoresis-based immunoassay (CEIA) is a sensitive and efficient tool for biomarker detection.[34] In this section, an antigen (24 kDa) and the protein-specific monoclonal antibody (150 kDa) is reacted to form an

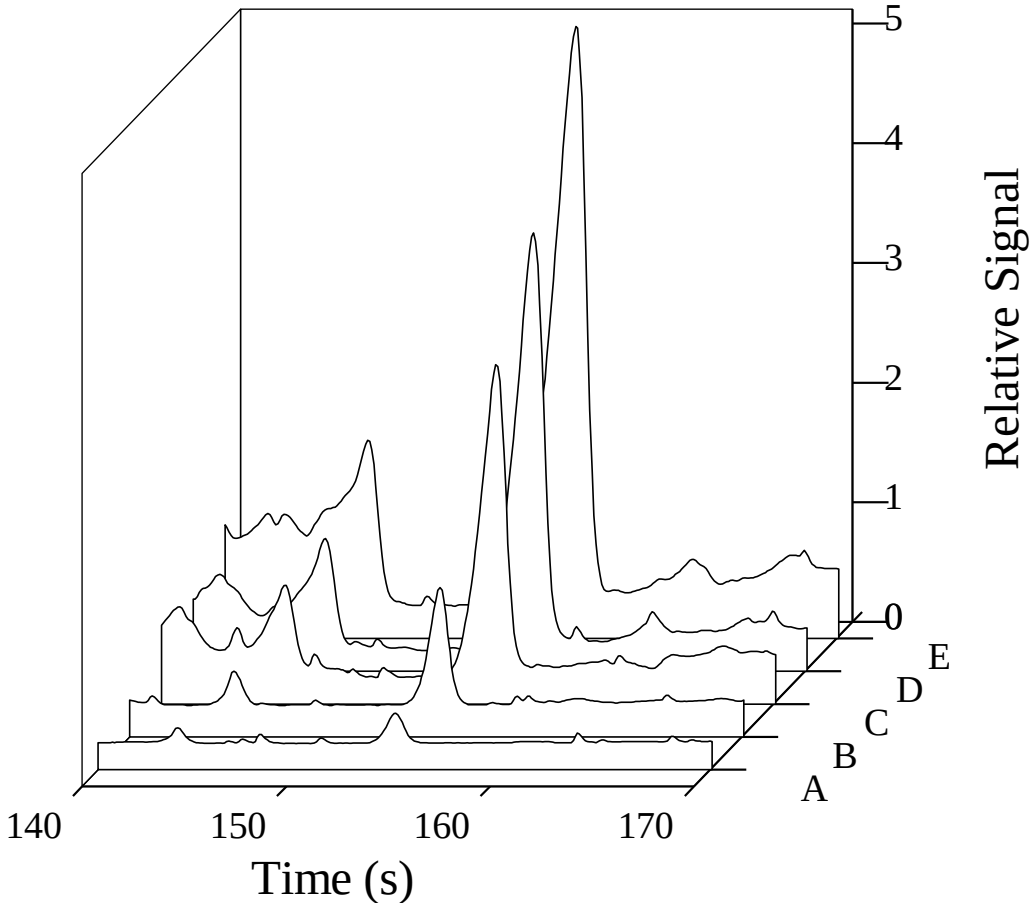

Figure 5.16 Electropherograms for quantification study for FITC-conjugated α-synuclein. Proteins are detected at different concentrations: (A) 28 μM, (B) 56 μM, (C) 84 μM, (D) 112 μM, and (E) 140 μM in 25 mM Tris-CHES buffer (pH 8.6). Capillary is rinsed with NaOH (0.1 M), water and UltraTrol, and running buffer (3% PEG, 100 mM Tris-CHES, and 0.1% SDS) for 3 minutes. Capillary: 75 μm i.d., 30 cm (15 cm effective length). 15.0 kV is applied for each run (reverse polarity). The sample is injected electrokinetically for 5 seconds. Detected by a 50 mW 473 nm laser.

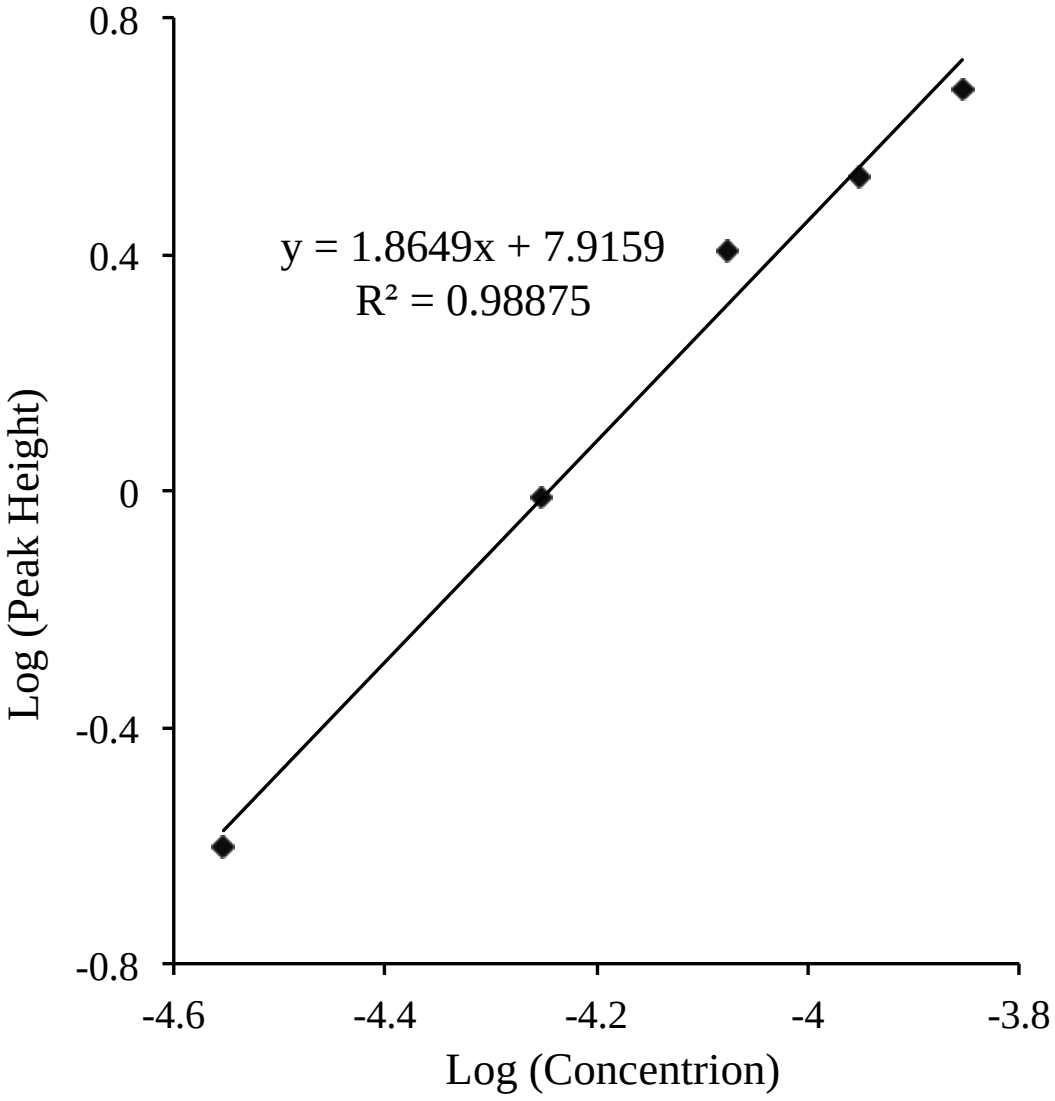

Figure 5.17 Quadratic dependence on concentration for FITC-conjugated α-synuclein with a slope of 1.87.

immunocomplex. Pre-reaction and post-reaction peak shifts are shown in Figure 5.18. The antigen and the monoclonal antibody are incubated for 1 hour at room temperature with a ratio of 1:1. The pre-reaction electropherogram shows an unreacted antigen at approximately 24 kDa. The post-reaction electropherogram shows a small peak of unreacted antigen and a large peak of an immunocomplex with molecular weight of 150 kDa. These studies show that antibodies can be used to increase the specificity of macromolecule detection by DFWM-CE and it can be utilized for α-synuclein.

5.5 Conclusion

Nonlinear absorption-based laser wave mixing provides ultrasensitive detection for FITC, QSY 35 and Chromeo P503-conjugated PD related protein. Best detection limits are obtained by FITC and Chromeo P503-conjugated analytes. Compared to native label-free detection, conjugating with high absorbance labels significantly improves sensitivity. In addition, the signal is a coherent laser-like beam that can be collected with excellent efficiency and high signal-to-noise ratios. Laser-wave mixing is convenient and faster than SDS-PAGE and ELISA in determining molecular weight of a protein for the purpose of investigating oligomeric forms. Potential applications include sensitive, reliable, fast and convenient detection of α-synuclein for early diagnosis of PD using a few drops of blood sample.

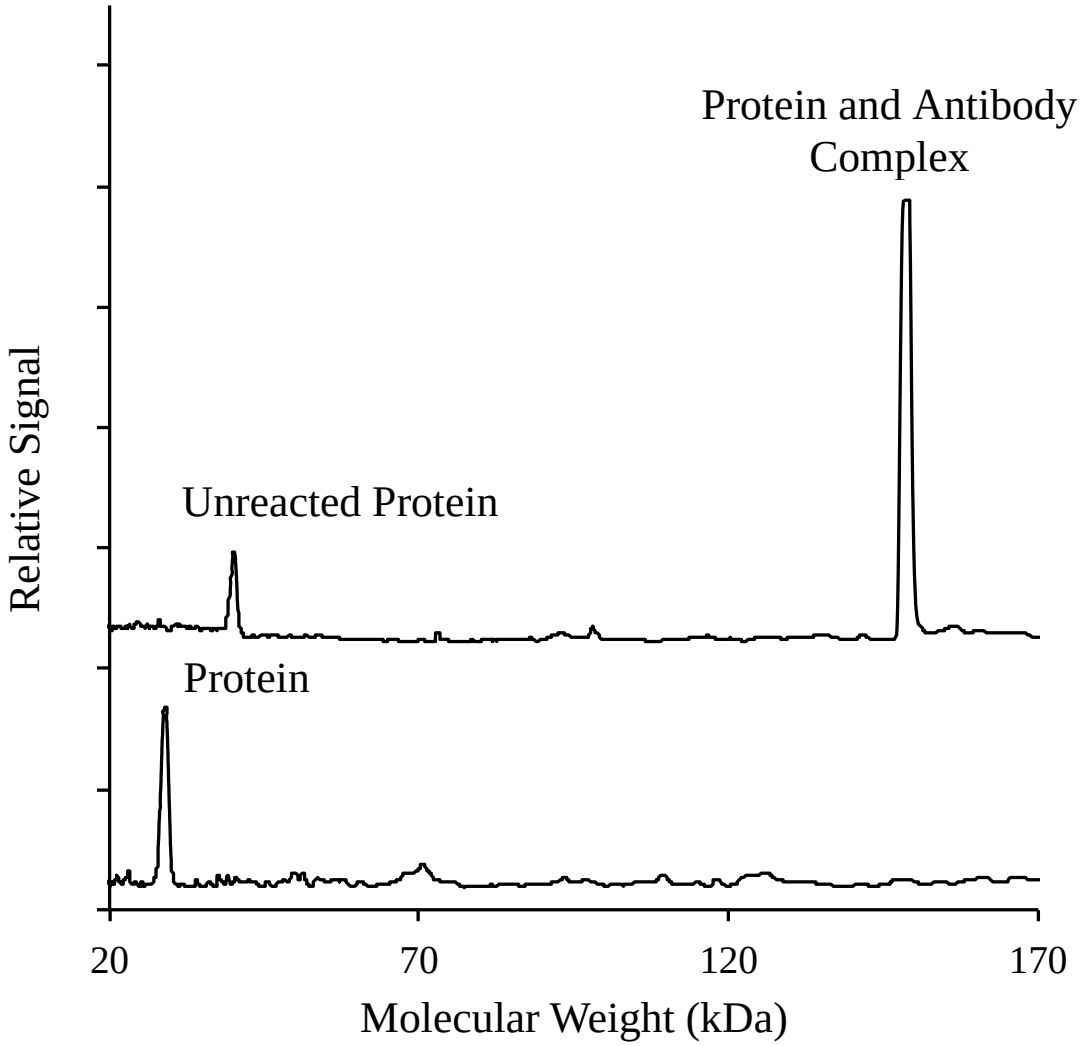

Figure 5.18 Electropherograms of pre- and post-reaction FITC-labeled antigen and its monoclonal antibody. The analytes are detected by a 50 mW 473 nm laser. Capillary: 75 μm i.d., 50 cm (30 cm effective length). UltraTro LN coated capillary is rinsed with NaOH (0.1M), water and background electrolyte (3% PEG, 100 mM Tris-CHES, and 0.1% SDS), -15 kV, 12 μA, 5 s injection.

5.6 Acknowledgement

The majority of the material for this chapter comes directly from a manuscript entitled “Sensitive Analysis of α-Synuclein by Nonlinear Laser Wave Mixing Coupled with Capillary Electrophoresis,” by Manna F. Iwabuchi, Marcel M. Hetu, and William G. Tong, submitted in Anal. Biochmeistry., 2015. The dissertation author is the primary author of this manuscript.

5.7 Reference

(1) McNeill, A.; Wu, R. M., *et al PLoS One* **2013**, *8*, e69190.

(2) Merola, A.; Zibetti, M., *et al Brain* **2011**, *134*, 2074.

(3) Bobby Thomas, a. M. F. B. *F1000 Medicine Reports* **2011**, *3*.

(4) Savica, R.; Rocca, W. A., *et al Arch Neurol-Chicago* **2010**, *67*, 798.

(5) Baba, M.; Nakajo, S., *et al Am J Pathol* **1998**, *152*, 879.

(6) Lee, J. C.; Langen, R., *et al Proceedings of the National Academy of Sciences of the United States of America* **2004**, *101*, 16466.

(7) Roberti, M. J.; Bertoncini, C. W., *et al Nat Methods* **2007**, *4*, 345.

(8) Choi, B. K.; Choi, M. G., *et al Proceedings of the National Academy of Sciences of the United States of America* **2013**, *110*, 4087.

(9) Goncalves, S.; Outeiro, T. F. *Molecular neurobiology* **2013**, *47*, 1081.

(10) Lee, V. M.; Trojanowski, J. Q. *Neuron* **2006**, *52*, 33.

(11) Kalia, L. V.; Kalia, S. K., *et al Ann Neurol* **2013**, *73*, 155.

(12) Thomas, B. *Antioxidants & redox signaling* **2009**, *11*, 2077.

(13) Bucciantini, M.; Giannoni, E., *et al Nature* **2002**, *416*, 507.

(14) Lotharius, J.; Brundin, P. *Nature reviews. Neuroscience* **2002**, *3*, 932.

(15) Hirsch, E.; Graybiel, A. M., *et al Nature* **1988**, *334*, 345.

(16) Halliday, G. M.; McRitchie, D. A., *et al Journal of clinical neuroscience : official journal of the Neurosurgical Society of Australasia* **1996**, *3*, 52.

(17) Fearnley, J. M.; Lees, A. J. *Brain* **1991**, *114 (Pt 5)*, 2283.

(18) Conway, K. A.; Rochet, J. C., *et al Science* **2001**, *294*, 1346.

(19) Burre, J.; Sharma, M., *et al Science* **2010**, *329*, 1663.

(20) Kensaku Kasuga, M. N., Takeshi Ikeuchi *International Journal of Alzheimer's Disease* **2012**, 1.

(21) Tokuda, T.; Salem, S. A., *et al Biochem Biophys Res Commun* **2006**, *349*, 162.

(22) B.Mollenhauer, V. C., I. Kahn et al *Experimental Neurology* **2008**, *213*, 315.

(23) L. Parnetti, D. C., G. Bellomo et al. *Movement Disorders* **2011**, *26*, 1428.

(24) Lee, P. H.; Lee, G., *et al J Neural Transm* **2006**, *113*, 1435.

(25) Duran, R.; Barrero, F. J., *et al Movement Disorders* **2010**, *25*, 489.

(26) Shi, M.; Zabetian, C. P., *et al Neurosci Lett* **2010**, *480*, 78.

(27) Guzman, N. A.; Blanc, T., *et al Electrophoresis* **2008**, *29*, 3259.

(28) Liu, C. T.; Wang, L., *et al Biochemistry-Us* **2013**, *52*, 5332.

(29) Turner, E. H.; Dickerson, J. A., *et al J Chromatogr A* **2008**, *1194*, 253.

(30) Craig, D. B.; Wetzl, B. K., *et al Electrophoresis* **2005**, *26*, 2208.

(31) de Jong, S.; Krylov, S. N. *Anal Chem* **2011**, *83*, 6330.

(32) Tim Bartels, J. G. C., and Dennis J. Selkoe *Nature* **2011**, *477*, 107.

(33) Shariff, K.; Ghosal, S. *Analytica Chimica Acta* **2004**, *507*, 87.

(34) Ou, J. P.; Chan, S. T. H., *et al J Chromatogr B* **1999**, *731*, 389.

CHAPTER 6
ZEPTO- AND YOCTO-MOLE DETECTION OF NATIVE AND LABELED NEUROTRANSMITTERS BY NONLINEAR WAVE-MIXING SPECTROSCOPY COUPLED WITH CAPILLARY ELECTROPHORESIS

6.1 Abstract

Deep brain stimulation (DBS) is an effective treatment for Parkinson's disease (PD). While its mechanisms are not yet fully understood, research has shown that it increases efflux of some neurotransmitters, including adenosine, dopamine, glutamic acid and γ-aminobutyric acid. Ultrasensitive detection of these analytes will help understand the mechanisms of DBS in order to design a smarter closed-loop controlled version of DBS. This chapter focuses on the detection and separation of key neurotransmitters using multi-photon laser wave-mixing spectroscopy, a compact and ultrasensitive detection method. The wave-mixing signal is a coherent laser-like beam that can be collected with excellent efficiency levels and high signal-to-noise ratios. Laser wave mixing offers inherent advantages over conventional absorption-based methods, including zeptomole and yoctomole-level detection sensitivity levels, picoliter probe volumes, small sample requirements, compact portable detector designs, and high spatial resolution. Concentration detection limits of 3.7×10^{-13} M and 2.1×10^{-9} M are determined for native adenosine and dopamine, respectively. Concentration detection limits of 1.1×10^{-9} M and 1.7×10^{-10} M are determined for labeled-glutamic acid (Glu) and γ-aminobutyric acid (GABA), respectively. These correspond to a mass detection limit of 2.0×10^{-23} mol for adenosine, 1.2×10^{-19} mol

for dopamine, 8.7 x 10^{-20} mol for Glu, and 1.3 x 10^{-20} mol for GABA.

6.2 Introduction

Ultrasensitive detection of neurotransmitters such as dopamine, adenosine, GABA and Glu (Figure 6.1) is key to a better understanding of the mechanisms of treatments for Parkinson's disease (PD). Accurate monitoring requires sensitive detection methods due to low basal levels of these chemicals, which can be as low as nanomolar concentrations (Table 6.1).[1-4] Studies have focused on methodologies to improve sensitivity and selectivity using various detection techniques.[5-7] Degenerate four-wave mixing (DFWM), a nonlinear absorption-based optical detection technique, offers coherent laser-like signal, and hence, ultrasensitive detection, and exhibits quadratic dependence on concentration, and hence, large swings in signal intensities are observed with small concentration change,[8] ideal for monitoring extracellular neurotransmitters.

Approved for Parkinson's by the FDA,[9] DBS is a surgical treatment in which implanted electrodes deliver controlled electrical pulses to a patient's brain (Figure 6.2).[10] The mechanism of the treatment remains unknown,[11] although numerous cases have shown that the therapy mitigates symptoms of Parkinson's disease and even diminishes some side effects of medications.[12] The treatment has been found to change concentrations of neurotransmitters,[11,13] so monitoring key neurotransmitters may lead to discovery of the precise mechanisms and better understanding of these actions. One hallmark of Parkinson's is a loss of dopaminergic neurons that leads to a sharp depletion of dopamine levels.[14] Dopamine, a catecholamine, shows increased

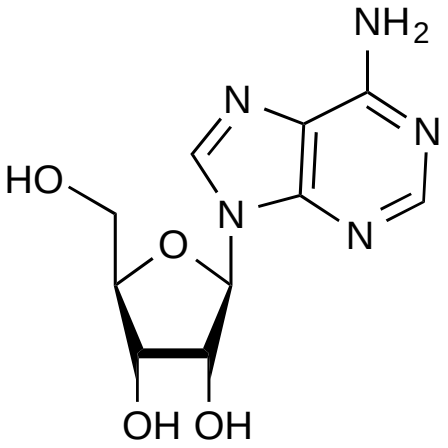

Adenosine

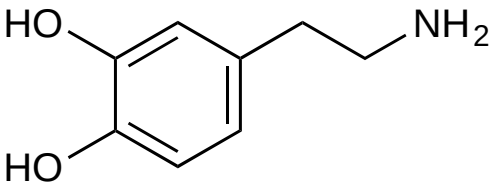

Dopamine

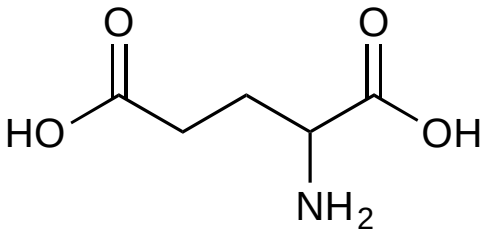

Glutamate

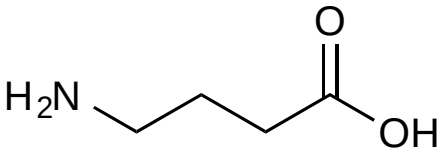

GABA

Figure 6.1 Molecular structures of neurotransmitters that change in concentration after DBS. Ultrasensitive detections are required due to the low extracellular level.

Table 6.1 Low basal levels of key neurotransmitters

Neurotransmitters	Basal Level	References
Adenosine	20-50 nM	(1)
Dopamine	20-30 nM	(2)
Glutamate	2.97 μM	(3)
GABA	52.8 nM	(4)

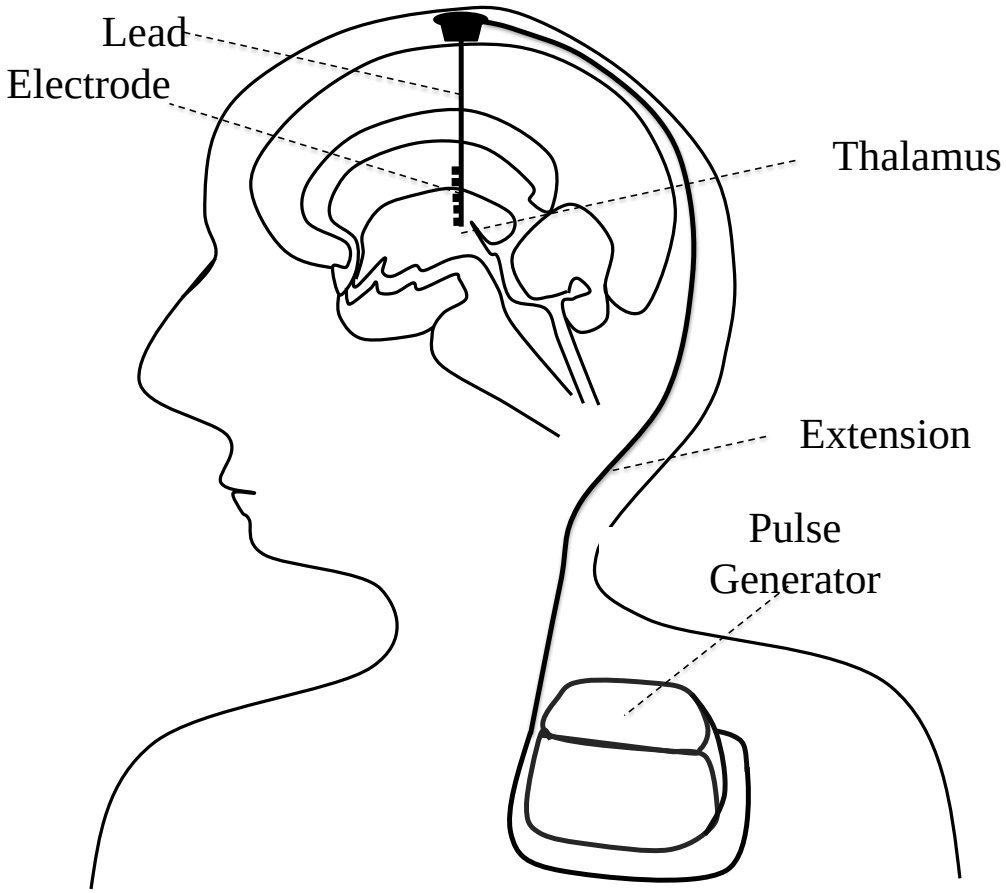

Figure 6.2 Deep brain stimulation is an effective treatment for Parkinson's disease. The battery operated pulse generator is surgically implanted under the skin of the patient's chest. The generator delivers continuous electrical pulses through the wire to the electrode at the target area of the brain.

efflux at the subthalamic nucleus (STN) when DBS treatment is employed.[13,15] Adenosine, an endogenous purine nucleoside, is another neurotransmitter that plays an important role in modulating neural activity.[14] Several studies report that DBS, specially modulated to work at high frequency, increases adenosine efflux.[11] The amino acid neurotransmitter Glu is a major excitatory neurotransmitter present in the mammalian central nervous system (CNS) with large amounts produced in the brain's synapse.[16] GABA is an inhibitory neurotransmitter in the CNS, where 10-40% of nerve terminals in the hippocampus and cerebral cortex may use GABA to transmit "close" signals.[17,18] Extracellular concentration levels of Glu are significantly higher in the globus pallidus (GP) and substantia nigra pars reticulata (SNr).[19] GABA efflux has been shown to increase at SNr with high frequency stimulation.[4,19]

At present, a wireless instantaneous neurotransmitter concentration system (WINCS), based on fast-scan cyclic voltammetry, is used to monitor neurotransmitters after a DBS system is installed. Cyclic voltammetry is appropriate for studying kinetic parameters of electrode reaction mechanisms; however, it is not as desirable as a sensitive detector due to its inability to detect nonelectroactive analytes.[20] Detection of nonelectroactive molecules, such as Glu and GABA, requires enzyme-linked electrodes.[21,22] Other optical detection techniques, such as laser-induced fluorescence coupled with CE, offer better sensitivity than conventional absorption techniques, but are limited to detecting fluorophores.[23] Liquid chromatography-mass spectrometry (LC-MS) has been used in detecting some neurotransmitters, but it is neither cost effective nor easily field-deployable.[24]

The wave-mixing signal has a quadratic dependence on extinction coefficient

and a cubic power dependence on laser power, as shown in the following equation.[25]

$$I_3 = \left(\frac{b}{8\pi}\right)^2 I_1^2 I_2 \frac{\lambda}{sin^4(\theta/2)} \left(\frac{dn}{dT}\right)^2 \frac{\alpha^2}{\kappa^2} \qquad (2.9)$$

The path length of the input laser beam is represented by b. I_3 represents the DFWM signal generated by probe and pump beams traveling forward with intensities I_1 and I_2, respectively. Probe beam I_1 has intensity lower than pump beam I_2. The wavelength of the laser source is λ, and θ represents an angle between the probe and pump beams. The parameter dn/dT shows a derivative of the refractive index with respect to solvent temperature change. The extinction coefficient is represented by α and thermal conductivity by κ. This equation shows some inherent features of the wave-mixing signal including a quadratic dependence on concentration and a cubic dependence on laser power. Both DFWM sensitivity and selectivity levels are enhanced when coupled with CE. High separation resolutions, short analysis time, and the small sample requirement[26,27] are some of the features that make DFWM-CE a powerful technique.

This chapter describes sensitive detection and separation of native and labeled target neurotransmitters by nonlinear DFWM, coupled with capillary electrophoresis (CE). A 266 nm UV laser is used to detect aromatic molecules and an optically pumped semiconductor 488 nm laser is used to detect dabsyl chloride (4-(dimethylamino)azobenzene-4'-sulfonyl chloride)-conjugated molecules. The derivatization reaction has a short reaction time and forms relatively stable products with the target neurotransmitter conjugates.[28] Concentration detection limits of 3.7 x 10^{-13} M (label-free native adenosine), 2.1 x 10^{-9} M (label-free native dopamine), 1.1 x

10^{-9} M (labeled Glu) and 1.7 x 10^{-10} M (labeled GABA) are determined using DFWM-CE. Based on the small DFWM probe volume, mass detection limits of 2.0 x 10^{-23} mol (adenosine), 1.2 x 10^{-19} mol (dopaminez), 8.7 x 10^{-20} mol (Glu), and 1.3 x 10^{-20} mol (GABA) are determined.

6.3 Experimental

6.3.1 Design and Optimization of Degenerate Four-Wave Mixing setup

Figure 6.3 shows a schematic diagram of a four-wave mixing optical setup interfaced to a CE system. A continuous-wave 40 mW 488 nm blue laser (Coherent, Santa Clara, CA, Sapphire) is used to detect dabsylated analytes. Blue diode laser operates at 447 nm, 25 mW is purchased from CNI (Changchun, China). A compact 20 mW 266 nm Q-switched UV pulsed laser (CNI, Changchun, China) is used to probe label-free native analytes.

The output of the laser beam is split by a 30:70 (R:T) beam splitter to form two input beams of low and high intensity input beams. The transmitted beam serves as both pump and probe beams while the reflected beam serves only as a pump beam. Two input beams travel equal distances to a biconvex lens that focuses the input beams at an angle of 0.95° (488 nm), 1.5 ° (447 nm), and 1.5° (266 nm laser). The diameters of the beams are 1.70 mm (488 nm), 4.00 mm (447 nm) and 1.10 mm (266 nm), yielding probe volumes of 79 pL (488 nm), 12 pL (447 nm) and 56 pL (266 nm), calculated using equations introduced in Chapter 5.

The sample cell is a 75 μm i.d., 360 μm o.d. fused-silica capillary (Molex, Lisle, IL). A small portion of the capillary coating is removed using a butane flame to

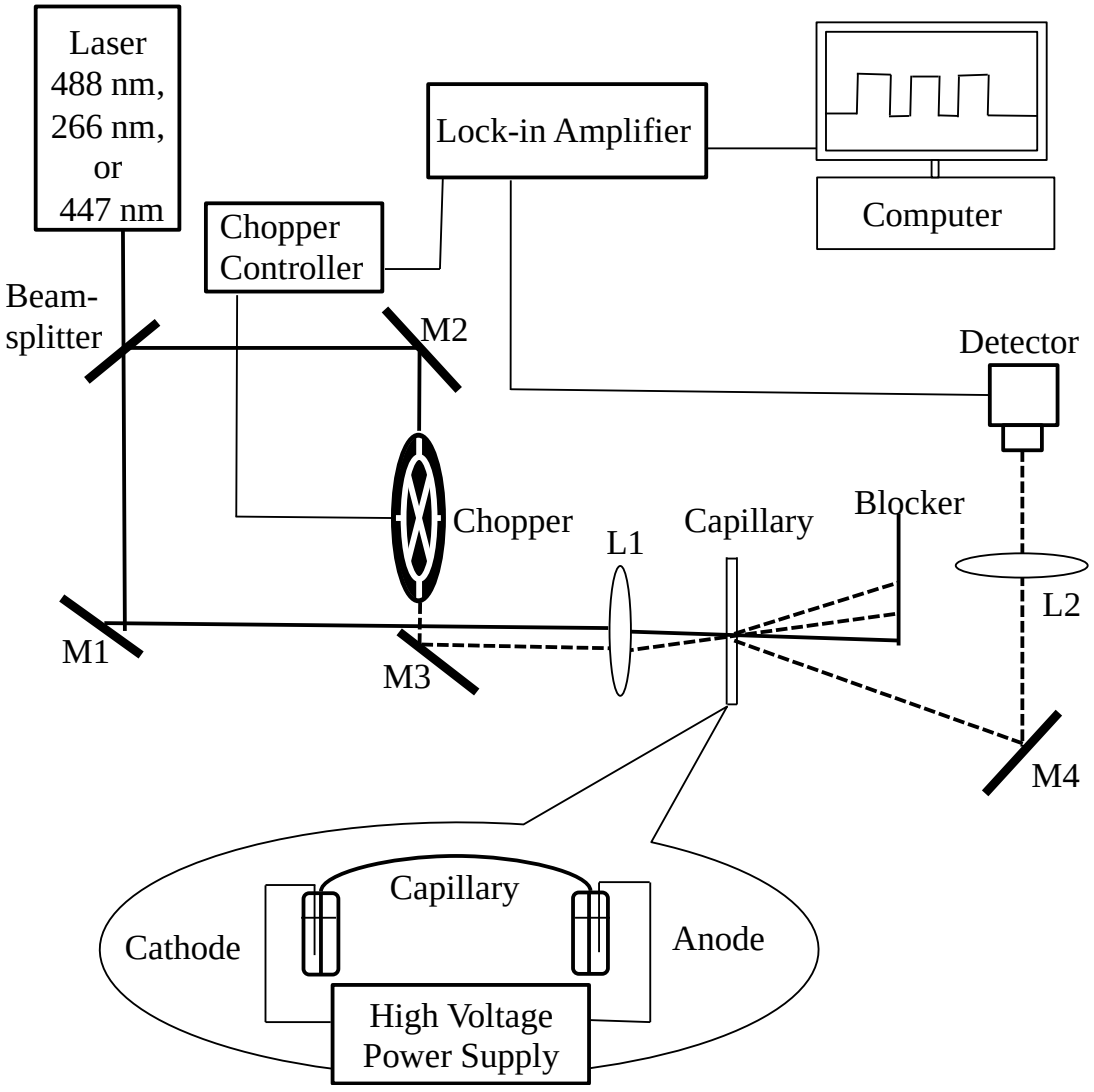

Figure 6.3 Ultrasensitive degenerate four-wave mixing detection setup coupled with custom-built CE system for detecting and separating neurotransmitters.

let the input laser beam propagate across the capillary. Two coherent wave-mixing signals are created by analytes that absorb at the wavelength of the laser. The signal is reflected by a mirror (M4) and focused by a 150 mm focal length biconvex lens (L2) to a photodetector (Thorlabs, Newton, NJ, PDA25K). The signal collected is digitized and monitored by a computer. An optical chopper (Stanford Research Systems, Sunnyvale, CA, SR541) is used to modulate one of the input beams (reflected beam) at 200 Hz. The chopper, photodetector and computer are interfaced to a DSP lock-in amplifier (Stanford Research Systems, Sunnyvale, CA, SR810).

6.3.2 CHEMICALS

Anhydrous sodium carbonate, sodium bicarbonate, methanol, acetone, acetonitrile, and NaCN are purchased from Fisher Scientific (Waltham, MA). Adenosine, glutamic acid, 4-aminobutyric acid (GABA), and methyl red are from Acros Organics (Morris Plains, NJ), and dopamine hydrochloride is from Alfa Aesar (Ward Hill, MA). HCl (37%), NaOH, borax, and sodium dodecyl sulfate are obtained from Sigma-Aldrich (St. Louis, MO). Naphthalene-2,3-dicarboxaldehyde (NDA) is purchased from Invitrogen (Carlsbad, CA).

6.3.3 NATIVE DETECTION FOR DOPAMINE AND ADENOSINE

All buffers are prepared using distilled water (Waterwise, Leesburg, FL, 4000). Borate buffer (20 mM, pH 8.3) is prepared by dissolving 1.9 g of borax into 250 mL of water and adjusting the pH with 1.0 M HCl. Adenosine is dissolved in the buffer for CE runs (1.0 mg/mL).

The borate buffer for the dopamine is prepared by dissolving 2.4g of borax

into 250 mL of water and adjusting the pH with 1.0 M HCl (25 mM, pH 9.0). Dopamine is prepared by dissolving 4.0 mg in 1.0 mL of the buffer. Solutions for UV-visible spectrophotometer are prepared by dissolving 1.0 mg of adenosine and 2.0 mg of dopamine in 1.0 mL of borate buffer (20 mM, pH 8.3).

6.3.4 LABELED GLU AND GABA

Dabsylated Glu and GABA are prepared using a slightly modified protocol reported previously for amino acid dabsylation.[29,30] Dabsyl chloride is prepared by dissolving 3.3 mg in 1.0 mL acetone. A pH 8.9 buffer is prepared from 27 mL of 0.1 M sodium bicarbonate solution and 3.0 mL of sodium carbonate solution. GABA and Glu solutions are prepared by dissolving 2.0 mg of each analyte in 1.0 mL of 0.1 M, pH 8.9 sodium carbonate buffer. Labeled neurotransmitters are prepared by adding 600 uL of dabsyl chloride into a 600 nmol neurotransmitter solution in a buffer at a total volume of 1,400 μL. The solution is heated at 70°C for 7 minutes until the reaction is completed. The labeled product is extracted three times with diethyl ether, and then the organic layer is discarded. The pH 8.9 aqueous layer is adjusted to pH 2.0 with 1.0 M hydrochloric acid. The color of the solution changes from orange to dark red. The labeled compounds are extracted five times with diethyl ether and the organic layer collected. Diethyl ether is evaporated and the dry labeled neurotransmitter is dissolved in 1.0 mL of pH 8.9, 25 mM sodium carbonate buffer. This solution is used to take UV-visible absorption spectra, run CE, and in continuous-flow measurement studies.

6.3.5 LABELED DOPAMINE

This protocol follows a previously reported reaction.[31] Sodium tetraborate buffer (0.1M, pH 9.0) is prepared by dissolving 1.90 g of borax in 50 mL distilled water. The following chemicals are mixed together in a glass vial: 700 μL of borate buffer, 100 μL dopamine hydrochloride (1.0 mM) in MeOH, 100 μL of NaCN (1.0 mM), and 100 μL of NDA (1.0 mM) to give a final concentration of 0.1m M for each component. The solution is incubated for 20 min in the dark until the reaction is completed. A previous study reported that NDA and CN^- reaction rate reached its maximum at around pH 9.0-9.5.[32]

The reaction is observed via UV-visible absorption spectra recorded at 20 s intervals until the reaction is completed.

6.3.6 CAPILLARY ELECTROPHORESIS

Capillary electrophoresis is performed using a custom-built CE system. The setup consists of a fused-silica capillary (Molex, Lisle, IL) with 75 μm i.d., 360 μm o.d., 30cm total length, and 15 cm effective length. Plastic vials containing buffer/analytes are positioned at each end of the capillary. The capillary is rinsed with 0.1 M NaOH, distilled water and CE running buffer for 15 min each using a peristaltic pump. The CE potential is supplied by platinum wires connected to a power supply (Glassman High Voltage, High Bridge, NJ). Current and voltage levels are controlled by a custom-built controller and monitored by voltmeters.

6.3.7 CONTINUOUS-FLOW DETECTION

For capillary continuous-flow analysis, the capillary is connected to a 0.25

mm i.d., 41 cm manifold pump tubing (Fisher Scientific, Hampton, NH) to supply analytes at a stable rate with a peristaltic pump (Rainin Instrument, Oakland, CA). The wave-mixing detector cell is a 75 μm i.d. fused silica capillary. A methyl red/methanol (5.0×10^{-5} M) solution is used to align and optimize the wave-mixing optical setup.

6.3.8 UV-VISIBLE SPECTROPHOTOMETER

A benchtop UV-visible diode-array absorption spectrometer (Agilent, Santa Clara, CA, 8453) is used for absorption measurements. A Quartz cuvette (1.0 cm path length) is used as the analyte cell. The instrument is blanked with buffers appropriate to dissolve each analyte.

6.4 Result and Discussion

6.4.1 EXCITATION LASER WAVELENGTHS FOR NATIVE AND LABELED NEUROTRANSMITTERS

Some of the target neurotransmitters require labeling to ensure that they absorb at the wavelength of the laser used in DFWM. Dabsyl chloride is used to label GABA and Glu to enhance absorption at 488 nm. Figure 6.4 shows simple labeling steps for a neurotransmitter with an amine group, which attacks sulfonyl chloride to obtain the sulfonamide product. UV-visible absorption spectra of native adenosine, dopamine and dabsylated GABA and Glu are shown in Figure 6.5. The extent of absorption at the wavelength of the DFWM laser source is crucial for detection sensitivity, since the nonlinear wave-mixing signals depend on the extinction coefficient. Native adenosine and dopamine have aromatic rings that absorb in UV wavelengths. Due to the extended conjugation in the molecular structure of

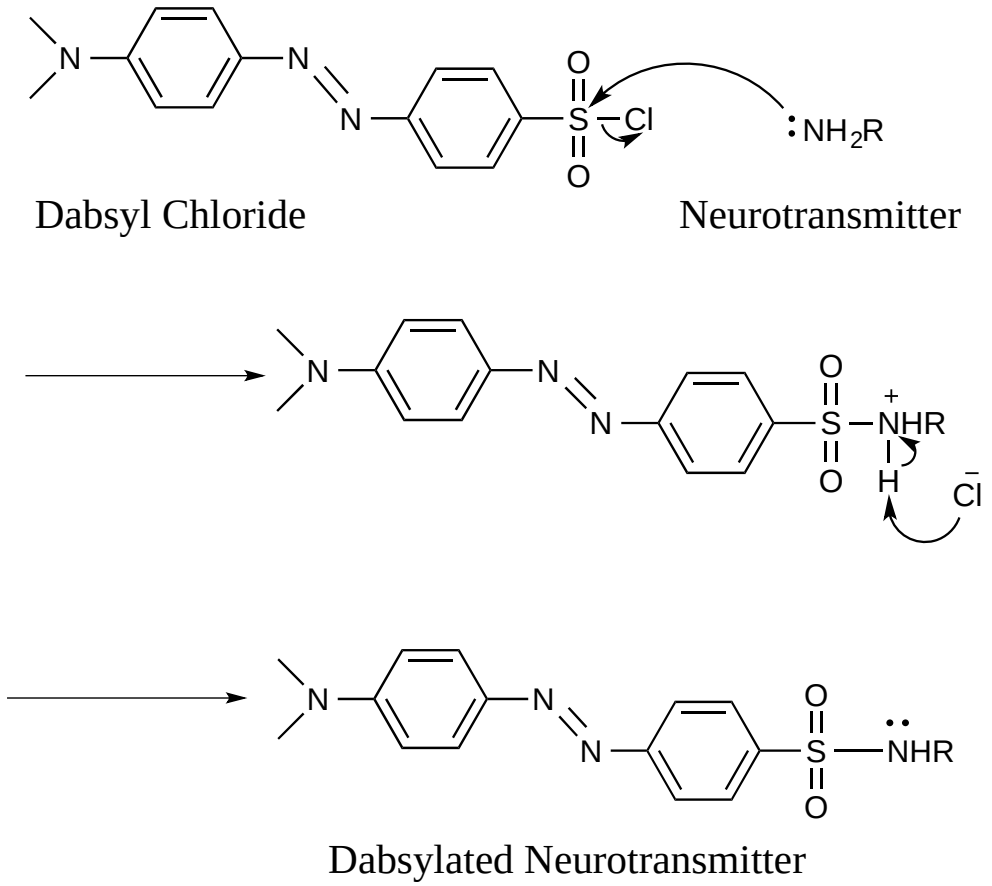

Figure 6.4 Dabsylation mechanism of neurotransmitter for enhancing absorption at 488 nm.

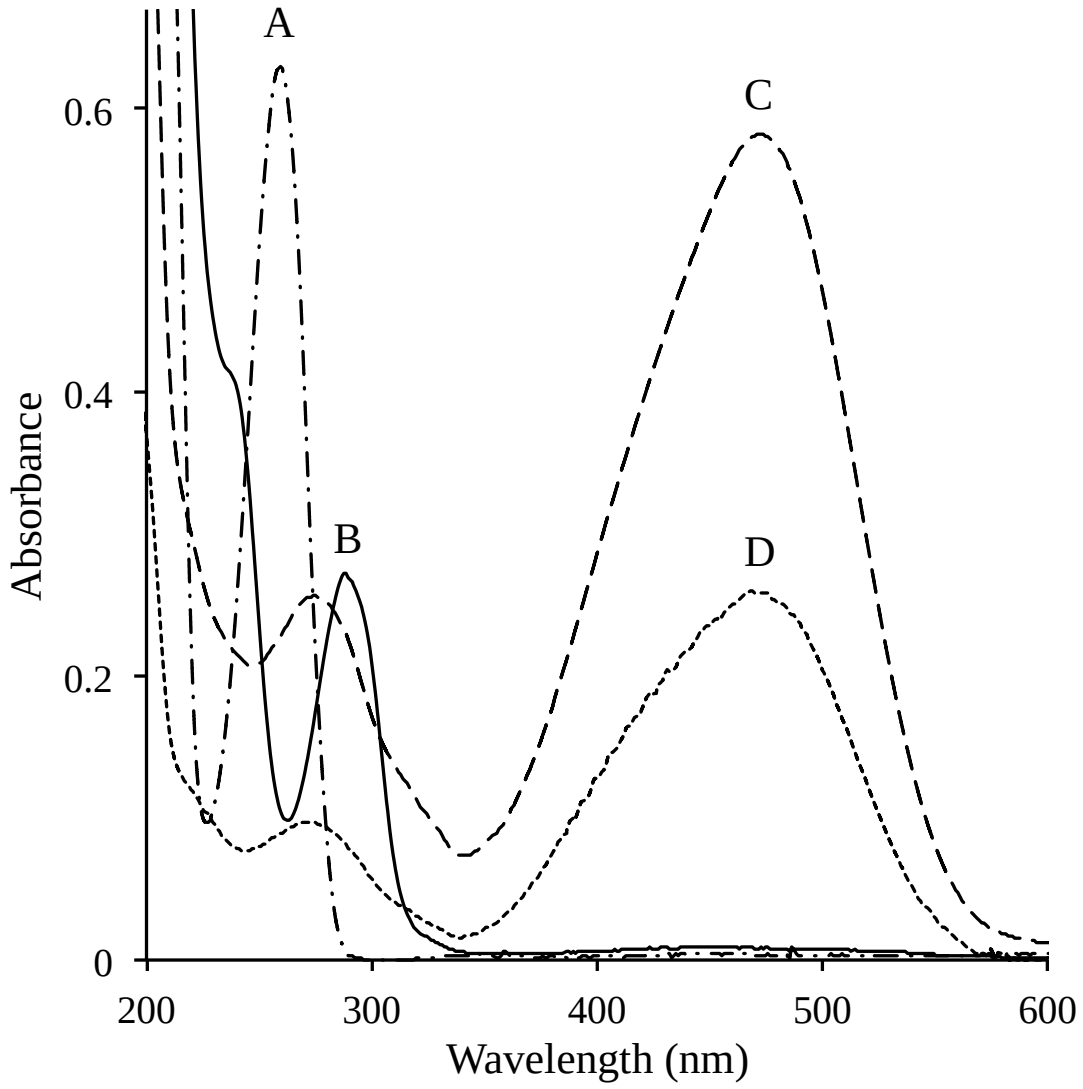

Figure 6.5 UV-visible absorption spectra of (A) native adenosine (3.7×10^{-5} M), (B) native dopamine (1.05×10^{-5} M), (C) dabsylated GABA (1.74×10^{-5} M), and (D) dabsylated Glu (7.8×10^{-6}M) in pH 8.9, 25 mM carbonate buffer. GABA and Glu can be probed with DFWM using visible lasers.

adenosine, its absorption is stronger than dopamine. Glu and GABA show no native absorption around UV or visible wavelengths. Dabsylated GABA and Glu can be detected with a 488 nm blue laser and they can be easily extracted from free dabsyl chloride. After extraction, CE electropherograms show no peaks for unreacted dabsyl label. Derivatization reaction yields are calculated using the Beer-Lambert law.

The extinction coefficient is calculated using the Beer-Lambert law for four neurotransmitters at the excitation wavelengths, 266 nm and 488 nm. The extinction coefficients of adenosine and dopamine at 266 nm are 14,324 $M^{-1}cm^{-1}$ and 10,000 $M^{-1}cm^{-1}$, respectively. Concentration levels of 7.8 x 10^{-6} M and 1.7 x 10^{-5} M, are determined for the dabsylated neurotransmitters, Glu and GABA, from the UV-visible spectra. Extinction coefficient of 30,901 $M^{-1}cm^{-1}$ and 31,258 $M^{-1}cm^{-1}$ are determined for Glu and GABA at 488 nm.

6.4.2 Optimization of Degenerate Four-Wave Mixing setup

Before CE runs, the DFWM setup is aligned and optimized using methyl red in methanol solutions (5.0 x 10^{-5} M) to obtain a visual signal, maximize signal intensities, and minimize background noise levels. The DFWM signal has a quadratic dependent on concentration and a cubic dependent on input laser power. Plotting a log(signal) vs log(concentration) plot and a log(signal) vs log(power) plot and obtaining a slope of 2 and 3, respectively, allows one to verify the true wave-mixing signal. The solution is drawn into a flexible plastic tubing by the pump at 2.1 μL/min. This flow rate provides optimum signal intensity for this wave-mixing setup. Faster flow rates yield inconsistent fluctuating signals due to a washout effect in the thermal

grating.

After the setup is optimized, analytes are injected. The four wave-mixing signal is confirmed by collecting finger plots at different concentrations, as shown in Figure 6.6, by systematically blocking the chopped beam and the unchopped beam in the laser setup. While instrumental noise from a chopped beam creates signal-like behavior from a solvent blank, this can be minimized in the DFWM setup by adding extra beam blockers to reduce incoherent scattered light.

6.4.3 Reproducibility of DFWM-CE runs

Consistent results for the analysis of neurotransmitters are readily obtained using CE and wave mixing. In a typical experiment, standard analytes are run under the same conditions as a mixture to measure elution times for analytes. The capillary cell is firmly mounted on a square clamp. A clear window on the capillary is created by burning off a portion of the polyamide coating. Residual polyamide is cleaned from the window using methanol. This unsheathing process often generates a clean but inconsistent surface that can cause scattered noise. The mount is fitted on a XYZ-translational stage where it can be adjusted to stay at the focal point of the focusing lens. To find the cleanest spot on the capillary, the mount is moved along the Y-axis while noise is monitored visually. CE peaks appear at reproducible migration times only when the mount is fixed at the same position through each run. Reproducible migration times can be obtained by maintaining voltage/current levels during separation runs, even when using different concentration levels. Figure 6.7 shows similar peak heights for different concentrations because sensitivity settings on the

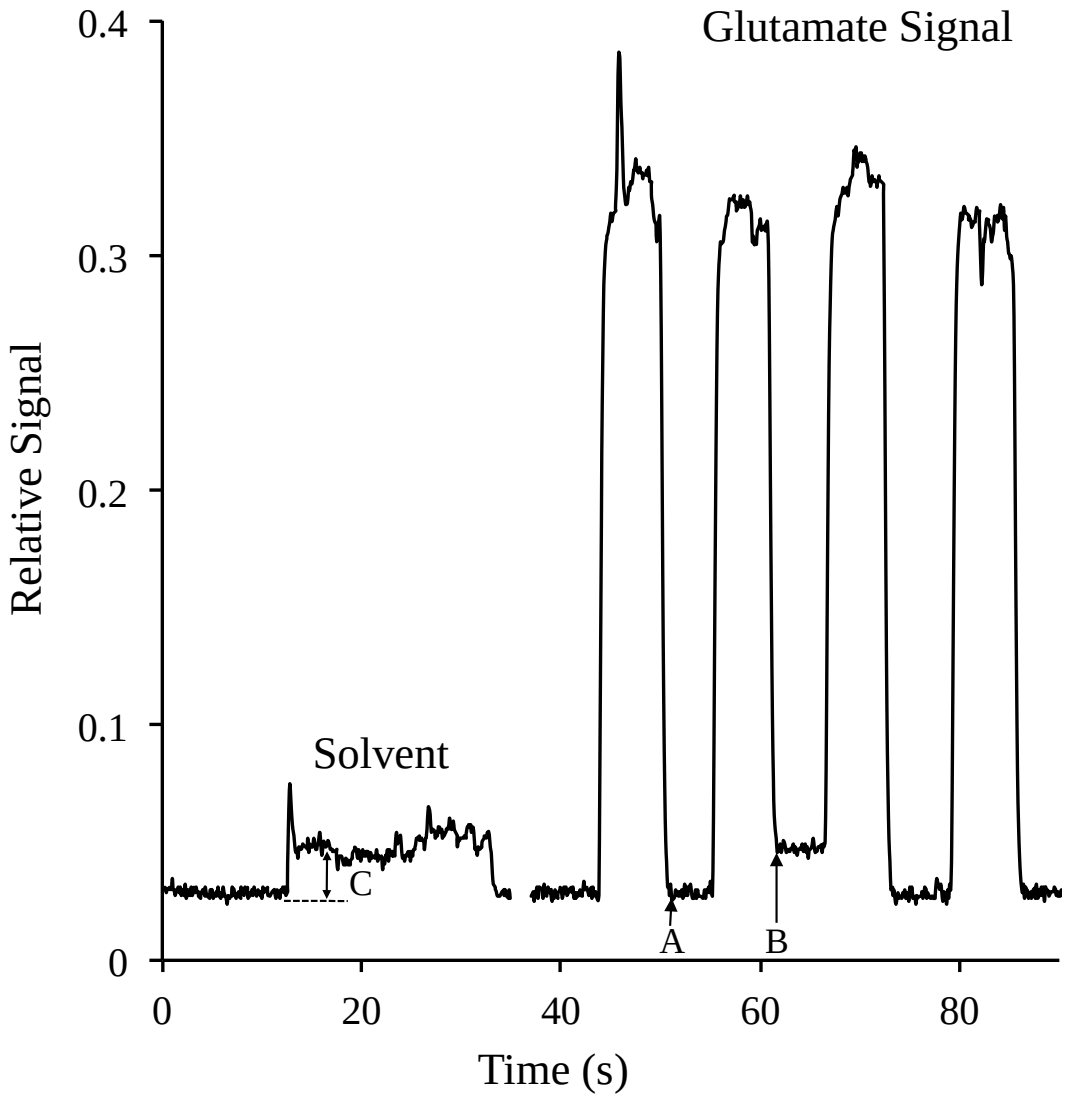

Figure 6.6 Detection of 4.6 x 10^{-6} M dabsylated Glu in 25 mM pH 8.9 sodium carbonate buffer. Wave-mixing signal is collected using a 20 mW 488 nm laser in the continuous-flow mode. The signal is verified by blocking (A) and unblocking (B) chopped and unchopped beams in the DFWM setup. Instrumental noise from the chopped beam (C) is also measured.

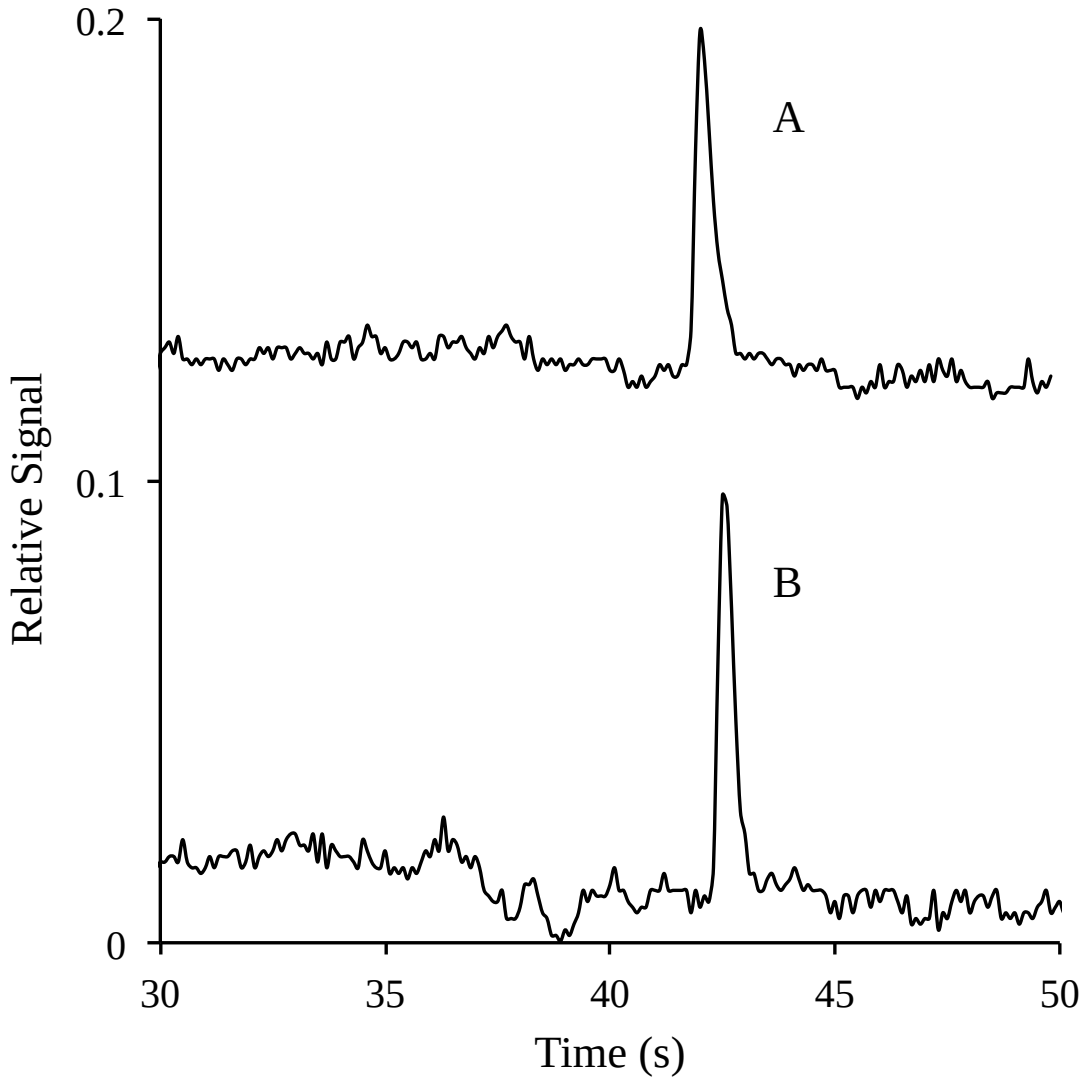

Figure 6.7 Reproducible electropherograms obtained by 488 nm DFWM-CE setup at 25 mW. Analyte: (A) 1.1 x 10^{-8} M Glu and (B) 1.1 x 10^{-9} M in 25 mM pH 8.9 sodium carbonate buffer. Running buffer: 50 mM pH 8.9 sodium carbonate buffer. Capillary: 30 cm, 75 μm i.d. The analytes are injected for 5 seconds and run at 15 kV.

lock-in amplifier are adjusted to fill the data acquisition screen. DFWM, coupled with CE, is a reliable detection method to separate and identify molecules even at low concentration levels.

6.4.4 Separation of neurotransmitters by UV and visible DFWM-CE

Native adenosine and dopamine are separated and detected by DFWM-CE using a 266 nm laser (Figure 6.8). A borate buffer is used as the running buffer, because it produces minimum noise for CE runs. Both neurotransmitters have migration times under 2 minutes. Sodium dodecyl sulfate (SDS) (60 mM) is used to perform micellar electrokinetic chromatography (MECK) discussed in Chapter 4. Dopamine and adenosine standards are used to verify peaks in the electropherograms. Label-free separation and identification of neurotransmitters eliminate the need for chromophore and fluorophore conjugation. Quick separation and identification of these neurotransmitters promise for a new method capable of fast, sensitive detection of neurotransmitters with very small sample size requirements.

Labeled GABA and Glu are separated and detected by DFWM-CE with a 488 nm laser (Figure 6.9). Field-amplified analyte stacking (FAAS) is used to enhance limit of detection (LOD). Dabsylated GABA and Glu are detected within 40 seconds with higher voltage applied. Peaks are identified by using internal standards. SDS (50mM) is also used for the separation. DFWM-CE offers relatively low background noise.

Both native and labeled neurotransmitters can be detected using a UV laser. Figure 6.10 shows the separation and detection of native adenosine, dopamine,

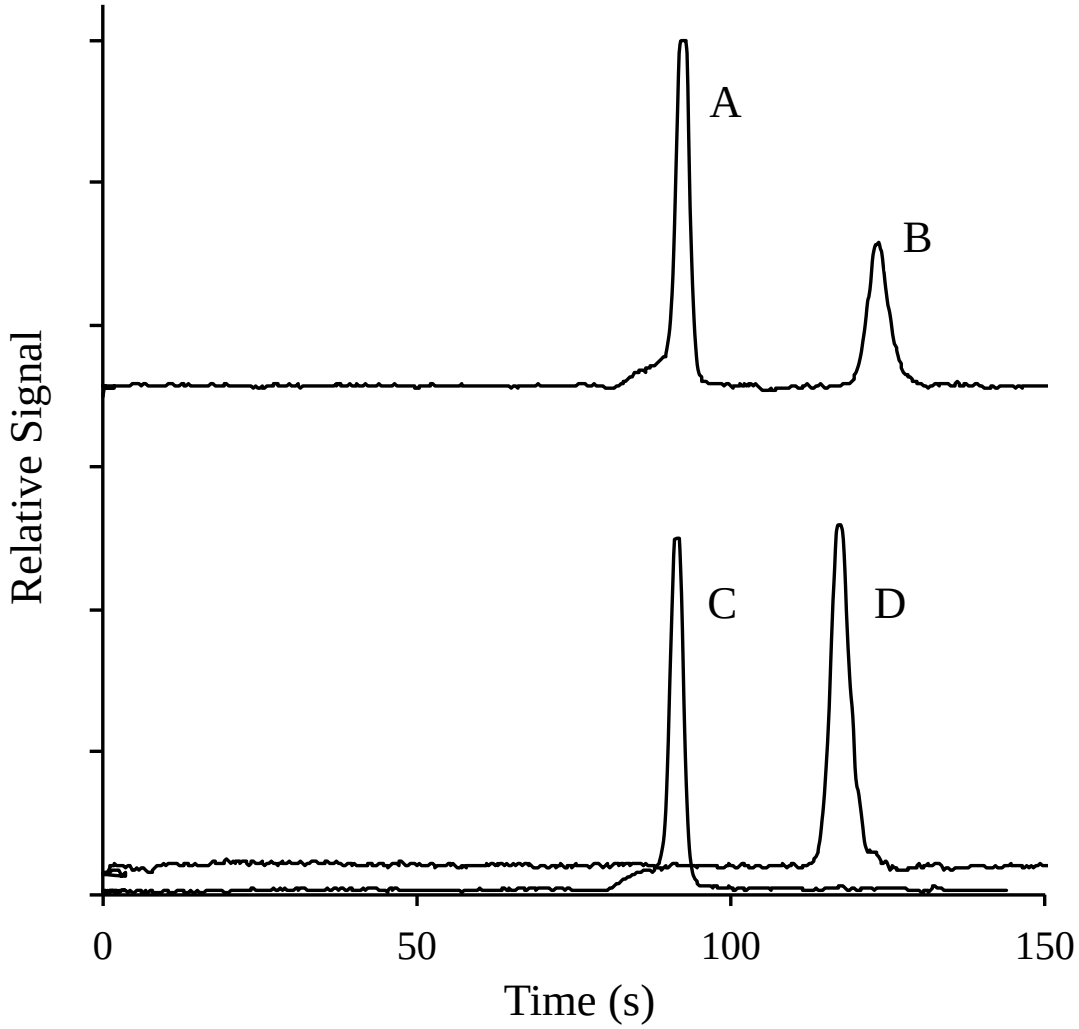

Figure 6.8 Electropherograms obtained for native adenosine and dopamine. Peak A and B: Mixture of dopamine (6.5 x 10^{-4} M) and adenosine (3.4 x 10^{-4} M), peak C: dopamine standard (6.5 x 10^{-4} M), peak D: adenosine standard (3.7 x 10^{-4} M). Running buffer: 20 mM borate buffer, pH 9.0, 60 mM SDS. Excitation source is a 266 nm laser at 20 mW. Capillary: 30 cm, 75μm i.d., 10 s electrokinetic injection, 12 kV separation.

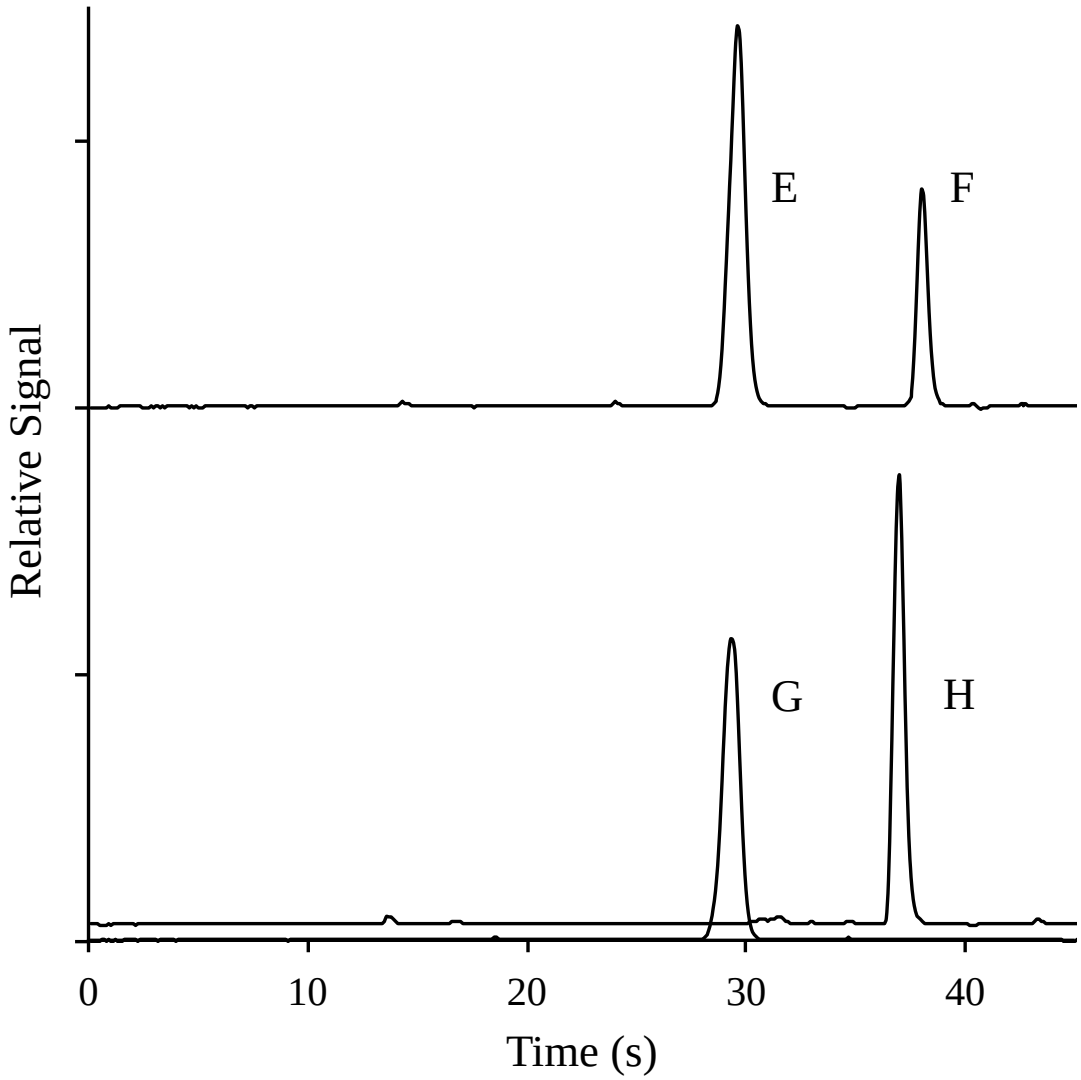

Figure 6.9 Peaks E and F: dabsylated GABA and Glu from one pot reaction, peaks G: dabsylated GABA standard (9.6 x 10^{-6} M), peak H: dabsylated Glu (9.0 x 10^{-6} M). Running buffer: 50 mM borate buffer, pH 8.6, 20 mM SDS. The excitation laser source is a 488 nm laser at 25 mW. Capillary: 30 cm, 75μm i.d., 10 s electrokinetic injection, 18 kV separation.

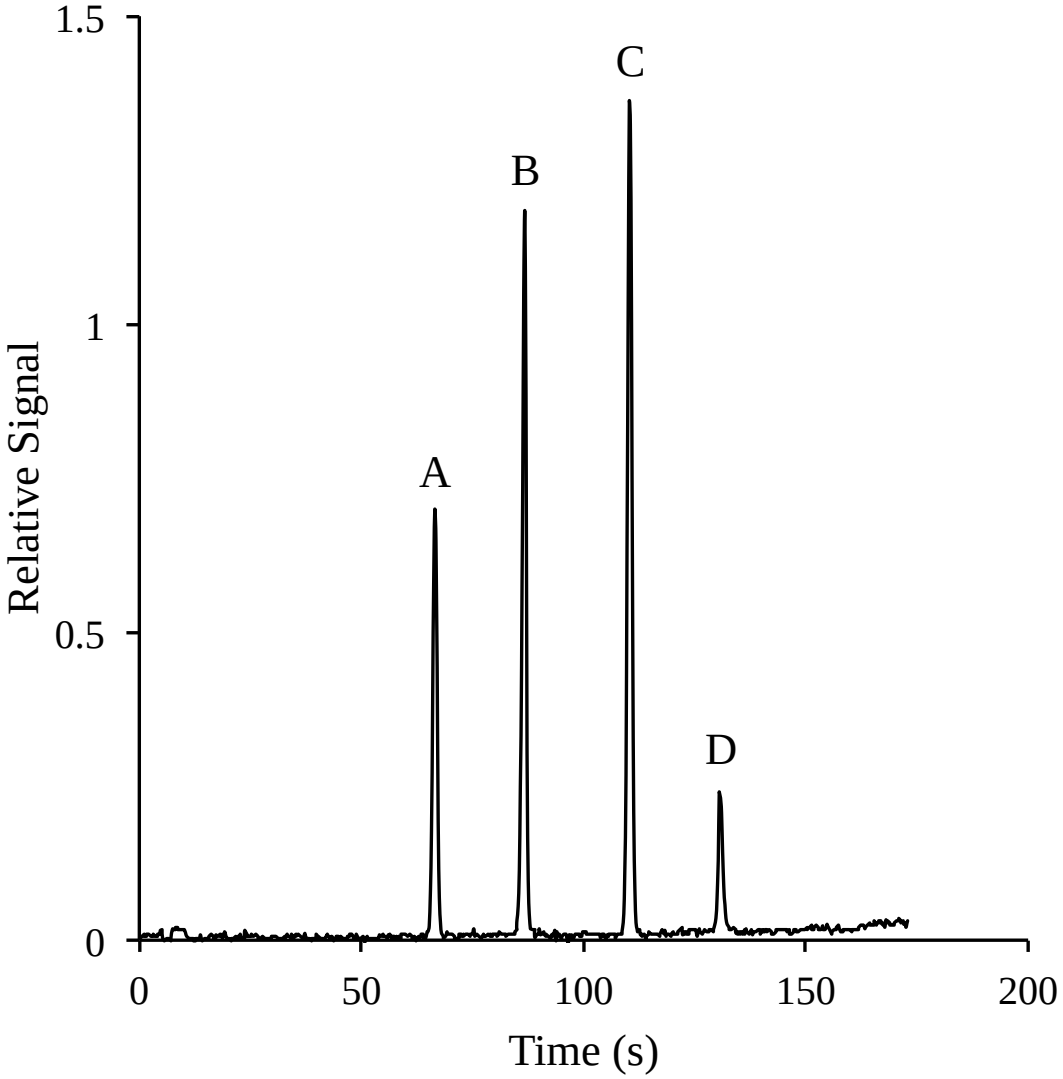

Figure 6.10 Peak A: native dopamine (1.6 x 10^{-3} M), B: native adenosine (1.0 x 10^{-3} M), C: dansyl-GABA (1.7 x 10^{-3} M), and D: dansyl-glutamate (2.0 x 10^{-3} M). Running buffer: 20 mM borate buffer, pH 9.0, 45 mM SDS. CE detection by a 20 mW 266 nm laser. Capillary: 30 cm, 75μm i.d, 5 s electrokinetic injection, 12 kV separation.

commercially available dansylated GABA and glutamate. Dansyl, one of the simplest sulfonamide derivatives, is an amine-reactive dye suitable for GABA and glutamate labeling. All the neurotransmitters are dissolved in 20 mM, pH 9 borate buffer (2.0 mg/mL). The mixture solution contains 100 μL of dopamine and adenosine, 200 μL of dansyl-GABA, and 300μL of dansyl-glutamate. Analysis times for native and fluorophore-labeled neurotransmitters are under 150 s and the results are reproducible.

6.4.5 Detection Limits by DFWM-CE

Native label-free detection, as demonstrated for adenosine and dopamine, is preferred since it is faster and does not need labels or time-consuming preparation steps. Both dopamine and adenosine are electroactive molecules, thus electrochemical detection techniques are commonly used to detect them in their native form.[33] CE yields efficient separation and is suitable for analyzing biological analytes due to the small sample size requirements (femtolitter to picoliter).[34] Often, CE is coupled to a laser-induced fluorescence detector where the analyte must be a fluorescent molecule or conjugated to a fluorescent tag in order to obtain ultrasensitive detection limits. Since adenosine and dopamine do not fluoresce, ultrasensitive detection in their native form is challenging using currently available methods. Nonlinear absorption-based wave-mixing techniques offer ultrasensitive detection limits for analytes that do not fluoresce. Numerous types of biological analytes, including small molecules, peptides and proteins with extended conjugation, inherently absorb at the 266 nm laser excitation wavelength.[35]

Nonlinear absorption-based wave-mixing detection sensitivity is verified by

running the target neurotransmitters at low concentration levels. Micromolar concentration analytes are analyzed first to verify separation efficiency and to measure relative analyte migration times. After successful CE runs, lower concentration analytes are separated and detected and the LOD determined.

Figure 6.11 shows the LOD of at 3.7×10^{-13} M, the best reported in these studies due to its high extinction coefficient. A mass detection limit of 2.0×10^{-23} mol is determined for native adenosine, which corresponds to approximately 13 molecules inside the wave-mixing probe volume. Although dopamine has a much lower extinction coefficient at 266 nm as compared to that of adenosine, an excellent concentration detection limit of 2.1×10^{-9} M (Figure 6.12) is determined for dopamine, corresponding to an excellent mass detection limit of 1.2×10^{-19} mol inside the probe volume.

Detection limits can be easily enhanced by using a simple labeling reaction for analytes with low extinction coefficients, such as GABA and Glu. Dabsyl chloride is an excellent reagent for target neurotransmitters, since it reacts with primary and secondary amines[36] to form compounds that absorbs visible light (Figure 6.5). This label is well-suited to detect amino acids and biogenic amines using HPLC.[30] Limited studies have reported using CE to analyze these small molecules as chromophores. Dabsyl chloride requires 7 min to complete a reaction with a molecule with amines. This is much faster than other amine reactive dyes such as fluorescence isothiocyanate (FITC), 4-Chloro-7-nitrobenzofurazan (NBD-Cl) and dansyl.[37-39] FITC has issues with both stability in solution and known impurities present in commercially available stock.[40] Unlike naphthalene-2,3-dicarboxaldehyde (NDA),

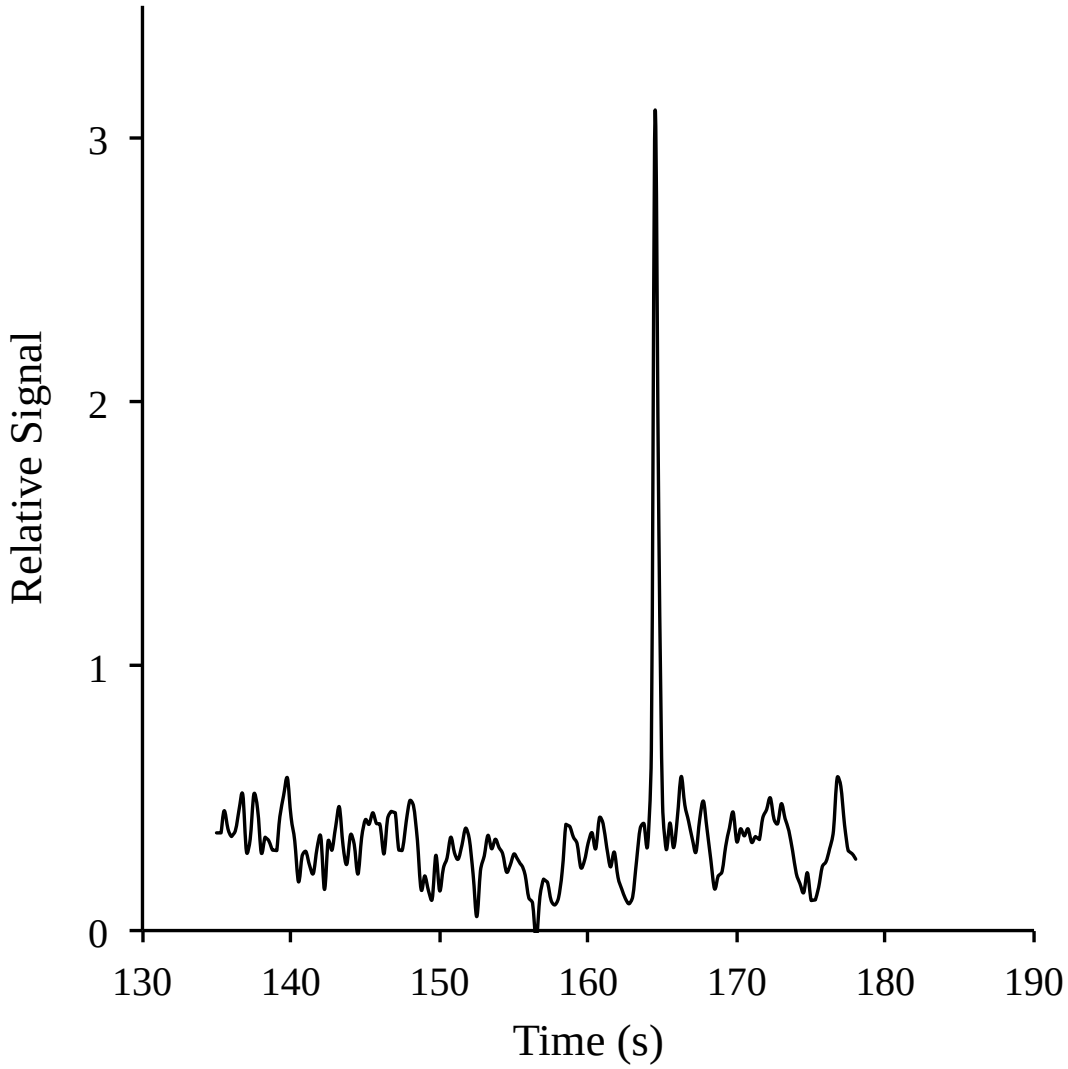

Figure 6.11 DFWM-CE electropherogram of adenosine at 3.7 x 10^{-13} M. Running buffer: 20 mM borate buffer, pH 9.0, 60 mM SDS. Detection by 20 mW 266 nm laser. Capillary: 30 cm, 75 μm i.d., 5 s electrokinetic injection, 12 kV separation.

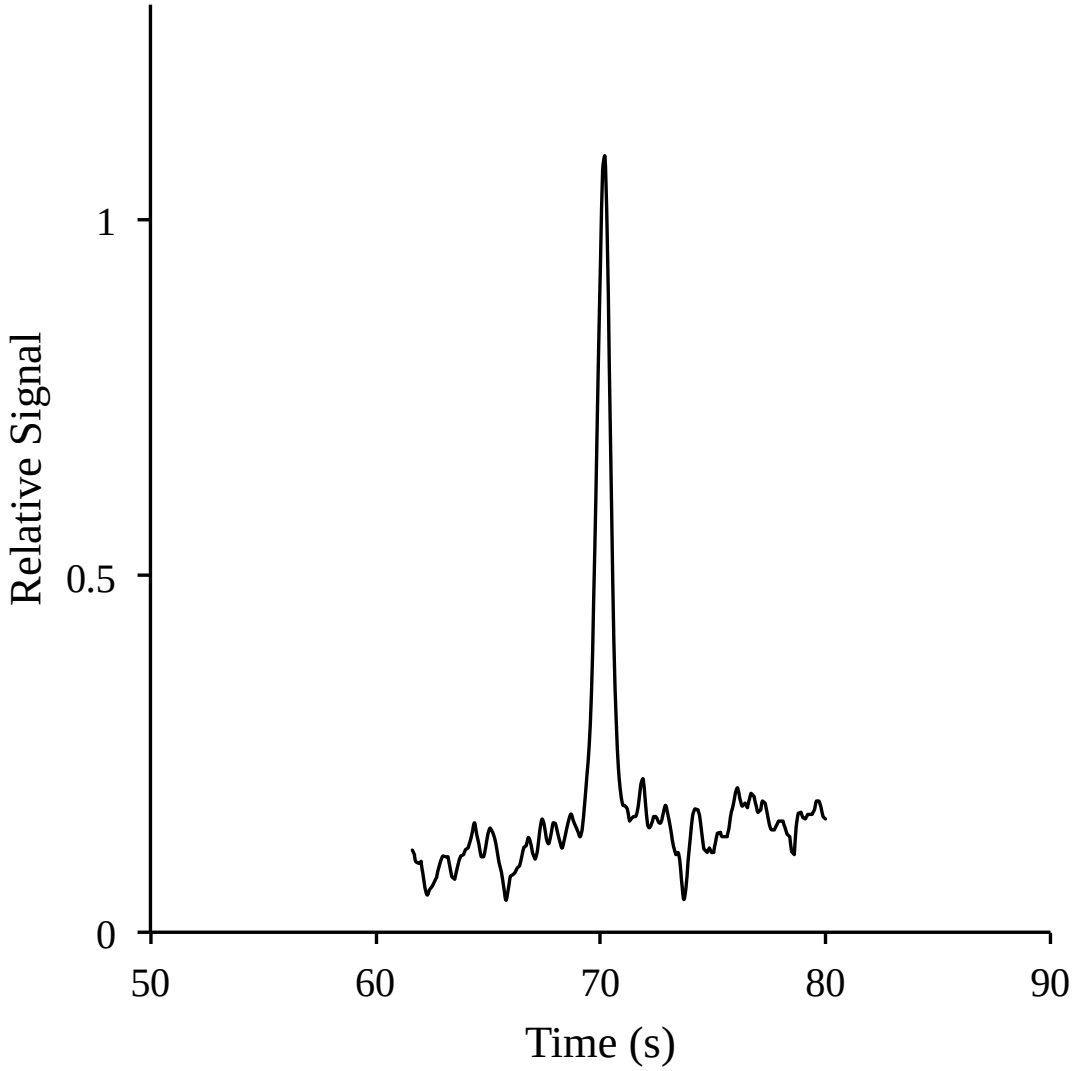

Figure 6.12 DFWM-CE electropherogram of dopamine at 2.1 x 10^{-9} M. Running buffer: 25 mM borate buffer, pH 9.0, 40 mM SDS. Detection by 20 mW 266 nm laser. Capillary: 30 cm, 75 μm i.d., 2 s electrokinetic injection, 8.1 kV separation.

dabsylation requires no toxic reagent such as NaCN.[41]

Extracted Glu and GABA are quantified by a UV-visible absorption spectrometer. The analytes are then serially diluted ten times with 25 mM sodium carbonate buffer (pH 8.9). Concentration detection limits of 1.1×10^{-9} M and 1.7×10^{-10} M are determined for Glu and GABA, respectively, corresponding to mass detection limits of 8.7×10^{-20} mol and 1.3×10^{-20} mol for Glu and GABA, respectively, inside the 79 pL probe volume of the 488 nm excitation laser (Figure 6.13 – 6.14).

6.4.6 DOPAMINE-NAPHTHALENE-2,3-DICARBOXALDEHYDE DETECTION USING A 447 NM LASER

Naphthalene-2,3-dicarboxaldehyde readily forms 1-cyanobenzisoindole derivative when a primary amine is present (Figure 6.15). The product conveniently absorbs at the blue/violet wavelength and it can be easily detected using visible laser wave mixing. A similar reaction takes place with o-phthalaldehyde (OPA), generating a fluorescence compound with a primary amine with just a trace amount of the analyte. Although OPA is widely used, it forms relatively unstable products.[32] On the other hand, NDA goes through a very similar reaction mechanism to form a more stable fluorescent molecule.

The extinction coefficients are calculated using the Beer-Lambert law at the 447 nm laser wavelength. UV-visible absorption spectra provide absorbance value for each component at 447 nm as shown in Figure 6.16. The extinction coefficients of free NDA, native dopamine and CBI-derivative are determined to be 66 $M^{-1}cm^{-1}$, 27 $M^{-1}cm^{-1}$ and 5,100 $M^{-1}cm^{-1}$. Unreacted NDA and native dopamine do not absorb

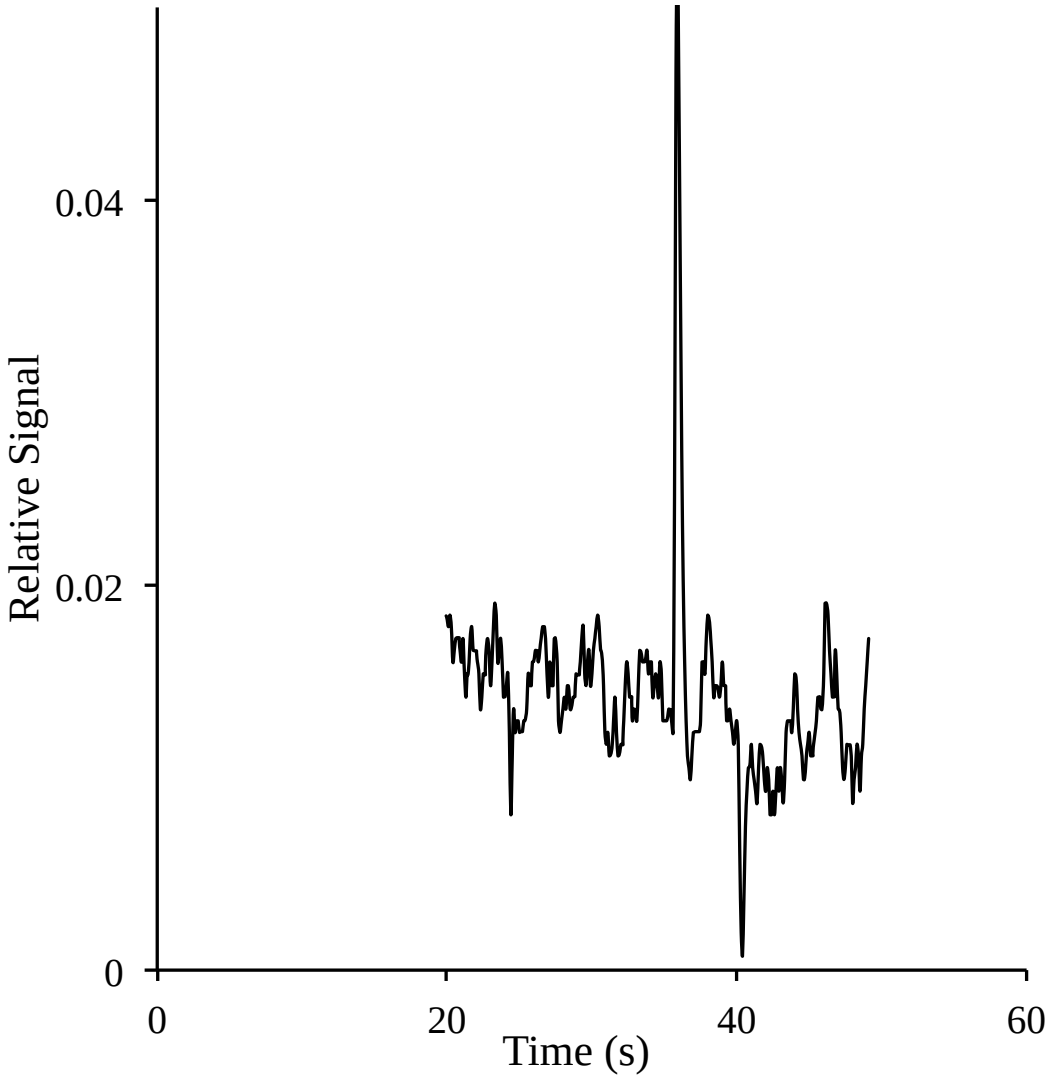

Figure 6.13 DFWM CE electropherogram of Glu at 1.1 x 10^{-9} M. Running buffer: 50 mM, pH 8.9, sodium carbonate buffer. Detection by 25 mW 488 nm laser. Capillary: 30 cm, 75 μm i.d, 10 s electrokinetic injection, 15 kV separation.

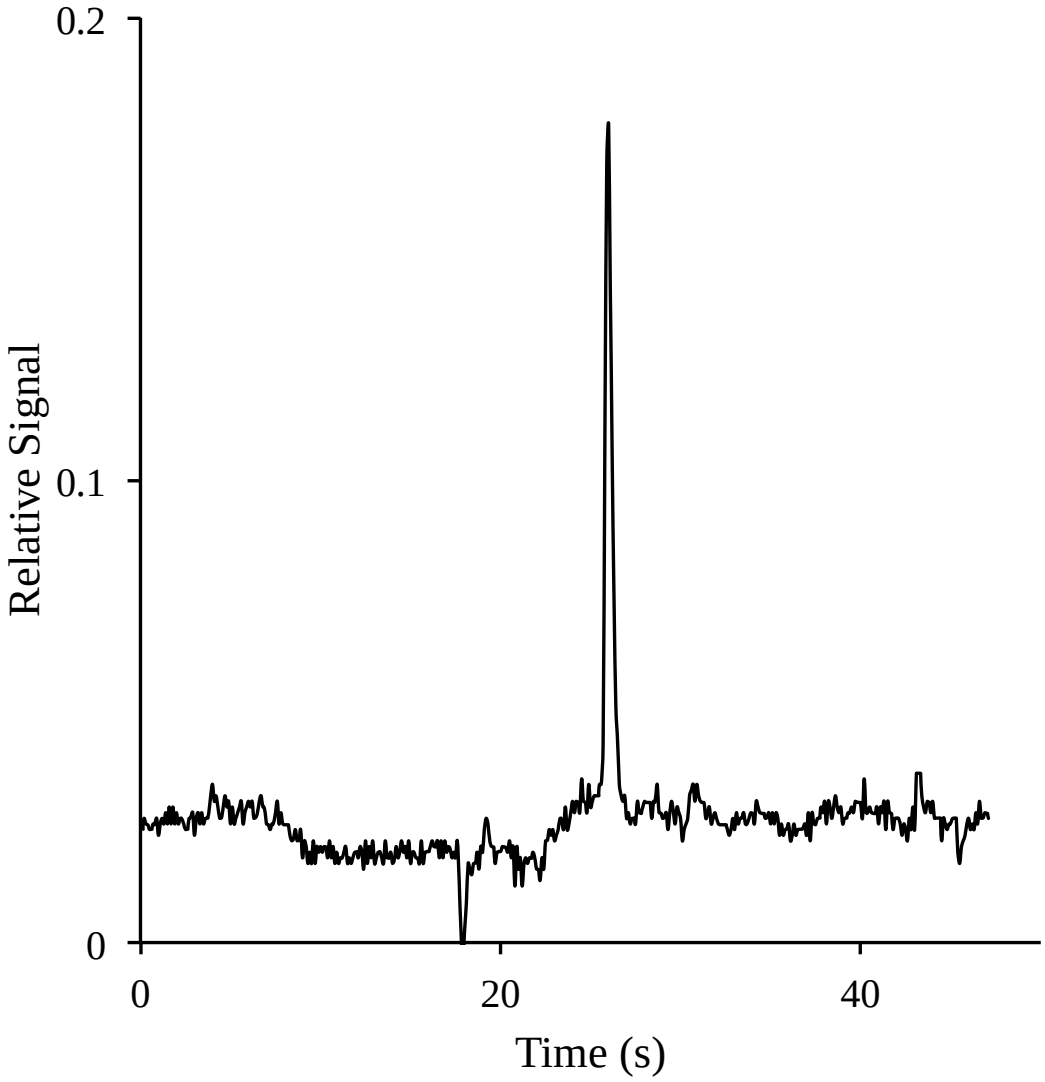

Figure 6.14 DFWM-CE electropherogram of GABA at 1.7 x 10^{-10} M. Running buffer: 50 mM, pH 8.9, sodium carbonate buffer. Detection by 25 mW 488 nm laser. Capillary: 30 cm, 75 μm i.d., 15 s electrokinetic injection time, 15 kV separation.

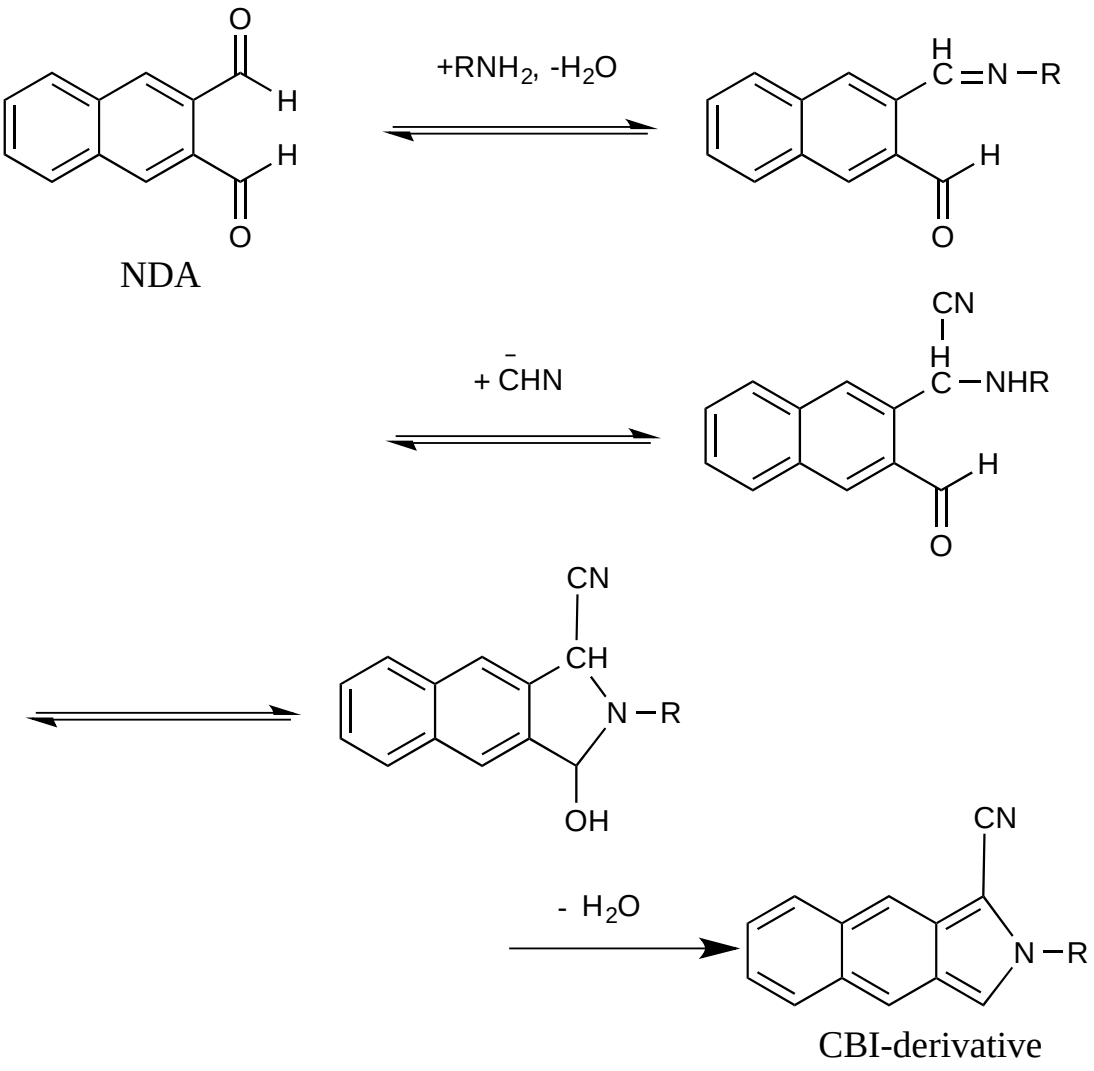

Figure 6.15 Reaction for NDA with a primary amine. The product, CBI-derivative, absorbs at the 447 nm laser excitation wavelength.

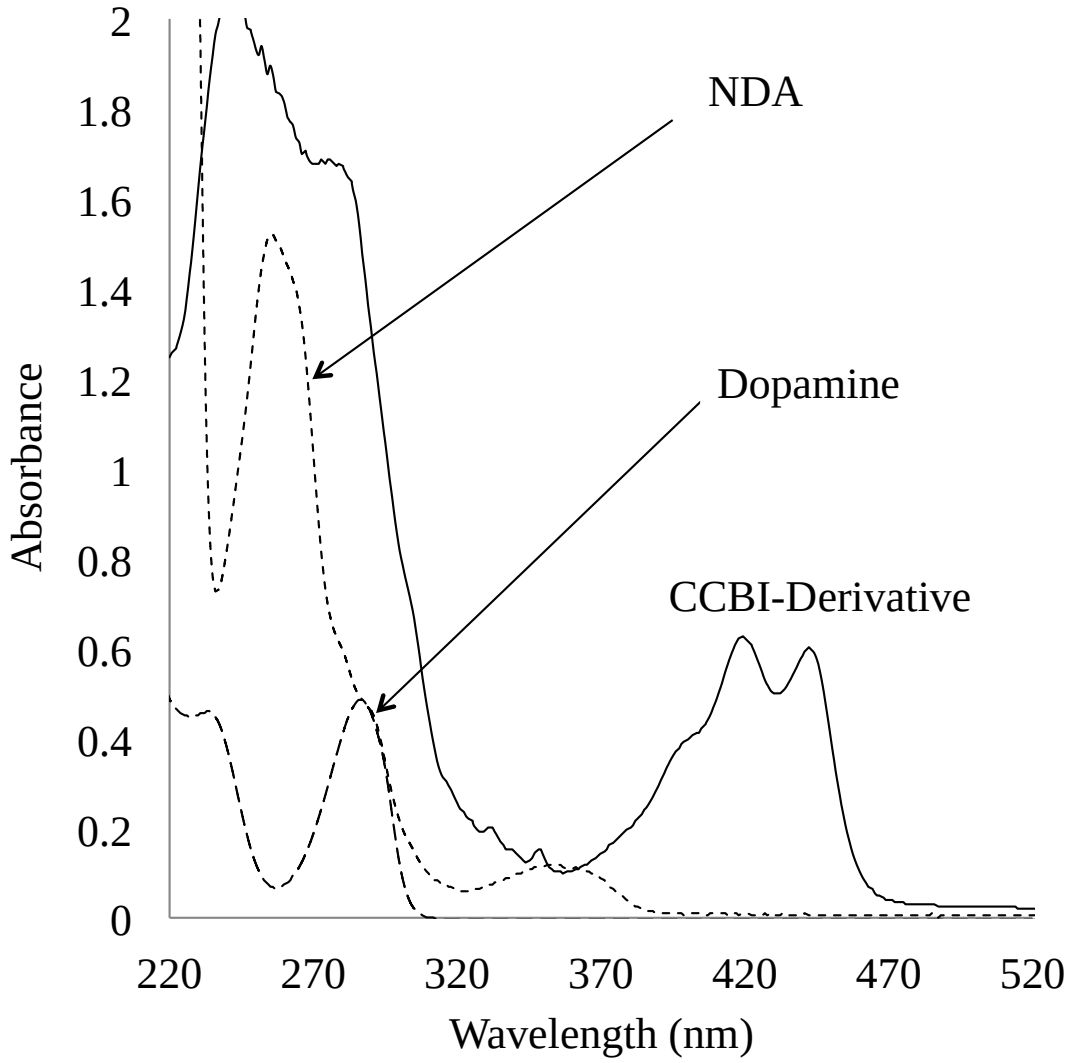

Figure 6.16 UV-visible absorption spectra of unreacted NDA, native dopamine and CBI-derivative. The product absorbs strongly at the 447 nm laser excitation wavelength.

significantly at 447 nm and are not detected by the laser.

Figure 6.17 shows UV-visible absorption spectra of NDA and its dopamine reaction products. UV-visible absorption spectra are taken in 20 s intervals after all the chemicals required for the reaction are mixed together. The spectrum of the lowest absorption is the beginning of the reaction. The first 110 seconds show a sharp increase in the products.

Figure 6.18 shows the rates of dopamine and NDA reactions. It shows that without the presence of dopamine, i.e., primary amine, absorption does not change with incubation time. On the other hand, dopamine, NDA and cyanide react to completion within 3 minutes to form products that absorb at 447 nm.

A typical DFWM setup is aligned and optimized first to obtain a visual wave-mixing signal, and then background noise levels minimized while the analyte flows through the capillary driven by a peristaltic pump. A flow rate of 2.1 μL/min yields an optimum signal for this wave-mixing setup.

The DFWM signal of dopamine-NDA is obtained by flowing it through the capillary and detecting it using a 447 nm laser. Figure 6.19 shows confirmation of the wave-mixing signal by blocking the chopped or the unchopped beam in the laser setup. To enhance the S/N, beam blockers, optical irises and pinholes are used to block background noise levels. The concentration of dopamine hydrochloride detected is 19 μg/mL, corresponding to a concentration detection limit of 1.9 μM (S/N of 2) and a mass detection limit of 228 attomole based on the 12 pL probe volume of the 447 nm laser.

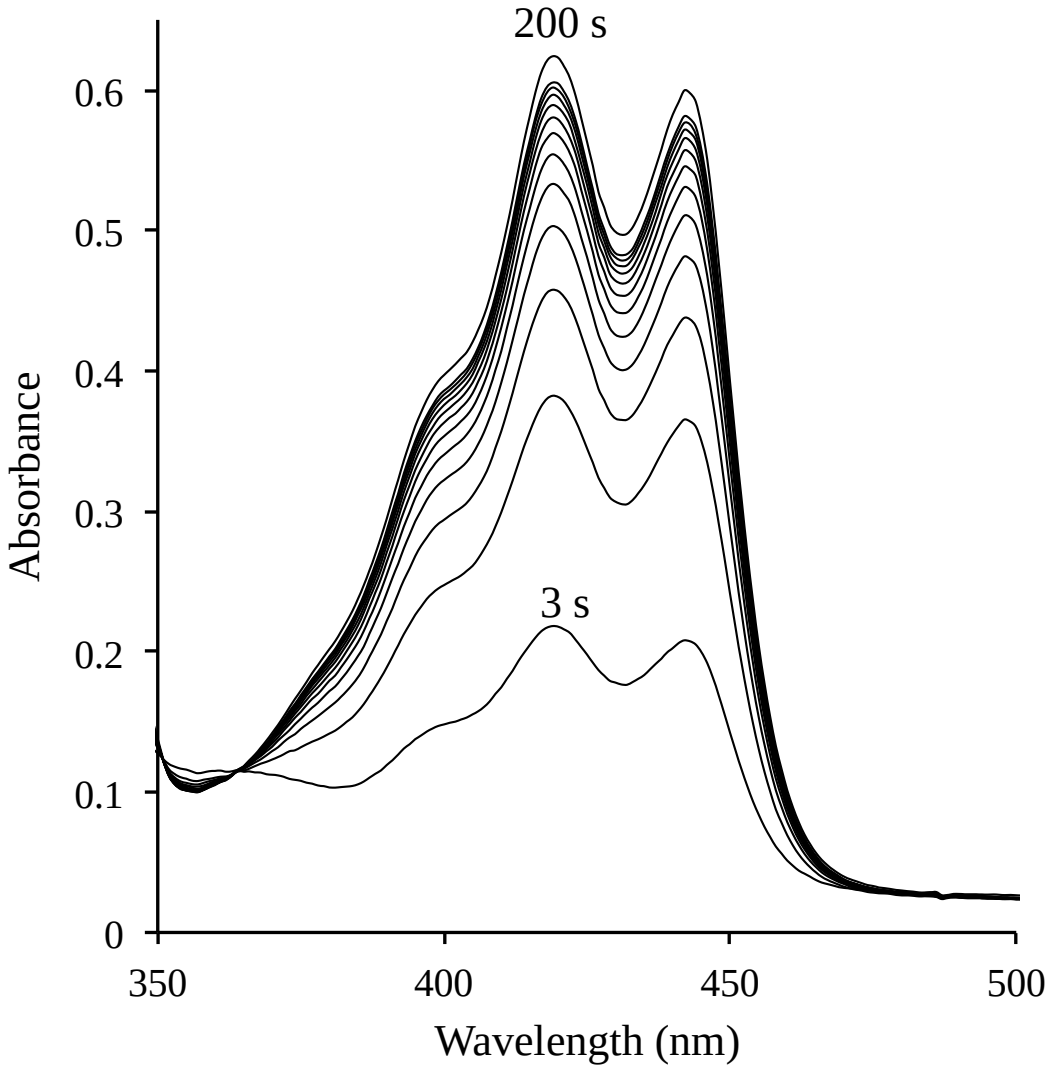

Figure 6.17 UV-visible absorption spectra of NDA and dopamine products at different times.

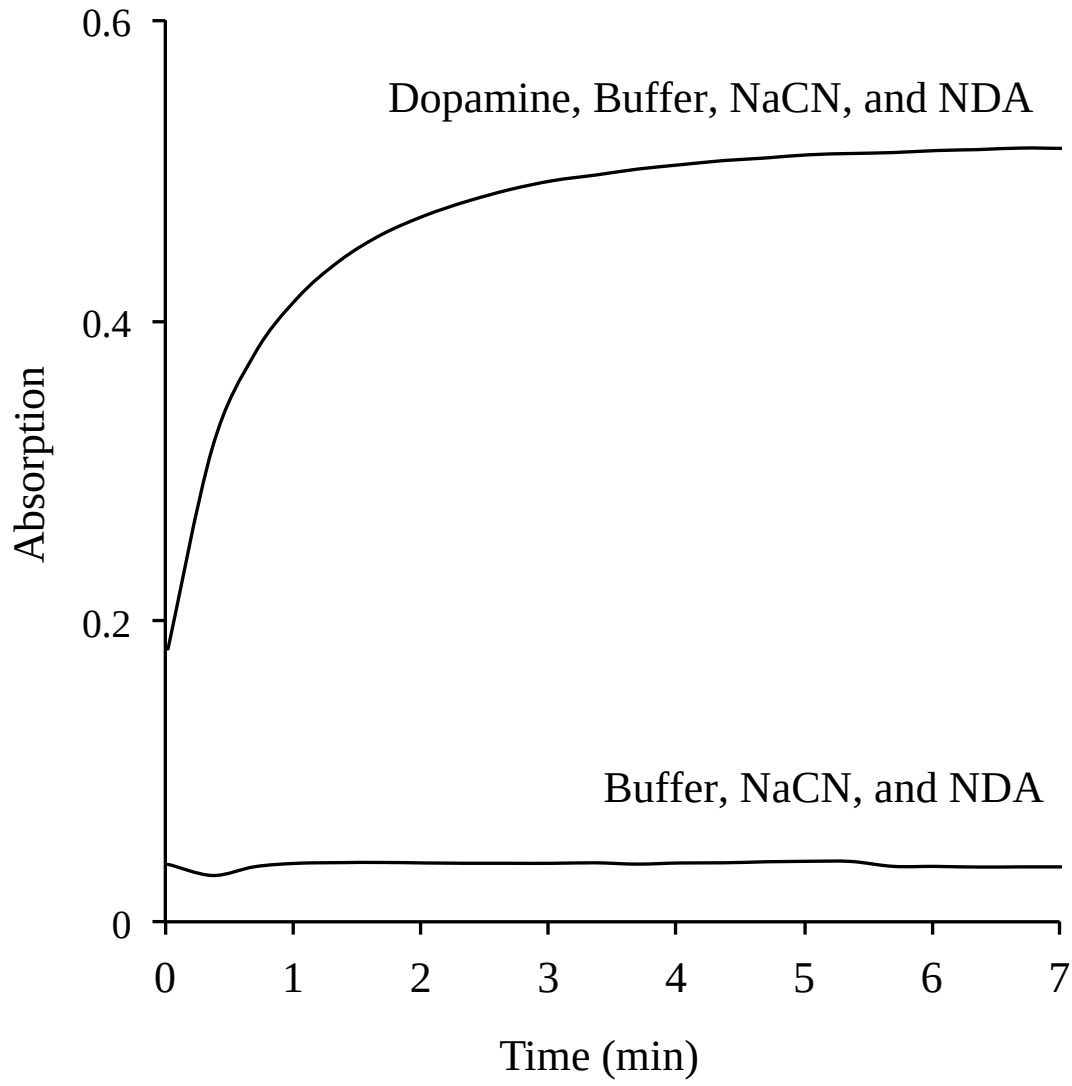

Figure 6.18 Reaction rate of NDA, dopamine and cyanide to form colored compound at 447 nm. The figure also shows that without dopamine, the reaction does not proceed.

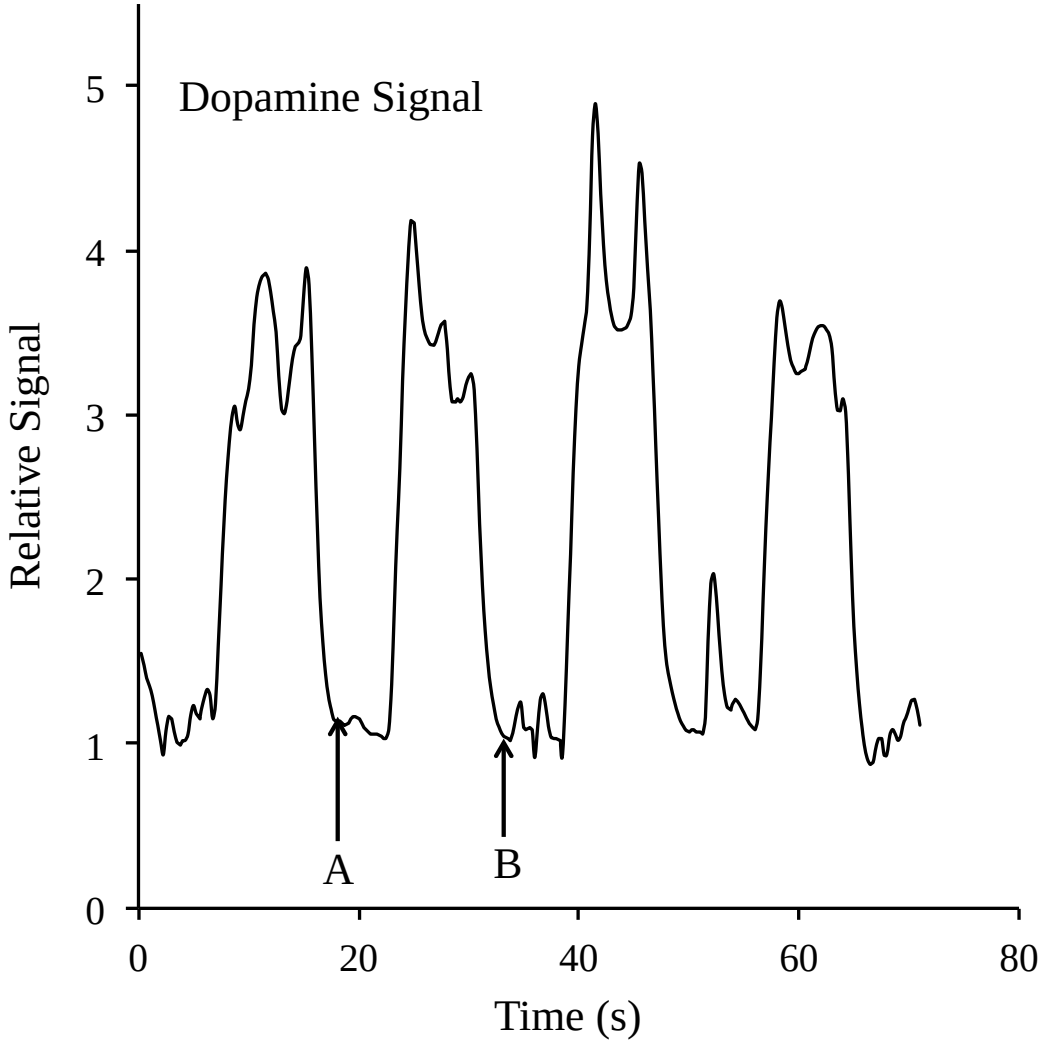

Figure 6.19 Detection of 19 μg/mL dopamine-NDA in 100 mM, pH 9.0, borate buffer. Wave-mixing signal detected by a 25 mW 447 nm laser in the continuous-flow mode. The signal is verified by blocking (A) and unblocking (B) the chopped and unchopped beams in the DFWM setup.

6.5 Conclusion

This chapter describes DFWM as an ultrasensitive absorption-based optical detection method for native and labeled neurotransmitters. DFWM-CE allows ultrasensitive (13 molecules) and selective detection of neurotransmitters (Table 6.2). Picoliter probe volume in DFWM yields ultrasensitive mass detection limits. Wave mixing allows ultrasensitive detection of both native and labeled neurotransmitters. Detection sensitivity for analytes with low extinction coefficients can be easily improved by labeling with dabsyl chloride or other agents. Laser wave mixing is more sensitive than conventional absorption techniques by orders of magnitude because the wave-mixing signal is a coherent laser-like beam. Since wave mixing is an absorption-based method, one can use both chromophores and fluorophores as labels. The technique offers unique and significant advantages including coherent laser-like signals, virtually 100% optical signal collection efficiency, yoctomole detection sensitivity, compact and portable detection setup, and low laser power requirements. Our custom-built CE offers excellent resolution and reproducibility. The separation methods presented here can resolve structurally similar molecules with similar molecular weights. DFWM-CE requires small sample volumes and offers short analysis time, and thus, it is excellent for measuring biological analytes of limited sizes in a wide range of applications including the study of brain chemistry.

Table 6.2 Detection limits for native and labeled neurotransmitters.

Neurotransmitter	Laser wavelength	Detection limit (S/N=2)	Mass detection limit (S/N=2)
Adenosine	266 nm (CE)	1.0×10^{-13} M	5.6×10^{-24} mol
Dopamine	266 nm (CE)	1.2×10^{-9} M	6.6×10^{-20} mol
Dabsylated Glu	488 nm (CE)	3.7×10^{-10} M	2.9×10^{-20} mol
Dabsylated GABA	488 nm (CE)	4.1×10^{-11} M	3.2×10^{-21} mol
Dopamine-NDA	447 nm (flow)	1.9×10^{-6} M	7.0×10^{-16} mol

6.6 Acknowledgement

The majority of the material for this chapter comes directly from a manuscript entitled “Zepto- and Yocto-mole Detection of Native and Labeled Neurotransmitters by Nonlinear Wave-Mixing Spectroscopy Coupled with Capillary Electrophoresi.,” by Manna F. Iwabuchi, Marcel M. Hetu, Sashary Ramos, and William G. Tong, to be submitted. The dissertation author is the primary author of this manuscript.

6.7 References

(1) Latini, S.; Pedata, F. *Journal of Neurochemistry* **2001**, *79*, 463.

(2) Owesson-White, C. A.; Roitman, M. F., *et al J Neurochem* **2012**, *121*, 252.

(3) Reisi, P.; Alaei, H., *et al Pathophysiology : the official journal of the International Society for Pathophysiology / ISP* **2009**, *16*, 63.

(4) Fedele, E.; Mazzone, P., *et al Exp Neurol* **2001**, *167*, 356.

(5) Hasanzadeh, M.; Shadjou, N., *et al Journal of neuroscience methods* **2013**, *219*, 52.

(6) Zinellu, A.; Sotgia, S., *et al Methods Mol Biol* **2013**, *919*, 35.

(7) Kanamori, K.; Kondrat, R. W., *et al Cell Mol Biol (Noisy-le-grand)* **2003**, *49*, 819.

(8) Mickadeit, F. K.; Berniolles, S., *et al Anal Chem* **2004**, *76*, 1788.

(9) Shih, L. C.; Tarsy, D. *Neuromodulation : journal of the International Neuromodulation Society* **2011**, *14*, 208.

(10) van Dijk, A.; Klompmakers, A. A., *et al J Neurochem* **2012**, *123*, 897.

(11) Shon, Y. M.; Chang, S. Y., *et al J Neurosurg* **2010**, *112*, 539.

(12) Liu, H. G.; Ma, Y., *et al Neuromodulation : journal of the International Neuromodulation Society* **2013**.

(13) Felicia S. Manciu, K. H. L., William G. Durrer, Kevin E. Bennet *Neuromodulation 2* **2012**, *XX*.

(14) Goyal, R. N.; Singh, S. P. *Carbon* **2008**, *46*, 1556.

(15) Lee, K. H.; Blaha, C. D., *et al The European journal of neuroscience* **2006**, *23*, 1005.

(16) Deng, Y. H.; Wang, H., *et al Journal of separation science* **2008**, *31*, 3088.

(17) Piepponen, T. P.; Skujins, A. *J Chromatogr B* **2001**, *757*, 277.

(18) Shah, A. J.; Crespi, F., *et al Journal of Chromatography B-Analytical Technologies in the Biomedical and Life Sciences* **2002**, *781*, 151.

(19) Windels, F.; Bruet, N., *et al Journal of Neuroscience Research* **2003**, *72*, 259.

(20) Lee, K. H.; Blaha, C. D., *et al Neuromodulation : journal of the International Neuromodulation Society* **2009**, *12*, 85.

(21) Agnesi, F.; Tye, S. J., *et al J Neurosurg* **2009**, *111*, 701.

(22) Agnesi, F.; Blaha, C. D., *et al Journal of neural engineering* **2010**, *7*, 26009.

(23) Cheng, Y. F.; Dovichi, N. J. *Science* **1988**, *242*, 562.

(24) Greco, S.; Danysz, W., *et al Analytica Chimica Acta* **2013**, *771*, 65.

(25) Nunes, J. A.; Tong, W. G. *Anal Chem* **1993**, *65*, 2990.

(26) Prata, C.; Bonnafous, P., *et al Electrophoresis* **2001**, *22*, 4129.

(27) García-Cañas, V.; Cifuentes, A. *Electrophoresis* **2008**, *29*, 294.

(28) Wu, Z. Q.; Tong, W. G. *J Chromatogr A* **1997**, *773*, 291.

(29) Chang, J. Y.; Knecht, R., *et al Biochem J* **1981**, *199*, 547.

(30) Krause, I.; Bockhardt, A., *et al J Chromatogr A* **1995**, *715*, 67.

(31) Tsai, C. H.; Huang, H. M., *et al Electrophoresis* **2003**, *24*, 3083.

(32) Demontigny, P.; Stobaugh, J. F., *et al Anal Chem* **1987**, *59*, 1096.

(33) Fang, H. F.; Pajski, M. L., *et al Anal Methods-Uk* **2013**, *5*, 2704.

(34) Lapainis, T.; Scanlan, C., *et al Anal Bioanal Chem* **2007**, *387*, 97.

(35) Schmid, F.-X. In *eLS*; John Wiley & Sons, Ltd: 2001.

(36) Romero, R.; Bagur, M. G., *et al Chromatographia* **2000**, *51*, 404.

(37) Xiong, S. X.; Han, H. W., *et al Biomed Chromatogr* **2001**, *15*, 83.

(38) Shi, X.; Liang, P., *et al Journal of separation science* **2012**, *35*, 548.

(39) De Mey, E.; Drabik-Markiewicz, G., *et al Food Chem* **2012**, *130*, 1017.

(40) Siri, N.; Lacroix, M., *et al Electrophoresis* **2006**, *27*, 4446.

(41) Wang, C.; Zhao, S., *et al Journal of chromatography. B, Analytical technologies in the biomedical and life sciences* **2006**, *833*, 129.

CHAPTER 7
ULTRASENSITIVE DETECTION OF ALZHEIMER'S DISEASE BIOMARKERS Aβ1-42 AND Aβ1-40

7.1 Abstract

Degenerate Four-Wave Mixing (DFWM), a nonlinear absorption-based technique, is an excellent analytical tool for biomedical applications such as early diagnosis of neurodegenerative diseases. Aβ is a potential biomarker for Alzheimer's disease (AD), but current detection techniques show inconsistent quantification results. The DFWM signal has a quadratic dependence on analyte concentration, and hence, it is effective for monitoring small changes in concentrations of peptides in plasma. Chromophores can be used as labels to enhance sensitivity and obtain better S/N as compared to using fluorophores as labels. In this chapter, a chromophore label, QSY 35 acetic acid succinimidyl ester, is used to detect amyloids. The wave-mixing signal is obtained by intersecting two focused laser beams inside a capillary where the analytes are separated and detected. The wave-mixing signal is a coherent laser-like beam and can be collected with virtually 100% efficiency with minimum optical background noise. Using DFWM, interfaced to capillary electrophoresis, concentration detection limits of 8.2×10^{-13} M and 1.2×10^{-12} M (S/N of 2) are determined for Aβ1-42 and Aβ1-40, respectively. Based on the sample probe volume used, mass detection limits of 6.5×10^{-23} mol and 9.5×10^{-23} mol are determined for Aβ1-42 and Aβ1-40, respectively.

7.2 Introduction

7.2.1 ALZHEIMER'S DISEASE

Alzheimer's disease (AD) is the most widespread neurodegenerative disease, affecting approximately 24 million people in 2001, and this number is estimated to increase up to 81 million by 2040.[1] The loss of neurons, intracellular neurofibrillary tangles, and extracellular senile amyloid resulting in dysfunction of adjacent axons and dendrites are the major pathological hallmarks of AD.[2] It has been reported that the degenerative process begins many years before the onset of clinical symptoms, such as cognitive impairment and mood change.[3-5] Early diagnosis at preclinical stages is currently limited and there is no cure for AD. Thus, presymptomatic diagnosis is crucial to the advancement of efficient and rapid treatment.[6-8]

7.2.2 BIOMARKERS AND DIAGNOSIS FOR ALZHEIMER'S DISEASE

A biomarker is an indicator whose presence, concentration and activity correlate with a disease. A biomarker plays crucial roles for accurate diagnosis, detecting early onset, and monitoring progression and therapeutic effects of a treatment.[9] An ideal biomarker is specific to the disease, able to accurately predict the course of the disease, and reflective of the extent of treatment. Biomarkers of AD have been extensively researched.[6,7]

Figure 7.1 describes a pathological pathway and potential biomarkers for AD.[10] Amyloid β (Aβ) 1-42 and other shorter Aβ fragments may be generated by amyloid precursor protein (APP) proteolytic cleavage by two proteolytic enzymes, β- and γ-secretase.[10] The aggregation of Aβ1-42 results in oligomerization and fibrillization that eventually lead to deposition of senile plaques. The toxicity of the

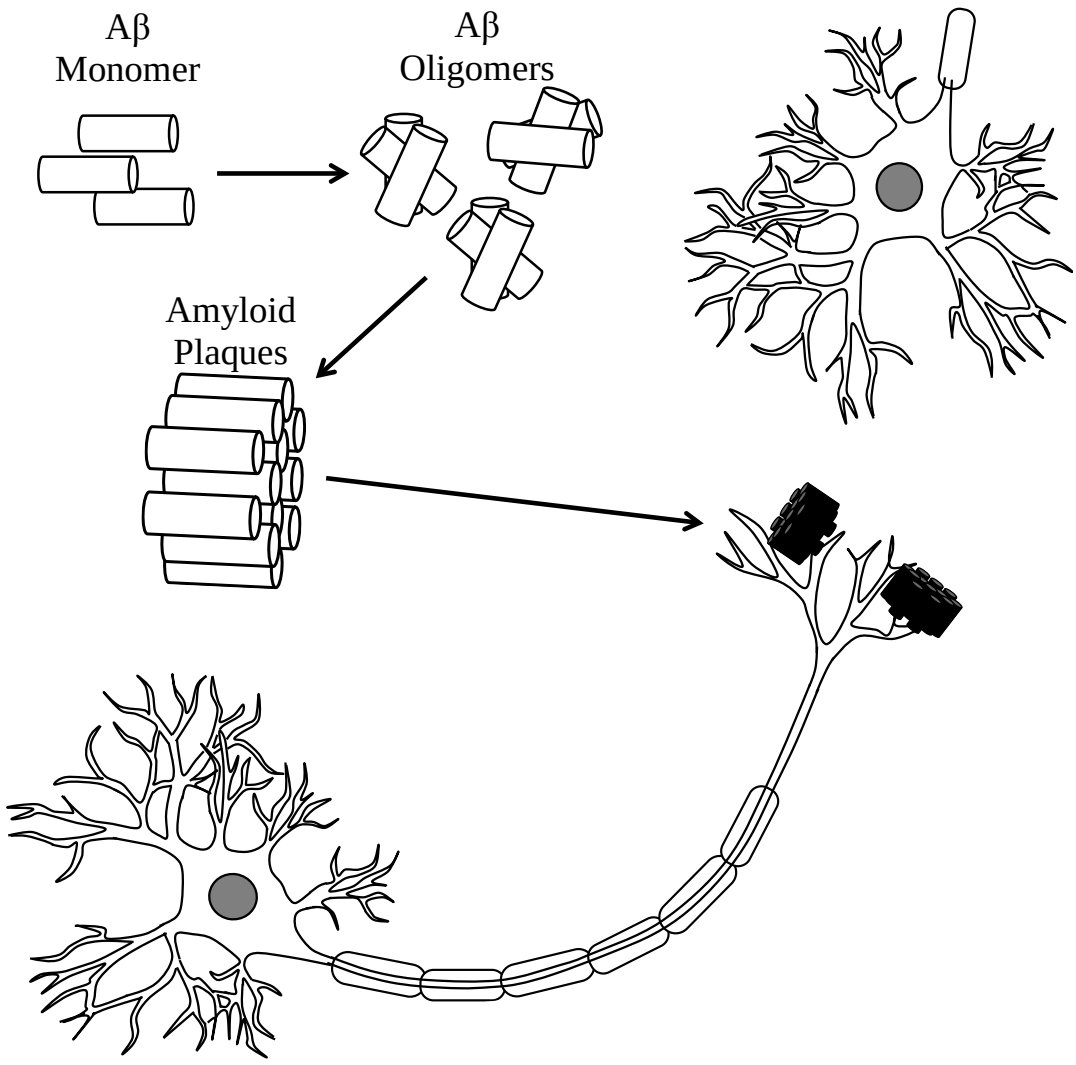

Figure 7.1 Pathological pathway and potential biomarker of AD. (Reference 10).

aggregation could lead to the tau-hyperphosphorylation cascade reaction. Tau stabilizes microtubules, but when hyperphosphorylated, tau dissociates from microtubules and aggregates into neurofibrillary tangles that eventually cause neuronal death.[11,12] Bodily fluids including cerebrospinal fluid (CSF), plasma, and urine are considered important sources for investigating biomarkers.

7.2.3 CEREBROSPINAL FLUID BIOMARKERS

Cerebrospinal fluid (CSF) has the potential to yield the most information. The subarachnoid space and ventricular system around the brain are occupied by CSF, and it provides basic mechanical and immunological protection of the brain inside the skull. However, CSF is collected by lumbar puncture, which is invasive and painful.[7]

Aβ1-42 is hydrophobic and forms oligomers and fibrils that accumulate to become a major component of extracellular plaques.[13] The reduction of the Aβ1-42 level is considered a robust biomarker of AD.[14-17] However, several other neurodegenerative or dementia diseases also show reductions in Aβ1-42.[18] Level of Aβ1-40 in CSF stays the same for AD patients, therefore the detection of a ratio of Aβ1-42/ Aβ1-40 serves as a more absolute AD diagnosis than the detection of Aβ1-42 alone.[19]

7.2.4 PLASMA BIOMARKERS

Investigating biomarkers in a plasma sample is less invasive and desirable, but it requires an assay or an instrument that can detect biomolecules at ultrasensitive levels. Plasma, the liquid portion of blood where red and white blood cells and platelets are suspended, can be easily isolated from blood by low speed centrifugation

in the presence of an anticoagulant. Multiple biomarkers are proposed for AD diagnosis, yet observing changes in levels of the analytes in plasma is challenging.[20] Different analytical methods utilized by various research groups disagree to some extent.[10] Some studies suggest no change in Aβ concentration in plasma, and others believe the Aβ1-42 : Aβ1-40 ratio could be an indicator for AD.[21,22]

7.2.5 DETECTION METHOD FOR BETA AMYLOID

Nonlinear absorption-based wave mixing, coupled with capillary zone electrophoresis (CE), offers ultrasensitive detection (picomolar and yoctomole levels) and high selectivity for Aβ1-42 and Aβ1-40. Detection limits of amyloid peptides by different methods as compared in Table 7.1.[23-26]

Typically, peptides in plasma are measured by using enzyme-linked immunosorbent assay (ELISA). However, results are inconsistent since some studies show higher concentrations of Aβ1-42 and Aβ1-40 in plasma, ratios that indicate risk factors for AD, and some research suggests no change in these analytes between AD patients and the healthy control.[21,22] The quantification of biomarkers in biological fluids is attempted by a combination of immunoprecipitation and matrix assisted laser desorption/ionization-time of flight (MALDI-TOF) to enhance selectivity.[27,28] Aβ1-42 and Aβ1-40 levels or the ratio may reflect the pathological process of AD and could theoretically differentiate AD patients from the healthy control group based on the analysis of the plasma; however, current analytical methods lack sensitivity, specificity and reproducibility to achieve this task.[10] Aβ level in plasma is in the 50 to 100 picomolar range, about100 times lower in concentration than in CSF.[29] Also,

Table 7.1 Detection limit of amyloid

Detection Method	Analytes	Molar Detection Limit	Mass Detection Limit	Reference
Sandwich ELISA	Aβ1-42	4.7×10^{-13} M	-	23
	Aβ1-40	4.2×10^{-13} M	-	23
LIF-CE	Amyloids	3.5×10^{-8} M	2.8×10^{-16} mol	24
HPLC	Aβ1-40	-	7.2×10^{-12} mol	25
MS	Amyloids	5.18×10^{-9} M	-	26
DFWM-CE	Aβ1-42	8.2×10^{-13} M	6.5×10^{-23} mol	This Work
	Aβ1-40	1.2×10^{-12}M	9.5×10^{-23} mol	

biological samples tend to be limited in size. DFWM interfaced with CE (DFWM-CE) only requires nanoliter sample sizes and it is inherently suitable for detecting these potential biomarkers in plasma or CSF. Verpillot *et al.* reported detection and separation of five amyloid peptides using capillary electrophoresis, but their sensitivity is not sufficient (0.300-0.500 micro-molar) to detect amyloids in plasma.[30]

This chapter presents sensitive detection of beta amyloid 1-40 and 1-42 at a sufficient sensitivity level in plasma using a chromophore label. DFWM is a nonlinear absorption-based technique that can conveniently detect analytes with both fluorophore and chromophore labels. Verpillot *et al.* studied detection limits of these peptides using multiple fluorescence methods.[24] They observed 35 nM to 750 nM analytes, corresponding to 280 attomoles, using CE laser-induced fluorescence (LIF).[24] DFWM yields a coherent laser-like signal that can be collected with high efficiency and high S/N, and hence, it is more sensitive than conventional absorption or fluorescence methods. A low-power laser can be used efficiently, since the wave-mixing signal has a cubic dependence on laser power. A concentration detection limit of 4.2 pM and 4.4 pM are determined for chromophore-conjugated Aβ1-42 and Aβ1-40, respectively. Based on the small sample size probed (79 pL), mass detection limits of 332 yoctomole and 348 yoctomole are determined for Aβ1-42 and Aβ1-40, respectively.

7.3 Experimental

7.3.1 Nonlinear Laser Wave-Mixing Setup

A forward-scattering nonlinear laser wave-mixing setup is used for amyloid analyses (Figure 7.2). A continuous-wave blue laser (488 nm) with adjustable power

(Coherent, Santa Clara, CA) tuned to 40 mW is used as the excitation source. The beam is divided in two by a beamsplitter (R:T 30:70). The stronger beam serves as both pump and probe beams while the reflected weaker beam serves only as the pump beam. Two parallel input beams travel equal distances to a lens where they are focused and mixed at an angle of 0.95°. The probe volume resulting from two overlapping input beams is determined to be 79 pL. The sample cell is a 75 μm i.d. fused-silica capillary (Molex, Lisle, IL). A portion of the capillary coating is removed by a butane flame or sulfuric acid to create a clear window for the input laser beams to propagate across the capillary. Two coherent wave-mixing signals are generated by the absorbing analytes. One of the input laser beams is chopped by an optical chopper (Stanford Research Systems, Sunnyvale, CA, SR541) at 200 Hz. The signal is collected by a photodetector (Thorlabs, Newton, NJ, PDA25K). The optical chopper, photodetector, and computer are interfaced to a lock-in amplifier (Stanford Research Systems, Sunnyvale, CA, SR810 DSP) where the signal is processed and amplified.

7.3.2 CHEMICALS

Distilled water from a compact water distillation system (Waterwise, Leesburg, FL, 4000) is used to prepare all the buffers in this study. Tris base, sodium dodecyl sulfate (SDS), sodium bicarbonate, and dialysis kit (MW_{CO} 1 kDa) are purchased from Sigma-Aldrich (St. Louis, MO). CHES, sodium hydroxide, and N,N-*dimethylformamide* (DMF) are purchased from Thermo Fisher Scientific (Waltham, MA). QSY 35 acetic acid succinimidyl ester is obtained from Life Technologies (Carlsbad, CA). The capillary cell is coated with Ultratrol LN (Target Discovery, Palo Alto, CA). Aβ1-42 and Aβ1-40 are purchased from American Peptide Company

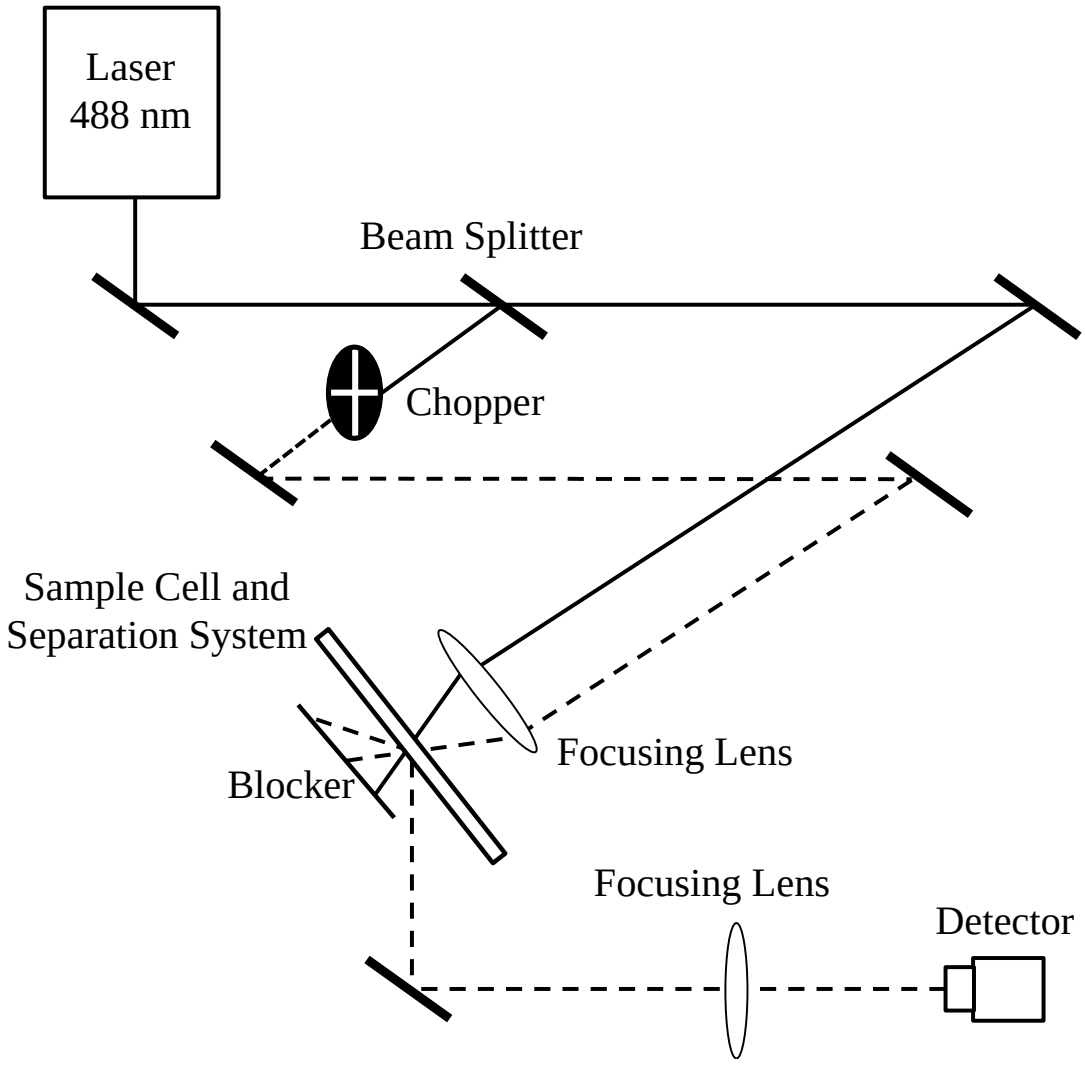

Figure 7.2 Nonlinear absorption-based wave-mixing setup for amyloid detection.

(Sunnyvale, CA).

7.3.3 Chromophore Labeling Reaction

Aβ1-42 and Aβ1-40 are resuspended in water to obtain 2.0 mg/mL protein solution in Tris buffer. The buffer is replaced by sodium carbonate-sodium bicarbonate reaction buffer (100 mM, pH 8.3) using the dialysis kit for peptides. Aβ1-42 and Aβ1-40 are reacted with QSY 35 (1:5) in DMF (20 mg/mL) for 1 hour in the dark. Excess dye is removed by dialysis while carbonate buffer is exchanged to Tris-CHES (25 mM) with 0.1% SDS.

7.3.4 Capillary Electrophoresis

Tris (1.04 g) and CHES (0.607 g) are dissolved in distilled water (100 mL), pH is adjusted to 9.0. All the CE runs are performed by a custom-built CE system. A fused silica capillary (Molex, Lisle, IL, USA) is used as the sample cell. Plastic reservoirs containing background electrolyte/analyte are placed at each end of the capillary. A high voltage power supply (Glassman High Voltage, High Bridge, NJ) is interfaced to a custom-built volage controller, and connected to platinum wires to power the anode and the cathode, placed in the reservoirs.

7.4 Results and discussion

7.4.1 Detection limit study for Aβ1-42 and Aβ1-40

Figure 7.3 shows reproducible electropherograms of QSY35-conjugated Aβ1-42 at different concentration levels. Multiple peaks are observed due to the three different labeling sites of the amyloid analyte. The injected concentrations of the amyloid are 0.42 nM and 4.2 pM. A concentration detection limit of 0.82 pM (S/N of

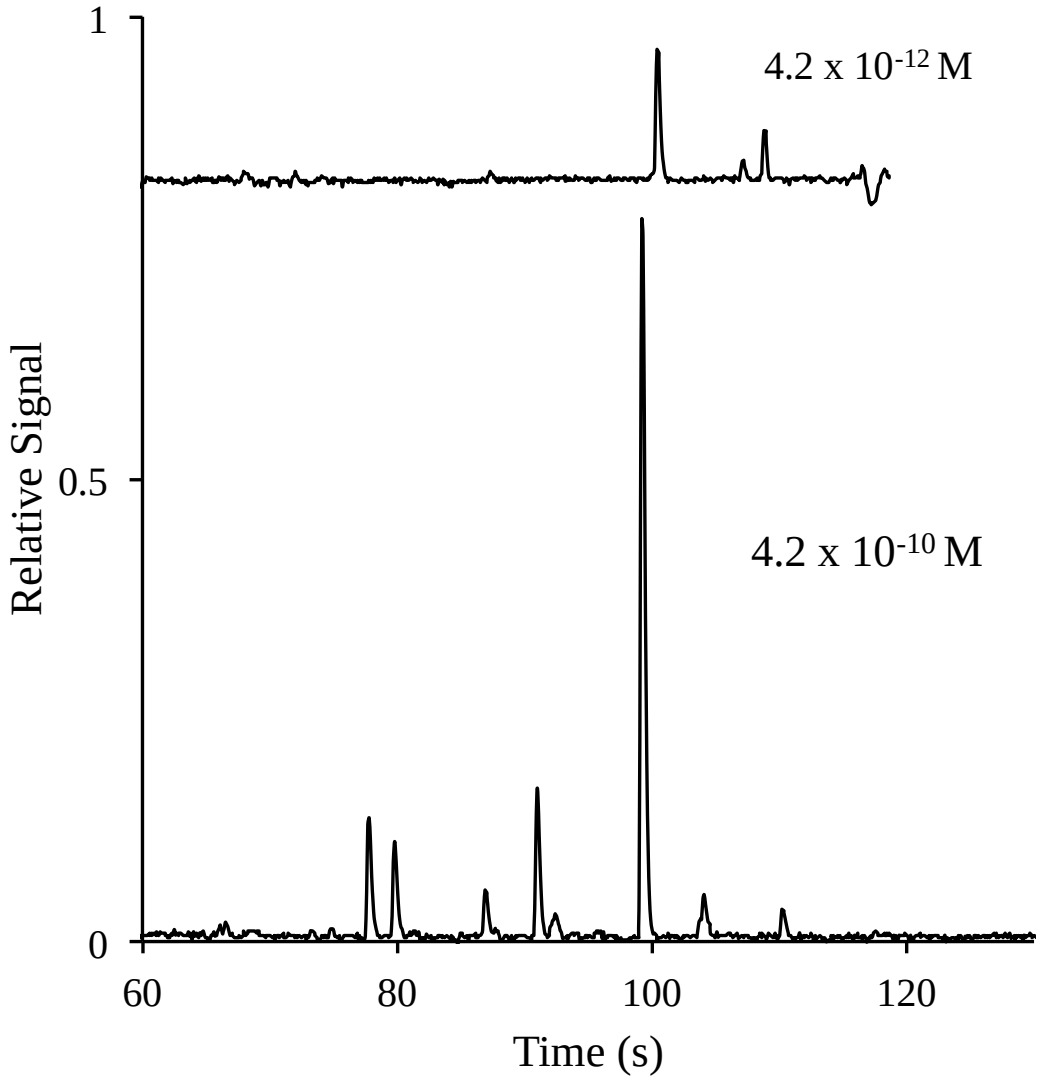

Figure 7.3 Electropherograms of QSY-conjugated Aβ1-42 (4.2 x 10^{-10} M and 4.2 x 10^{-12} M). The capillary is rinsed with NaOH (0.1 M), water UltraTrol LN and run buffer (100 mM Tris-CHES, 0.1% SDS). Capillary: 75 μm i.d., 34 cm, 16 cm effective length, -18.0 kV, 26 μA, 25 s electrokinetic injection. Detection by 40 mW 488 nm laser.

2) is determined for QSY35-conjugated Aβ1-42. Based on the probe volume used, a mass detection limit of 6.5 yoctomol is determined for QSY35-conjugated Aβ1-42, corresponding to only 39 Aβ1-42 peptides inside the DFWM probe volume.

Figure 7.4 shows electropherograms of 44 μM and 4.4 pM QSY-35-conjugated Aβ1-40. A concentration detection limit of 1.2 pM (S/N of 2) and a mass detection limit of 9.5 yoctomol are determined for QSY35-conjugated Aβ1-40.

Compared to the other analytical methods listed in Table 7.1, DFWM offers better sensitivity levels, especially mass detection limits, as compared to other techniques. The DFWM sensitivity can be enhanced by using simple chromophore or fluorophore labeling reactions to enhance optical absorption. The sandwich ELISA method listed in Table 7.1 provides comparable sensitivity; however, it produces inconsistent results as discussed earlier. DFWM is a reproducible detection method without the variables and the uncertainties of ELISA. DFWM-CE offers promising features and inherent advantages for the separation and detection of Aβ1-42 and Aβ1-40 in plasma.

7.4.2 POTENTIAL TO SEPARATE Aβ1-42 AND Aβ1-40

As shown in Figure 7.5, Aβ1-42 has a shorter migration time as compared to that of Aβ1-40 since capillary zone electrophoresis (CZE) separates molecules depending on charge-to-size ratios. A mass spectrometer (MS) separates molecules depending on mass-to-charge ratios and MS is not as sensitive as DFWM-CE. Verpillot *et al.* achieved separation of Aβ1-42, Aβ 1-40, Aβ 1-39, Aβ 1-38 and Aβ 1-37 by CZE using a UV laser.[30] Separation of these amyloids is challenging since the peptides, especially Aβ1-42, tend to oligomerize and fiberize within 6-15 hours

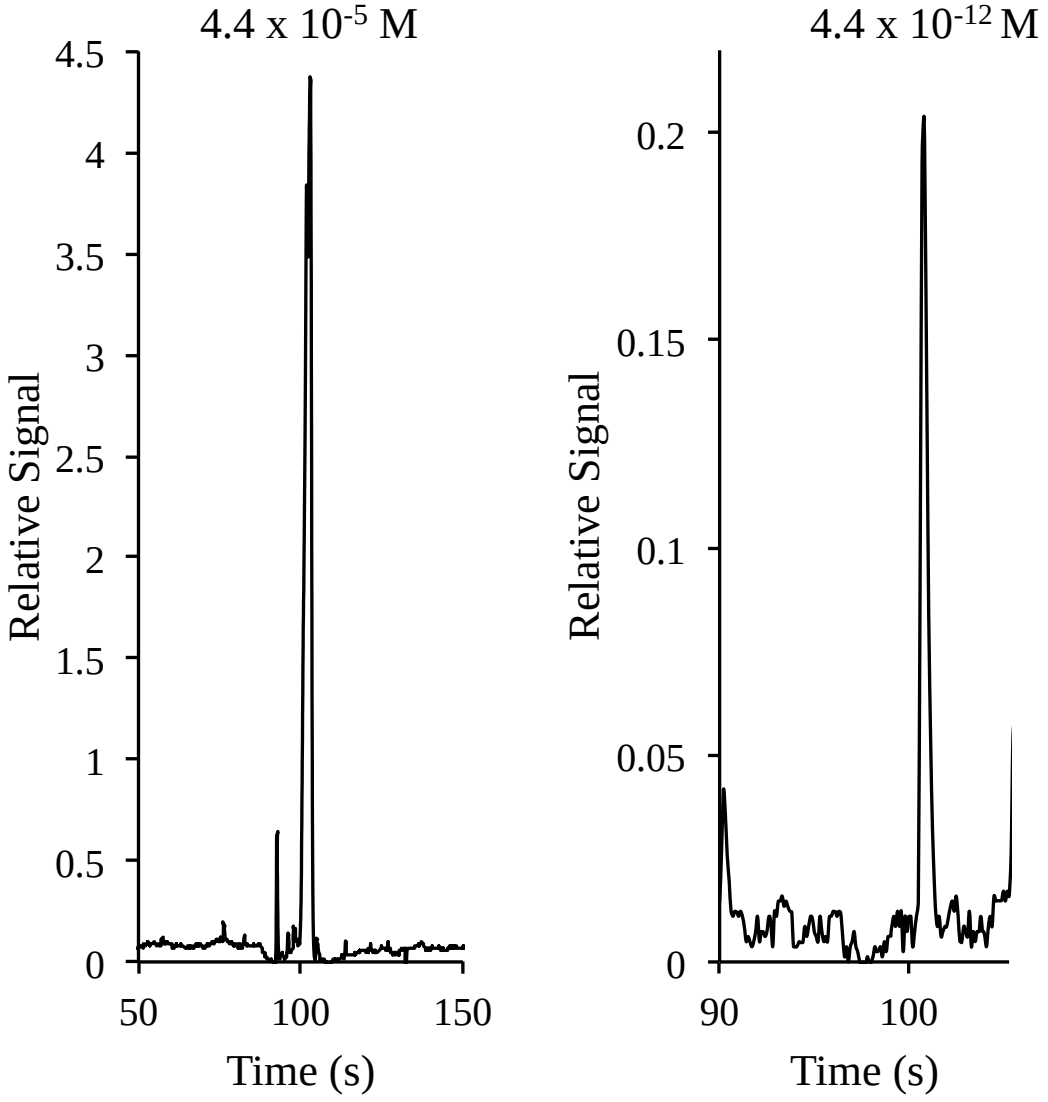

Figure 7.4 Electropherograms of QSY-conjugated Aβ1-40 (4.4 x 10^{-5} M and 4.4 x 10^{-12} M). Capillary is rinsed with NaOH (0.1 M), water, UltraTrol and run buffer (100 mM Tris-CHES, 0.1% SDS). Capillary: 75 μm i.d., 34 cm,16 cm effective length, -18.0 kV, 26 μA, 5 s and 25 s electrokinetic injection. Detection by 40 mW 488 nm laser.

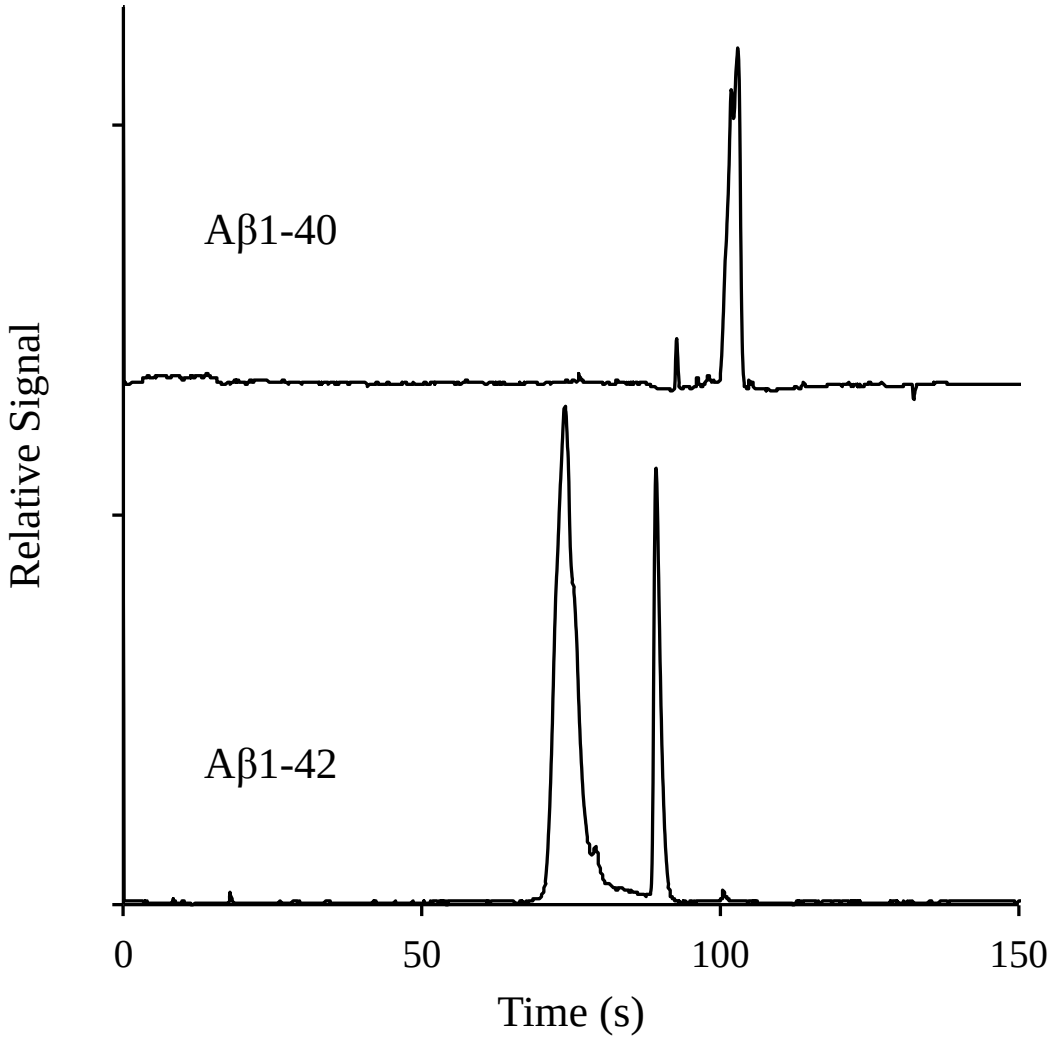

Figure 7.5 Electropherograms of QSY-conjugated Aβ1-42 and Aβ1-40 (4.2 x 10^{-5} M and 4.4 x 10^{-5} M, respectively). Capillary is rinsed with NaOH (0.1 M), water and UltraTrol for 3 minutes followed by filling with run buffer (100 mM Tris-CHES, 0.1% SDS). Capillary: 75 μm i.d., 34 cm (16 cm effective length), -18.0 kV, 5 s electrokinetic injection. Detection by 40 mW 488 nm laser.

depending on the type of pretreatment used to avoid aggregation.[31]

The monomeric form of the peptide is observed followed by the oligomeric form, as shown in Figure 7.5. The electropherogram shown is taken 48 hours after the peptide solution is prepared. A dialysis kit takes 3 hours to exchange buffer or remove free labels, and the Chromeo P503 label takes only 30 minutes to complete labeling reaction. The excess free label does not have to be removed since the absorption wavelength of the label is far away from those of the analyte after conjugation.

When a UV laser is used as the excitation source, amyloids can be detected by DFWM-CE label-free in their native form. DFWM-CE can overcome sensitivity issues faced by other methods, and DFWM offers promising advantages for the detection of amyloids in plasma, a less invasive technique for the diagnosis of early-stage AD.

7.5 Conclusion and future work

Nonlinear absorption-based laser wave mixing, coupled with CE, has the potential to detect Aβ1-42 and Aβ1-40 in plasma, and promises a noninvasive and reliable diagnosis tool for AD. Laser wave mixing offers many advantages as an ultrasensitive detection technique for chromophore-conjugated peptides. Ultrasensitive picomolar and yoctomole detection limits are obtained in CZE using dynamic coating for the capillary. The use of low-power lasers yields a compact portable wave-mixing design for the detection and identification of amyloid peptides. Wave-mixing detection is fast (< 2 minutes) and hence, it is suitable for a biochemical sample that degrades quickly.

7.6 Acknowledgement

The majority of the material for this chapter comes directly from a manuscript entitled “Ultrasensitive Detection of Alzheimer’s Disease Biomarkers Aβ1-42 and Aβ1-40,” by Manna F. Iwabuchi, Marcel M. Hetu, and William G. Tong, to be submitted. The dissertation author is the primary author of this manuscript.

7.7 Reference

(1) Lui, J. K.; Laws, S. M., *et al Journal of Alzheimer's disease : JAD* **2010**, *20*, 1233.

(2) Selkoe, D. J. *Nature cell biology* **2004**, *6*, 1054.

(3) Fernandez, M.; Gobartt, A. L., *et al BMC neurology* **2010**, *10*, 87.

(4) Morris, J. C. *Neurobiology of aging* **1997**, *18*, 388.

(5) Morris, J. C.; Price, J. L. *Journal of molecular neuroscience : MN* **2001**, *17*, 101.

(6) Perrin, R. J.; Fagan, A. M., *et al Nature* **2009**, *461*, 916.

(7) Blennow, K.; Hampel, H., *et al Nature reviews. Neurology* **2010**, *6*, 131.

(8) Clark, C. M.; Davatzikos, C., *et al Neuro-Signals* **2008**, *16*, 11.

(9) Aluise, C. D.; Sowell, R. A., *et al Bba-Mol Basis Dis* **2008**, *1782*, 549.

(10) Anoop, A.; Singh, P. K., *et al International journal of Alzheimer's disease* **2010**, *2010*.

(11) Grundke-Iqbal, I.; Iqbal, K., *et al J Biol Chem* **1986**, *261*, 6084.

(12) Grundke-Iqbal, I.; Iqbal, K., *et al Proceedings of the National Academy of Sciences of the United States of America* **1986**, *83*, 4913.

(13) Roher, A. E.; Lowenson, J. D., *et al Proceedings of the National Academy of Sciences of the United States of America* **1993**, *90*, 10836.

(14) Motter, R.; Vigo-Pelfrey, C., *et al Ann Neurol* **1995**, *38*, 643.

(15) Kanai, M.; Matsubara, E., *et al Ann Neurol* **1998**, *44*, 17.

(16) Shoji, M.; Matsubara, E., *et al Journal of the neurological sciences* **1998**, *158*, 134.

(17) Fukuyama, R.; Mizuno, T., *et al European neurology* **2000**, *43*, 155.

(18) Mollenhauer, B.; Esselmann, H., *et al J Neural Transm* **2011**, *118*, 691.

(19) Thal, L. J.; Kantarci, K., *et al Alzheimer disease and associated disorders* **2006**, *20*, 6.

(20) Fukumoto, H.; Tennis, M., *et al Arch Neurol-Chicago* **2003**, *60*, 958.

(21) Irizarry, M. C. *NeuroRx : the journal of the American Society for Experimental NeuroTherapeutics* **2004**, *1*, 226.

(22) Graff-Radford, N. R.; Crook, J. E., *et al Arch Neurol* **2007**, *64*, 354.

(23) Pesini, P.; Perez-Grijalba, V., *et al International journal of Alzheimer's disease* **2012**, *2012*, 604141.

(24) Verpillot, R.; Esselmann, H., *et al Anal Chem* **2011**, *83*, 1696.

(25) Du, C.; Ramaley, C., *et al Journal of biomolecular techniques : JBT* **2005**, *16*, 356.

(26) Cheng, X.; van Breemen, R. B. *Anal Chem* **2005**, *77*, 7012.

(27) Gelfanova, V.; Higgs, R. E., *et al Briefings in functional genomics & proteomics* **2007**, *6*, 149.

(28) Portelius, E.; Tran, A. J., *et al Journal of proteome research* **2007**, *6*, 4433.

(29) Maler, J. M.; Klafki, H. W., *et al Proteomics* **2007**, *7*, 3815.

(30) Verpillot, R.; Otto, M., *et al J Chromatogr A* **2008**, *1214*, 157.

(31) Ryan, T. M.; Caine, J., *et al PeerJ* **2013**, *1*, e73.